NASA CONTRACTOR REPORT

NASA CR-1568

HYPERSONIC CRUISE VEHICLE WING STRUCTURE EVALUATION

by P. P. Plank, I. F. Sakata,
G. W. Davis, and C. C. Richie

Prepared by
LOCKHEED MISSILES & SPACE COMPANY
Sunnyvale, Calif.
for Langley Research Center

NATIONAL AERONAUTICS AND SPACE ADMINISTRATION • WASHINGTON, D. C. • MAY 1970

call no.
NASA CR-1568

HYPERSONIC CRUISE VEHICLE

WING STRUCTURE EVALUATION

By P. P. Plank, I. F. Sakata, G. W. Davis, and C. C. Richie

May 70

Prepared under Contract No. NAS 1-7573 by
m. e. LOCKHEED MISSILES & SPACE COMPANY
Sunnyvale, Calif.

for Langley Research Center

NATIONAL AERONAUTICS AND SPACE ADMINISTRATION

For sale by the Clearinghouse for Federal Scientific and Technical Information
Springfield, Virginia 22151 – CFSTI price $3.00

ABSTRACT

HYPERSONIC CRUISE VEHICLE WING STRUCTURE EVALUATION

by

P. P. Plank, I. F. Sakata, G. W. Davis, and C. C. Richie

An analytical and experimental evaluation was performed to determine the best primary structure, heat shield, and leading edge for design of a Mach 8 hypersonic transport wing. Selections were based on least total system cost for a fleet of airplanes. Results indicate that a semimonocoque wing structure of Rene´ 41 with spanwise stiffened panels consisting of a single beaded sheet provided lowest weight and lowest total-system-cost. Large corrugated heat shields with multiple supports cover the exposed wing surfaces. The heat shields are made of TD NiCr adjacent to the leading edge and of Rene´ 41 on the remaining surfaces. Segmented leading edges of TD NiCr complete the concepts selection. Reported herein are design criteria, descriptions of concepts, procedures, results, and discussion of significant findings.

CONTENTS

ILLUSTRATIONS

TABLES

SYMBOLS

a,b	X and y distances between simply supported edges of plate
a/b	Panel aspect ratio
BL	Butt line
b	Flat width
b_s	Pitch
C	Wing chord; geometric chord
C_p	Specific heat
CER	Cost-estimation relationship
dB	Decibel
e	Strain
E_c	Compressive Young's modulus
F	Allowable stress
FS	Fuselage station
F_{cy}	Compression yield strength
F_{tu}	Ultimate tensile strength
F_{ty}	Tensile yield strength
$F_{0.7}$	Stress corresponding to modulus of $0.7\,E_{el}$
f	Stress
f_a	Alternating stress
f_m	Mean stress
GTOW	Gross takeoff weight
g	Gravitational acceleration
H	Altitude
h	Height; bead height
K	Thermal conductivity
K_Q, K_T	Fatigue quality indices
L	Length
L_{max}	Maximum length
L/D	Lift-to-drag ratio
MS	Margin of safety
N	Number of cycles periodically repeated until failure
n	Ramberg-Osgood parameter
N_x, N_y, N_{xy}	Extensional and shear forces in XY coordinate system per unit length
p	Pressure; pitch of stiffeners for waffle panel
$p_{ult.}$	Ultimate pressure load
q	Dynamic pressure
R	Radius
RT	Room temperature
S	Cell size
S_{REF}	Wing reference area
T	Temperature
t	Thickness, time
t_s	Skin thickness

t_w	Stiffener thickness
$\bar{t}$	Equivalent thickness
z	Distance from neutral axis to extreme fiber
W	Weight
w	Unit weight of panel, lb/ft^2
α	Mean coefficient of thermal expansion; angle of attack
Δp, ΔT	Pressure difference; temperature difference
ΔW_f	Fuel increment due to leading-edge drag penalty, lb.
δ	Deflection; depth of oxidation penetration
ϵ	Emittance; depth of panel distortion
ϵ_T	Elastic thermal strain
ϵ_{ht}	Hemispherical total emittance
$\epsilon_{\lambda\ 0.65}$	Spectral emittance measured at a wavelength of 6500A
$\bar{\eta}$	Plasticity correction factor
λ	Dynamic pressure parameter; pitch of panel distortion in airstream direction
λ_{CR}	Value of dynamic pressure parameter at flutter
μ	Pitch of panel distortion perpendicular to airstream direction
ρ	Density
Σn	Cumulative number of occurrences
$\Sigma \bar{t}$	Summation of equivalent thicknesses

Subscripts

c	Pertaining to core of honeycomb-core sandwich; pertaining to compression
clip	Pertaining to heat shield clip
FLAT	Associated with flat section of leading edge
HS	Associated with heat shield
LE	Associated with leading edge
NOSE	Associated with nose section of leading edge
u, l	Pertaining to upper and lower surfaces of the convex-beaded panel
1, 2	Lower and upper faces of honeycomb-core sandwich

HYPERSONIC CRUISE VEHICLE WING STRUCTURE EVALUATION

By P. P. Plank, I. F. Sakata,* G. W. Davis, and C. C. Richie
Lockheed Missiles & Space Company

SUMMARY

An investigation was conducted to provide both theoretical and experimental data to support the selection of the best structural concept for the design of a hypersonic wing structure.

Various combinations of promising primary structures, heat shields, and leading-edge design concepts were analyzed for the wing of a specified hypersonic cruise vehicle to operate at Mach 8, at a maximum dynamic pressure of 2200 lb/ft^2, and with a life-span of 10 000 hr. The results of earlier studies were supplemented by an in-depth analysis, which was conducted in accordance with design criteria and included extensive computer modeling, transient structural thermal and load predictions, and synthesis procedures for structural optimization. After initial and intermediate screening, six wing-structure concepts, as shown in the table on page 2, were selected and subjected to in-depth structural analysis, including: optimum rib and spar spacing, optimum thermal-protection arrangements, oxidation penetration, eccentricities, nonoptimum factors, manufacturing penalties, panel flutter, wing flutter, sonic fatigue, load fatigue, and creep. Since the wing's leading edge exists in an even more severe environment than the remainder of the wing, the leading edge required additional and separate analyses, such as low-cycle fatigue.

The various wing concepts were evaluated with respect to weight, cost, performance, and reliability. These factors were then interrelated to yield a relative comparison, based on minimum-total-system cost for a payload range requirement of 205 billion ton-miles. Concurrently, subelement tests were conducted to provide material-screening data, joining-technique capabilities, and formability parameters. Compression tests (end closeouts, crippling, column) and shear tests on panel elements were also conducted to assess and refine concept designs.

Based on a constant-weight vehicle (baseline), the ranking of the primary-structure design concepts shown in the table on page 2 was obtained. When these primary-structure concepts were applied to a minimum-total-system-cost vehicle – by an interaction evaluation of weight, cost, performance, and reliability – the ranking of the primary-structure concepts was unchanged and the relative cost increases shown in the table on page 2 were obtained.

The relative cost increases show conclusively the great effect that structural efficiency has on overall total-system cost. Small weight inefficiencies evaluated under range-payload constraints can and do raise costs to prohibitive levels.

*Lockheed California Company

Wing primary-structure concept	Weight comparison for baseline-size vehicle[a]		Minimum TSC[b] comparison for optimum-size vehicles[c]
	Wing weight,[d] lb/ft^2	Relative weight	Relative cost
(1) Semimonocoque spanwise beaded	6.20	1.000	1.000
(2) Semimonocoque spanwise tubular	6.53	1.053	1.083
(3) Monocoque honeycomb-core	6.58	1.061	1.110
(4) Statically determinate spanwise beaded	6.77	1.092	1.263
(5) Semimonocoque chordwise tubular	7.41	1.195	1.431
(6) Monocoque unflanged waffle	10.38	1.674	5.741

[a]Gross takeoff weight = 550 000 lb.
[b]TSC = procurement cost and operating costs for a 205 x 10^9 ton-mile fleet mission.
[c]Gross takeoff weight and fleet size = variable.
[d]Wing weights are given in lb per ft^2 of planform wing area.

The most favorable heat-shield concept for use with the primary structures is a large corrugated shield with multiple supports. A segmented leading edge, insulated from the primary load-carrying structure, was found to be the most favorable.

The superalloy René 41 was shown to be the best material for the primary structure and for most of the heat shields; dispersion-strengthened TD NiCr was shown best for the leading edge and for the row of heat shields adjacent to the leading edge.

The concept-selection procedures developed in this study provide a sensitive, rational basis for comparing both overall-design arrangements and skin-panel configuration variations. The results demonstrate that wing structural weights relate directly to total-system cost and that substantial cost differences exist between the various primary-structure concepts. A significant finding is the relatively large importance of weight-saving compared, for example, to initial cost.

INTRODUCTION

The utility of a hypersonic cruise vehicle depends upon a low structural mass fraction in a high-temperature environment. This requirement exceeds the limits of state-of-the-art structures. The only hypersonic structures flown to date have been the X-15 research airplane and the ASSET unmanned lifting reentry test vehicle, both of which have structures that are too heavy and therefore unsuitable for cruising flight.

For the past several years, the NASA Langley Research Center and other agencies have been investigating promising structural concepts, such as those discussed in references 1, 2, and 3, and the 1967 Conference on Hypersonic Aircraft Technology (ref. 4) was devoted to the subject.

The investigation now being reported was conducted to subject six promising wing concepts to the same in-depth analyses, including all known environmental structural considerations that could affect the four comparison parameters: weight, cost, performance, and reliability. These factors were then interacted in a total-system-cost study for a system range-payload capability of 205 billion ton-miles to provide the basis for selecting the best structural concept for a lightweight hot-wing structure of minimum total-system-cost.

First, the potential approaches were assessed and screened. Then, a combination of structural-design concepts that satisfied the requirement for sustained operation at Mach 8 to a maximum dynamic pressure of 2200 psf was selected and validated. This involved a comprehensive theoretical structural optimization and experimental investigation of the primary structures, the heat shields, and the leading edges for a hot-wing structure integrally attached to a hot-fuselage structure. The basic structural concepts included:

(1) Biaxially stiffened structures with smooth external surfaces (waffle, honeycomb, etc.)

(2) Uniaxially stiffened structures, stiffened either in the chordwise or spanwise direction: sheetmetal constructions – beaded, tubular, and corrugated – that relieve thermal stresses, but that in some cases require fairings for aerodynamic smoothness

(3) Statically determinate structures, consisting of a series of spanwise single-cell box beams, slip jointed at the ribs and fuselage, with potentially lower thermal stresses

The bases of selection were weight, vehicle cost, performance, and reliability, with minimum total-system cost including direct and indirect operating costs as the common denominator for overall evaluation and selection of the concepts.

Only the most significant results of the study are presented in this volume. The details of the analyses and substantiation of results are given in reference 5, which includes sections on weight, cost, performance, reliability, and total system cost.

DESIGN CRITERIA

Requirements for the analysis of the structural concepts for the wing of a specified hypersonic cruise vehicle are defined in this section in terms of vehicle configuration, vehicle performance, and structural criteria.

CONFIGURATION CRITERIA

Detailed analyses were based on the wing section of the representative Mach 8 hypersonic cruise vehicle shown in figure 1. The study area, as defined in this figure, was subjected to the detail analysis with temperature and loads determined in a gross sense for the entire vehicle.

Specifically, the evaluation was based on an integral hot-fuselage and hot-wing structure, with separate liquid-hydrogen tanks and pressurized compartments suspended within the fuselage.

The following specifications were used:

(1) Total wing area	10 000 ft^2
(2) Reference area (rear delta-wing area)	8 330 ft^2
(3) Vertical tail area	574 ft^2
(4) Engine capture area	306 ft^2
(5) Zero-lift line	3 deg

The masses assigned to the various components of the baseline vehicle (fig. 1) are listed below as fractions of the gross takeoff weight of 550 000 lb.

Fuel	0.40	Propulsion	0.15
Structure	0.27	Equipment	0.05
Landing gear	0.03	Payload	0.10

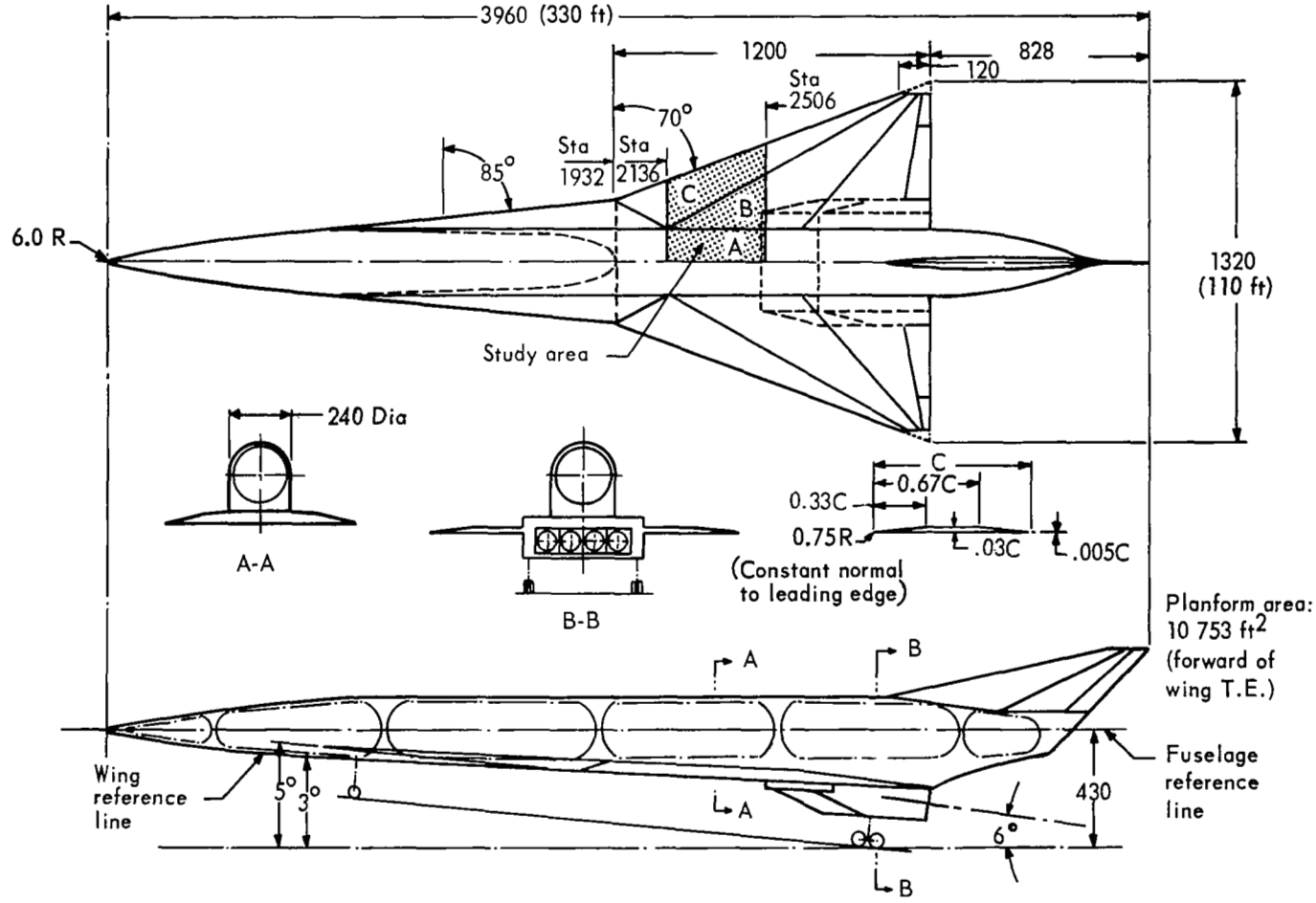

Figure 1. Hypersonic cruise vehicle

PERFORMANCE CRITERIA

The flight schedule, altitude versus mach number, is shown in figure 2 in which lines of constant dynamic pressure q are indicated. In the load and trajectory analysis, a skin-roughness drag of 1.10 times the smooth-surface skin drag was assumed.

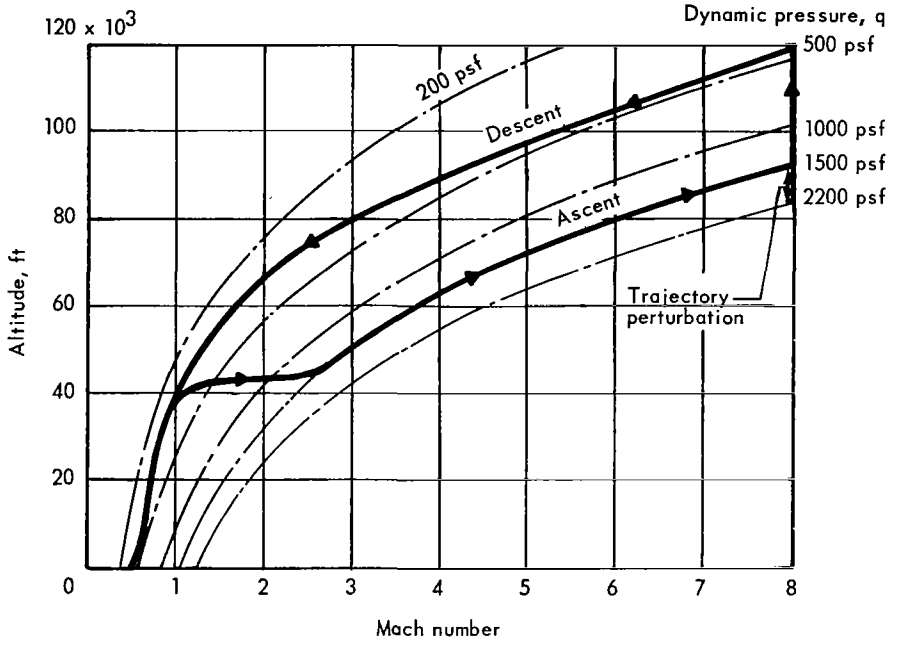

Figure 2. Hypersonic cruise vehicle flight schedule

A maximum forward acceleration of 0.2g was assumed in the trajectory analysis for the ascent period to Mach 8. At initiation of cruise, a nominal climb at constant Mach 8 occurs until maximum lift-to-drag ratio (L/D) is approached, followed by a +1.0-g flight at maximum L/D. A constant deceleration of 0.2g, caused by drag augmentation, was postulated for descent flight. The altitude at termination of cruise was taken as that which provides the required fuel for descent. It was assumed that 90 percent of the flights have this schedule.

The indicated schedule perturbation (10 percent of flights) at Mach 8 was used to determine limit loads. This perturbation is assumed to exist at the initiation of cruise (Mach 8, q = 1500 psf) and results from a -1.5-g (-1.5 +1.0 gravity = -0.5-g) nosedown maneuver. This -0.5-g condition is followed by a +2.0-g pullup maneuver (which does not exceed q = 2200 psf) and is held at a constant acceleration during a smooth transition to maximum L/D. This is followed by a +1.0-g nominal flight condition at maximum L/D for the remainder of the cruise period. The negative-limit load condition is the critical combination of thermal and air loads that occurs during the nosedown maneuver; the positive-limit load condition is the critical combination of thermal and air loads that occurs during the pullup maneuver. In life analyses, the maneuver loadings were used for every tenth flight.

STRUCTURAL CRITERIA

Evaluations of the structure and heat-shield concepts were based on a life of 10 000 hours, with environment and loading durations determined from design-trajectory analyses.

A maximum permanent deformation of 0.5 percent due to creep was considered for the life of the structure, thereby permitting future improvement in materials without seriously penalizing the weight of the study vehicle.

Boundary-layer and engine-noise levels were considered in developing acoustic-(sonic-) fatigue criteria. Areas of the wing experiencing laminar and turbulent flow are assumed to be subject to root-mean-square sound-pressure levels equal to 0.70 percent of freestream dynamic pressure (0.007 q). The wing-surface area adjacent to the transition line from laminar to turbulent flow is assumed to be subject to significantly higher sound-pressure levels of 0.022 q.

The limit loads for the vehicle structure occur during the specified maneuver at Mach 8, dynamic pressure of 2200 psf, and +2.0-g acceleration normal to the wing plane. The temperatures resulting from this limit-load maneuver were used as the limit temperatures for structural-material analysis. To ensure an ultimate-load factor of safety of 1.5, an additional factor of 1.3 was used to account for further degradation of material properties resulting from increases in temperature above limit loads. Therefore, ultimate airloads are (1.5x1.3) times limit airloads.

For thermal stresses, 1.3 times limit thermal stresses (strains) were combined to stresses (strains) due to ultimate airloads. Tensile thermal stresses tending to relieve compressive airload stresses were conservatively ignored.

For both panel and vehicle flutter, a factor of safety of 1.3 times dynamic pressure was used for thermal-protection (heat shields) and structural panels.

The wing cavity was assumed to be vented to the upper surface pressures; however, a limit-load Δp of ± 0.5 psi (resulting from internal pressure lag) was assumed for the upper surface primary-structure panels. The lower surface primary-load-carrying panels are designed for the calculated aerodynamic pressures. These pressures are uniformly distributed over the primary-structure panels (based on complete venting through the heat-shield panels) or with 0.5 psi applied to the heat shield and introduced at the heat-shield support interface, with the balance of the pressure uniformly distributed over the structure panels. The heat-shield panels are designed for a limit Δp of ± 0.5 psi.

The allowable material stress was compared to stresses based on thermal and air loads, predicted temperatures, and appropriate fatigue or creep spectra. Limit thermal and air load stresses were not allowed to exceed the 0.2 percent material yield or two-thirds of the material ultimate strength (the lower for the appropriate temperature). For compression members, the ultimate allowable stress was considered to be the critical buckling stress of the members supporting the primary loads.

STRUCTURAL CONCEPTS

The structural concepts for a hypersonic wing were divided into the three major problem areas: primary load-carrying structures, thermal-protection systems, and leading edges.

PRIMARY STRUCTURE

The three general types of primary load-carrying structural concepts that were evaluated are as follows:

(1) Monocoque – biaxially stiffened panels

(2) Semimonocoque – uniaxially stiffened panels

(3) Statically determinate – a series of spanwise single-cell box beams, slip jointed in the chord direction

Monocoque

Monocoque construction consists of biaxially stiffened panels, which support the principal load in both the span and chord directions, as indicated in figure 3. The wing substructure and a typical heat shield are also shown.

While monocoque construction has a smooth skin that results in minimum aerodynamic drag, heat shielding may be required to limit structural temperatures or may be desirable to minimize thermal stress. The biaxially stiffened panels shown in figure 4 were considered.

The unflanged waffle-grid configurations were assumed to be electrochemically milled, while the flanged-waffle configurations were diffusion bonded. The core of the honeycomb-sandwich configuration was assumed to be spotwelded to the face sheets. Both diffusion bonding and spotwelding were considered for the truss-core sandwich panel configuration.

In the monocoque concept, as well as in all other primary-structure concepts, circular-arc (sine-wave) corrugated webs are used for rib and spar webs. The caps of the ribs and spars are inplane with the surface panels, and the fastener shear force is aligned with the centroidal axis of the panel where applicable.

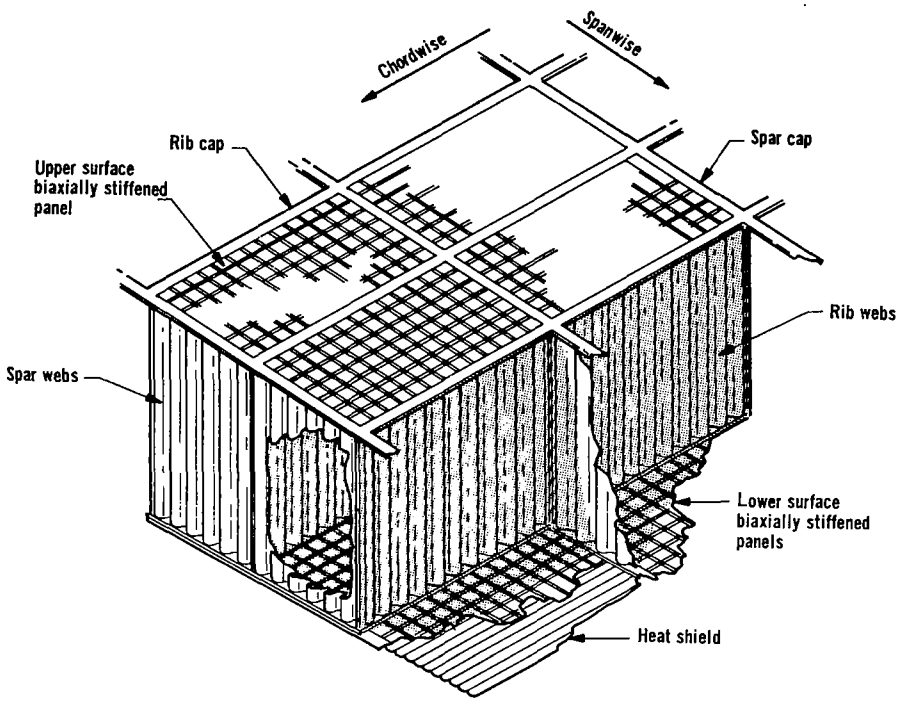

Figure 3. Monocoque biaxially stiffened primary-structure concept

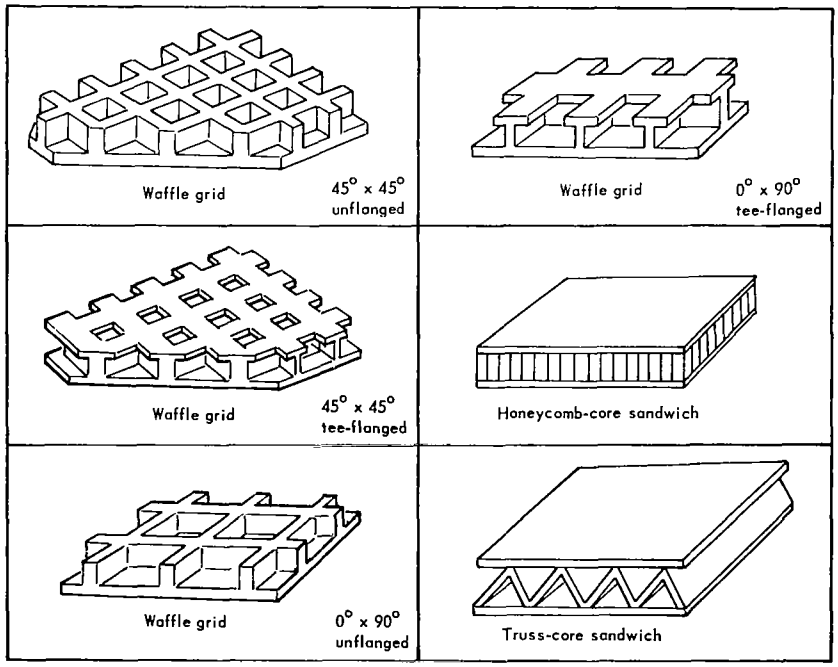

Figure 4. Monocoque panel constructions

Semimonocoque

Biaxial stiffening often produces minimum-weight structural designs, However, one objective of this hot-wing study in which thermal stresses can be significant is to evaluate concepts that alleviate thermal strains, such as the concept shown in figure 5. The two types of semimonocoque concepts studied are (1) panels supporting loads in the spanwise direction, and (2) panels supporting loads in the chordwise direction. Both have the same type of rib and spar caps as the monocoque structure; but since the panels cannot support biaxial loads, either spar caps or rib caps must have sufficient area to support inplane loads acting normal to the panel stiffeners.

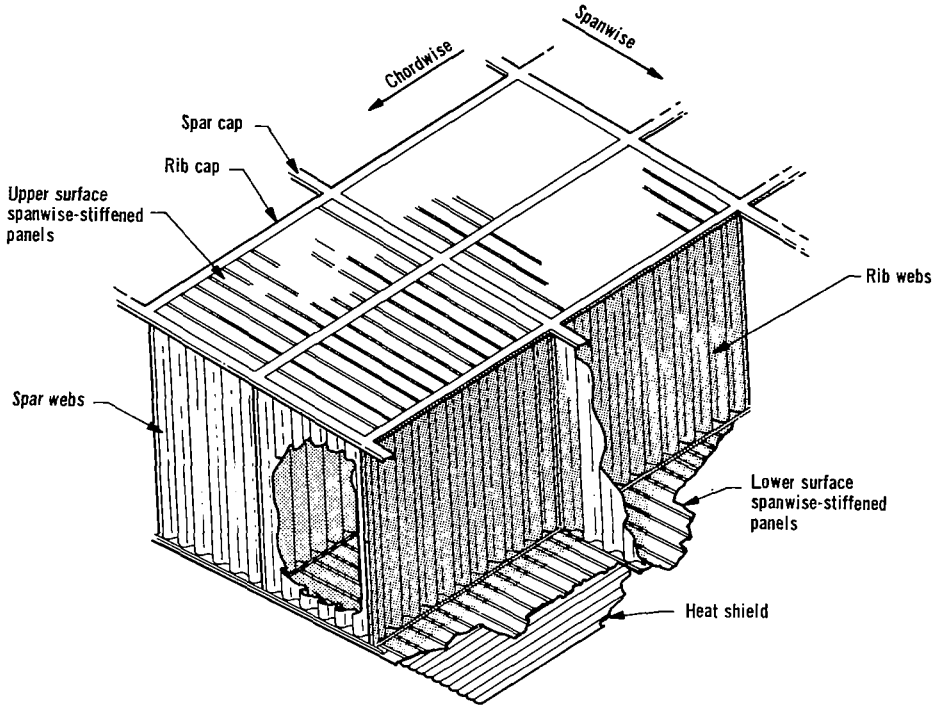

Figure 5. Semimonocoque spanwise-stiffened primary-structure concept

Spanwise. – The spanwise-stiffened wing concept, including spar and rib substructure, is shown in figure 5. The surface-panel configurations studied, shown in figure 6, have effective load-carrying capability in their stiffened direction. Panel chordwise thermal stresses are minimized by allowing thermal expansion (deformation) in the chordwise direction for all but the corrugation-stiffened skin concept. Aerodynamic fairings or heat shields are required in all areas to maintain smoothness for all spanwise-stiffened concepts except the corrugation-stiffened skin. For regions subject to most severe heating, all concepts may require heat shields to limit structural temperatures and reduce thermal stress.

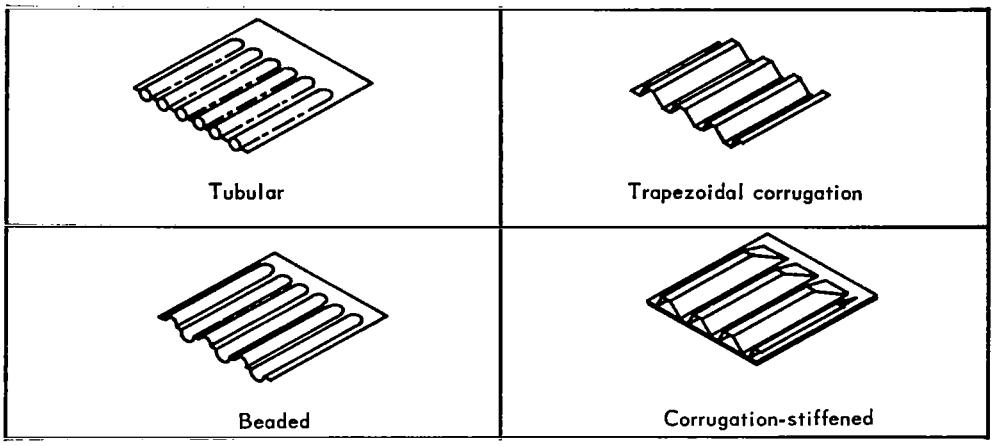

Figure 6. Semimonocoque spanwise-stiffened panels

The tubular panel is made of two beaded sheets, joined by spotwelding. The tubular, beaded, and corrugation-stiffened skin constructions are produced by stretch forming, with integrally formed end-closeouts. The trapezoidal-corrugation configuration is formed by a power brake. All of the double-skin configurations and the end-closeout doublers are resistance spotwelded.

Chordwise. – The chordwise-stiffened panel and wing substructure are shown in figure 7.

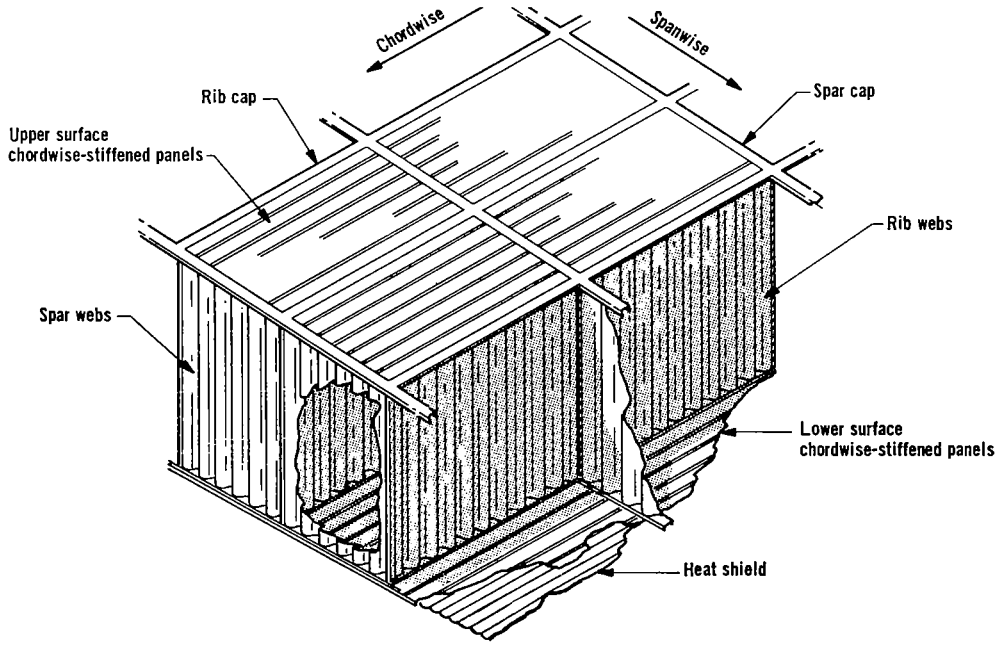

Figure 7. Semimonocoque chordwise-stiffened primary-structure concept

The panel surface configurations studied are shown in figure 8A. Except for the convex-beaded and corrugation-stiffened constructions, the chordwise-stiffened panel configurations are similar to the spanwise configurations studied. Since the chordwise

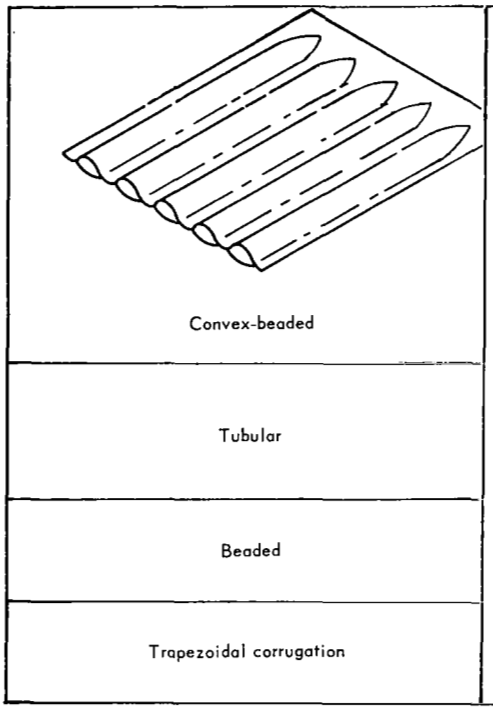

Figure 8A. Semimonocoque chordwise-stiffened panels

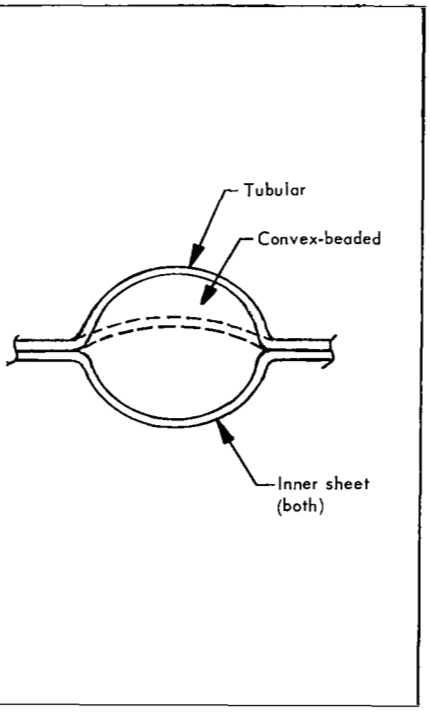

Figure 8B. Tubular and convex-beaded construction

concept has stiffening in the airstream direction, a saving in weight may be possible by deleting aerodynamic fairings. The deep tubular construction at the top in figure 8B requires fairings. However, if thermal considerations permit, shielding is not required on the outer surface of the lower-profile convex-beaded construction. As shown in the figure, the inner sheet of both concepts has full-depth circular-arc beads.

Stretch forming and resistance spotwelding are used in producing the convex-beaded panel, while the other configurations are formed by the same methods as the spanwise configurations.

Statically Determinate

The statically determinate structure shown in figure 9 is a series of spanwise single-cell box-beams attached at the forward end of each beam to the fuselage. At rib intersections and at the fuselage, a slip joint is provided between adjacent beams. This method of attachment allows rotational freedom between beams while affording deflectional compatibility in the vertical and spanwise directions. The slip joints

shown in figure 9 provide vertical shear continuity only; no axial or moment continuity is present between adjacent beams.

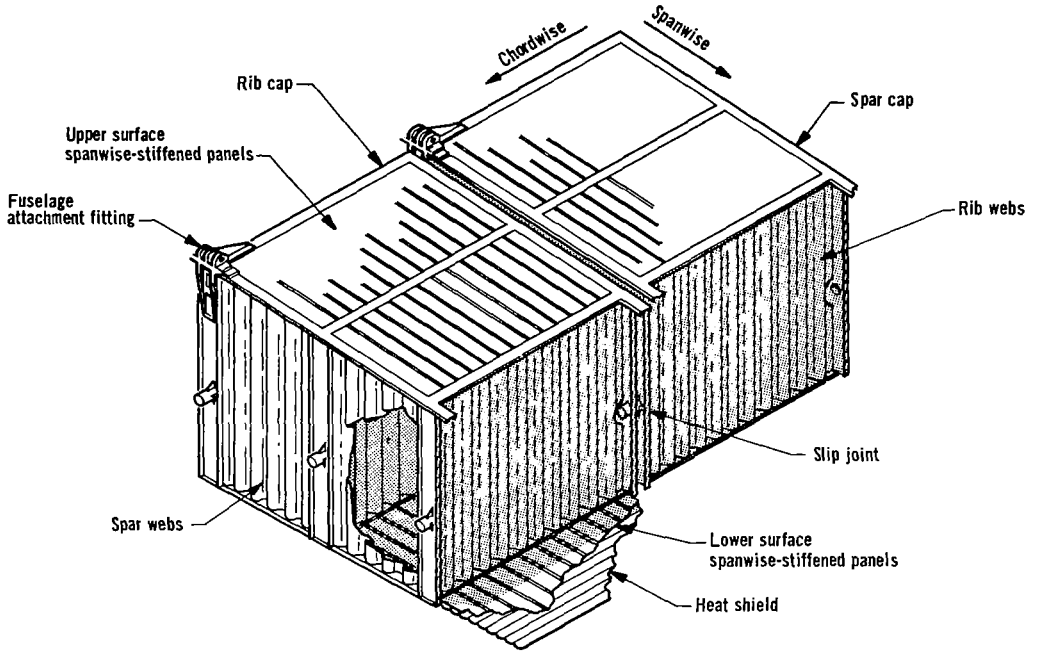

Figure 9. Statically determinate spanwise-stiffened primary-structure concept

Surface smoothness is provided by an aerodynamic fairing or heat shield; and only the forward end of each spanwise beam is attached to the fuselage. Since neither the panels nor ribs provide chordwise bending continuity and since the slip joints do not allow axial thermal strains to be transmitted in the chord direction, diminished chordwise thermal stresses can be expected from this concept. Because spanwise stiffening is employed in the statically determinate design, the spanwise primary-structure panel configuration of lowest weight was used for the statically determinate in-depth analysis.

Edge Closeouts and Cap Arrangements

Typical edge closeouts for panels and cap (flange) arrangements for ribs and spars are shown in figure 10.

Rib or spar caps (flanges) of one- and two-piece construction were considered. Melt-through weld techniques were used to join the corrugated webs to the caps. The spar or rib-web intersections consist of integrally formed web flanges plus separate angles to satisfy assembly tolerance considerations. Joining is by spotwelding and riveting.

The panel-closeout attachment sketches show the panel centroidal axis aligned with the shear plane of the attachment fastener. Exceptions are the trapezoidal corrugation in which a doubler with a zee-shear transfer member is used and the honeycomb close-out which utilizes a splice plate and channel edge member.

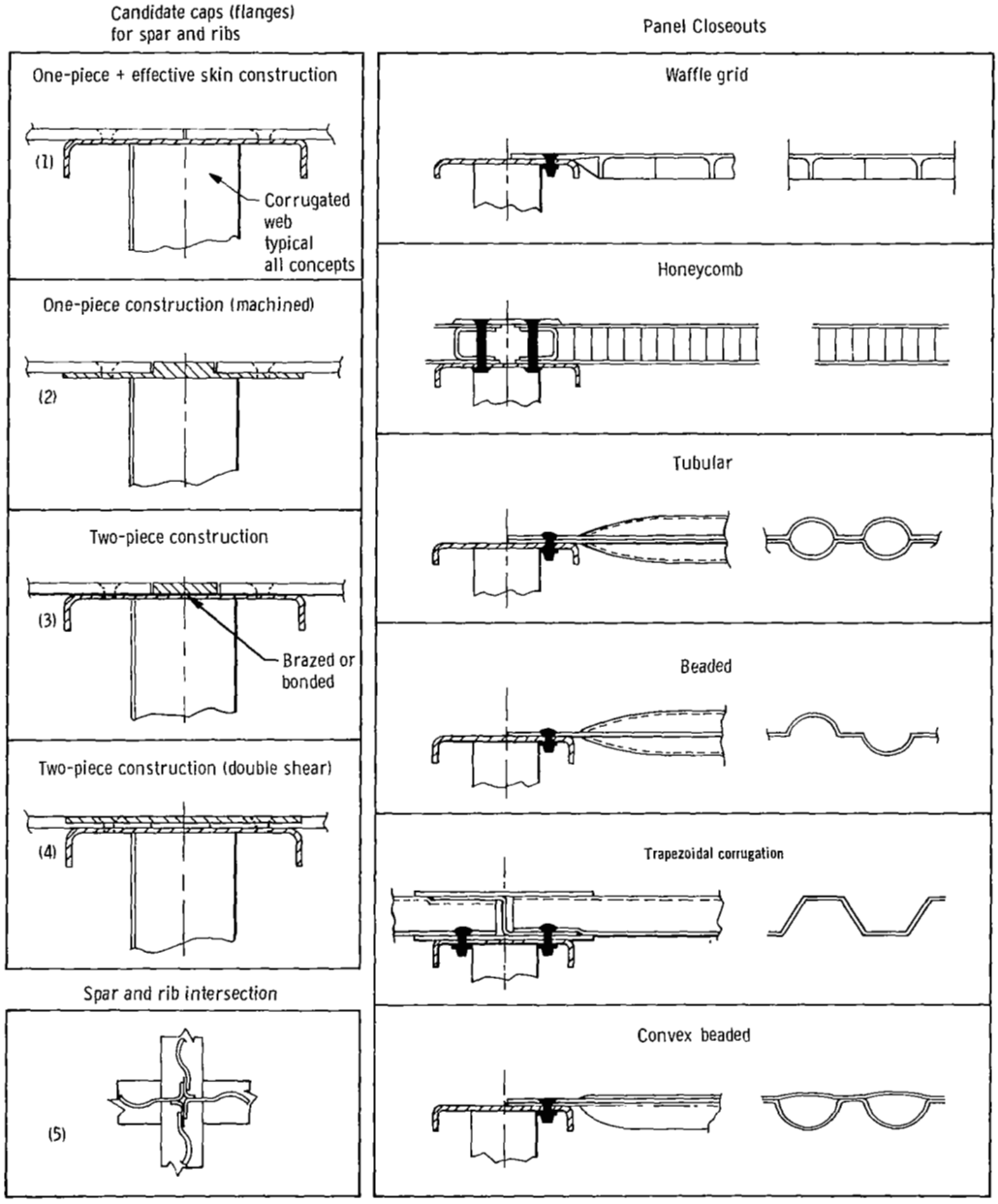

Figure 10. Attachment configurations for typical spar or rib caps and panel closeouts

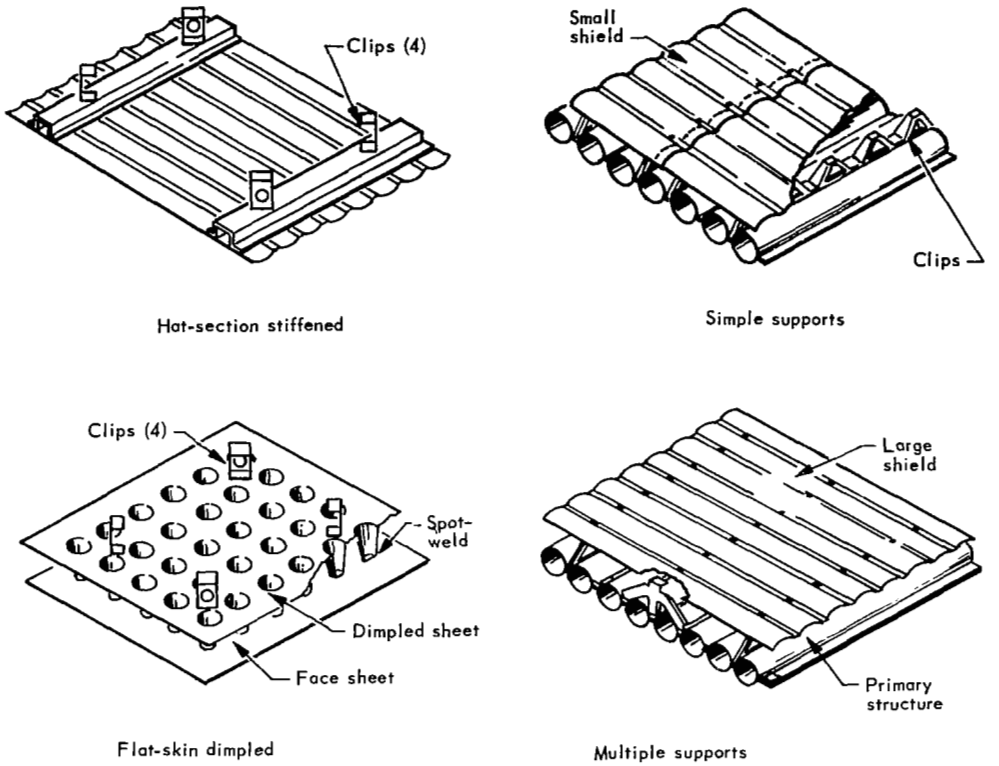

Figure 11. Refurbishable heat shields

THERMAL-PROTECTION SYSTEM

Both refurbishable and permanently attached metallic heat shields were considered for the thermal-protection system, and fibrous quartz packaged in foil was selected for the insulation.

Refurbishable Heat Shields

The refurbishable heat shields investigated were of the corrugated-skin and flat-skin dimple-stiffened designs shown in figure 11. The corrugated shields are attached to the primary structure by stiffened hat-sections or by clips (simply supported or with multiple supports). The flat-skin dimple-stiffened shields are attached by flexible standoff supports.

Permanently Attached Shields

The permanently attached shields are modular heat shields which are strips corrugated in the chordwise direction, and are either simply supported or cantilevered. The simply supported shield shown in figure 12 is resistance spotwelded to the primary

structure at the rear and interlocked forward. The cantilevered version is resistance spotwelded to the primary structure at the forward portion of the corrugated strip and overlapped at the aft portion.

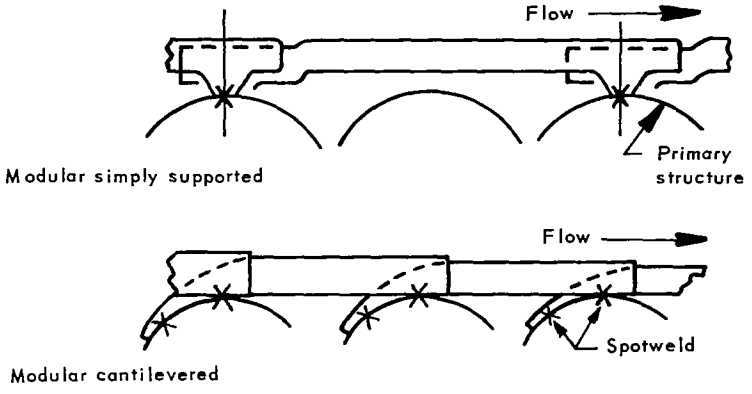

Figure 12. Permanently attached heat shields

LEADING EDGE

Both continuous and segmented leading-edge concepts were considered. In both, the chord length of the removable section was selected to assure maximum fastener temperatures of less than 2200°F, thus allowing the use of nonrefractory metal fasteners.

Continuous Leading Edge

Two design variations of the continuous leading-edge concept were considered: (1) designs which sustain thermal stresses without buckling and (2) designs in which thermal stresses are alleviated.

The first design variation consists of relatively long pieces that overlap in sealed nonslip joints. This design, as applicable to a heat shield and to monocoque structure is shown in figure 13.

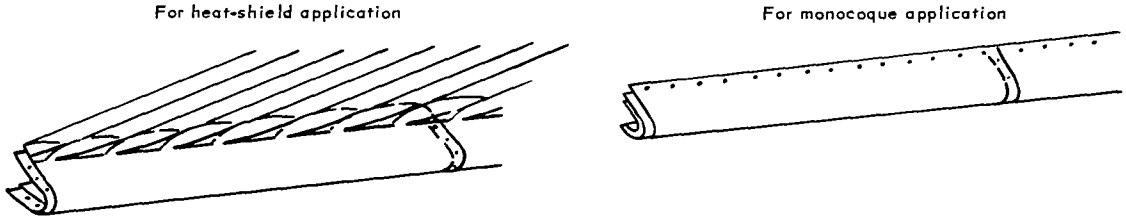

Figure 13. Continuous leading-edge concept

In the other continuous variation, thermal stresses are alleviated. Flexibility parallel to the leading edge is provided by beads oriented normal to the leading edge, as shown in figure 14.

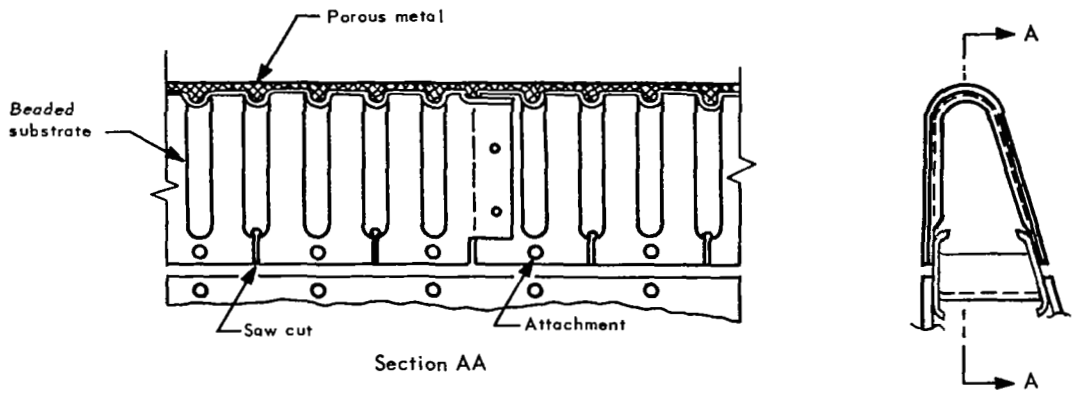

Figure 14. Porous-metal continuous leading-edge concept

A smooth exterior is provided by a layer of porous-metal which is diffusion-bonded to the beaded sheet; the porous-metal fills the cavities formed by the beads and is impregnated with an oxidation-protective material.

Segmented Leading Edge

The segmented leading-edge concept consists of short overlapping pieces with slip joints at the overlaps, as shown in figure 15. Segment lengths are optimized to prevent the buildup of thermal stresses.

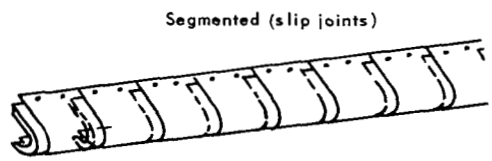

Figure 15. Segmented leading-edge concept

CONCEPT EVALUATION PROCEDURE

To provide a rational basis for evaluating the structural concepts, methods were established for applying specific factors of weight, cost, performance, and reliability, as follows:

(1) The specified vehicle configuration and structural design criteria were used to develop environmental data consisting of trajectory, loads, and aerodynamic heating. These data were then used in evaluating leading-candidate superalloy and refractory-metal materials and in establishing parameters for conducting critical material tests.

(2) The promising panel concepts for monocoque, semimonocoque, and statically determinate structures were screened in terms of weight on the basis of compressive inplane loading for a selected panel size.

(3) A more detailed weight evaluation was conducted on the structure concepts found to be the more promising as a result of the screening. This evaluation, extending to panels, substructure, insulation, and heat shields, was made on the basis of compressive inplane and pressure loads. These weights provided an intermediate screening of primary structures. Six concepts were selected for in-depth analysis.

(4) One heat-shield and one leading-edge concept was selected from several that had been evaluated in terms of the four evaluation factors.

(5) Final evaluation of the six different primary structures, using the selected heat shield and leading edge, was made on the basis of weight, cost, performance, and reliability. The optimized weights were determined on the basis of multiple modes of failure from compression, bending, and shear loads.

(6) Results of these analyses were then used in an interaction evaluation, in which total-system cost (including initial investment cost of the vehicle and direct and indirect operating costs) was used as the basis for evaluation. In this final phase of the investigation, vehicle data derived from using each of the wing structures (as extrapolated from the wing-section analysis to the baseline-vehicle wing) was made to vary as a function of wing size by scaling equations. All six final structures were evaluated in terms of a constant range of 4600 statute miles, a fleet size of 200 baseline vehicles, 550 000-lb gross takeoff weight, 55 000-lb payload, and 10 000-hr life (8110 missions) over 10 years.

These procedures are described under the headings of environment, materials, weight, cost, performance, reliability, and rating-factor interaction.

ENVIRONMENT

The flight-trajectory characteristics of the vehicle were determined from the aerodynamic data (ref. 6) by using the mission-analysis procedure described in reference (7). Net vehicle loads, based on the vehicle configuration and trajectory, were determined in a general sense for the entire airframe. Aerodynamic loadings over the vehicle at the design condition at Mach 8 (-0.5-g, +2.0-g, and cruise condition) were determined on the basis of oblique shock and Prandtl-Meyer expansion relationships (ref. 8). Newtonian impact theory was used for estimating the loadings on the nose of the vehicle (ref. 9).

Boundary-layer and engine-noise levels were considered in establishing acoustic (sonic) fatigue effects (refs. 10 and 11). A fatigue spectrum was established for the specified maneuver perturbation occurring every tenth flight for the 10 000-hr vehicle life (ref. 12).

Accurate predictions of aerodynamic heating and resulting temperatures were determined for materials selection, structural design, and insulation requirements. Theoretical and empirical methods (refs. 13 through 28) were employed to predict aerodynamic-heating rates, and prediction techniques required for structural-temperature determination were based on transient structural-heating analyses (ref. 18).

MATERIALS

From the temperature data, leading candidate materials were evaluated and material-screening tests were performed. Design allowables were evaluated for structural use by parametric analysis, based on published data and concurrent tests (basic material properties, joining, and formability).

Superalloys (nickel and cobalt base) were considered for wing primary structures. Dispersion-strengthened alloys, as well as the nickel- and cobalt-base superalloys, were considered for heat shields. For leading-edge requirements, dispersion-strengthened materials and alloys of columbium and tantalum were evaluated. Fibrous quartz materials were considered for the lower surface thermal insulation.

WEIGHT

Weights for the primary structure, the thermal-protection system (heat shields and insulation), and the leading edges, were determined in detail for the 550 000-lb baseline vehicle by the methods discussed in the following section. Weights for vehicles of other sizes were obtained by appropriate scaling relationships.

Initial Screening

Initial panel weights were determined from preliminary loads and radiation-equilibrium temperatures for a selected rib and spar spacing. Superalloy materials were investigated for several candidate monocoque and semimonocoque constructions. The nonoptimum panel factors were calculated on the basis of varying the geometry of the closeout to align the fastener shear force with the neutral axis of the panel. The goals of the initial panel screening were to eliminate the less promising constructions, to develop data for use in calculating internal redundant-model loads, and to guide the selection of the material (allowables and manufacturing) and panel tests, and to enable material selection.

The redundant-analysis procedure used to determine internal loads was a computerized structural-analysis solution based on the matrix force method (ref. 29). Optimization procedures (refs. 30 and 5), applied to inplane loading conditions, were used for evaluating the various structural wing-panel configurations.

During the initial screening, panel-element tests were initiated for seven compression columns (30 in. long by 17 in. wide), eight compression crippling panels, one cap-beam crippling panel, two cap-web shear panels, and three panel-end closeouts. The tests were conducted at room temperature and at 1400°F for the evaluation of end-closure designs; joining methods; combined effects of temperature and load; and substantiation of element and panel shear, crippling, and column buckling stresses. Results of these tests were used to refine the methods of analysis and concept design for determining weight.

Intermediate Screening

In a more detailed monocoque and semimonocoque intermediate screening, normal as well as inplane loadings for total wing cross-section optimization were considered as rib and spar spacings were varied. To determine internal loads, a redundant-loads analysis was performed using the stiffness results of the initial screening. Calculated weights included those for the primary structure, typical heat shields, spars and ribs, and panel closeouts. In addition to eliminating certain configurations, the intermediate screening provided the necessary structural data for determining the final redundant-model inputs.

Final Structural Analysis

The final structural analysis of each of the structural concepts remaining after intermediate screening generally consisted of the following steps:

(1) External surface temperature distributions were calculated for the three flight conditions (-0.5-g, +2.0-g, and cruise) assuming radiation-equilibrium conditions. In addition to these temperatures, a transient thermal analysis was performed for several thermal-protection arrangements.

(2) A redundant-force analysis for one thermal-protection arrangement was performed, using the stiffnesses derived from the intermediate screening and

temperature distributions determined in step (1). Additional iterations as required were performed until reasonable convergence was attained between the stiffness input and those obtained from the final panel proportions, step (7).

(3) A plane-strain analysis of the vehicle cross-section yielded chordwise thermal strains for each thermal-protection arrangement investigated.

(4) The results of the plane-strain analysis that correspond to the thermal-protection arrangement of the redundant-force analysis were compared with the results of the redundant-force analysis. The ratio of the thermal strain was applied to the chordwise thermal strain of the other thermal-protection arrangements. The resulting chordwise thermal strains and chordwise airloads obtained from the redundant-force analysis resulted in a set of airloads and thermal strains for each of the thermal-protection arrangements.

(5) Spanwise thermal loads were those of the one redundant-force analysis adjusted by the ratio of the plane-strain chordwise thermal loads (strains) for the particular thermal-protection arrangement to the chordwise thermal loads (strains) of the one redundant-force analysis.

(6) The spanwise airloads were those of the redundant-force analysis which were added to the adjusted spanwise thermal loads to obtain spanwise airloads and thermal strains for each thermal-protection arrangement.

(7) Panel proportions and rib and spar spacing were then optimized for each thermal-protection arrangement. In addition to the inplane loads (expressed as airloads and thermal strains) and normal pressure, this optimization included eccentric edge loading, initial deflection due to manufacturing, and bowing to a temperature gradient through the panel thickness.

In all phases of structural sizing, plastic deformation was taken into account with the use of the Ramberg-Osgood stress-strain relationship and the octahedral shear-stress theory. Postbuckling strength was not considered. Provisions for side constraints (for example, minimum thicknesses) were included. In addition, the amount of plastic deformation was restricted by imposing a lower limit on the ratio of tangent-modulus to elastic-modulus.

Panel- and vehicle-flutter analysis. – Panel-flutter analyses of the wing surface panels were conducted to assure that the structure remains stable throughout the entire flight trajectory. The method of Bohon and Anderson (ref. 31), which takes into account the influence of spring-supported edges on the critical flutter dynamic pressure, was employed. By using the analysis procedure of reference 32, vehicle-flutter analyses were then performed.

Sonic-fatigue analysis. – Sonic-fatigue analyses were conducted to determine the effects of random sound pressure on the wing structures by the analytical and empirical approaches of references 33 through 38.

Structural-fatigue analysis. – Fatigue analyses were conducted to establish allowable design stresses, based on the spectra of anticipated loadings and environmental conditions for the design life of each primary structure (ref. 39).

Creep analysis. – Creep analyses of the final structures were conducted to establish margins of safety. The allowable compressive stresses under creep conditions were approximated by using isochronous stress-strain curves. The creep allowable stresses were based on the average temperature during cruise and the total time at cruise for a vehicle life of 10 000 hr.

The final concept weights were obtained from the final-sized primary-structure panels, spars and ribs (webs and caps), closeouts and fasteners, heat shields, insulation and material depth-of-attack effects due to oxidation for the 10 000-hr vehicle life.

The final weight comparison of all structural concepts was made in terms of lb/ft^2 for the center area (centerline of vehicle to intersection of wing and fuselage), inboard area (intersection of wing and fuselage to wing one-third chordline), outboard area (one-third chordline to wing leading edge), and average weight of the selected wing section. These areas are referred to as A, B, and C, respectively, hereafter.

Total wing weights for the baseline 550 000-lb vehicle were obtained by establishing mass scaling relationships for each concept. The scaling was accomplished by using the internal loads data from the redundant analyses to calculate detail weights required to transmit these loads at acceptable stress levels. The stress levels were determined through detailed analysis of rib and spar caps and webs at selected areas of the wing. Panel requirements were determined through comparison with areas of similar loading and temperature.

Heat-Shield Weights

A weight analysis of several materials for a selected heat shield and load yielded data that enabled material selection as a function of temperature to be carried out. The candidate heat-shield concepts, described in the structural concepts section, were then analyzed on the basis of shielding a spanwise tubular structure with the best material for most shields. Weight determination was based on the predicted temperatures, three candidate materials, and lateral pressure loadings. Analyses of heat shields of various sizes included deflection considerations and minimum gages. In this minimum-weight approach, heat-shield aspect ratio and width based on a multiple of the overall primary load-carrying panel dimensions were considered, using the specified 0.5 psi positive and negative pressure heat-shield loading. In addition, bending due to nonuniform thermal deflection of supports and forced deflection due to bowing of stiffened structural panels under loading were considered. In the analysis of the minimum-weight configurations and candidate materials, the closed-form method of optimization (ref. 5) was used. Flow disturbance, local heating, panel flutter including flexibility of the primary structure, sonic fatigue, reliability, and cost were factors used to select a heat shield to be adapted to each final primary structure.

The selected heat shield was weight-optimized for each primary structural concept as a function of panel size, insulation placement, loads, and temperatures. Material oxidation weights were also determined.

Leading-Edge Weights

Material selection was the first objective of the leading-edge investigation. The candidate leading-edge structural arrangements and proposed materials were subjected to temperature and load/strength analyses, analyses of thermal strains, local buckling, and reusability requirements (refurbishment), in which depth of oxide penetration, coating life, insulation placement, and low-cycle fatigue (refs. 40 and 41) were considered. Performance and heating penalties due to leading-edge distortion are evaluated along with attachment considerations. A selection of the lowest-weight leading-edge based on the desired life requirements without refurbishment (cost) was made.

The selected leading edge was adapted to each structural design concept on a lowest-weight basis. The leading-edge load boundary conditions were established by using the redundant-analysis results of the primary structures.

COST

All costs (expressed in 1968 dollars) were developed for comparison purposes only, using current labor rates and material prices. Facilities and process-development costs were not included. It is assumed that cleanroom conditions are available for the fabrication of vehicle components, that suitable controlled-atmosphere furnaces and process baths have been installed, and that required special equipment and machine tools have been developed and installed.

Detail costing of the primary-structure concepts for the selected wing investigation area was accomplished through consideration of the total wing cross-section, consisting of surface panels, heat shields, ribs and spars (webs and caps), and panel closeouts. Costs for each of the concepts, which were premised upon structural-element interfaces from the design drawings, involved consideration of labor, material, and tooling requirements. Detail designs were developed for each of the component and substructure joints to assure realistic cost estimates. Labor costs were developed from an outline of the required manufacturing operations and an appropriate labor rate. Material costs were computed from an estimate of the net weight of each component and extended by material cost requirements. Tooling costs were obtained by applying tooling cost rates to the anticipated tooling. Cumulative cost estimates per unit for 100 vehicles were obtained.

Total wing costs were obtained for the baseline 550 000-lb vehicle. Based on the detailed wing-section costs, cost-estimation relationships (CERs) were developed for the wing areas: A (under the fuselage), B (outboard of the fuselage but inboard of the wing one-third chordline), and C (outboard of the one-third chordline in the upper wing surface). To develop CERs for the total wing, the wing-section costs indicated above were factored to account for other sheetmetal parts and machined parts required at interfaces between manufacturing segments of the vehicle. These CERs were used in developing total wing costs for each structural concept.

PERFORMANCE

To determine effects of the various concepts on performance, methods and parametric design data were established for evaluating performance degradation (aerodynamic drag losses) due to surface roughness and wing distortion (refs. 42 through 48). In terms of fuel increment, performance degradation was investigated for the following types of roughness and distortion of the wing:

(1) Uniformly distributed or equivalent sand-grain roughness

(2) Sheetmetal joints and fasteners

(3) Two-dimensional surface waviness, in which the wave crests are perpendicular to the wing chord

(4) Three-dimensional surface bumps or depressions

(5) Surface corrugations parallel to the wing chord

(6) Deformation of the primary wing structure

The incremental drag changes resulting from the six types of roughness and distortion represent the drag difference between a rough distorted wing and an ideally smooth undistorted wing. The wing of the nominal vehicle was specified to have an amount of roughness and distortion that would produce a drag increase equal to 10 percent of the smooth-wing friction drag. Therefore, the fuel penalty used in the concepts-evaluation procedure is the difference between the fuel increment determined for the candidate wing concept and the fuel increment resulting from the roughness and distortion specified for the nominal wing of the baseline vehicle.

RELIABILITY

The basic approach in the reliability evaluation was to establish a consistent standard that was adequate for measurement of mission performance over the vehicle lifespan. However, insufficient data exist on which to base a statistical numerical probability analysis. Therefore, the key factors affecting the relative reliability (sensitivity) of the structural concepts, as measured by weight, were evaluated. These key factors, involving factors of safety, creep, fatigue, and maintainability, were used for low, nominal, and high levels of structural reliability of -0.5-g, +2.0-g, and cruise conditions, as shown in table 1. It was assumed that an increase in factor of safety is an increase in reliability and that at a given level of factor of safety each different structural concept has the same reliability.

The reliability factor of maintainability (or repairability) was assessed by evaluating refurbishment requirements of leading edges and heat shields. For example, weight due to oxidation penetration to satisfy life requirements was included. Accessibility for interior wing inspection and repair was satisfied by using mechanical fasteners on the wing panels.

The final reliability results were compared for all structural concepts as a function of factor of safety. While absolute definition cannot be made as to what reliability any one of the levels is for any type of structure or what reliability the three levels represent, weight sensitivity to the factor-of-safety change is the index of comparison of the adaptability of the various concepts to meet a given structural reliability level. Therefore, the basis of the final comparison was minimum weight at a particular level of reliability.

TABLE 1. – SUMMARY OF RELIABILITY PARAMETERS

-0.5-g and +2.0-g load conditions (applied to operating limit loads)			Life criteria for primary structure (fatigue and creep allowables)		
Reliability level	Ultimate load factor	Ultimate thermal strain factor	Reliability level	Fatigue[a] scatter factor	Creep[b] scatter factor
Low	1.5	1.1	Low	1.0	1.0
Nominal	2.0	1.3	Nominal	1.5	1.5
High	2.5	1.5	High	2.0	2.0

[a]Applied to fatigue spectra.

[b]Cruise limit loads; 0.5-percent total creep tensile strain; creep buckling based on isochronous stress-strain curves.

RATING-FACTOR INTERACTION

A rating-factor interaction evaluation was conducted by interrelating the total wing factors of weight, cost, performance, and reliability to a total-vehicle-system cost for each wing structural concept.

Interaction Procedure

A common denominator, minimum total-system-cost, was selected as the basis for evaluating and comparing the wing-structure concepts. The baseline mission range requirement of 4600 statute miles and a fleet size of 200 vehicles (550 000 lb each) with a payload of 55 000 lb satisfying 10 000 hr of life (8110 missions) for 10 years resulted in a fleet payload-range requirement of 205 billion ton-miles (statute) for each concept.

The total wing weights and costs for the three levels of reliability and fuel mass fractions associated with roughness drag performance (resulting in payload changes for the wing structural concept of the baseline 550 000-lb vehicle) were submitted for integration into a whole vehicle system. Except for the statically determinate concept, which requires additional fuselage weight, identical weight and cost scaling relationships were used for the remaining portion of the vehicle. The vehicle integration was simulated by an analytical vehicle weight-cost sizing evaluation model.

Vehicle Weight-Cost Sizing Method

A vehicle weight-sizing analysis procedure (ref. 49) was coupled with a cruise-transport economics model. Basic input data included weight and volume coefficients, propulsion-system data, specific geometrical characteristics, and cost coefficients.

For the vehicle weight-sizing analysis, the vehicle gross weight W, reference wing area S_{REF}, and total fuel weight to vehicle gross weight (fuel fraction) were used. The vehicle configuration was assumed to be geometrically similar and to have a constant takeoff wing loading for all sizes of vehicles.

Vehicle procurement costs were established through using the economics model of reference 50 and an economics subroutine employing supersonic-transport-cost model techniques to determine the direct and indirect operating costs.

The established baseline-vehicle cumulative cost estimates per unit for 100 vehicles was used. The labor cost was then factored along a learning curve to obtain labor costs for any required number of aircraft. Material costs were similarly factored along a learning curve. (A learning curve is an expression of the rate at which production cost per unit decreases as the number of units produced increases.) The learning curves cited here are based on airframe industry standards (ref. 51). Total tooling costs were amortized over the appropriate production quantity. A summation of airframe manufacturing labor and material, avionic, and propulsion costs provided total vehicle costs for the established production quantity. One-time investment costs, including spares, facilities, and production tooling required to bring the system to operational status were then added to obtain the initial investment cost for the established number of operational vehicles.

All of the aforementioned constraints as well as boundary limits for the payload were input into the weight-scaling synthesis model loop, in which wing reference area is the primary scaling parameter. As the vehicle gross weight parameter varied, variations in fuel requirements to perform the 4600-mile mission resulted in payload capability variations. Once the weight and sizing conditions were satisfied for the basic mission requirements, the data were input into the economics model, in which each element cost was varied linearly with vehicle weight change. Then, the vehicle procurement (including anticipated spares), direct operating cost, indirect operating cost, and total system cost were computed in detail for the specified mission. Because of structural efficiency variations between the wing concepts, the output provided variable fleet sizes and vehicle gross weights to satisfy the 205 billion ton-mile (statute) fleet payload-range requirement, as well as total system cost.

EVALUATION RESULTS

Environmental data were developed for use in material selection for the hypersonic-vehicle structures and thermal-protection systems. Evaluation results are reported in terms of weight, cost, performance, and reliability. The interactions of these factors are then determined to find the ranking of the primary structure, heat shields, and leading-edge designs based on the minimum total-system-cost.

ENVIRONMENTAL ANALYSES

Trajectory Analysis

The trajectory analysis, based on the cruise mission and maneuver perturbation, yielded the data shown in figure 16 for dynamic pressure, angle of attack, altitude, and Mach number.

The thrust and drag schedule was for a power-on descent from end of cruise (q = 470 psf), following a varying dynamic-pressure path to an altitude of 40 000 feet. Drag augmentation was provided to effect a constant deceleration of 0.20g.

The basic trajectory duration of 1.23 hr extends to 1.25 hr when the maneuver perturbation is included. For both, a criterion of 8110 flights per 10 000 hr of life was established. This amounts to 8978.4 hr for the former and 1013.75 hr for the latter. The maneuver perturbation requires only 16 hr of the 10 000-hr vehicle life, while the cruise condition requires 4460 hr. The ascent requires 2840 hr and the descent 2684 hr.

Aerodynamic-Heating Analysis

In calculating the vehicle external-surface temperature distributions, radiation-equilibrium conditions were assumed. Radiation heat transfer from lower surfaces to space, from lower surface to upper surface, and from upper surface to space was considered.

Initial temperature distributions resulting from the radiation-equilibrium analysis are shown in figures 17, 18, and 19 for the -0.5-g, +2.0-g, and cruise conditions.

The trajectory perturbations at the end of climb cause large changes in the peak heating rates of the upper surface (-0.5-g condition) and on the lower surface (+2.0-g condition). Temperatures for the transient +2.0-g condition average 400°F higher than for the cruise condition. For the -0.5-g condition, upper wing-surface temperatures are higher than lower surface temperatures, because of the negative 2.2-deg angle-of-attack relative to the wing reference line. However, expansion of the flow over the upper surface results in decreasing temperatures, so at the aft portion of the wing, upper and lower surface temperatures are almost identical. The effect of radiation heat transfer between the wing surfaces may be seen in the unusual temperature patterns on the lower wing surface, which reflect the different temperature levels on the various sloped portions of the upper surface.

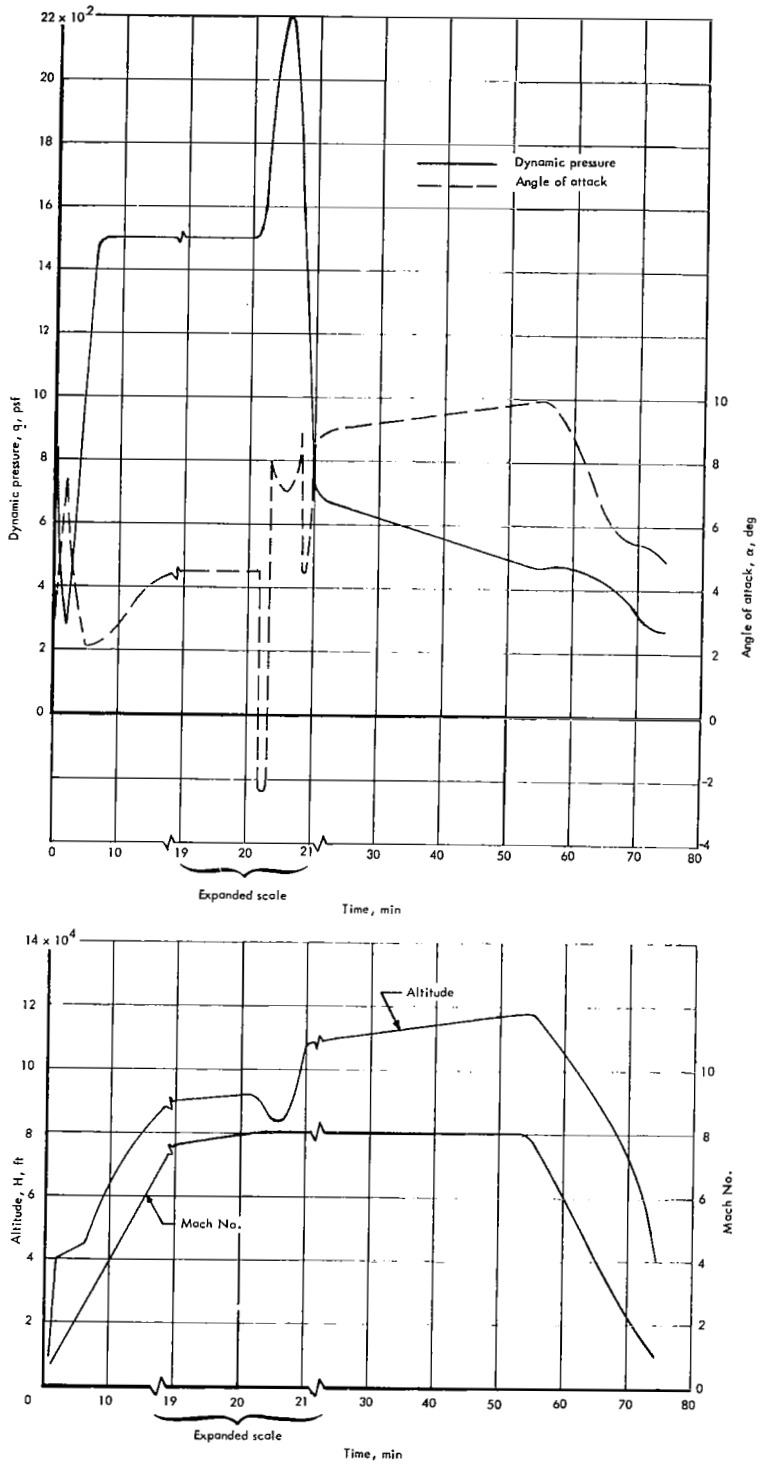

Figure 16. Trajectory plus maneuver perturbation

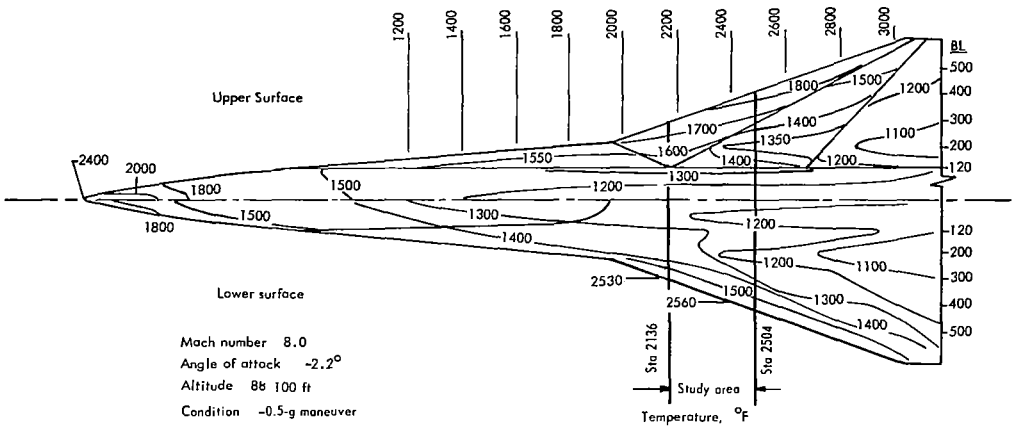

Figure 17. Temperature distribution for the −0.5-g maneuver

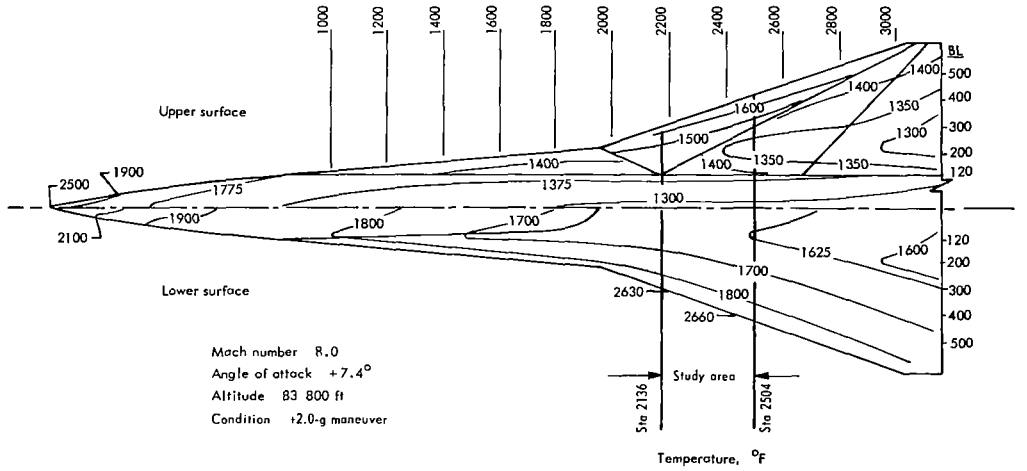

Figure 18. Temperature distribution for the +2.0-g maneuver

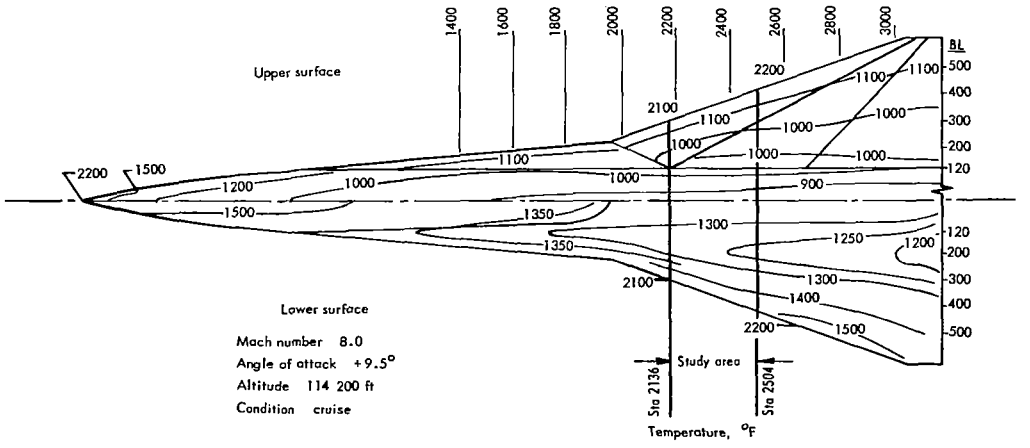

Figure 19. Temperature distribution for cruise condition

Vehicle Loads Analysis

Unit load distributions were established to represent aerodynamic, inertial, elevon, and thrust loadings. In addition, normal and axial balance were determined with the resultant thrust vector running approximately through the vehicle center-of-gravity. Balanced loadings were distributed to provide a loading function for determination of the elastic load distributions which inherently determine vehicle balance.

Rigid load analyses were conducted for the -0.5-g, +2.0-g, and cruise conditions. Also, aeroelastic analyses were conducted for both the positive maneuver (+2.0-g) and cruise conditions. It was found that the lower loadings experienced during the negative maneuver condition (-0.5-g) are not significantly changed by flexibility effects.

Evaluation of the elastic load distribution indicated that the magnitude of the loads at the wing study area does not vary significantly from the rigid load values. The effect of elasticity is to deflect the trailing edge aft of station 2580 upward, thus inducing a negative angle-of-attack on the affected panels. The attendant incremental negative loading necessitates additional trailing-edge down-elevon deflection (positive load) for trim. Significant changes in loading resulting from elastic effects were noted in the area of trailing-edge and tip region as well as the nose. Net loads in the tip area decrease the local angle-of-attack, but this loss in lift is made up for by the additional elevon deflection required for trim, which further increases trailing-edge deflection.

Pressure loadings over the wing-study-area panel points were defined, as shown in table 2. The pressures are average values for the panel sizes shown. Pressure loadings for the vehicle lower and upper surfaces are shown in table 3.

The limit wing differential pressures used for the structural analysis of the various concepts are shown in table 4. The design pressures include heat shield and panel pressures on the upper and lower wing surfaces, based on aerodynamic and transient venting pressures.

Fatigue-load analysis. – A fatigue spectrum established for determining cyclic loadings included the specified maneuver perturbation that occurs every tenth flight. Figure 20 shows the design fatigue spectra for ascent, cruise, and descent flights. The ground-handling (taxi) cycle was included to permit definition of forces on the vehicle throughout the ground-air-ground cycle.

Boundary-layer and engine-noise level loads. – Estimated overall sound-pressure levels from boundary-layer noise are shown in the two upper curves of figure 21. The two lower curves also show the octave band sound-pressure levels for the hypersonic wing panels which fall in the panel natural frequency octave band level of 37.5 to 150 Hz. For each set of curves, the decibel levels are based on the criterion that the root-mean-square pressure is proportional to the dynamic pressure q times a constant. The upper wing surface and the lower wing inboard surface are turbulent and subject to 0.7 percent of q, while the lower surface from the leading edge to 3 ft inboard is in a transition area from laminar to turbulent flow and is subject to the 2.2 percent of q criterion during the cruise portion of the flight.

TABLE 2. – PRESSURE LOADINGS FOR WING INVESTIGATION SECTION

Panel number	Limit pressure loading, psi					
	-0.5-g		+2.0-g		1.0-g	
	Upper surface	Lower surface	Upper surface	Lower surface	Upper surface	Lower surface
1–4	0.1623	0.0320	0.0929	0.4692	0.0454	0.2300
5	0.1892	0.0172	0.0500	0.5492	0.0245	0.2685
6–8	0.1461	0.0124	0.0359	0.9615	0.0175	0.4692
9	0.1892	0.0172	0.0500	0.5492	0.0245	0.2685
10–12	0.1461	0.0124	0.0359	0.9615	0.0175	0.4692
13–22	0.1646	0.0368	0.1065	0.4754	0.0521	0.2331

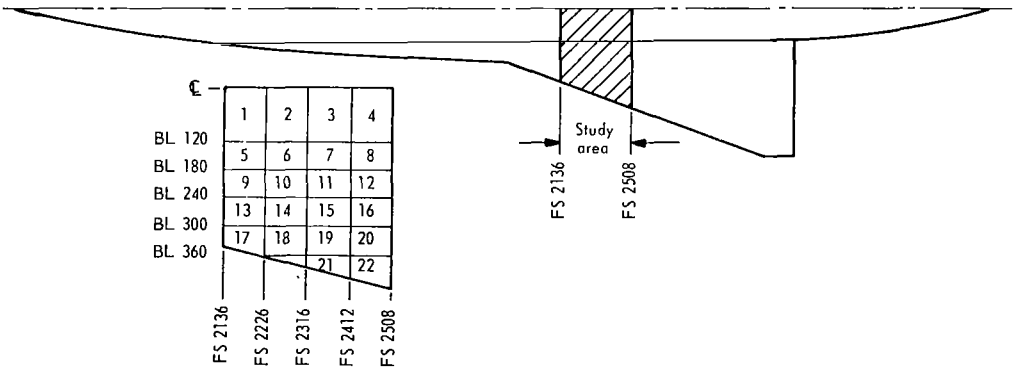

TABLE 3. – PRESSURE LOADINGS FOR ENTIRE WING

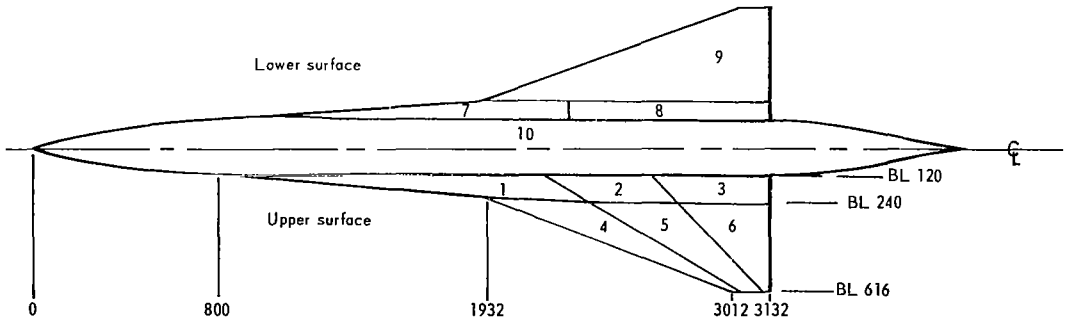

Wing area	Limit pressure loading[a], psi		
	Design condition		
	-0.5-g	-2.0-g	-1.0-g
1	0.1892	0.0500	0.0245
2	0.1461	0.0359	0.0175
3	0.0549	0.0097	0.0038
4	0.1646	0.1065	0.0521
5	0.1243	0.0358	0.0168
6	0.0463	0.0096	0.0037
7	0.0172	0.5492	0.2685
8	0.0124	0.9615	0.4692
9	0.0368	0.4754	0.2331
10	0.0320	0.4692	0.2300

[a]Ramp pressure not included.

TABLE 4. – WING DESIGN PRESSURE

Location \ Condition	Limit pressure Δp, psi [a, b, c]								
	BL 0-120			BL 120-212			BL 212-350		
	-0.5-g	+2.0-g	Cruise	-0.5-g	+2.0-g	Cruise	-0.5-g	+2.0-g	Cruise
Lower surface structural panels	-0.53	-0.97	-0.73	-0.51	-1.46	-0.97	-0.54	-0.98	-0.73
All heat shields & upper surface panels	±0.50								

[a]For ultimate design pressures, multiply (1.3) (1.5) by limit pressures shown.
[b]Negative values indicate inward-acting pressures;positive values indicate outward-acting pressures.
[c]Sta. 2274-2366.

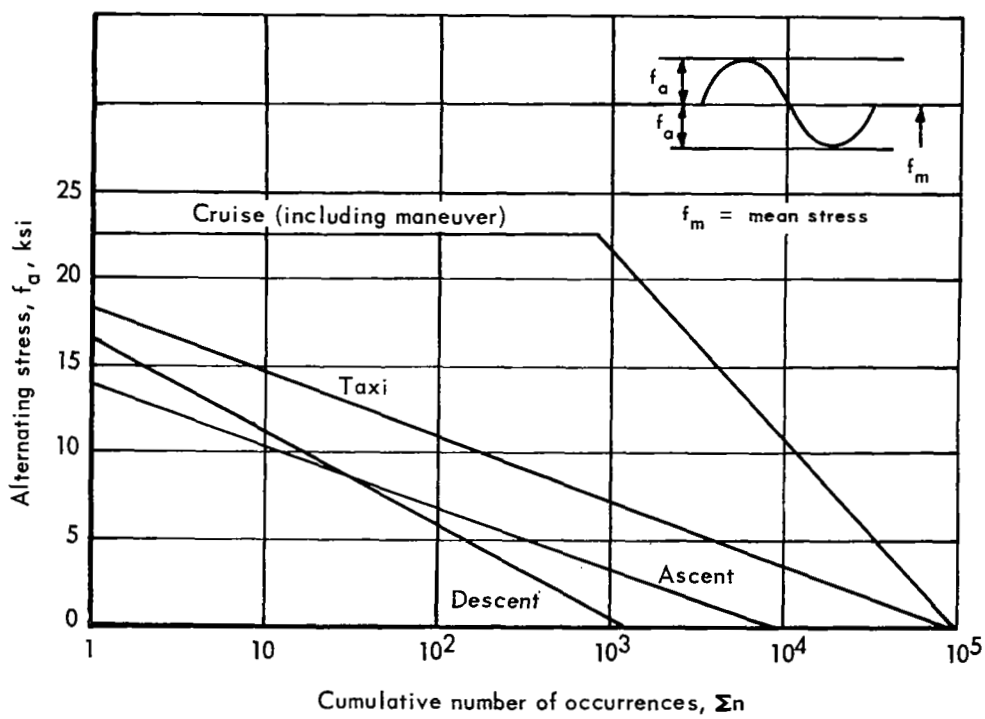

Figure 20. Fatigue spectra for wing-structure life determination

Sound-pressure levels from engine noise were determined, using the thrust and flow relationships for the type of turbojet engine required for the vehicle. The engine-noise levels were found to be less critical than the noise levels from boundary-layer considerations in the local wing area of the investigation.

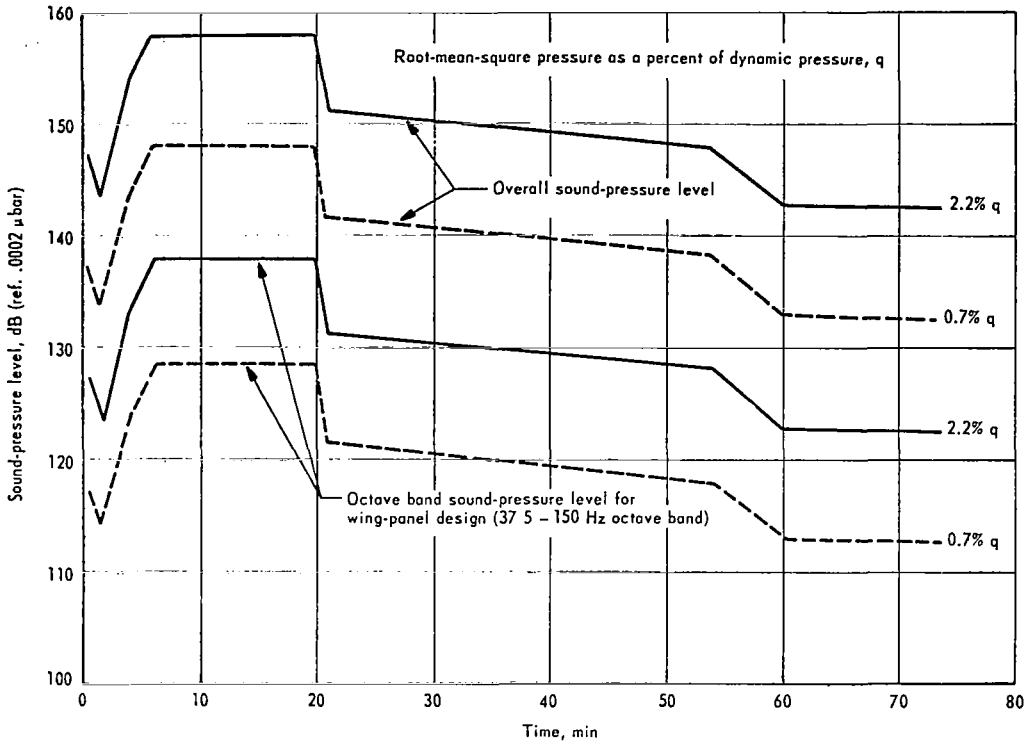

Figure 21. Variation of boundary-layer noise during design trajectory

MATERIALS ANALYSES

The materials listed below were evaluated parametrically for wing-structure application based on established property data and additional screening tests.

Leading candidates	Density, lb/in^3	Application
René 41	0.298	Primary structure
Haynes 25	0.330	
René 41	0.298	Heat shields
Haynes 25	0.330	
TD NiCr	0.306	
Ta-10W	0.608	Leading edge
Cb-752	0.326	
TD NiCr	0.306	

Parametric Analysis

Merit indexes relating materials to various design parameters provide an efficient index for comparison. Figures 22 and 23 show density-compensated ultimate tensile and compressive-yield stresses versus temperature for the leading candidate materials. The allowable stresses divided by the density ρ show advantages for Rene 41 in the temperature ranges (1200° to 1600°F) of the major portion of the wing structure.

The compressive buckling weight index, $\frac{\rho}{\overline{\eta}(E_c)^{1/2}}$, is plotted in figure 24 versus the applied compressive stress f_c for temperatures of 1200°, 1300°, and 1400°F. The index $\frac{\rho}{\overline{\eta}(E_c)^{1/2}}$ is an expression of a material's structural stability characteristic in relation to weight (ref. 2). The terms of the expression are: ρ is density, E_c is compression modulus, and $\overline{\eta}$ is the plasticity correction factor.

The curves of figure 24 indicate that a prohibitively large weight increase due to plasticity occurs for Haynes 25 if the working stress is increased beyond 20 000 psi for the temperature range of 1200° to 1400°F. However, Rene 41 can be used at stresses around 100 000 psi before plasticity begins to have a significant effect. Thus, for a given compressive load, the higher permissible stress for the Rene 41 results in panels that weigh considerably less than Haynes 25, provided minimum gage does not constrain the results.

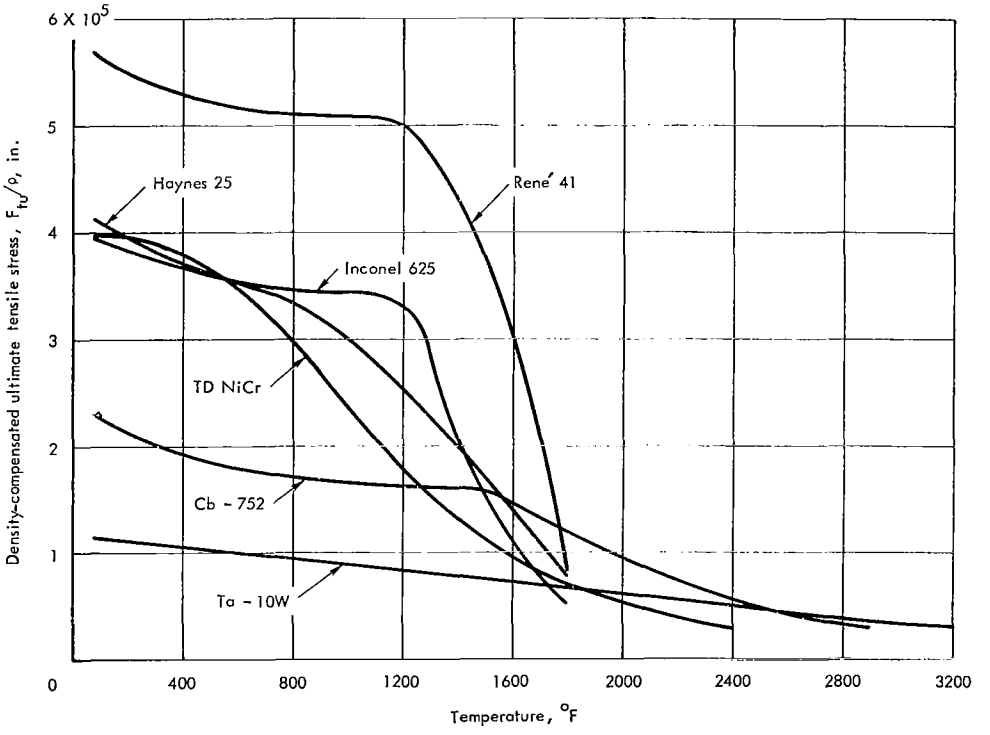

Figure 22. Density compensated ultimate tensile stress vs temperature of candidate high-temperature materials

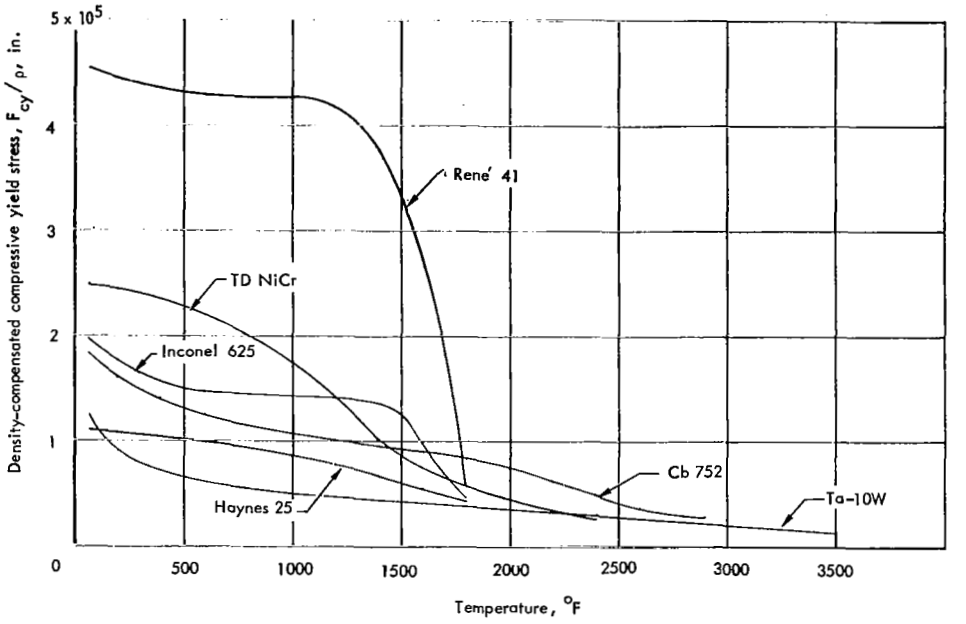

Figure 23. Density compensated compressive yield stress vs temperature of candidate high-temperature materials

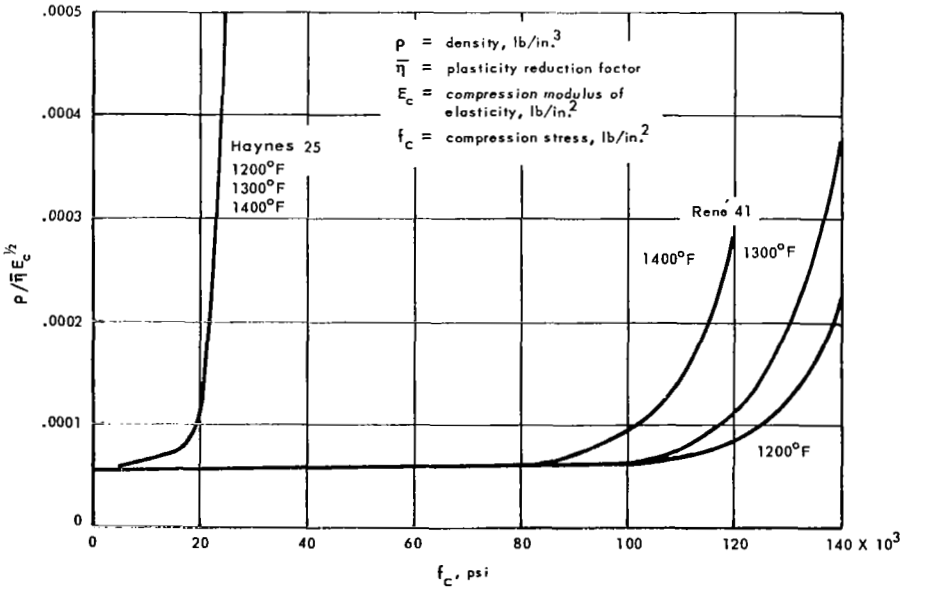

Figure 24. Compression stress vs weight index for Rene' 41 and Haynes 25

Other factors considered (see ref. 5) included fabricatability, physical properties (α, K, C_p, and emissivity), creep, fatigue, minimum gages, oxidation characteristics, and metallurgical stability. As an example of elevated-temperature considerations, figure 25 shows René 41 constant-life fatigue diagrams at 1400°F for various stress levels. Variations of mechanical properties of René 41 from room temperature to 1600°F are shown in table 5 for both A and B probability values (ref. 52).

A typical isochronous stress-strain diagram used for creep analysis is shown in figure 26. The temperature environment is 1300°F for the René 41 sheet material in the 1400°F aged condition. The 4460 hr corresponds to the cruise condition, at the low level of reliability; the other two curves correspond to nominal and high reliability levels. F_{cy} (0.2 percent strain) and the 0.5 percent strain for tensile creep are indicated on figure 26.

Materials Testing

Material-screening tests were performed in conjunction with parametric analysis. Existing data, supplemented by data generated under this test investigations, provided the design allowables used in the structural analysis.

Material property tests. – Oxidation and thermal stability, tensile property, emittance, and metallurgical examination tests were conducted for René 41, Haynes 25, and TD NiCr during the materials screening (176 tests). Emittance tests were also conducted for the Cb-752 and Ta-10W alloys.

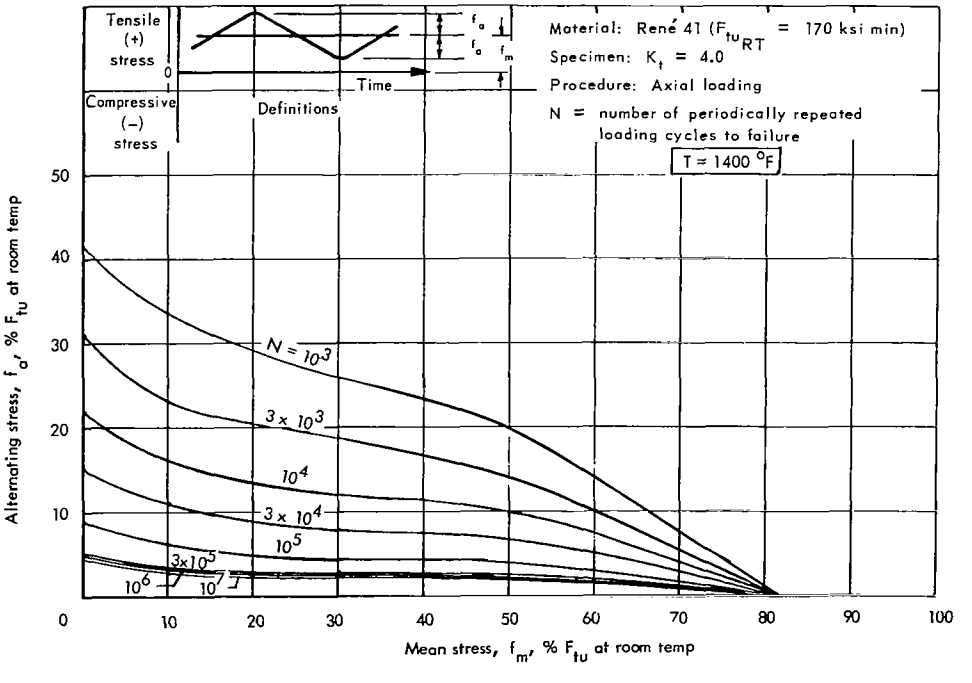

Figure 25. Constant-life diagram of René 41 (K_t = 4.0) at 1400°F

TABLE 5. – MECHANICAL PROPERTIES OF RENE 41

Rene 41 sheet and strip (1400°F aged); t ≤ 0.187 in.													
Temp, °F	Grain	Basis	n[a]	$F_{0.7}$, ksi a	E_c, 10^6 psi	F_{cy}, ksi	Temp, °F	Grain	Basis	n	$F_{0.7}$, ksi	E_c, 10^6 psi	F_{cy}, ksi
75	L	A	25	134.5	31.6	135.0	1400	L	B	15	112.4	22.8	112.0
75	T	A	25	140.7	31.6	141.0	1400	T	B	15	118.4	22.8	117.6
75	L	B	25	139.7	31.6	140.0	1500	L	A	10	79.3	20.9	81.0
75	T	B	25	147.0	31.6	147.0	1500	T	A	10	83.3	20.9	84.6
1200	L	A	15	130.7	24.6	129.6	1500	L	B	10	82.6	20.9	84.0
1200	T	A	15	137.0	24.6	135.4	1500	T	B	10	87.2	20.9	88.2
1200	L	B	15	135.9	24.6	134.4	1600	L	A	10	55.7	18.0	58.0
1200	T	B	15	143.2	24.6	141.1	1600	T	A	10	58.4	18.0	60.6
1400	L	A	15	108.1	22.8	108.0	1600	L	B	10	58.0	18.0	60.2
1400	T	A	15	113.3	22.8	112.8	1600	T	B	10	61.2	18.0	63.2

[a]Ramberg Osgood Parameters, NACA-TN 902

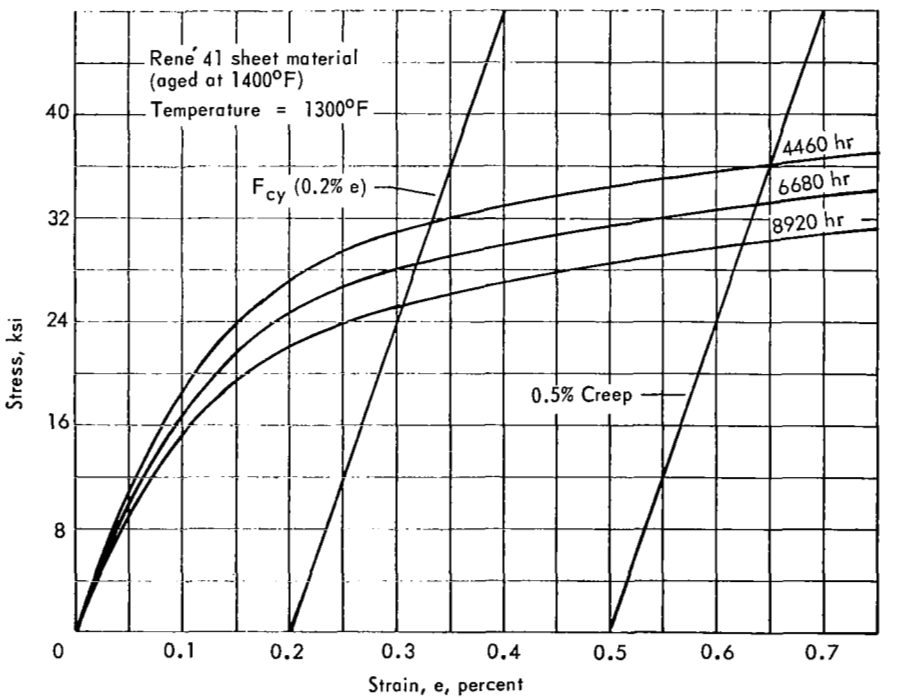

Figure 26. Typical isochronous stress-strain diagram for René 41 at 1300°F

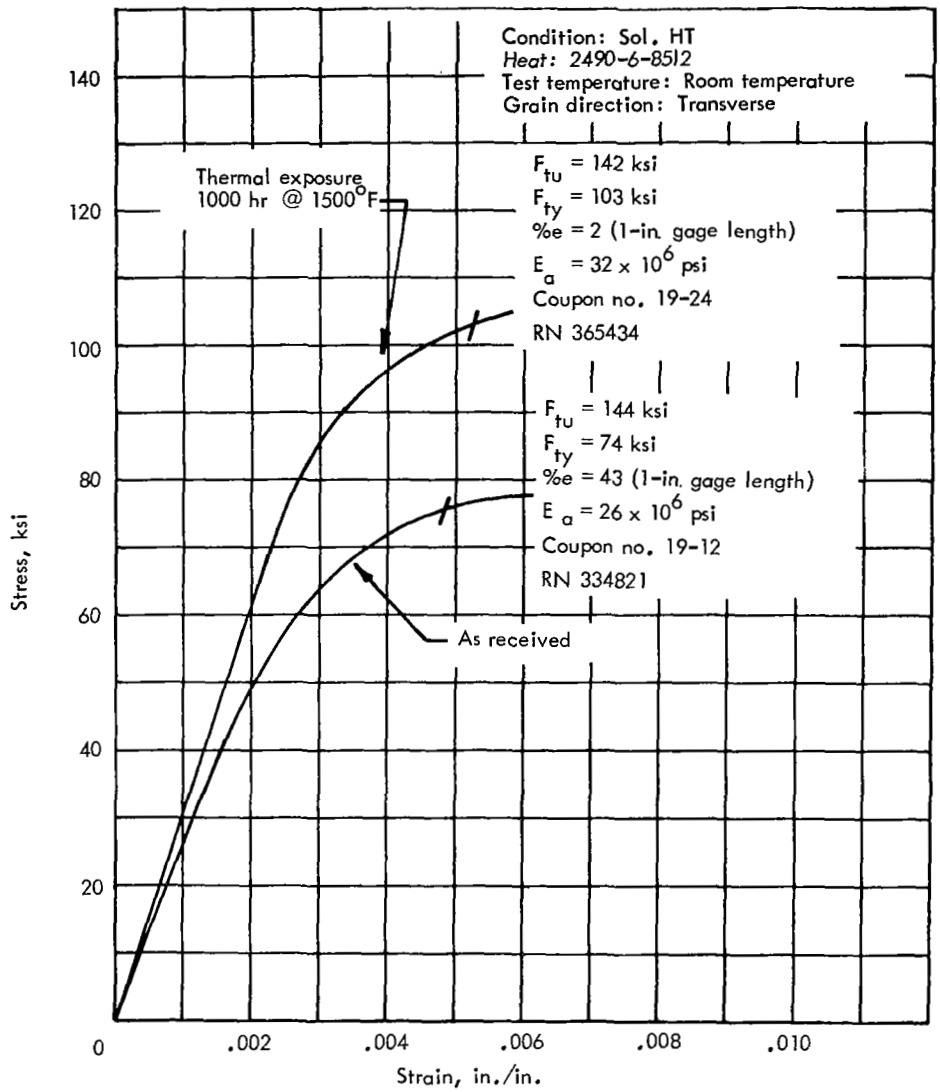

Figure 27. Room-temperature tensile stress-strain test data for 0.015 René 41

Tensile test data for René 41 and Haynes 25 included room-temperature tests of solution heat-treated (annealed) material after exposure to the thermal environment. The normal aging response of annealed René 41 as well as Haynes 25 causes a sharp increase in yield strength, as shown in figure 27. Therefore, it was found that René 41 is the most favorable material to satisfy elevated temperature strength requirements, provided it is aged after fabrication to provide the predictable allowables required for design.

Emittance-test data obtained over expected temperature ranges for René 41, Haynes 25, TD NiCr, Cb-752, and Ta-10W, were used in the thermal structural analyses. René 41 emittance-test data are shown in figure 28, and as a result, an emittance of 0.8 was used for designing with René 41.

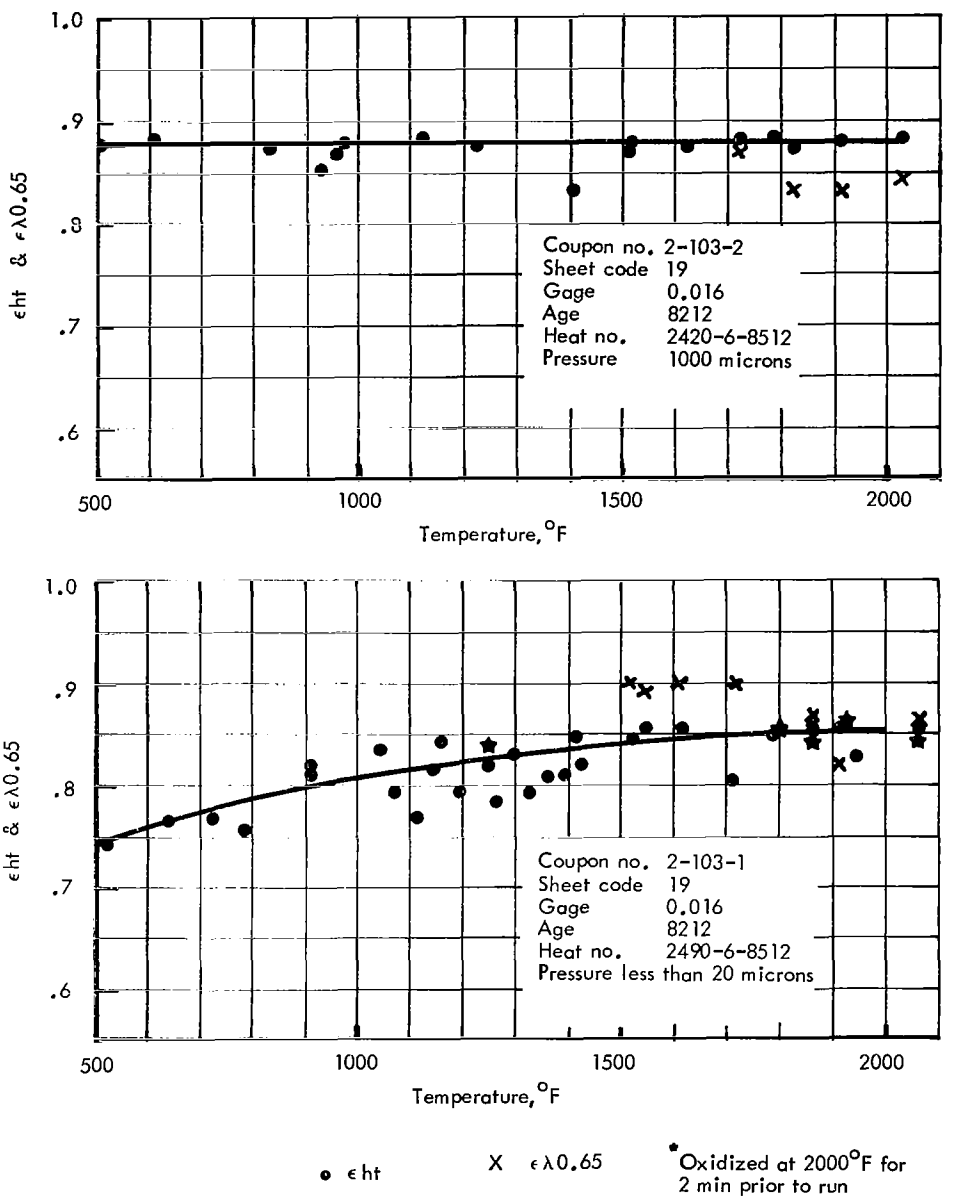

Figure 28. Emittance data for René 41

Coating tests for leading edge. – Initial radiation-equilibrium temperature predictions (see fig. 18) indicated that refractory metals would be required for leading-edge applications. Accordingly, screening tests for coated refractory-metal systems were performed. Two leading-edge refractory material candidates were fabricated and tested in a plasma arc under simulated flight conditions. The first, a porous metal, was a 50-percent dense powder-metallurgy product of Ta-10W sintered to a Ta-10W backing sheet. A protective coating of Sylcor R505 (Al-25Sn) was applied to the assembly and

vacuum fired at 1900°F for 1 hr. The second candidate fabricated and tested was a Ta-10W sheet leading-edge specimen disilicide-coated with Sylcor R512C (Si-20Ti-10Mo). This coating was diffused in a vacuum at 2580°F for 1 hr.

The two leading-edge material arrangements (porous and sheet) were tested at 2800°, 3000°, and 3100°F for cyclic conditions of temperature to determine the failure point of each. Six-minute cycles were selected to correspond with earlier leading-edge tests (ref. 53). The leading-edge test results are shown in figure 29.

As shown, the sheet concept did not fail after 39 six-minute cycles at 2800°F. Although the porous metal failed after 12 six-minute cycles at 2800°F, there were indications of improvements by a factor of 2 over earlier tests with the same type of coating (ref. 53). The mode of oxidation that occurs in the porous Ta-10W/R505 concept produces local hot spots. Failure was attributed to a combination of progressive Ta oxidation and thermal stress. The results indicate that adequate oxidation protection

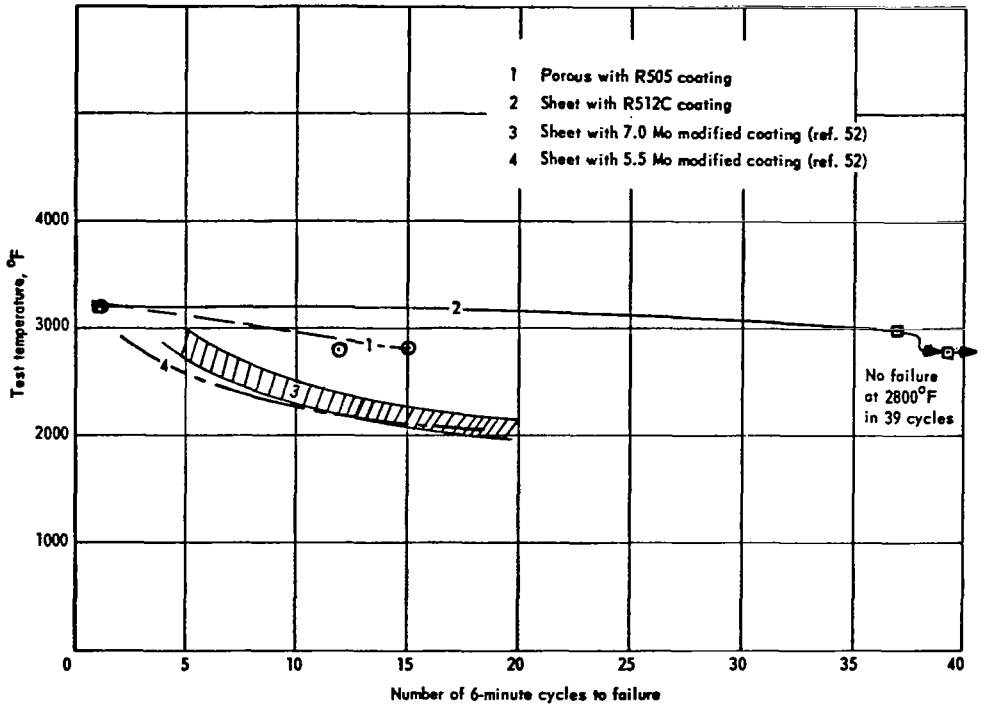

Figure 29. Leading-edge plasma-arc test results

at 3100°F is not practical with either of the concepts tested (each failed during the first cycle), whereas limited oxidation protection is afforded at 3000°F with the Ta-10W sheet coated with R512C (37 six-minute cycles).

Structural joint tests. – Representative structural joints and splices were selected for evaluation (330 tests). Resistance spotwelding and diffusion spot-bonding were evaluated for René 41. For Haynes 25, resistance spotwelding was investigated. Diffusion spot-bonding, brazed-spot, continuous-braze, and riveted techniques were used for TD NiCr.

The joint-technique evaluation results, shown in table 6, indicated that higher joint strengths at elevated temperatures are possible for the resistance spotwelded specimens than for the diffusion-bonded specimens. Radiographic inspection of the René 41 spots indicated crackfree welds; therefore, resistance spotwelding was selected for use in test-panel fabrication of René 41. For the TD NiCr materials, the riveted specimens provided the highest strengths at elevated temperatures, as shown in table 7.

TABLE 6. – RENÉ 41 LAP-JOINT TEST DATA

Material	Heat no.	Gage, in.	Condition[a]	Method of joining	Thermal Exposure		Ultimate load, lb/spot		
					hr	°F	RT	1200°F	1500°F
René 41	2490-6-8512	0.015	Aged	Resistance spot	None		612	405	294
			Annealed				532	442	234
			Aged		250	1500	632	–	–
			Annealed				629	–	–
	2490-7-8513		Aged		None		682	516	301
			Annealed				579	461	286
			Aged		250	1500	560	–	–
			Annealed				586	–	–
	2490-6-8512		Aged	Diffusion spot	None		557	313	181
			Annealed				524	420	163
			Aged		250	1500	548	–	–
			Annealed				559	–	–

[a]Aging cycle: heated in air to 1400°F, held at 1400°F for 16 hr, then cooled in air to room temperature.

TABLE 7. – TD NiCr LAP-JOINT TEST DATA

Material	Heat no.	Gage, in.	Material condition	Method of joining	Test temperature			
					RT	RT	2000°F	2200°F
					Ultimate, lb/spot	Yield	Ultimate, lb/spot	Ultimate, lb/spot
TD NiCr	2862-1	0.010	Annealed	Diffusion spot bond	247	–	38	31
	2862-1	0.030	Annealed	Diffusion spot bond	942	–	63	40
	2862-1	0.010	Annealed	Brazed spot	488	–	52	39
	2862-1	0.030	Annealed	Brazed spot	1098	–	92	67
	2901	0.030	Annealed	Riveted	596[a]	367[a]	84[a]	73[a]
	2891	0.060	Annealed	Riveted	1730[a]	915[a]	220[a]	176[a]
	2862-1	0.010	Annealed	Continuous braze	1910[b]	–	180[b]	118[b]

[a]Pounds per rivet.
[b]Total load on specimen (brazed area 1 in. by 2 in.).

Formability tests. – Room-temperature formability tests for the leading candidate materials were conducted to establish fabrication limits and procedures for the manufacture of the panel-element and structural design.

Beading, flanging, bending, and dimpling of Rene 41, within the formability limits of this material, can be accomplished with no difficulty. Elongations up to 17 percent (0.010 to 0.020 gage) can be achieved from the solution-treated condition in single operations. Elongations of more than 17 percent require interstage annealing. Total elongations of 25 to 30 percent can be achieved with two and three interstage annealings, respectively, for 0.010 to 0.020 gage Rene 41.

A minimum bend radius of 1.5t for both longitudinal and transverse grain directions was achieved for 0.010 to 0.025 gage Rene 41.

Minimum-Gage Selection

Minimum gage for fabrication of acceptable structural elements, sheet-thickness availability, and sheet-thickness variation were considered in the structural concept optimization. Table 8 presents minimum metallic material thicknesses that were selected for the concepts evaluation. The basis of selection was suitability to fabrication processes involved and to damage resistance.

TABLE 8. – MATERIAL MINIMUM GAGE FOR STRUCTURAL CONCEPTS

Structural concept	Element	Min. thickness, in.	
Monocoque panels			
Waffle grid,	Skin	0.020	0.015[a]
$0^o \times 90^o$ and $45^o \times 45^o$	Stiffener	0.020	0.015[a]
Honeycomb-core sandwich	Skin, exterior	0.015	
	Skin, interior	0.010	
	Core	0.002	
Truss-core sandwich	Skin, exterior	0.015	
	Skin, interior	0.010	
	Core	0.006	
Semimonocoque panels			
Tubular	Skin	0.010	
Beaded	Skin	0.015	
Trapezoidal corrugation	Skin	0.015	
Corrugation-stiffened skin	Skin, exterior	0.015	
	Skin, interior	0.010	
Convex beaded	Skin, exterior	0.015	
	Skin, interior	0.010	
Ribs & spars			
Caps	Flanged sheetmetal	0.030	
Webs	Corrugation	0.015	
Heat shields			
Corrugated	Skin	0.010	
Dimple-stiffened	Skin, exterior	0.015	
	Skin, interior	0.010	
Modular	Skin	0.010	

[a]These gages applicable to bonded construction.

Materials Selection

Final selections were René 41 for the primary structure and for most of the heat shields, and TD NiCr for the leading edge and for the heat shields adjacent to the leading edge.

Primary structure and heat shields. – René 41 was selected for use in the detailed evaluation of the primary structure and heat shields because of its excellent high-temperature buckling strength and acceptable fabricatability. As indicated in figures 22, 23, and 24, René 41 is the most efficient superalloy at the elevated temperature range in which the structure must operate. The loss in material weight resulting from oxidation at the operational temperatures and flight durations of this program was included in the analysis.

Leading edge. – For service temperatures from 2200° to 2500°F, the Cb-752/R512E material would be selected; for service from 2500°F to 3000°F, the Ta-10W/R512C material system would be chosen. On the basis of radiation-equilibrium temperatures, Ta-10W was originally considered to be the leading candidate. However, the two-dimensional transient thermal analysis described in the section on leading-edge weight shows that reasonable metal thicknesses lead to a maximum operating temperature of 2200°F, allowing use of TD NiCr without the oxidation coating requirement of refractory metals.

Insulation materials. – Several insulation materials were considered for the thermal-protection system between the heat shields and the primary structure. Of the three leading candidate low-density silica fibrous materials, two (Micro-Quartz and Dyna-Flex) are feltlike materials and one, Dyna-Quartz, is a block-tile material. The following tabulation shows the characteristics of the leading candidate insulation materials.

Insulation	Density, lb/ft^3	Maximum utilization temperatures, °F
Micro-Quartz	3.5 (3.0 nominal)	1600
Dyna-Quartz (heat stabilized Micro-Quartz)	4.5	2750
Dyna-Flex	6.0	2800

Micro-Quartz does not satisfy the maximum temperature requirement for this program (about 2000°F), and Dyna-Quartz is brittle and therefore has doubtful resistance to vibration loads. On the basis that Dyna-Flex satisfactorily meets the requirements for the application, it was selected.

PRIMARY-STRUCTURE WEIGHT ANALYSIS

Data obtained from an analysis of trajectory, vehicle loads, aerodynamic heating, and candidate materials were applied to an in-depth weight analysis of the primary structure which was performed after an initial screening and an intermediate screening. Concepts analyses are described in the structural concepts section of this report.

Initial Weight Screening

Table 9 shows the loads and temperature data used for the initial panel-weight screening. The loads resulted from preliminary redundant-model loads analyses. Panels of selected sizes were designed and optimized according to methods discussed in the section on evaluation procedures. Initial weight-screening results are shown in table 10 for monocoque and semimonocoque spanwise- and chordwise-stiffened primary structures constructed of Rene' 41 and Haynes 25 materials.

Monocoque. – The weight data and panel details presented in table 10 led to the selection of the 45 deg by 45 deg and 0 deg by 90 deg unflanged waffle grid configurations for further evaluation.

Initially, only the waffle panel was retained for further analysis. However, as the study progressed, the waffle weight was found to have increased significantly, primarily as a result of pressure loads and the fact that the waffle panel is less efficient when applied to the complete wing structure than other concepts. Thus, the waffle results did not present the best choice for a monocoque concept, and consequently, honeycomb-core sandwich was chosen as the panel exhibiting the greatest potential for support of pressure and inplane loadings for monocoque studies. The honeycomb-core sandwich was thus selected for final detailed analysis.

Rene' 41 was selected as the primary-structure panel material since upper and lower surface panel weights were less than those of Haynes 25 for all concepts, as shown in table 10.

TABLE 9. – LOADS AND TEMPERATURES USED FOR INITIAL PANEL-WEIGHT SCREENING

		Wing surface			
		Upper	Lower		
N_x	lb/in.	-84	-1000	Chordwise	
N_y	lb/in.	-300	±325	Spanwise	
N_{xy}	lb/in.	-132	-32	Shear[a]	
Temp.	°F	1400	1600[b]		

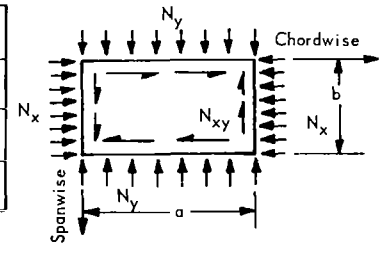

[a] Used for monocoque only.

[b] 1400°F was used for shielded panels.

TABLE 10. – INITIAL PANEL-WEIGHT SCREENING RESULTS

Panel construction	Panel dimensions, in.		Nonoptimum factor	Rene 41 Panel unit weight,[a] lb/ft^2	Haynes 25 Panel unit weight,[a] lb/ft^2
	"a"	"b"			
Monocoque					
45° by 45° Unflanged waffle	40	20	1.24	4.37	7.96
45° by 45° Tee-flanged waffle	40	20	1.30	4.70	N.A.[b]
0° by 90° Unflanged waffle	40	20	1.38	4.56	8.72
0° by 90° Tee-flanged waffle	40	20	1.40	4.86	8.92
Honeycomb sandwich	40	20	1.80	5.18	10.79
Truss-Core sandwich	40	20	1.50	6.24	9.58
Semimonocoque spanwise					
Tubular	43	30	1.15	4.51	5.16
Beaded skin	43	30	1.17	3.75	4.34
Trapezoidal corrugation	43	30	1.20	3.79	4.39
Corrugation-stiffened	43	30	1.20	3.92	4.34
Semimonocoque chordwise					
Convex-beaded	30	43	1.20	3.20	4.32
Tubular	30	43	1.15	4.51	6.19
Beaded-skin	30	43	1.17	3.75	5.48
Trapezoidal corrugation	30	43	1.20	4.20	5.92

[a]Includes upper and lower surface weights.

[b]Not available.

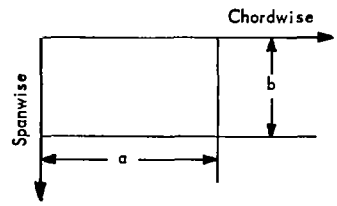

Semimonocoque. – Panel weight, closeout weight, minimum gages, and typical heat-shield weight were considered in the initial screening of all candidate semimonocoque spanwise- and chordwise-stiffened panels. Nonoptimum factors were based on the weights obtained from panel-edge closeout designs in which the fastener shear force and panel centroidal axis were aligned. The typical heat-shield weight was based on a refurbishable corrugated skin with two transverse hat-section stiffeners and four post supports.

Spanwise concepts: The results of the initial spanwise panel screening given in table 10 indicate that all of the spanwise panel configurations are of approximately the same efficiency. The heaviest is indicated to be the tubular panel; however, this panel showed the potential for much greater efficiency at longer lengths than used. Therefore, during the intermediate screening, all four configurations were subjected to an additional detailed panel evaluation in which total wing cross-section weights were considered. Results showed that the Haynes 25 alloy panels were not competitive with the Rene' 41 panels.

Chordwise concepts: The results of the initial chordwise panel screening presented in table 10 show that the convex-beaded version (unshielded design) has the lowest weight. However, selection was not made until results of the intermediate analyses of the spanwise concepts were known. This delay was to allow a better evaluation of the weight of these primary-structure concepts as a function of panel size and to allow selection of

a concept identical to one of the spanwise concepts in order to make a direct comparison of panel orientation.

Statically determinate. – The statically determinate structure shown in figure 9 is spanwise stiffened. The lowest-weight panel concept for the spanwise semimonocoque structure would also be very efficient for the statically determinate panels, since the loading conditions are similar. Thus, no screening was done for the statically determinate structure, and the panel selected for final weight analysis of this type of structure was the lowest-weight spanwise-stiffened semimonocoque panel.

Intermediate Weight Screening

The intermediate screening considered normal pressure as well as inplane loadings for total wing cross-section optimization; rib and spar spacings were varied. Preliminary considerations for thermal protection (heat shield) were included to keep the primary-structure temperatures below 1600°F. Calculated weights included Rene' 41 primary structure, typical heat shields, spars and ribs, and panel closeouts. Heat-shield weight was based on a refurbishable corrugated skin with two transverse hat-section stiffeners and four post supports. In addition to eliminating certain panel constructions, the intermediate screening provided the necessary structural data for determining the final redundant-model loads analysis inputs.

The loads used for the intermediate weight evaluation were based on a redundant-model loads analysis which utilized the monocoque stiffnesses obtained from the initial screening. These loads are shown in table 11.

TABLE 11. – INTERMEDIATE REDUNDANT-MODEL LOADS (AVERAGE LOADS BETWEEN STA. 2274 AND 2366)

Wing panel location	Direction	Ultimate loads, lb/in.[a]					
		-0.5-g condition		+2.0-g condition		Cruise condition	
		Upper	Lower	Upper	Lower	Upper	Lower
℄ to BL 120 Area A	N_x	-64 (-1659)	-182 (-737)	-330 (2120)	-555 (-1400)	-158 (-1659)	-251 (-737)
	N_y	168 (-62)	-118 (-29)	-510 (46)	550 (143)	-251 (-62)	268 (-29)
	N_{xy}	-2 (14)	-13 (-36)	-34 (13)	-5 (-35)	-18 (14)	-5 (-36)
BL 120 to BL 212 Area B	N_x	-42 (1635)	-170 (-363)	-270 (1380)	-495 (-900)	-131 (1635)	-222 (-363)
	N_y	116 (-112)	-78 (26)	-375 (-72)	420 (165)	-180 (-112)	-194 (26)
	N_{xy}	-7 (112)	-28 (-39)	-156 (118)	89 (-71)	-66 (112)	41 (-39)
BL 212 to BL 350 Area C	N_x	-26 (1136)	-111 (-1097)	-120 (910)	-210 (-1600)	-69 (1136)	-99 (-1097)
	N_y	44 (-127)	-32 (72)	-173 (-357)	195 (169)	-77 (-127)	87 (72)
	N_{xy}	-5 (80)	-30 (-99)	-106 (-92)	95 (-225)	-48 (80)	42 (-99)

[a] Values within parentheses are thermal loads; values not within parentheses are airloads; negative values indicate compression, positive values indicate tension.

A survey of the preliminary transient-temperature data for the three flight conditions (-0.5-g, +2.0-g, and cruise) and the loads of table 11 led to the choice of the +2.0-g maneuver condition as controlling the design for the intermediate screening. The thermal strains, rather than the thermal loads of table 11, were used in combination with the airloads and the temperatures of the preliminary transient analysis for each concept. The semimonocoque arrangements were optimized for bending and compression. The waffle optimization included shear, bending, and compression.

The results of the intermediate weight screening are shown in table 12 and include temperatures, rib and spar spacings, and weights (lb/ft^2) for the primary-structure concepts investigated.

Monocoque. – A parametric aspect-ratio study involving 45-deg by 45-deg and 0-deg by 90-deg waffle panels indicated that a geometrical configuration in which $a/b = 2.0$, with rib spacing b of 20 in., provides optimum weights. This 20-in. by 40-in. size was then used for the panel evaluations shown in table 12. Since the 45-deg by 45-deg grid was more efficient, the panel geometry and weights were determined for the 45-deg grid to provide input data for obtaining final redundant-analysis loads.

TABLE 12. – INTERMEDIATE WEIGHT-SCREENING RESULTS

Primary structure	Location area	Spacing, in.		Design temperature, °F		Weight,[a] lb/ft^2
		Rib	Spar	Lower surface	Upper surface	
Monocoque						
45° by 45° Unflanged waffle	B	20	40	1600	1400	8.90
	C	20	40	1600	1400	8.50
0° by 90° Unflanged waffle	B	20	40	1600	1400	9.24
Semimonocoque spanwise						
Trapezoidal corrugation upper surface panel	B	30	90	–	1300	1.20[b]
Corrugation-stiffened upper surface panel	B	30	90	–	1400	3.26[b]
Tubular	B	40	90	1400	1300	5.70
	C	44	90	1500	1400	5.11
Beaded-skin	B	48	90	1400	1300	4.93
	C	50	90	1500	1400	4.42
Trapezoidal corrugation	B	30	90	1400	1300	6.56
	C	31	90	1500	1400	5.64
Semimonocoque chordwise						
Tubular	B	90	46	1400	1300	6.44
Tubular lower convex-beaded upper surfaces	B	90	46	1400	1400	5.92

[a]Includes upper and lower surface panels, heat shields, spars and ribs, and closeouts; material René 41.

[b]Upper surface panels only.

Semimonocoque spanwise. – All semimonocoque spanwise-stiffened structures, except the smooth corrugation-stiffened panels, employed heat shields on all exposed surfaces to reduce temperatures and provide aerodynamic smoothness.

The beaded skin and tubular panel concepts were based on a constant semiapex angle of 77.5 deg, reduced from the earlier 90-deg arc because of the limitations of fabrication stretch-forming. The corrugation-stiffened configurations had a 60-deg interior angle and a flat to slant-height ratio of 0.80, which is nonoptimum, also as a result of the fabrication stretch-forming limitations. The trapezoidal corrugation was analyzed for the optimum 60-deg interior angle and a flat to slant-height ratio of 0.85.

By this intermediate structural screening, the corrugation-stiffened skin was eliminated, since it was found to be considerably heavier than the other three candidates. For example, for a 30-in. rib spacing, the upper surface corrugation-stiffened panel is 2-1/2 times as heavy as the upper surface trapezoidal corrugation, as shown in table 12.

The goal of the intermediate screening was the selection of the two lightest-weight semimonocoque spanwise structures for final sizing. These are the tubular and beaded-skin concepts (table 12). The trapezoidal corrugation was found to be about 30 percent heavier than the beaded-skin and about 13 percent heavier than the tubular concept.

Semimonocoque chordwise. – The results for spanwise stiffening eliminated both corrugation-stiffened skin and trapezoidal-corrugation concepts. Of the remaining semimonocoque panel concepts, tubular and beaded, only the tubular buckling analysis had been verified by tests at the time the selection of a panel concept was made for the chordwise weight analysis. Therefore, the tubular concept was selected for intermediate weight analysis. A variation of the tubular concept (convex-beaded) that does not use heat shields on the upper surface and that reduces the exposed bead height to provide a smoother surface was also considered. This variation permitted a comparison of the chordwise tubular concept with the spanwise tubular concept. As a result of the lateral pressure loads and excessive temperatures when unshielded, tubular panels instead of convex-beaded panels were necessary on the lower surface. The rib and spar spacing weight results, including the substructure, are shown in table 12. On the basis of these results, the lightest-weight structure consists of tubular lower surface and convex-beaded upper-surface panels, so this construction was selected for final chordwise evaluation.

Final Structural Weights

In final structural sizing of the René 41 primary structure, various thermal-protection arrangements were considered to determine the most compatible arrangement of wing-fuselage temperatures and to determine the structure with the lowest weight. With respect to the heat shields and insulation, the major objective was to minimize weight by reducing thermal stress and by limiting primary-structure temperatures to a maximum of 1600°F.

Monocoque waffle concept. – Thermal-protection arrangements for the 45-deg by 45-deg waffle primary structure were assessed on the basis of lowest weight, practicality of design for the given wing cross-section, and detailed thermal-analysis data. These arrangements were for (1) no heat shields and no insulation, (2) lower surface heat shields outboard of the one-third wing chordline with and without insulation and, (3) heat shields on the entire lower surface with insulation outboard of one-third chordline and without insulation.

The thermal-analysis data included transient effects on structural temperatures and isotherms generated for each candidate thermal-protection arrangement. The transient effects were based on a general thermal model, which included effects of heat-shield placement, lower surface insulation, and spar and rib size. Isotherms for the waffle primary structure, with outboard lower surface heat shields and insulation, are shown in figure 30 for the +2.0-g flight condition. The transient analysis indicates surface temperatures that are 100° to 200°F below the steady-state predictions, shown on figure 18, that result from the radiation-equilibrium analysis.

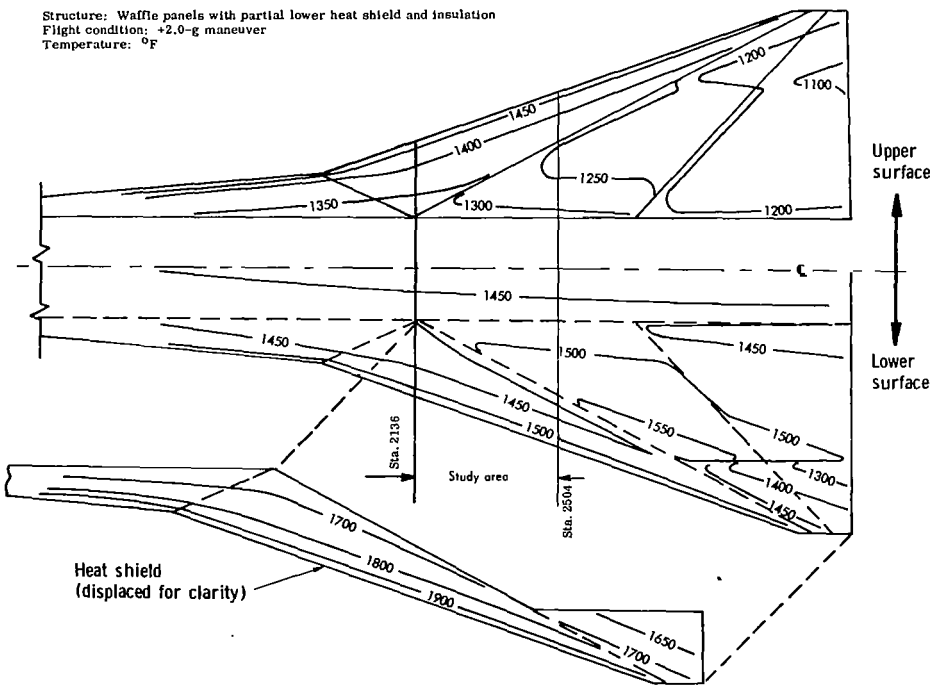

Figure 30. Wing isotherms at +2.0-g condition for waffle panels and heat shield

Figure 31 presents wing-fuselage temperatures (+2.0-g condition) for the candidate thermal-protection system arrangements and indicates the temperature-gradient matching aspects of the fuselage and wing. The most vertical wing-temperature profiles of figure 31 indicate the lowest difference in thermal gradients through the wing-fuselage cross-section. When the various wing butt-line temperature profiles are close together horizontally, the spanwise wing-surface thermal gradients are the lowest. The thermal-protection arrangement that yields the best match between wing depth and fuselage gradients and the lowest spanwise wing gradients results in lowest thermal stress. The arrangement of figure 31c with lower surface heat shields and insulation outboard of the one-third wing chord provides the lowest wing spanwise thermal gradients and the best match between wing-fuselage cross-section thermal gradients. Therefore, this thermal-protection arrangement would offer lowest thermal stress and hence was selected for optimizing rib and spar spacing.

From the panel sizing results of the intermediate screening, which were based on the intermediate screening redundant-model load analysis, the equivalent extensional and shear stiffnesses of the 45-deg by 45-deg waffle were input into the final redundant-model analysis. Poisson's effect on the 45-deg by 45-deg unflanged waffle grid was accounted for by a modification of the element flexibility matrix in the redundant model. Thermal data ($\alpha\Delta T$) based on temperature isotherms were input for each flight condition. Final redundant-analysis average internal loads are shown in table 13 for the thermal-protection arrangement with lower surface heat shields outboard and no insulation. The redundant-model airloads were used for all the thermal-protection arrangements; however, the thermal strains were obtained for other arrangements by plane-strain analyses, which, for the same thermal-protection arrangement, indicated generally good agreement with the redundant model results of table 13.

Optimum rib and spar spacing for wing waffle construction in inboard area B (BL 120 to BL 212) was determined for the thermal-protection arrangement with lower surface heat shield and insulation outboard of the one-third chordline. Forty upper and lower surface panels were optimized for panel-aspect ratios of 0.5, 1.0, 2.0, 3.0, and 4.0 and panel widths of 10, 20, 30, and 40 in. Figure 32 shows that aspect ratio has no effect on weight, provided both spanwise and chordwise dimensions can be varied. As shown in figure 32, the panel width of 20.0 in. with $a/b = 1$ has a slight advantage for wing area B. However, final selection of optimum rib and spar spacing was based on a comparison of average unit weights for the entire wing investigation section, in which a panel spanwise width of 20 in. and panel aspect ratios of 1.0 and 2.0 were considered. Average unit weight for aspect ratios of 1.0 was 10.764 lb/ft^2 and for 2.0 was 10.494 lb/ft^2. Consequently, a waffle-panel spanwise width of 20 in. and a chordwise length of 40 in. resulting in a panel aspect ratio of 2.0, was selected for final sizing of the five thermal-protection arrangements.

A summary of average unit weights for the various arrangements of lower surface thermal protection is shown in table 14. The arrangement with the lowest weight has heat shields and insulation only on the lower surface outboard of the wing one-third chordline. Deleting the outboard insulation results in a 3-percent weight penalty and decreasing the panel-aspect ratio from 2 to 1 causes a 2.6-percent weight penalty. Extending the heat shield over the entire lower surface results in a 5.6-percent weight penalty (higher without outboard insulation). Deleting both heat shield and insulation results in an 11-percent weight penalty. The lowest-weight wing was achieved when the thermal-protection arrangement imposed temperatures that resulted in a temperature gradient through the depth of the wing that nearly matched the temperature gradient through the fuselage depth, both at the same station (figure 31C).

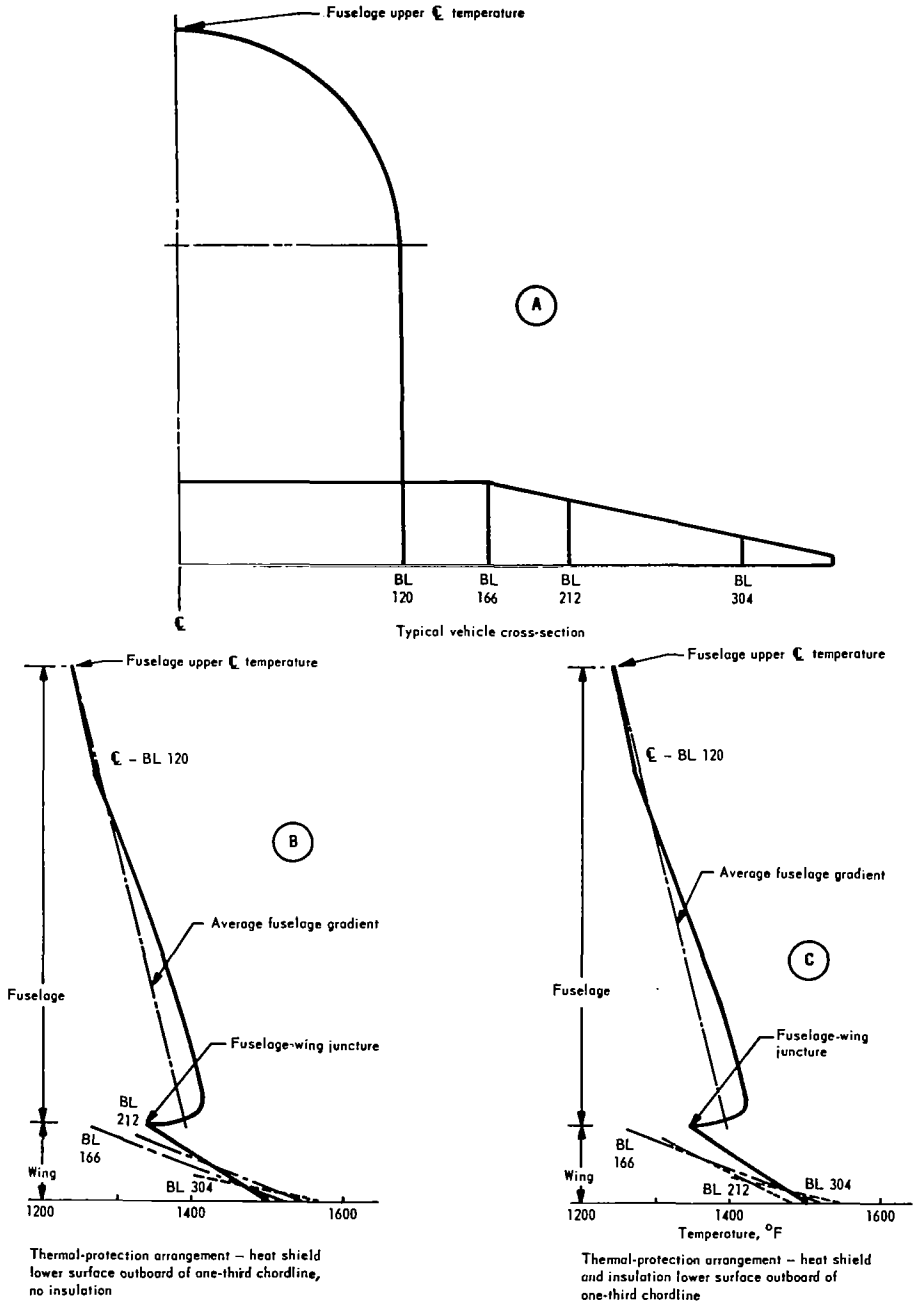

Figure 31. Wing/fuselage cross-section temperatures for candidate thermal-protection arrangements, +2.0-g condition

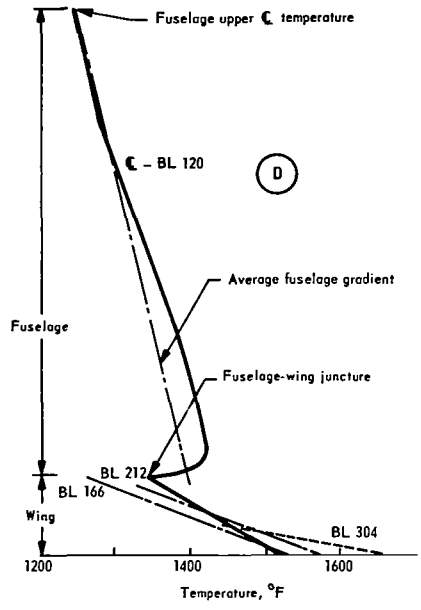

Thermal-protection arrangement – no heat shield, no insulation

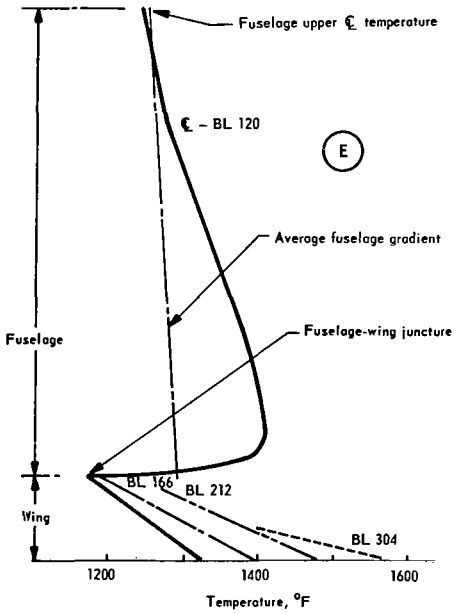

Thermal-protection arrangement – heat shields on entire lower surface, no insulation

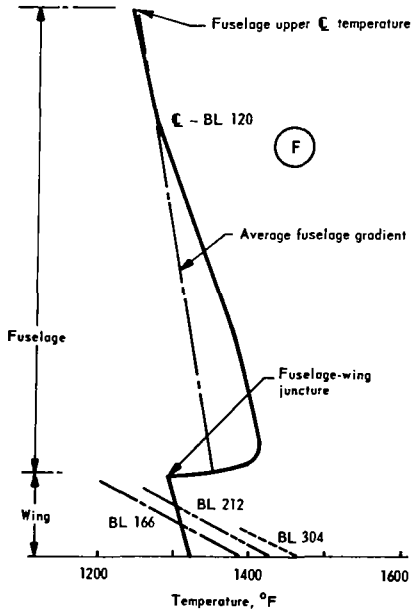

Thermal-protection arrangement – heat shield on entire lower surface, insulation lower surface outboard of one-third chordline

Figure 31. Concluded

TABLE 13. – FINAL REDUNDANT-MODEL LOADS FOR MONOCOQUE WAFFLE PANELS (AVERAGE LOADS BETWEEN STA. 2274 AND 2366)

Wing panel location	Direction	Ultimate loads, lb/in.[a]					
		-0.5-g condition		+2.0-g condition		Cruise condition	
		Upper	Lower	Upper	Lower	Upper	Lower
℄ to BL 120 Area A	N_x	-24 (+216)	-152 (+341)	-152 (+468)	-508 (-376)	-75 (-567)	-234 (-540)
	N_y	+140 (+62)	-110 (+150)	-857 (-65)	+804 (+59)	-387 (-81)	+369 (-58)
	N_{xy}	-24 (+4)	+42 (-18)	-56 (0)	+20 (+9)	-20 (-50)	+2 (-34)
BL 120 to BL 212 Area B	N_x	-22 (+220)	-131 (+156)	-144 (+801)	-459 (-641)	-71 (572)	-213 (-376)
	N_y	+62 (+43)	-34 (+123)	-807 (-115)	+768 (+52)	-364 (-137)	+340 (-30)
	N_{xy}	-12 (+108)	-48 (+42)	-414 (+154)	+278 (-23)	-176 (+106)	+143 (-12)
BL 212 to BL 350 Area C	N_x	-68 (-650)	-145 (-255)	-25 (+513)	-226 (-568)	-34 (710)	-134 (-294)
	N_y	+107 (-231)	-19 (+135)	-396 (-198)	+384 (+128)	-160 (-108)	+166 (+90)
	N_{xy}	-16 (+431)	-31 (+156)	-349 (-67)	+318 (-15)	-150 (+139)	+132 (-12)

[a]Values within parenthesis are thermal loads, values not within parentheses are airloads; negative values indicate compression, positive values indicate tension.

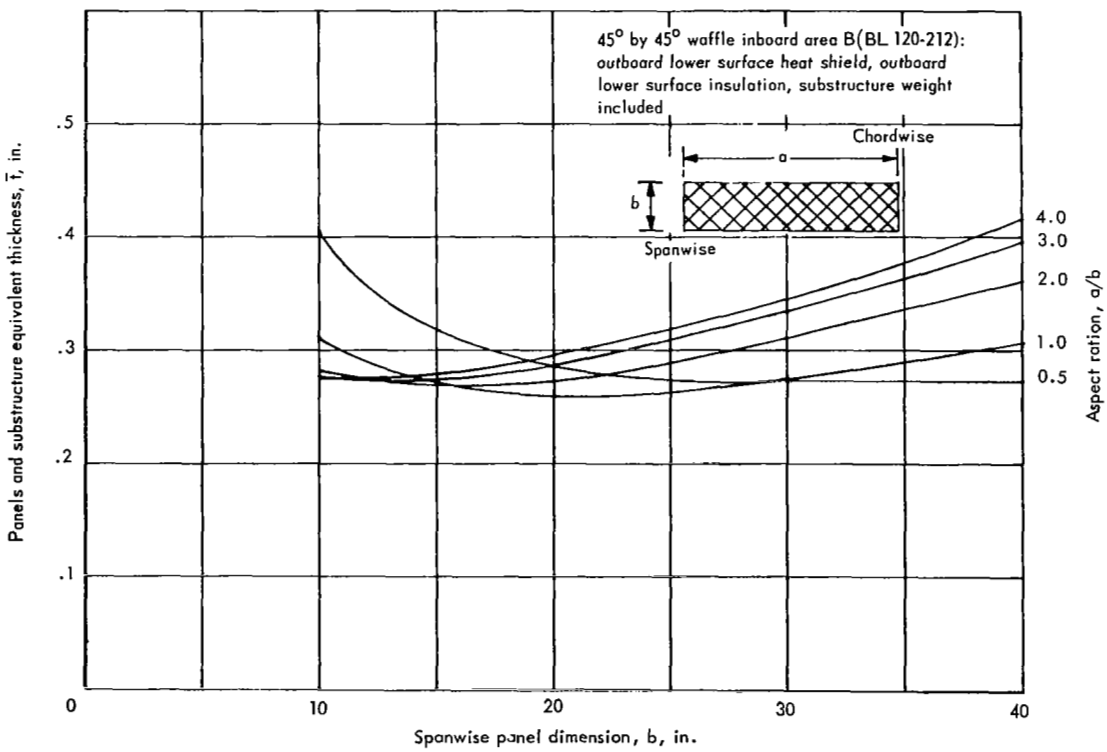

Figure 32. Aspect ratio weight summary, waffle construction

TABLE 14. – WEIGHTS OF MONOCOQUE WAFFLE PANEL AND VARIOUS THERMAL-PROTECTION ARRANGEMENTS

Aspect ratio	Thermal-protection arrangement		Weight, lb/ft^2			
	Heat shields	Insulation	Center Area A	Inboard Area B	Outboard Area C	Weighted average
2	Lower surface outboard area	Yes	10.717	12.033	9.437	10.494[a]
2	Lower surface outboard area	No	10.355	11.896	10.637	10.811
1	Lower surface outboard area	Yes	10.668	11.645	10.367	10.764
2	Entire lower surface	No	11.785	11.427	11.698	11.670
2	Entire lower surface	Outboard area	11.343	11.506	10.609	11.084
2	None	No	10.298	11.664	12.907	11.652

[a]Lowest weight.

A summary of the waffle-panel configuration with lowest-weight thermal-protection arrangement is presented in table 15 for the center, inboard, and outboard areas of the wing section investigated. A detail breakdown of wing equivalent thicknesses and weights for waffle panels shown in table 16 includes weights of panels, single shear cap and closeouts, rib and spar webs, web intersection, Dyna-Flex-insulation, corrugated heat shield, oxidation losses, and fasteners. A spanwise weight distribution was used to obtain an average unit weight for the entire wing cross-section. The waffle panels represent approximately 55 percent of the total wing weight.

TABLE 15. – FINAL GEOMETRY FOR MONOCOQUE WAFFLE PANELS

	Center Area A		Inboard Area B		Outboard Area C	
	Upper	Lower	Upper	Lower	Upper	Lower
Item \ Temp., °F	1330	1500	1260	1530	1370	1450
$\bar{t}$, in.	0.071	0.066	0.079	0.082	0.068	0.045
h, in.	0.708	0.621	0.726	0.714	0.644	0.464
p, in.	1.076	0.799	1.031	1.022	1.105	0.831
t_s, in.	0.021	0.020	0.020	0.027	0.020	0.020
t_w, in.	0.040	0.031	0.044	0.042	0.044	0.024

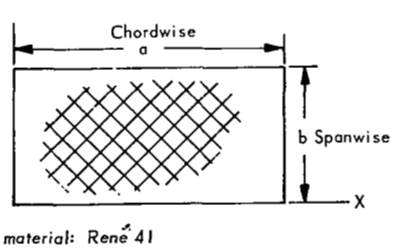

material: Rene 41
a = 40 in., b = 20 in., a/b = 2.0

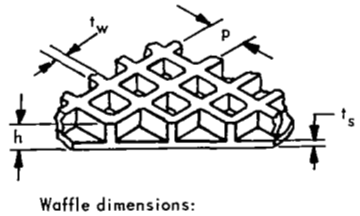

Waffle dimensions:
h = overall waffle height
p = pitch of stiffeners
t_s = skin thickness
t_w = stiffener thickness
$\bar{t}$ = panel equivalent thickness

TABLE 16. – BREAKDOWN OF WING WEIGHTS FOR MONOCOQUE WAFFLE CONCEPT WITH LOWER SURFACE OUTBOARD HEAT SHIELD AND INSULATION

Item		Equivalent thickness $\bar{t}$, in.		
		Center, A	Inboard, B	Outboard, C
Panels	Upper	0.0708	0.0790	0.0684
	Lower	0.0658	0.0822	0.0452
Caps (minimum gage)	Spar, upper	0.00173	0.00173	0.00173
	Spar, lower	0.00173	0.00173	0.00173
	Rib, upper	0.00345	0.00345	0.00345
	Rib, lower	0.00345	0.00345	0.00345
Closeouts	Upper	0.0222	0.0245	0.0207
	Lower	0.0180	0.0217	0.0108
Webs	Rib web	0.0363	0.0363	0.0182
	Spar web	0.0182	0.0182	0.0091
Web intersections	Total	0.00225	0.00225	0.00112
Insulation	Total	–	–	0.00348
Heat shields	Corrugation	–	–	0.0166
	Clip	–	–	0.00485
Oxidation	Total	0.00047	0.00050	0.00566
Fasteners	Total	0.00541	0.00541	0.00541
Total equivalent thickness, in.		0.2498	0.2804	0.2199
Total unit weight, lb/ft^2		10.72	12.03	9.44
Average unit weight, lb/ft^2		10.49		

[a] a = 40 in., b = 20 in., a/b = 2.

The final structural design offering the lowest-weight waffle thermal-protection arrangement is shown in figures 33A and 33B. Center, inboard, and outboard areas (designated A, B, and C) were used in determining total wing weight and cost. A rib spacing of 22.30 in. (in area B) and a spar spacing of 41.05 in. were used so that the one-third wing chord lies along the panel diagonal. This arrangement provides maximum uniformity of panel design.

Out-of-plane loads at the one-third chordline were resisted by full-depth webs along the panel diagonal. A minimum-gage (0.015 in.) 60-deg circular-arc corrugation was used for rib and spar webs. Flush Hi-Lok fasteners were used to attach the upper surface panels to the rib and spar caps. Spar and rib caps are flanged sheet burn-through welded to the corrugated web. For attachment of lower surface panels, countersunk screws and nut plates were used. (Removal of the upper surface primary-structure panels is accomplished by first removing the lower surface panels.)

At rib and spar web intersections, combinations of integrally formed flanges and separate angles were joined by resistance spotwelding. Dyna-Flex insulation, varying from 0.25 in. in thickness near the leading edge to 0.125 in. inboard, was packaged in Inconel X-750 foil.

Leading edges and heat shields were attached by externally accessible flush screws. Cross-sections of the corrugated heat shield and the segmented leading edge are shown in figure 33B.

Monocoque honeycomb-core sandwich concept. – The honeycomb-core sandwich primary structure was evaluated with lower surface heat shields and insulation outboard of the one-third wing chord, since this arrangement has the lowest weight for the monocoque waffle concept.

After detailed evaluation, it was determined that René 41 honeycomb-core sandwich could not be adequately brazed by using existing techniques. Therefore, resistance welding was selected for welding the cellular-shaped foil-ribbon core to the face sheets.

Using the loads from the final redundant-model analysis of the waffle concept, honeycomb-core sandwich panels were sized, and these extensional and shear stiffnesses were then input into the final honeycomb redundant-model analysis. Thermal data ($\alpha\Delta T$) for each flight condition were based on the temperatures obtained from a detailed transient thermal analysis. Table 17 shows the final internal loads, resulting from the redundant-model analysis, used for the final structural analysis of honeycomb-core sandwich.

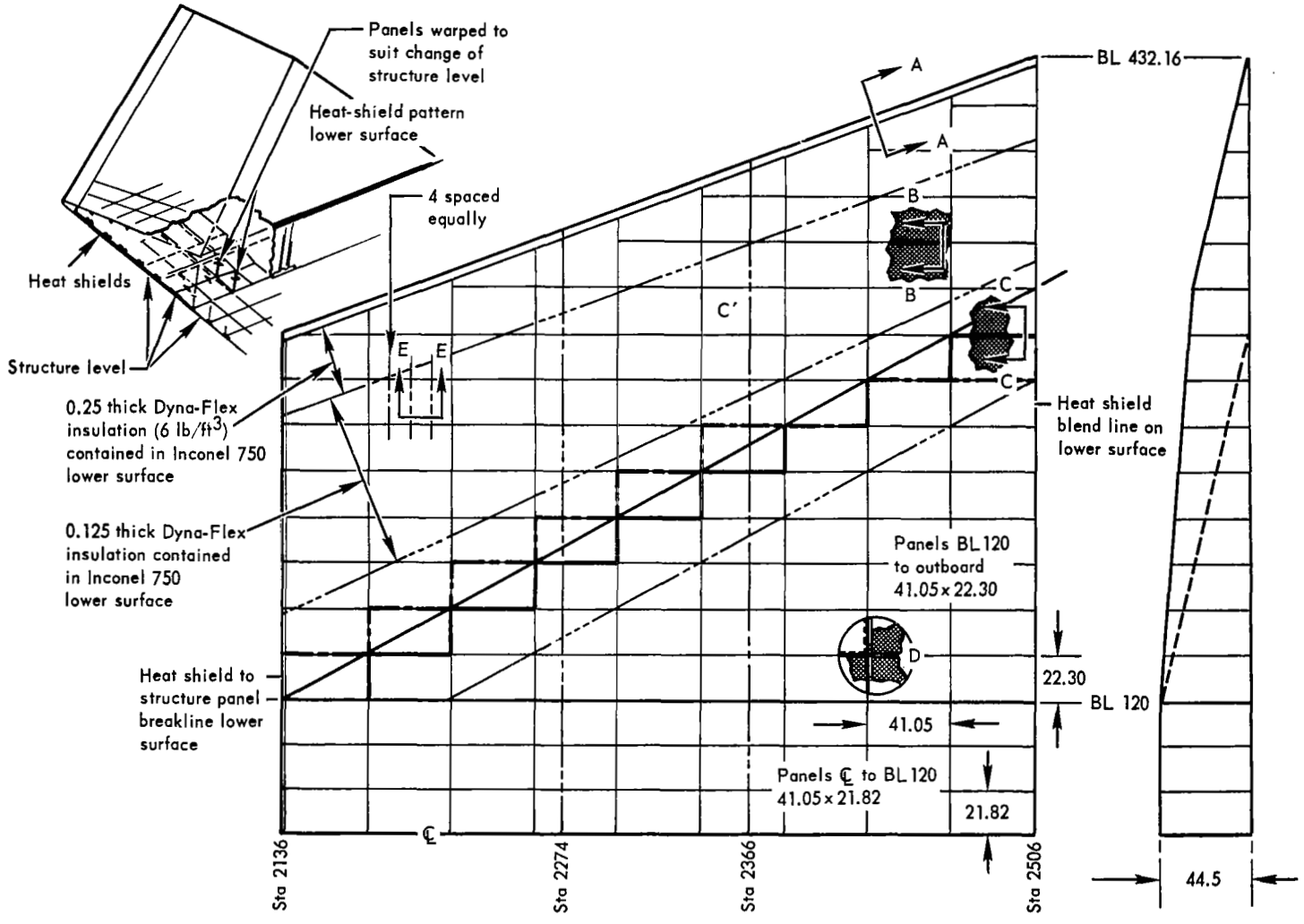

Figure 33 A Final design of monocoque waffle primary-structure concept

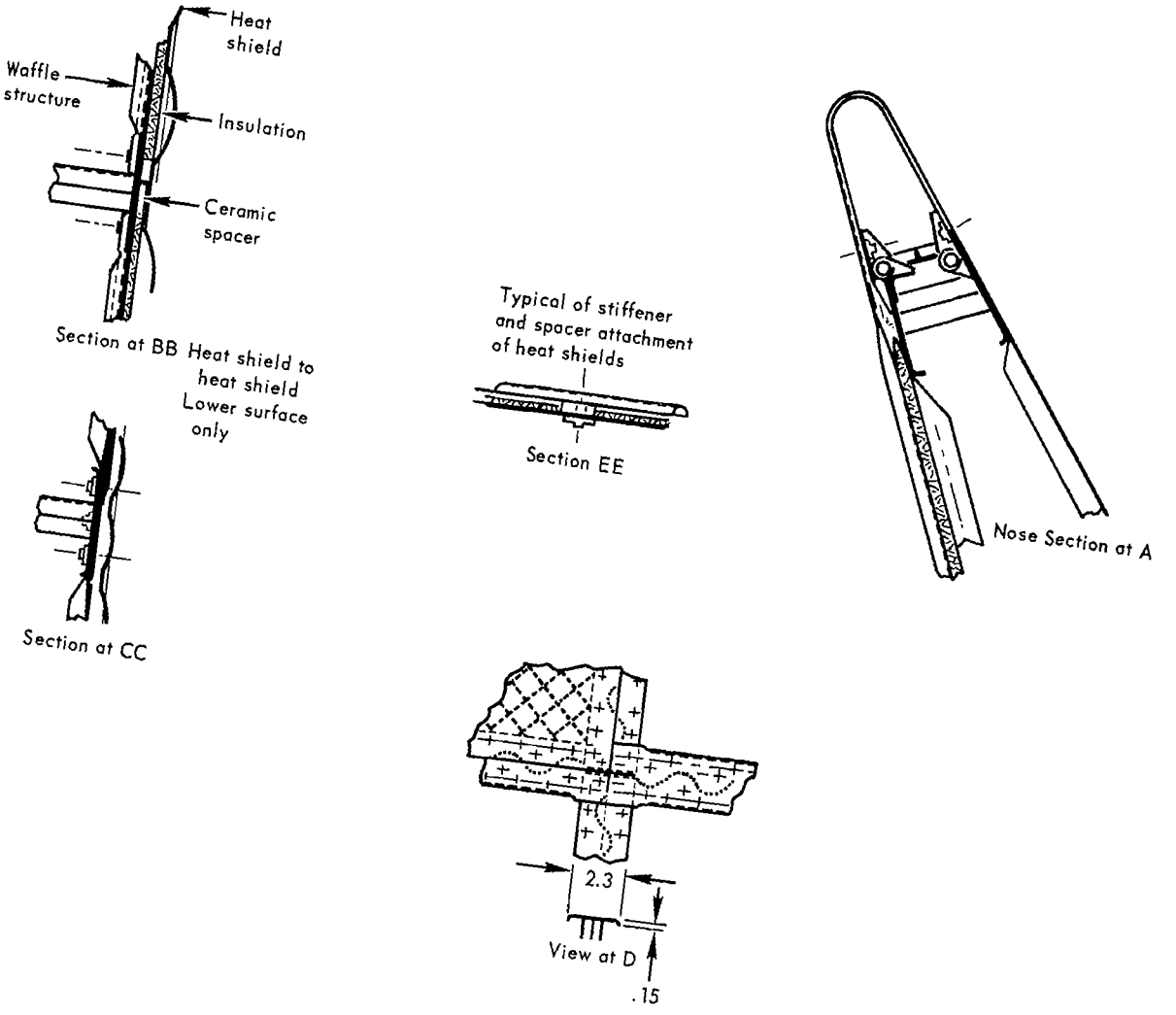

Figure 33B. Details of final design of monocoque waffle primary-structure concept

TABLE 17. – FINAL REDUNDANT-MODEL LOADS FOR MONOCOQUE HONEYCOMB-CORE SANDWICH PANELS (AVERAGE LOADS BETWEEN STA. 2274 AND 2366)

Wing panel location	Direction	Ultimate loads, lb/in.[a]					
		-0.5-g condition		+2.0-g condition		Cruise condition	
		Upper	Lower	Upper	Lower	Upper	Lower
℄ to BL 120 Area A	N_x	6 (161)	-186 (470)	-400 (674)	-297 (-771)	-187 (-1174)	-142 (-658)
	N_y	211 (47)	-178 (293)	-651 (-85)	587 (74)	-307 (-205)	285 (-230)
	N_{xy}	15 (20)	34 (41)	26 (-16)	3 (-45)	7 (65)	-24 (-64)
BL 120 to BL 212 Area B	N_x	11 (51)	-177 (461)	-331 (899)	-387 (-959)	-152 (894)	-185 (-397)
	N_y	88 (57)	-78 (261)	-589 (-96)	559 (100)	-266 (-129)	258 (-162)
	N_{xy}	12 (63)	-50 (186)	-302 (109)	-193 (181)	-130 (47)	84 (-92)
BL 212 to BL 350 Area C	N_x	-49 (-1080)	-96 (-16)	-101 (452)	-64 (-235)	-42 (1376)	-40 (558)
	N_y	33 (-214)	-31 (141)	-242 (-156)	242 (174)	-111 (40)	109 (142)
	N_{xy}	-2 (-614)	-39 (141)	-192 (-127)	-148 (171)	-86 (346)	73 (286)

[a]Values within parentheses are thermal loads; values not within parentheses are airloads; negative values indicate compression; positive values indicate tension.

The honeycomb-core venting problem was approached in two ways: (1) complete venting to the atmosphere, and (2) sealed panels, evacuated to a low pressure and filled with helium. Honeycomb-core vented to the atmosphere simplifies heat-shield attachment and fabrication. However, this approach permits oxidation and corrosion (from condensation of water vapor) of both core and interior-skin surfaces plus greater temperature drops through the panels. Honeycomb-core sealed, evacuated, and filled with helium at 2 psia eliminates oxidation and corrosion of the panel interior and offers lower temperature drops in the panel, but causes severe fabrication problems, since under existing techniques the panel pressure seal is extremely difficult to achieve (adequate welding of closeouts). However, since honeycomb-core sandwich offers a low weight potential and adequate sealing techniques may be developed for future application, the sealed approach was used for this investigation.

A detailed transient thermal analysis was conducted to determine local stresses and deflections caused by temperature gradients through the panel structure. Figure 34 shows structure and heat-shield temperatures for the lower surface insulation outboard arrangement (+2.0-g condition). The thermal-protection system may need to be extended to cover the small region on the lower surface where structural temperatures between 1650°F and 1700°F are indicated. Additional temperature and thermal gradient data are shown in table 18 for the three flight conditions. During the structural sizing, various combinations of face thicknesses, core densities, and sandwich heights were considered to minimize the panel thermal gradients. All interior surfaces were preoxidized and the panels were helium filled. As indicated in table 18, the largest thermal gradient (323°F) occurs on the lower surface panel under the fuselage.

Optimum rib and spar spacing were determined as shown in figure 35, considering surface panels, rib and spar caps, vertical webs, heat shields, closeouts, fasteners, insulation, oxidation penetration, and vertical posts. To assure that no weight decrease occurs due to the relieving effect of local thermal gradients, weights were determined with and without thermal gradients. Fifty-four panels were optimized for panel aspect ratios of 1.0, 1.5, and 2.0. Panel widths of 40 in., 50 in., and 60 in. were considered.

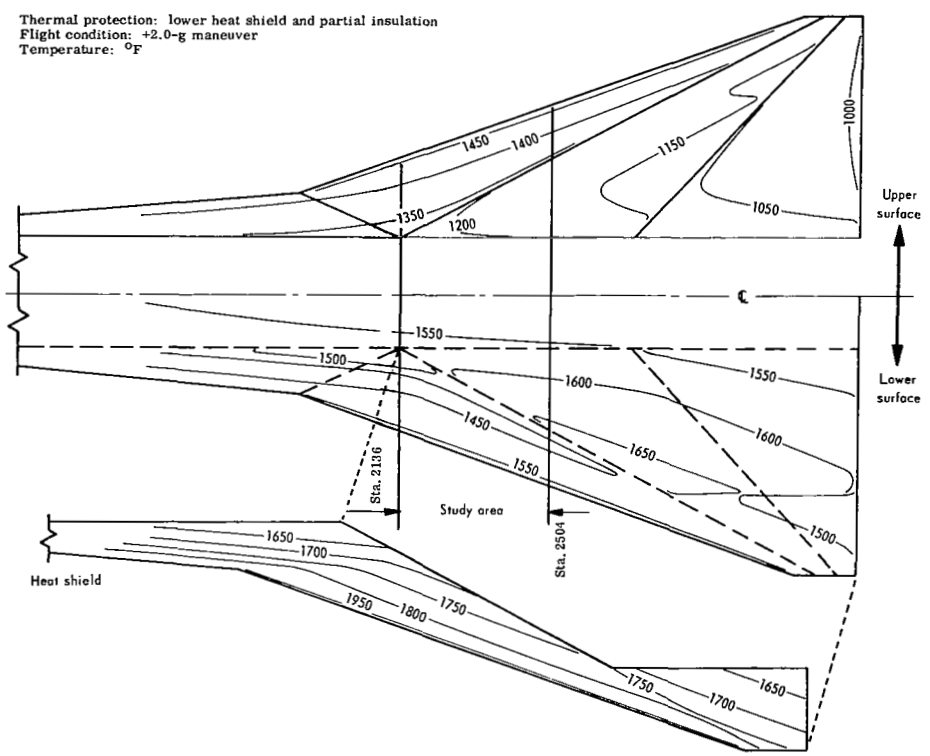

Figure 34. Temperature isotherms for honeycomb sandwich panels and heat shields, +2.0-g condition

TABLE 18. – TEMPERATURES AND THERMAL GRADIENTS FOR MONOCOQUE HONEYCOMB-CORE SANDWICH PANELS WITH OUTBOARD LOWER SURFACE HEAT SHIELD AND INSULATION

Loading condition	Wing panel location	Item[a]	Face sheet temperature, °F			
			BL 60	BL 166	BL 258	BL 350
-0.5-g	Upper	T_1	980	1312	<u>1588</u>	<u>1661</u>
		T_2	1055	1225	1386	1416
		ΔT	-74	86	201	244
	Lower	ΔT	95	41	21	17
		T_2	1166	1286	1396	1403
		T_1	1260	1327	1416	1420
		T_{HS}	–	–	1366	1425
+2.0-g	Upper	T_1	1007	1172	1362	1409
		T_2	1077	1252	1409	1443
		ΔT	-70	-79	-47	-33
	Lower	ΔT	<u>323</u>	257	122	18
		T_2	1211	<u>1323</u>	1434	1437
		T_1	1534	1579	1557	1456
		T_{HS}	–	–	<u>1693</u>	<u>1828</u>
Cruise	Upper	T_1	1240	888	946	945
		T_2	1276	1107	1137	1085
		ΔT	-35	-219	-191	-139
	Lower	ΔT	28	120	104	84
		T_2	1298	1215	1241	1149
		T_1	<u>1326</u>	1335	1344	1233
		T_{HS}	–	–	1402	1494

[a]Symbols: T_1 = External face sheet temperature
T_2 = Internal face sheet temperature
ΔT = $T_1 - T_2$
T_{HS} = Heat-shield temperature
Maximum temperatures are underlined.

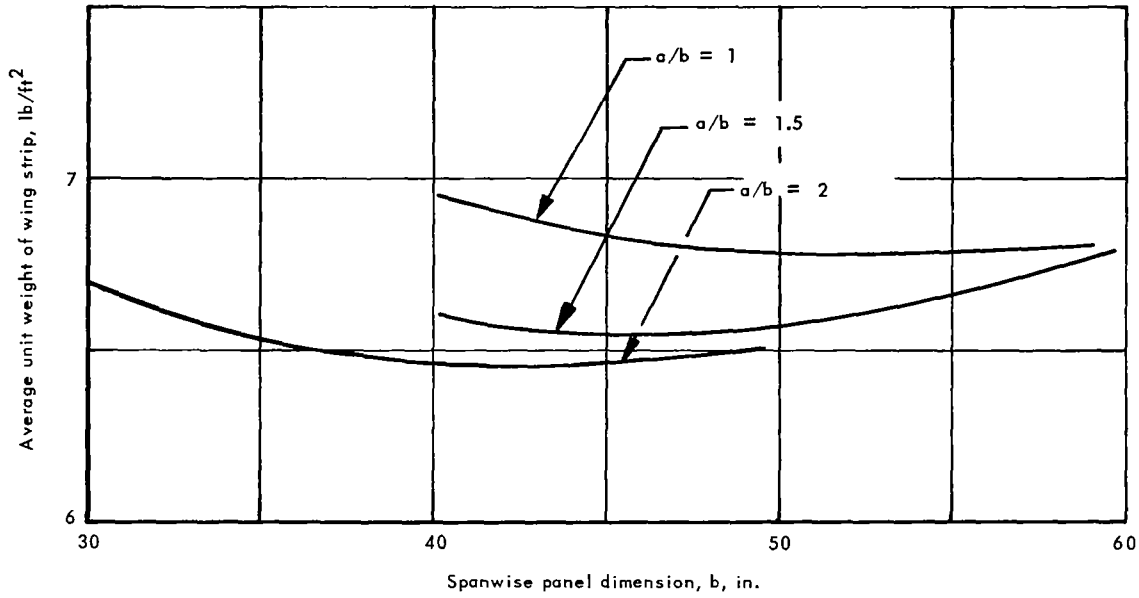

Figure 35. Honeycomb-core sandwich panel size requirements

The effective design condition for the center and outboard upper surface panels was cruise and -0.5-g, respectively. All other panels were designed by the +2.0-g condition.

As indicated in figure 35, a panel aspect ratio of 2.0 and a spanwise panel dimension of 40 in. provides minimum weight for the spar spacings considered. This is in agreement with the panel size selected for final redundant-model loads and thermal analysis. A comparison between the shear and extensional thickness used as input for the honeycomb redundant-model load analysis and the final panel stiffnesses indicated excellent agreement.

A summary of the honeycomb-sandwich panel design temperatures and geometry is presented in table 19 indicating that the height h varies from 0.71 to 0.96 in. with internal face thicknesses varying from 0.012 to 0.018 in., and external face thicknesses varying from 0.015 to 0.018 in. The maximum face-sheet temperatures of table 19 were conservatively used to determine material properties for both face sheets and core. The detail breakdown of equivalent thicknesses and wing weights for honeycomb-core sandwich panels shown in table 20 includes weights of panels, caps, closeouts, webs, web intersections, Dyna-Flex insulation, corrugated heat shield, oxidation losses, and fasteners. A relatively low core density of 1.25 percent of the density of the face sheet was used to assure a minimum-weight honeycomb-core structure. A spanwise weight distribution was used to obtain an average unit weight of 6.47 lb/ft^2 for the entire wing cross-section. The panels represent approximately 59 percent of the wing weight.

TABLE 19. - FINAL TEMPERATURES AND GEOMETRY FOR MONOCOQUE HONEYCOMB-CORE SANDWICH PANELS WITH OUTBOARD LOWER SURFACE HEAT SHIELD AND INSULATION

		Center		Inboard		Outboard	
		Upper	Lower	Upper	Lower	Upper	Lower
Max. face sheet temp., °F	-0.5-g	1003	1263	1313	1335	1595	1412
	+2.0-g	1026	1534	1245	1572	1408	1515
	Cruise	1277	1327	1130	1340	1123	1315
$W^{(c)}$, lb/ft^2		1.820	1.800	1.760	1.970	1.990	1.520
ρ_c, lb/ft^3		7.600	7.120	6.690	7.070	5.740	6.160
$\bar{t}$, in.		0.042	0.042	0.041	0.046	0.046	0.035
h, in.		0.935	0.898	0.950	0.937	0.963	0.714
t_1, in.		0.015	0.015	0.015	0.018	0.018	0.015
t_2, in.		0.014	0.015	0.014	0.015	0.018	0.012
t_c, in.		0.002	0.002	0.002	0.002	0.002	0.002
S, in.		0.271	0.291	0.308	0.294	0.358	0.334
$\bar{Z}$, in.		0.450	0.449	0.461	0.420	0.492	0.319
$W_o^{(d)}$, in.		-0.910	1.610	-0.820	0.230	1.160	-0.950

[a] a = 80 in., b = 40 in., a/b = 2.0.

[b] Effective design condition underlined.

[c] Nominal, does not include core flanges and corrugations.

[d] Midpanel deflection.

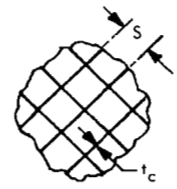

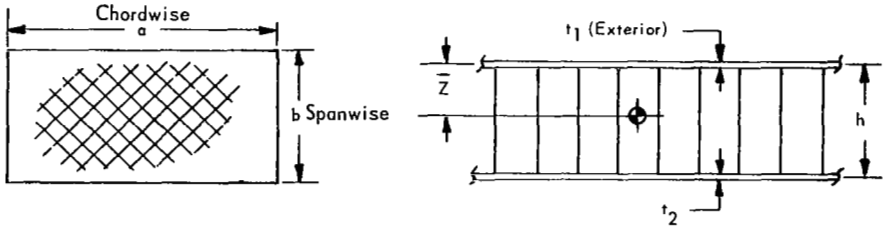

$\bar{t}$ = panel equivalent thickness

w = panel equivalent unit weight

ρ_c = density

TABLE 20. – BREAKDOWN OF WING WEIGHTS FOR MONOCOQUE HONEYCOMB-CORE SANDWICH CONCEPT WITH LOWER SURFACE OUTBOARD HEAT SHIELD AND INSULATION

Item		Equivalent thickness, $\bar{t}$, in.		
		Center, A	Inboard, B	Outboard, C
Panels	Upper[a]	0.0449	0.0434	0.0480
	Lower[a]	0.0443	0.0482	0.0372
Caps (minimum gage)	Spar, upper	0.00097	0.00097	0.00097
	Spar, lower	0.00097	0.00097	0.00097
	Rib, upper	0.00195	0.00195	0.00195
	Rib, lower	0.00195	0.00195	0.00195
Closeouts	Upper	0.00878	0.00888	0.00888
	Lower	0.00868	0.00878	0.00848
Webs	Rib web	0.0182	0.0182	0.0091
	Spar web	0.0091	0.0091	0.0046
Web intersections	Total	0.00056	0.00056	0.00028
Insulation	Total	–	–	0.00348
Heat shields	Corrugation	–	–	0.01660
	Clip	–	–	0.00485
Oxidation	Total	0.00110	0.00077	0.00599
Fasteners	Total	0.00417	0.00421	0.00404
Total equivalent thickness, in.		0.1456	0.1479	0.1573
Total unit weight, lb/ft^2		6.25	6.35	6.75
Average unit weight, lb/ft^2		6.47		

[a]Includes weight due to core corrugation and flanges.

A drawing of the final honeycomb-core sandwich structural design is shown in figures 36A and 36B. Center, inboard, and outboard areas A, B, and C were used in determining total wing weight and cost. Rib spacing of 40 in. and spar spacing of 80 in. were used. Other details are identical to those described on page 56 for the waffle concept. A minimum-gage (0.015 in.) 60-deg circular-arc corrugation was used for the rib and spar webs.

Semimonocoque spanwise concepts. – Two spanwise-stiffened primary-structure concepts were analyzed for final structural weight: tubular and beaded primary structures with heat shields on both upper and lower surfaces. Insulation on the lower surface outboard of the one-third wing chord was considered, since this arrangement produced lowest thermal stress and lowest weight for the waffle concept. From the panel-sizing results of the intermediate screening, which were based on the intermediate-screening redundant-model load analysis, the equivalent extensional and shear stiffnesses of the tubular concept (representative of the spanwise concepts) was input into the final redundant-model analysis. Thermal data ($\alpha\Delta T$) for each flight condition were based on the temperatures obtained from a detailed transient thermal analysis at 30 wing locations with insulation at the lower surface outboard area.

Tubular: Detailed transient thermal analyses were conducted to determine local stresses and deflections caused by temperature gradients through the panel structure. Isotherms were derived. Figures 37 and 38 show structure and heat-shield temperatures for the lower surface insulation outboard arrangement (+2.0-g condition). Insulation was placed so as to maintain the 1600°F material limit to minimize thermal gradients in the spanwise direction, and to match gradients through the wing and fuselage depth, thereby reducing thermal stresses. Figure 39 shows typical distribution of thermal stresses resulting from the use of insulation.

The internal loads resulting from the spanwise redundant-model analysis are shown in table 21. These loads were used for evaluating both spanwise structures. Good agreement between assumed and actual stiffnesses was noted; nevertheless, a plane-strain analysis was conducted to determine thermal loads for each structure type.

Optimum rib and spar spacings were determined by considering surface panels, rib and spar caps, vertical webs, heat shields, closeouts, fasteners, insulation, oxidation penetration, and vertical posts. The surface panels were analyzed for their most critical flight condition, the +2.0-g maneuver.

The 60-deg circular-arc (sine wave) spar webs were analyzed for total minimum $\bar{t}$ across the three wing areas A, B, and C for critical shear stability. An optimum spar spacing of 90 in. allowed minimum-gage webs of 0.015-in. René 41 in the center A and outboard C wing areas and 0.018 in. in the inboard B section.

Using the optimum 90-in. spar spacing, total wing cross-section and various wing-element effective thicknesses were determined as a function of rib spacing. The optimization results for inboard area B, summarized in figure 40, indicate an optimum rib spacing of 37 in. for the tubular concept. This same type of rib-spacing optimization was accomplished for areas A and C of the wing investigation section. In all cases, the rib spacing for minimum wing $\bar{t}$ was low enough for minimum-gage (0.015-in.) rib webs.

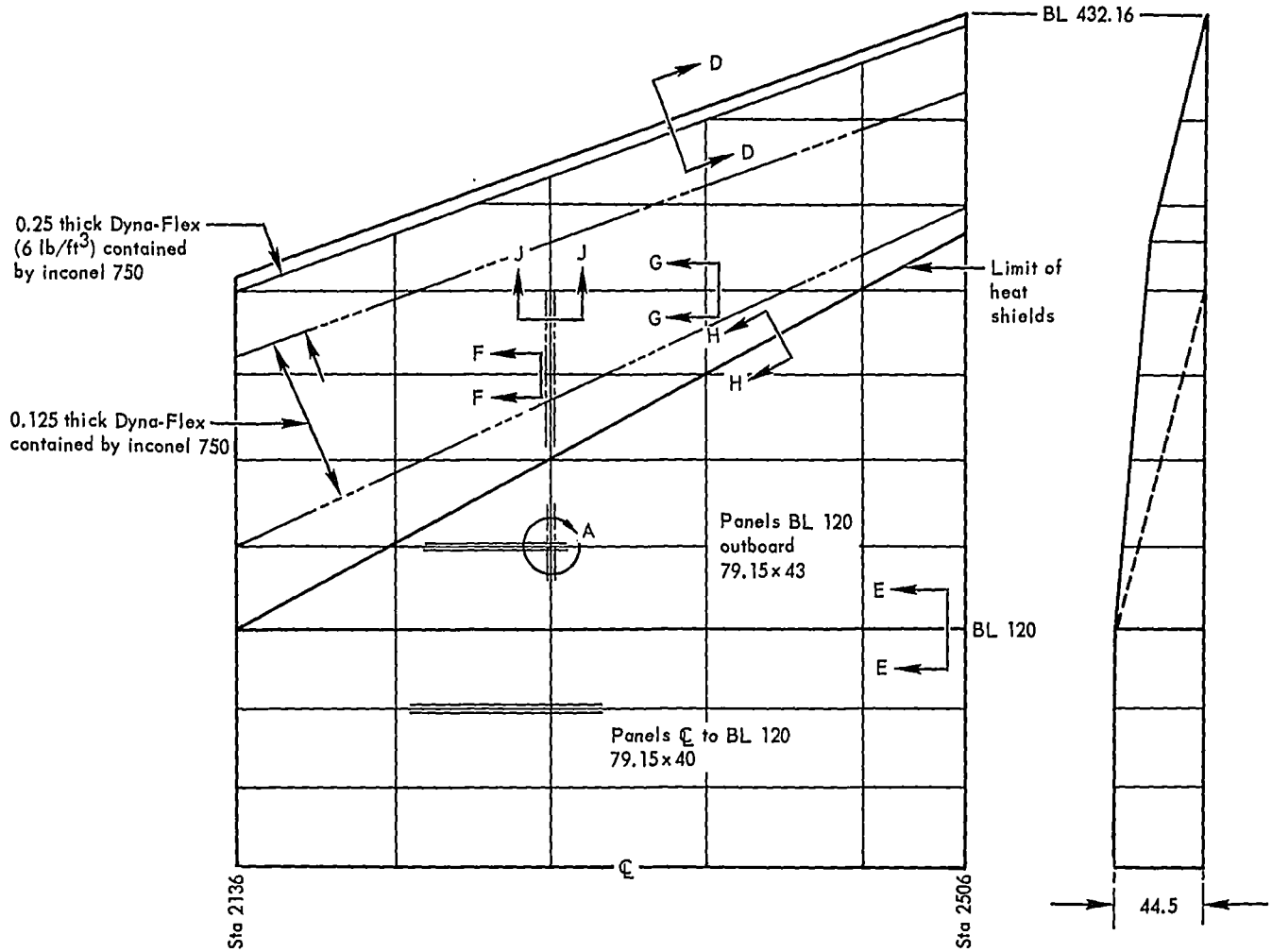

Figure 36A. Final design of monocoque honeycomb-core sandwich primary-structure concept

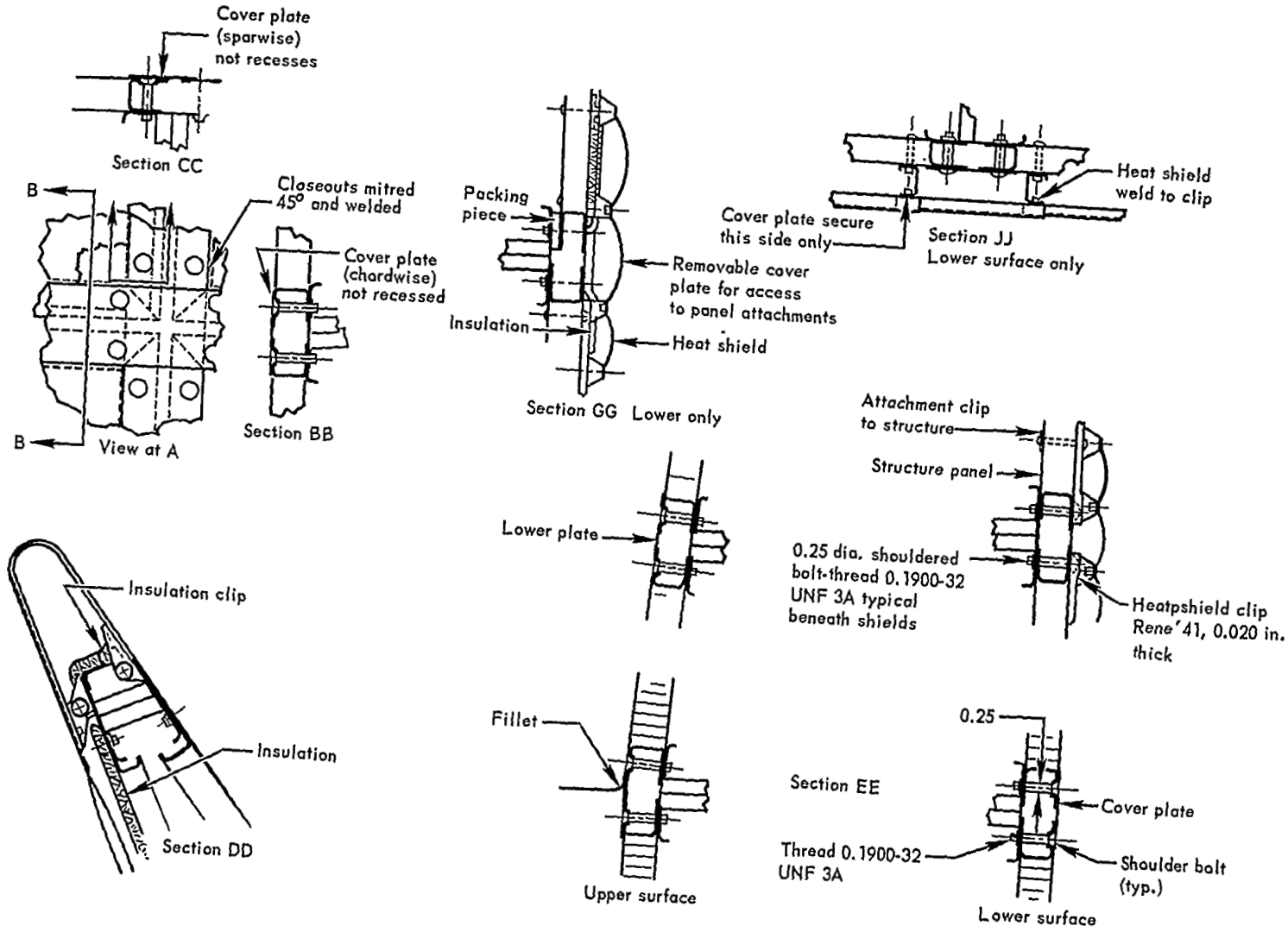

Figure 36B. Details of final design of monocoque honeycomb-core sandwich primary-structure concept

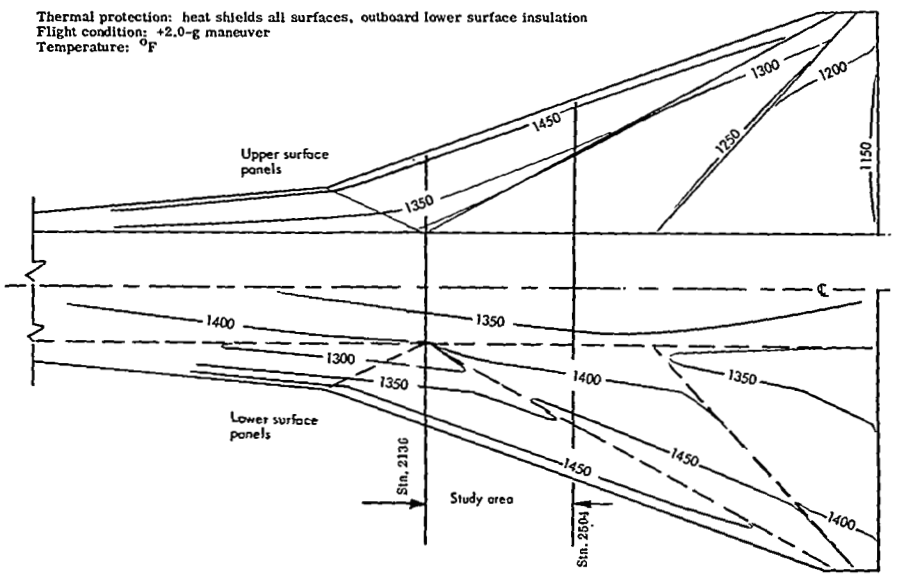

Figure 37. Primary-structure temperatures for spanwise-stiffened concept

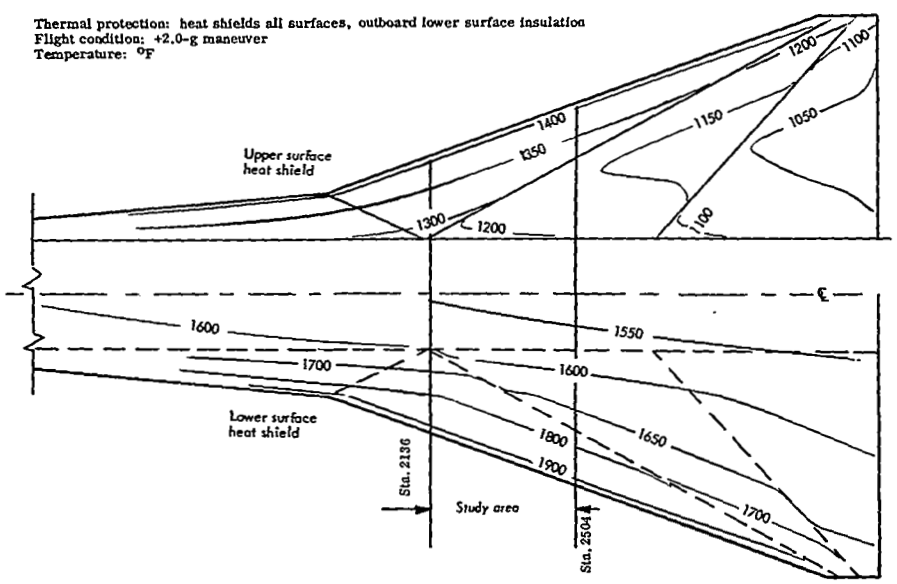

Figure 38. Heat shield temperatures for spanwise-stiffened concept

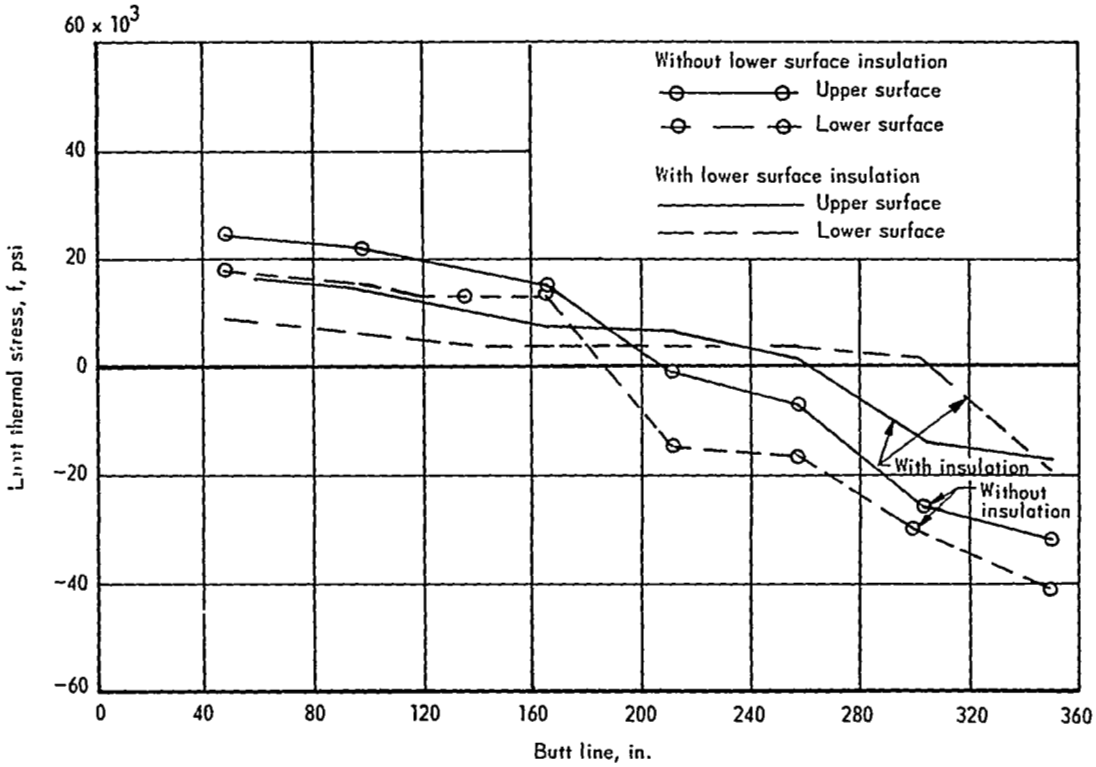

Figure 39. Limit chordwise thermal stresses for the +2.0-g condition for semimonocoque spanwise-stiffened panels with and without insulation

TABLE 21. – FINAL REDUNDANT-MODEL LOADS FOR SEMIMONOCOQUE SPANWISE-STIFFENED PANELS (AVERAGE LOADS BETWEEN STA. 2274 AND 2366)

Wing panel location	Direction	Ultimate loads, lb/in.[a]					
		-0.5-g condition		+2.0-g condition		Cruise condition	
		Upper	Lower	Upper	Lower	Upper	Lower
℄ to BL 120 Area A	N_x	-72 (319)	-117 (46)	-269 (174)	-385 (39)	-129 (-344)	-179 (-364)
	N_y	210 (-34)	-177 (76)	-563 (-23)	644 (49)	-269 (-65)	309 (-4)
	N_{xy}	-4 (2)	23 (3)	-15 (-3)	19 (19)	-7 (-10)	3 (-13)
BL 120 to BL 212 Area B	N_x	-74 (83)	-116 (-24)	-269 (127)	-385 (10)	-128 (-50)	-181 (-192)
	N_y	98 (-40)	-72 (63)	-496 (-32)	576 (51)	-231 (-64)	265 (24)
	N_{xy}	-8 (-5)	-38 (21)	-176 (-11)	139 (14)	-77 (9)	64 (4)
BL 212 to BL 350 Area C	N_x	-55 (-79)	-84 (-73)	-135 (-27)	-210 (-40)	-65 (210)	-102 (122)
	N_y	78 (-85)	-33 (59)	-197 (-67)	215 (106)	-92 (-57)	72 (29)
	N_{xy}	-7 (-107)	-35 (56)	-138 (-92)	112 (49)	-63 (67)	48 (62)

[a]Values within parentheses are thermal loads; values not within parentheses are airloads; negative values indicate compression; positive values indicate tension.

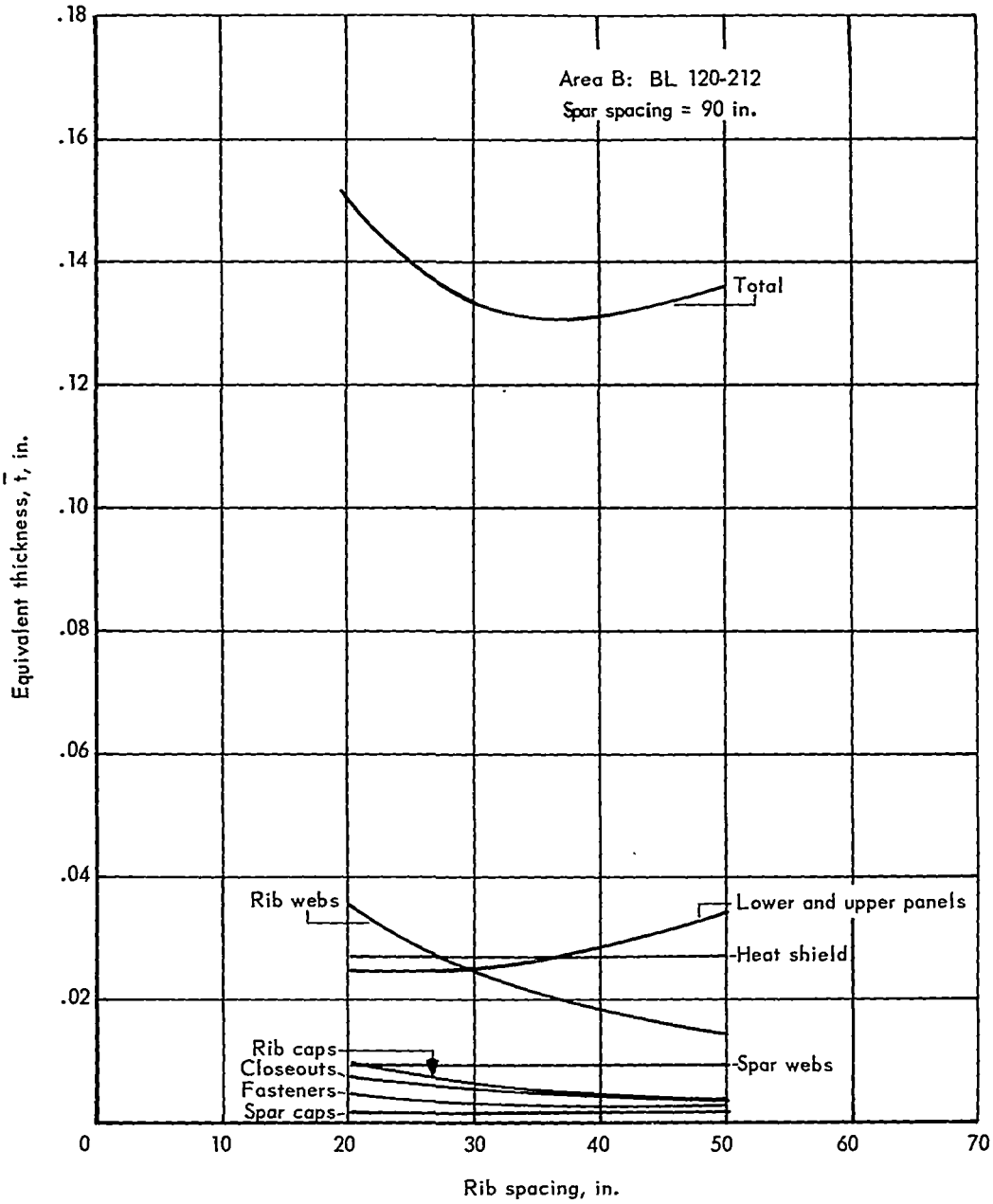

Figure 40. Optimum rib spacing for spanwise-stiffened tubular concept with partial insulation outboard

As a result of the heat-shield evaluation (described later), the refurbishable corrugated heat shield with multiple supports was used in this analysis. Oxidation weight was based on a depth of oxide penetration commensurate with the exposure time and temperature.

A summary of the panel geometry of the tubular structure is presented in table 22 for the center, inboard, and outboard areas of the wing section investigated. To provide heat-shield support-clip attachment surfaces, the flats between tubes were set at 0.50 in. The tubular panel semiapex angle was held constant at 77.5 deg, as in the intermediate sizing. As indicated in table 22, the panel geometry is near minimum gage (t = 0.010 in.) for the three wing areas.

TABLE 22. - FINAL GEOMETRY FOR SEMIMONOCOQUE SPANWISE-STIFFENED TUBULAR PANELS

Wing Area	Surface	$\bar{t}$, in.	t, in.	R, in.	L, in.	Pitch, in.
A (C_L - 120)	Upper	0.0292	0.011	1.500	50	3.429
	Lower	0.0258	0.010	0.800	50	2.062
B (120-212)	Upper	0.0287	0.011	0.950	40	2.355
	Lower	0.0284	0.011	0.800	40	2.062
C (212-350)	Upper	0.0258	0.010	0.750	40	1.964
	Lower	0.0254	0.010	0.600	40	1.672

$\bar{t}$ = panel equivalent thickness.
L = panel length (rib spacing).
b = 0.5 in. flat.
Pitch = center-to-center of stiffener.
Critical flight condition all wing areas = +2.0 g.

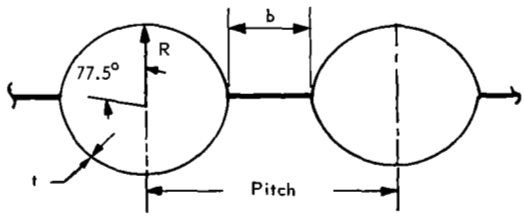

A detail breakdown of wing equivalent thicknesses and weights for spanwise-stiffened tubular panels shown in table 23 includes primary-structure panels, rib and spar caps, panel closeouts, webs and post, Dyna-Flex insulation, corrugated heat shields, oxidation losses, and fasteners. A spanwise weight distribution was used to obtain an average unit weight of 5.38 lb/ft^2 for the entire wing cross-section. The primary-structure panels are approximately 45 percent of the total wing weight.

A final structural design is shown in figures 41A and 41B. The tubular concept has panel dimensions of 90 in. by 48 in., 90 in. by 40 in., and 90 in. by 40 in., respectively, for the three sections from center to outboard. Ribs and spars are identical to those described on page 56 for the waffle concept.

The heat-shield attachment clips are spotwelded to the shield and panel on both surfaces. Since the heat shield is slightly smaller than the structural panel, corrugated cover strips are attached mechanically to the spars. The placement of foil-packaged Dyna-Flex insulation and its thickness are indicated in figure 41A.

TABLE 23. – BREAKDOWN OF WING WEIGHTS FOR SEMIMONOCOQUE SPANWISE-STIFFENED TUBULAR CONCEPT WITH FULL HEAT SHIELDS AND LOWER SURFACE OUTBOARD INSULATION

Item		Equivalent thickness, $\bar{t}$, in.		
		Center, A	Inboard, B	Outboard, C
Panels	Upper	0.0292	0.0287	0.0258
	Lower	0.0258	0.0284	0.0254
Caps	Spar, upper	0.0011	0.0011	0.0011
	Spar, lower	0.0011	0.0011	0.0011
	Rib, upper	0.0027	0.0028	0.0032
	Rib, lower	0.0032	0.0034	0.0028
Closeouts	Upper	0.0032	0.0029	0.0024
	Lower	0.0020	0.0025	0.0021
Webs	Rib web	0.0151	0.0180	0.0120
	Spar web	0.0084	0.0096	0.0047
Web intersections	Total	0.00042	0.00050	0.00029
Insulation	Total	–	–	0.00685
Heat shields	Total	0.0131	0.0263	0.0358
Oxidation	Total	0.00453	0.00246	0.00633
Fasteners	Total	0.00254	0.00294	0.00294
Total equivalent thickness, in.		0.1124	0.1307	0.1328
Total unit weight, lb/ft^2		4.82	5.61	5.70
Average unit weight, lb/ft^2		5.38		

[a]Area A: a = 90, b = 50, a/b = 1.8.

Area B and C: 2 = 90, b = 40, a/b = 2.25.

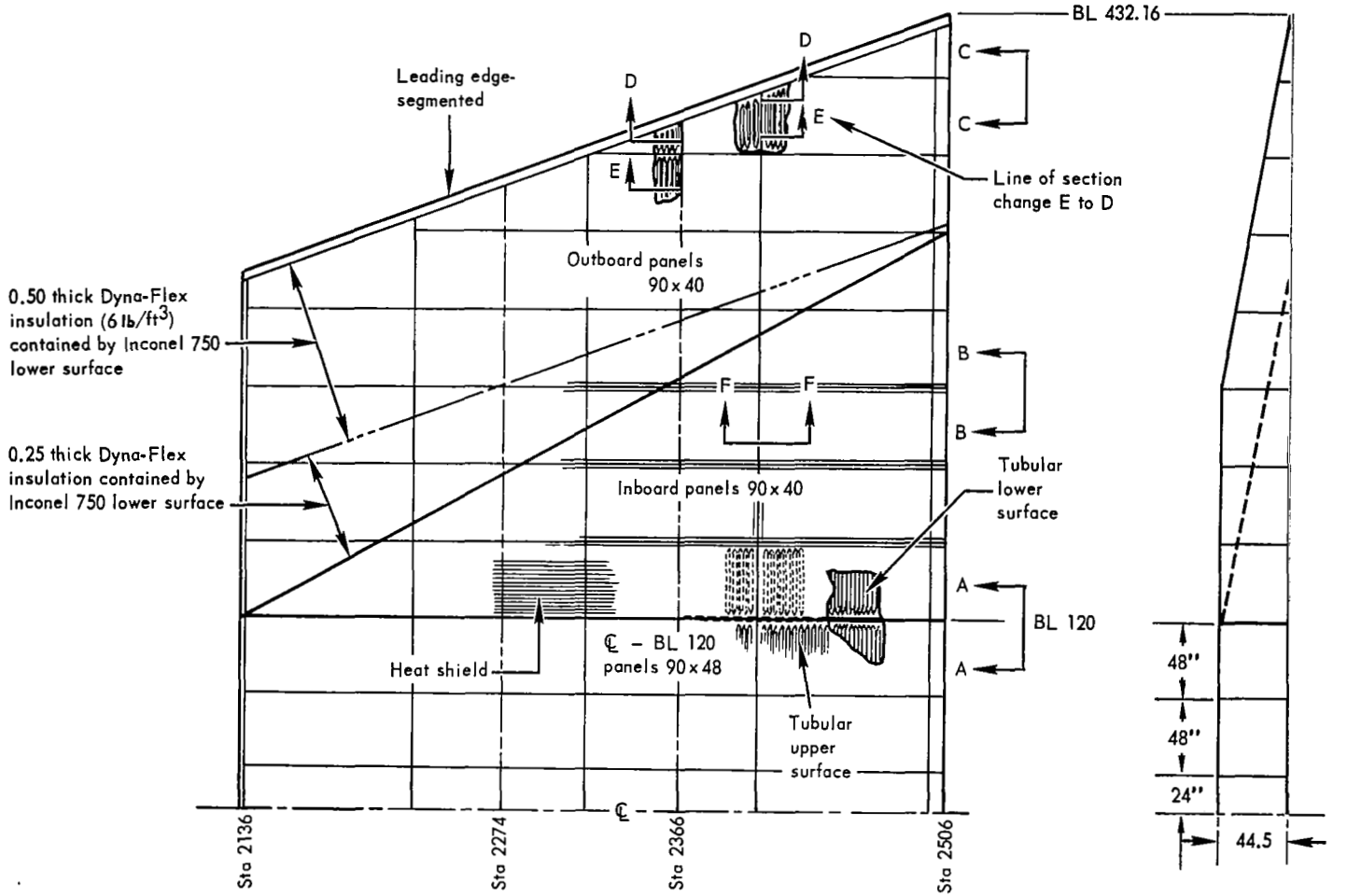

Figure 41A. Semimonocoque spanwise-stiffened tubular primary-structure concept

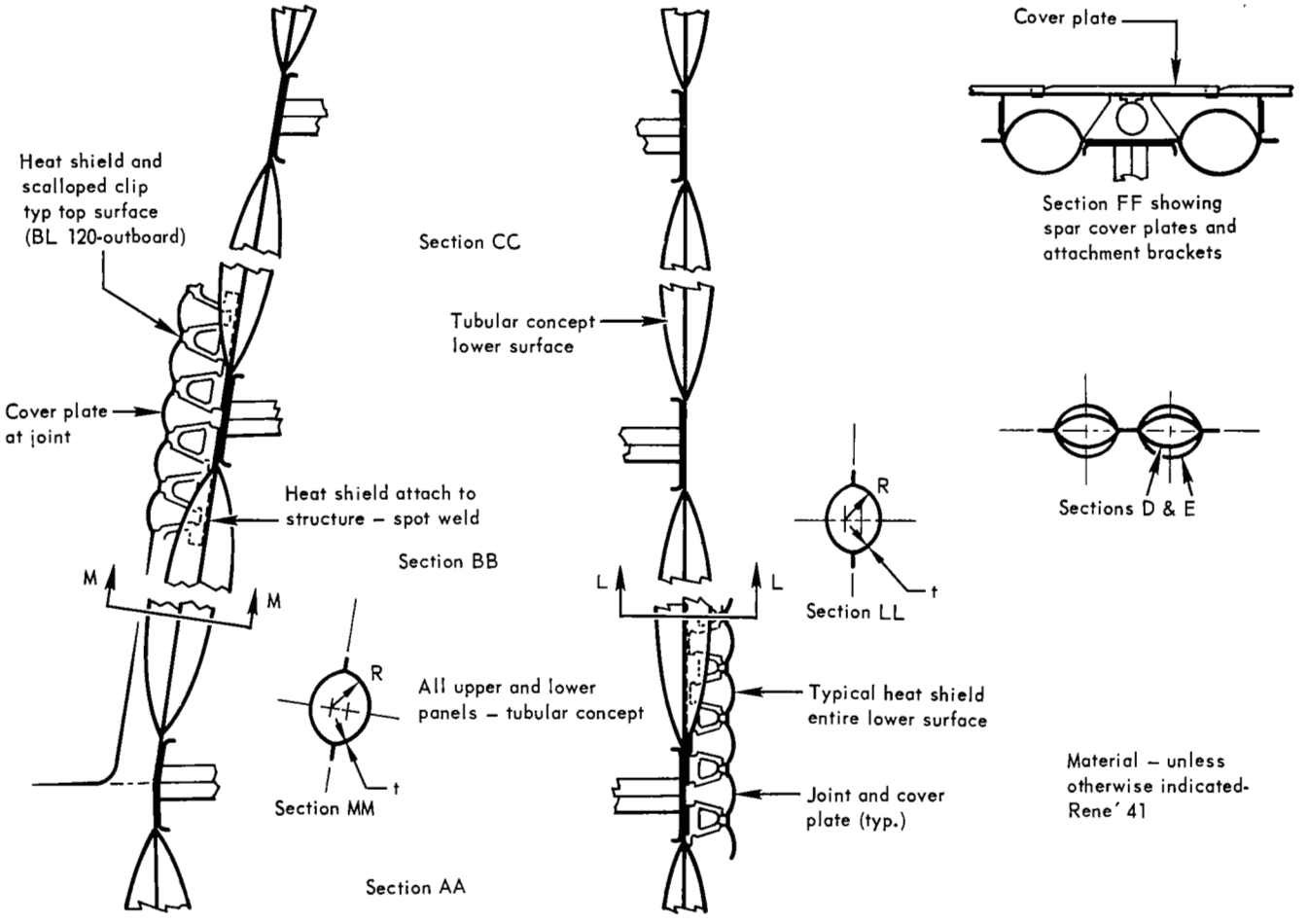

Figure 41B. Details of semimonocoque spanwise-stiffened tubular primary-structure concept

Beaded skin: A thermal-protection arrangement with insulation on the lower surface outboard of the one-third chordline was considered. The loads of table 21 were used to evaluate the beaded structure. The beaded-panel thermal analyses were those reported in the tubular discussion (figures 37 and 38). The tubular-structure optimum 90-in. spar spacing was used for the beaded skin concept to determine total wing cross-section and various wing-element effective thicknesses as a function of rib spacing. The optimization results for inboard area B, summarized in figure 42, indicate an optimum rib spacing of 40 in. for the beaded concept.

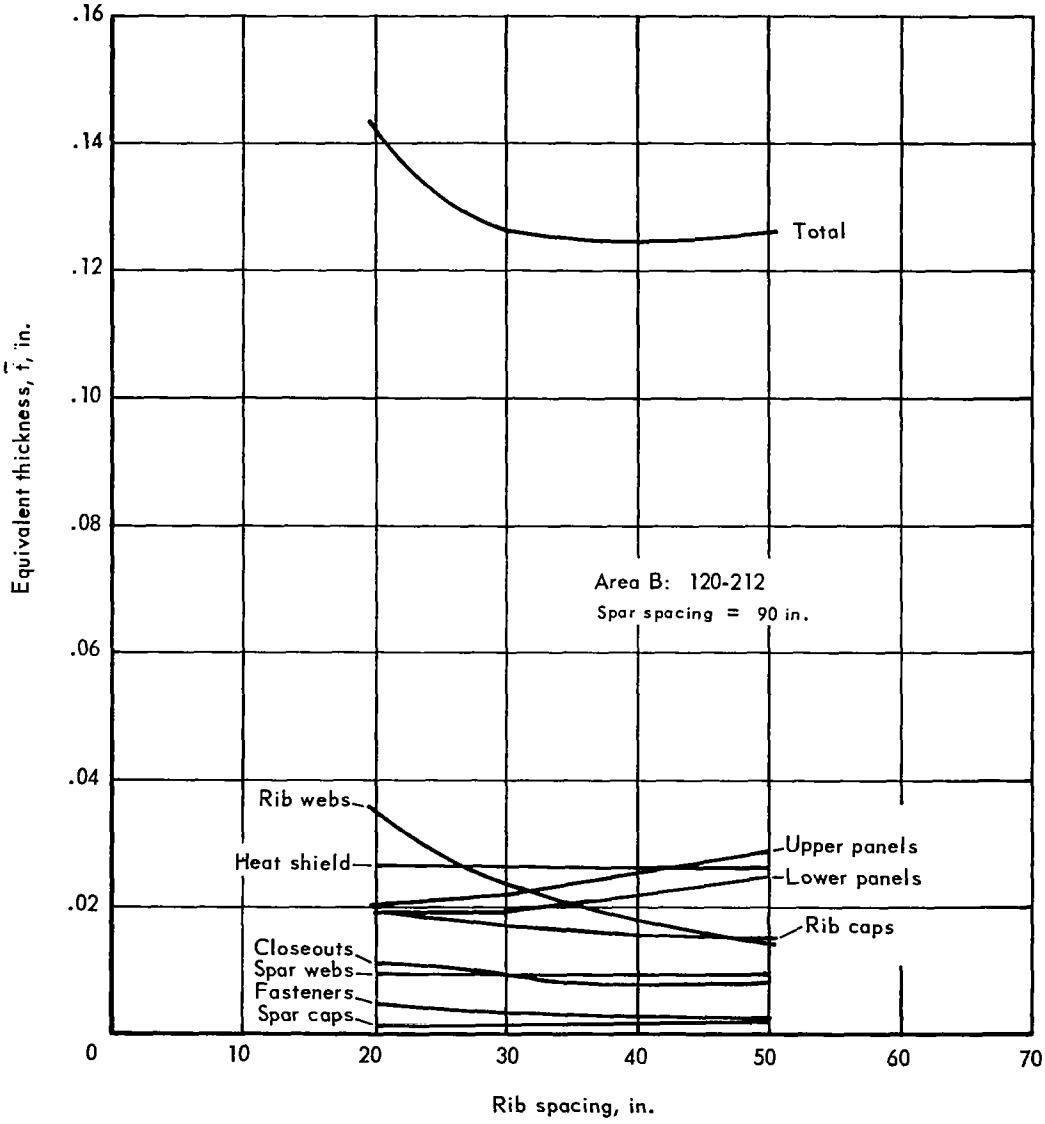

Figure 42. Optimum rib spacing for semimonocoque beaded skin concept

This same type of rib-spacing optimization was accomplished for areas A and C of the wing investigation section. In all cases, the rib spacing for minimum wing $\bar{t}$ was low enough that minimum-gage (0.015-in.) rib webs were sufficient.

The refurbishable corrugated heat shield with multiple supports was used in this analysis. Oxidation weight was based on a depth of oxide penetration commensurate with the exposure time and temperature.

A summary of the beaded-panel geometry is presented in table 24 for the center, inboard, and outboard areas of the wing section investigated. The panel gages shown in table 24 range from minimum gage of $t = 0.015$ to $t = 0.020$. To provide heat-shield support-clip attachment surfaces, the flats between beads were set at 0.50 in. The beaded-panel semiapex angle was held constant at 77.5 deg, as in the intermediate sizing.

A detail breakdown of wing equivalent thicknesses and weights is shown in table 25 for primary structural panels, rib and spar caps, panel closeouts, webs and posts, Dyna-Flex insulation, corrugated heat shields, oxidation losses, and fasteners. A spanwise weight distribution was used to obtain an average unit weight of 5.06 lb/ft^2 for the entire wing cross-section. The primary-structure panels are approximately 45 percent of the total wing weight.

TABLE 24. – FINAL GEOMETRY FOR SEMIMONOCOQUE SPANWISE-STIFFENED BEADED PANELS

Wing Area	Surface	$\bar{t}$, in.	t, in.	R, in.	L, in.	Pitch, in.
A $\mathcal{L}_L$ - BL 120	Upper	0.0263	0.020	1.150	50	5.491
	Lower	0.0196	0.015	1.050	50	5.100
B BL 120-212	Upper	0.0262	0.020	1.100	40	5.296
	Lower	0.0224	0.017	1.250	40	5.881
C BL 212-350	Upper	0.0221	0.017	0.900	40	4.515
	Lower	0.0197	0.015	1.150	40	5.491

$\bar{t}$ = panel equivalent thickness.
L = panel length (rib spacing).
b = 0.5 in. flat.
Critical flight condition all wing areas = +2.0 g.

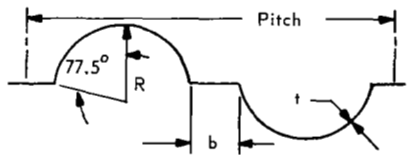

TABLE 25. – DETAIL BREAKDOWN OF WING WEIGHTS FOR SEMIMONOCOQUE SPANWISE-STIFFENED BEADED CONCEPT WITH FULL HEAT SHIELDS AND LOWER SURFACE OUTBOARD INSULATION

Item	Equivalent thickness, $\bar{t}$, in.		
	Center, A	Inboard, B	Outboard, C
Panels			
Upper	0.0263	0.0262	0.0221
Lower	0.0196	0.0224	0.0197
Caps			
Spar, Upper	0.0011	0.0011	0.0011
Spar, Lower	0.0011	0.0011	0.0011
Rib, Upper	0.0027	0.0028	0.0032
Rib, Lower	0.0032	0.0034	0.0028
Closeouts			
Upper	0.0037	0.0038	0.0030
Lower	0.0040	0.0053	0.0036
Webs			
Spar	0.0084	0.0096	0.0047
Rib	0.0151	0.0180	0.0120
Posts	0.00042	0.00050	0.00029
Insulation	–	–	0.00685
Heat shield	0.0131	0.0263	0.0358
Oxidation	0.00254	0.00173	0.00602
Fasteners	0.00254	0.00294	0.00294
Total, in.	0.1039	0.1253	0.1252
Unit wt., lb/ft^2	4.46	5.38	5.37
Average unit wt., lb/ft^2		5.06	

[a]Area A: a = 90 in., b = 50 in.

Area B and C: a = 90 in., b = 40 in.

The final structural design for the beaded concept is shown in figures 43A and 43B. The panel dimensions are 90 in. by 48 in., 90 in. by 40 in., and 90 in. by 40 in., respectively, for the three sections from center to outboard. Other design aspects of figure 43 for the beaded concept are the same as discussed earlier for the tubular concept.

Semimonocoque chordwise concept. – The primary-structure weight for the concept with tubular lower surface and convex-beaded upper surface was determined with insulation on the lower surface outboard of the one-third chordline. From the panel-sizing results of the intermediate screening, which were based on the loads obtained from the intermediate screening redundant-model analysis, the equivalent extensional and shear stiffnesses of the tubular lower surface and convex-beaded upper surface concept were input into the final redundant-model loads analysis. As in the case of the spanwise concept investigation, thermal data ($\alpha \Delta T$) for each flight condition were based on the temperatures obtained from a detailed transient thermal analysis at 30 wing locations with insulation at the lower surface outboard area. The chordwise redundant-model internal loads are shown in table 26.

Detailed transient thermal analyses were conducted to determine local stresses and deflections caused by temperature gradients through the panel structure. Isotherms were derived. Figures 44 and 45 show structure and heat-shield temperatures for the shielded lower surface with insulation outboard arrangement (+2.0-g condition).

The 60-deg circular-arc (sine wave) rib webs were analyzed for the total minimum $\bar{t}$ across wing areas A, B, and C for shear stability. A rib spacing of 60 in. in the center (one-half fuselage) and 75 in. in the inboard B and outboard C areas allowed minimum-gage webs of 0.015-in. René 41 to be used.

Using these rib spacings, total wing cross-section and various wing-element equivalent thicknesses were determined as a function of spar spacing. The optimization results for inboard area B (BL 120 to BL 212), summarized in figure 46, indicate an optimum spar spacing of 30 in., but the minimum-weight spar spacing when areas A, B, and C were optimized was 24 in., for this concept. In all cases, the spar spacing for minimum wing weight was low enough for minimum-gage (0.015-in.) spar webs to be used.

The tubular semiapex angle and the convex-beaded inner semiapex angle were held constant at 77.5 deg. The bead height-to-width ratio for the unshielded convex-beaded surfaces was held constant at 0.10 to reduce performance (aerodynamic drag) penalties.

As a result of the heat-shield evaluation described later, the refurbishable corrugated heat shield with multiple supports was used in this analysis. Oxidation weight was based on a depth of oxide penetration commensurate with the exposure time and temperature.

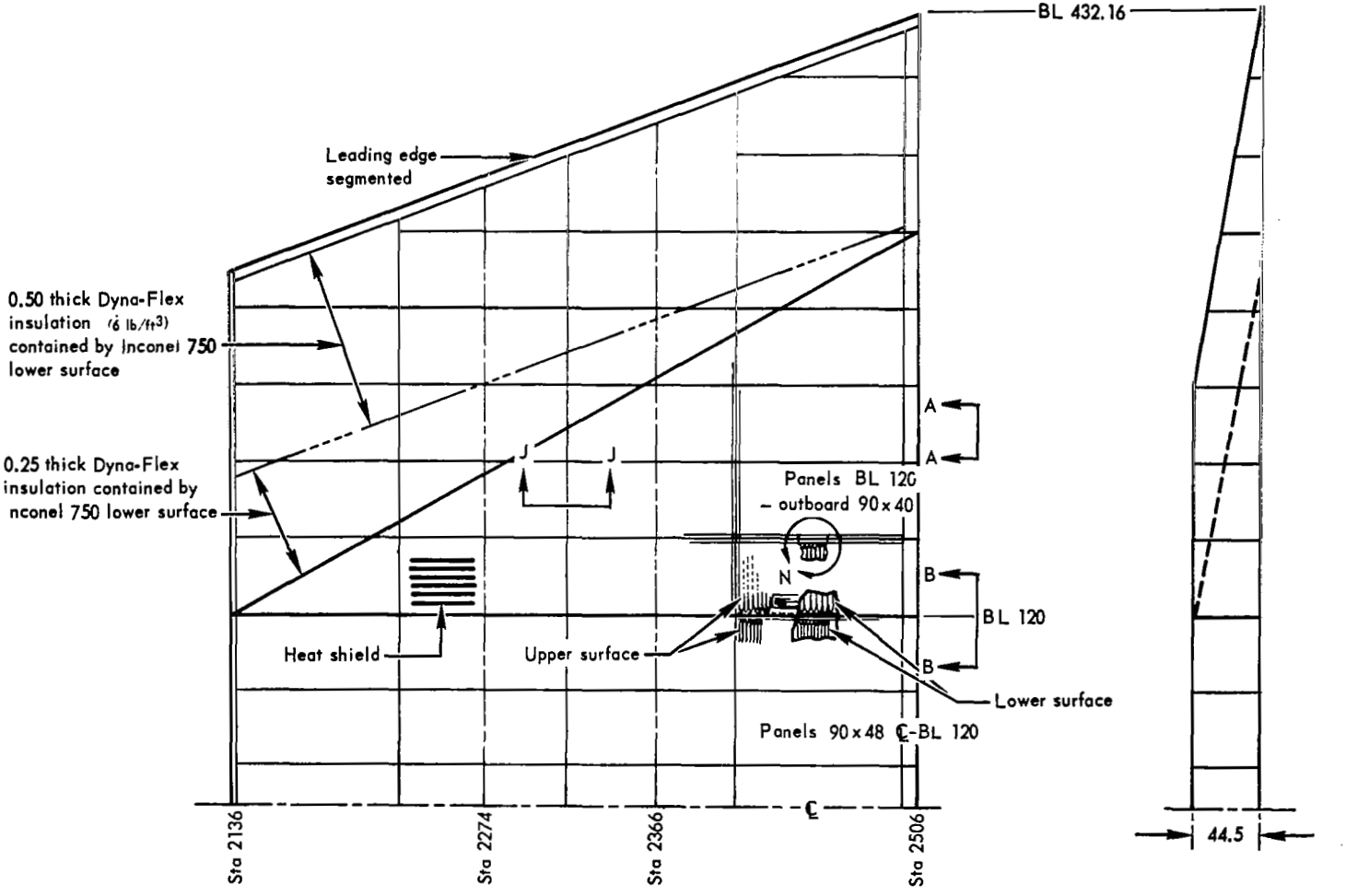

Figure 43A. Semimonocoque spanwise-stiffened beaded primary-structure concept

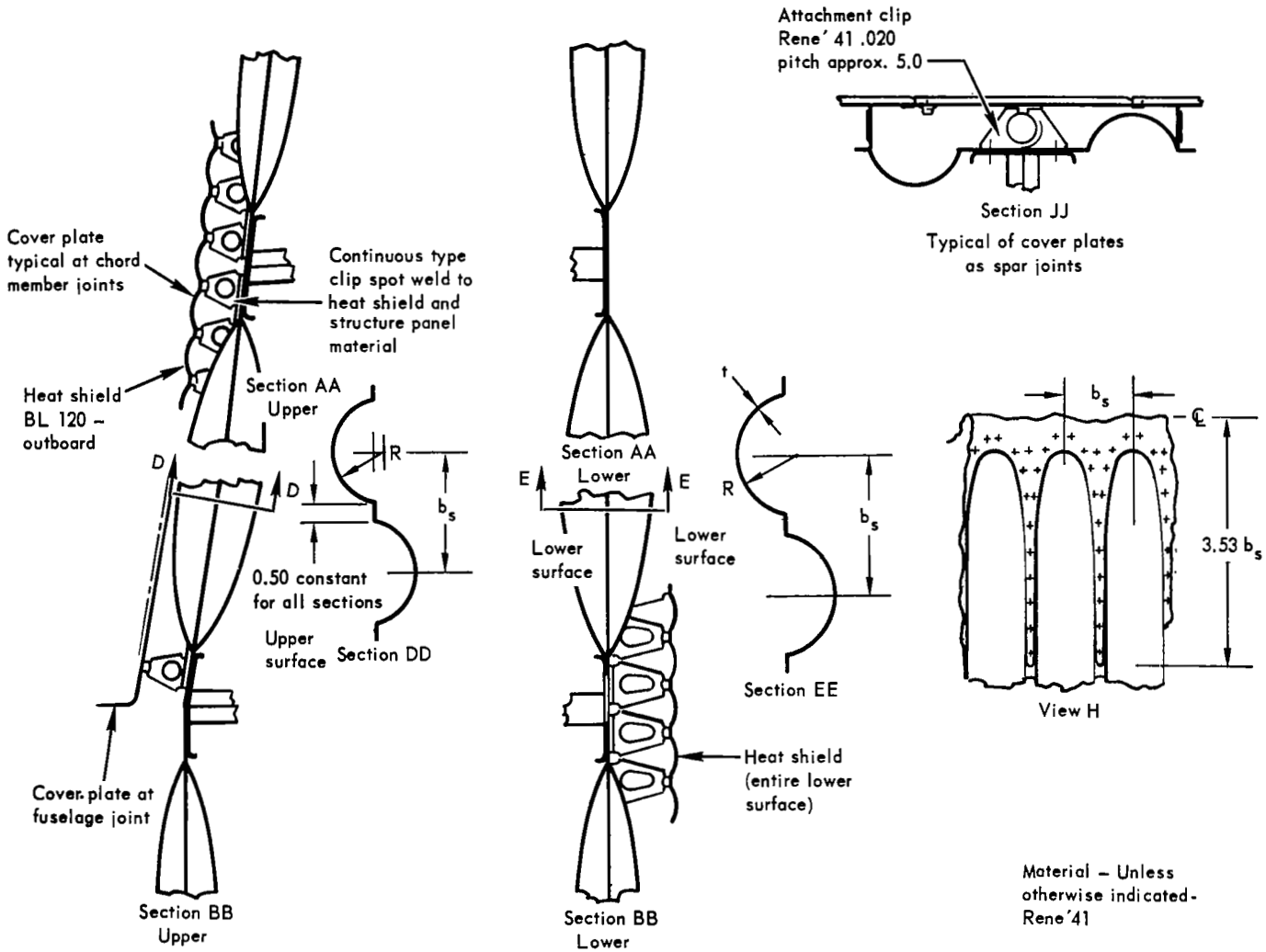

Figure 43B. Details of semimonocoque spanwise-stiffened beaded primary-structure concept

TABLE 26. – FINAL REDUNDANT-MODEL LOADS FOR SEMIMONOCOQUE CHORDWISE-STIFFENED PANELS

Wing panel location	Direction	Ultimate loads, lb/in.[a]					
		-0.5-g condition		+2.0-g condition		Cruise condition	
		Upper	Lower	Upper	Lower	Upper	Lower
$\mathcal{L}$ - BL 120 Area A	N_x	-50(470)	-157(138)	-300(320)	-547(-280)	-142(-1205)	-253(-950)
	N_y	182(143)	-153(156)	-992(78)	885(60)	-443(-217)	405(-145)
	N_{xy}	-12(17)	14(22)	-54(38)	19(-17)	-24(44)	4(19)
BL 120 to BL 212 Area B	N_x	-55(25)	-168(190)	-353(658)	-680(-327)	-155(1153)	-315(-283)
	N_y	64(94)	-31(140)	-965(27)	865(99)	-420(-151)	380(-70)
	N_{xy}	-24(115)	-37(46)	-461(206)	359(-38)	-191(190)	155(-39)
BL 212 to BL 350 Area C	N_x	-62(-600)	-72(-40)	-146(-120)	-138(-160)	-134(1077)	-50(159)
	N_y	20(-169)	-4(61)	-418(-144)	433(95)	-181(-20)	186(34)
	N_{xy}	-16(-339)	9(-59)	-290(-220)	425(64)	-122(269)	175(79)

[a]Values within parentheses are thermal loads; values not within parentheses are airloads; negative values indicate compression; positive values indicate tension.

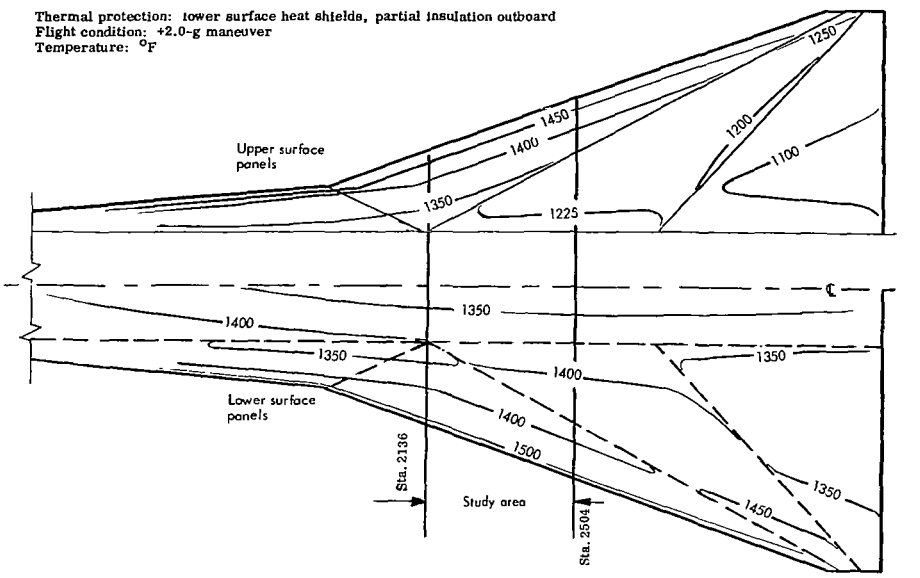

Figure 44. Primary-structure temperatures for chordwise-stiffened concept

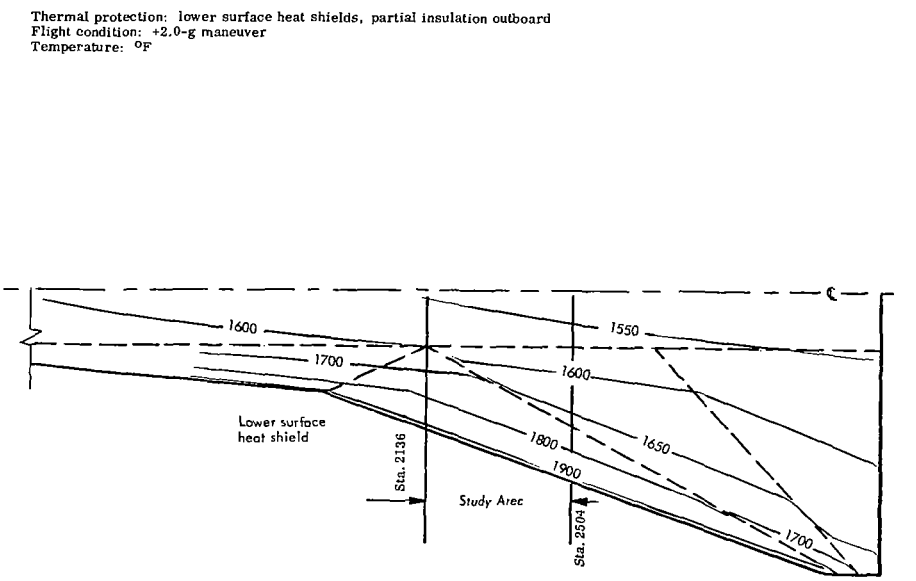

Figure 45. Heat-shield temperatures for chordwise-stiffened concept

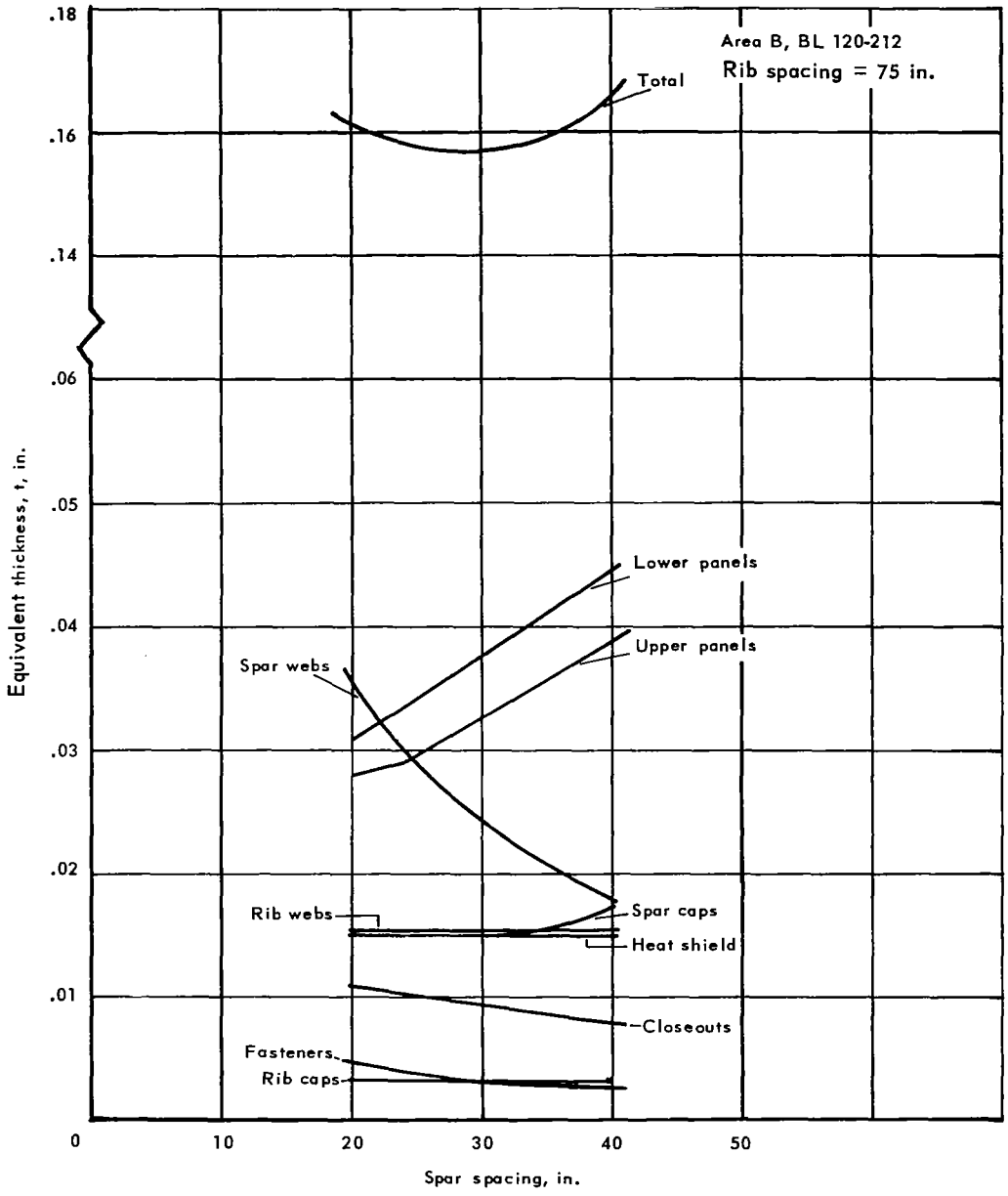

Figure 46. Optimum spar spacing for semimonocoque chordwise-stiffened concept

A summary of the final panel configuration is presented in table 27 for the center, inboard, and outboard areas of the wing-section investigation. As indicated, the tubular-panel thicknesses range from minimum gage (t = 0.010 in.) to 0.013 in. The convex-beaded panel gages are near minimum gage (t_{upper} = 0.015 in., and t_{lower} = 0.010 in.) for Area B and slightly larger than minimum gage at Area C.

The detail breakdown of wing equivalent thicknesses and weights for the convex-beaded/tubular concept is shown in table 28 for primary-structure panels, and close-outs, rib and spar caps, webs and posts, Dyna-Flex insulation, corrugated heat shield, oxidation losses, and fasteners. A spanwise weight distribution was used to obtain an average unit weight of 6.67 lb/ft^2 for the entire wing cross-section. The primary-structure panels represent approximately 40 percent of the total wing weight.

The final structural design for the chordwise concept shown in figures 47A and 47B has panel dimensions of 60 in. by 24 in. for the center area and 75 in. by 24 in. for the inboard and outboard areas. The vertical webs and caps are similar in design to those of the spanwise concept.

The lower surface, which is the only surface requiring thermal protection, is shielded from aerodynamic heating by a corrugated heat shield supported on truss-type clips (multiple supports). Dyna-Flex insulation, packaged in Inconel foil, is located on the lower outboard wing surface.

Statically determinate concept. – The statically determinate structure is a series of spanwise-stiffened beams, decoupled at the chordwise-rib intersections. The slip joints at the beam-rib intersections provide vertical shear continuity only, thereby maintaining the wing contour (shape) but providing neither bending nor axial load paths. Thus, the minimum-weight semimonocoque spanwise-stiffened construction was the logical choice for the detailed statically determinate analysis. Heat shields covered all exposed surfaces and three thermal-protection arrangements were considered: (1) no insulation, (2) insulation on the lower surface of the center A and inboard B areas, and (3) insulation at the lower surface outboard of the one-third wing chordline.

The second thermal-protection arrangement (inboard) was studied to investigate structural temperatures even lower than 1600°F to provide minimum-gage panel designs, since the spanwise loads were low. Because of noncontinuous slip-jointed ribs and the allowable wing rotation at the fuselage, wing-to-fuselage temperature compatibility is not important in this concept.

TABLE 27. – FINAL GEOMETRY FOR SEMIMONOCOQUE CHORDWISE-STIFFENED TUBULAR AND CONVEX-BEADED PANELS

Panel Concept	Area	Surface	$\bar{t}$, in.	t, in.	R, in.	Pitch, in.	Critical Condition
Tubular	A $\mathrm{C_L}$–BL 120	Upper	0.0286	0.011	0.900	2.257	Cruise
	A $\mathrm{C_L}$–BL 120	Lower	0.0261	0.010	0.950	2.355	Cruise
	B BL 120–212	Lower	0.0337	0.013	0.850	2.160	+2.0-g
	C BL 212–350	Lower	0.0254	0.010	0.600	1.672	-2.0-g

Convex Beaded	Area	Surface	$\bar{t}$, in.	t_u in.	t_ℓ in.	R_u in.	R_ℓ in.	Pitch, in.	Critical Condition
	B BL 120–212	Upper	0.0292	0.016	0.010	2.031	0.800	2.062	+2.0-g
	C BL 212–350	Upper	0.0382	0.022	0.012	2.538	1.000	2.453	-0.5-g

Panel length = 24 in. (spar spacing)
b = 0.5 in. flat
$\bar{t}$ = panel equivalent thickness

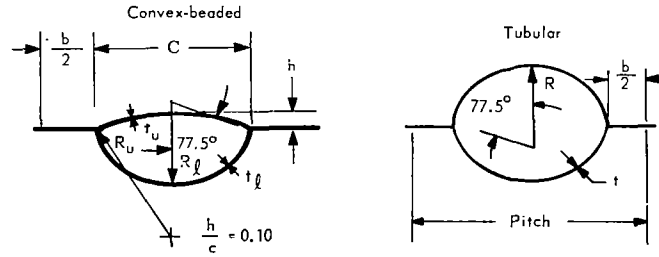

TABLE 28. – DETAIL BREAKDOWN OF WING WEIGHTS FOR SEMIMONOCOQUE CHORDWISE-STIFFENED TUBULAR/CONVEX-BEADED CONCEPT WITH FULL LOWER SURFACE HEAT SHIELD AND OUTBOARD LOWER SURFACE INSULATION

Item	Equivalent thickness, $\bar{t}$, in.		
	Center, A	Inboard, B	Outboard, C
Panels			
Upper	0.0286	0.0292	0.0381
Lower	0.0261	0.0337	0.0254
Caps			
Spar, Upper	0.0070	0.0069	0.0051
Spar, Lower	0.0070	0.0083	0.0041
Rib, Upper	0.00167	0.00163	0.00145
Rib, Lower	0.00167	0.00163	0.00145
Closeouts			
Upper	0.00865	0.00420	0.00491
Lower	0.00805	0.00613	0.00348
Webs			
Spar	0.0329	0.0300	0.0176
Rib	0.0150	0.0155	0.0056
Posts	0.00131	0.0010	0.00058
Insulation	–	–	0.00685
Heat shields	0.0143	0.0143	0.0230
Oxidation	0.00525	0.00173	0.00588
Fasteners	0.0044	0.0041	0.0041
Total, in.	0.1619	0.1584	0.1476
Unit wt, lb/ft^2	6.95	6.80	6.33
Average unit wt, lb/ft^2		6.67	

[a]Area A: a = 24 in., b = 60 in.

Area B and C: a = 24 in., b = 75 in.

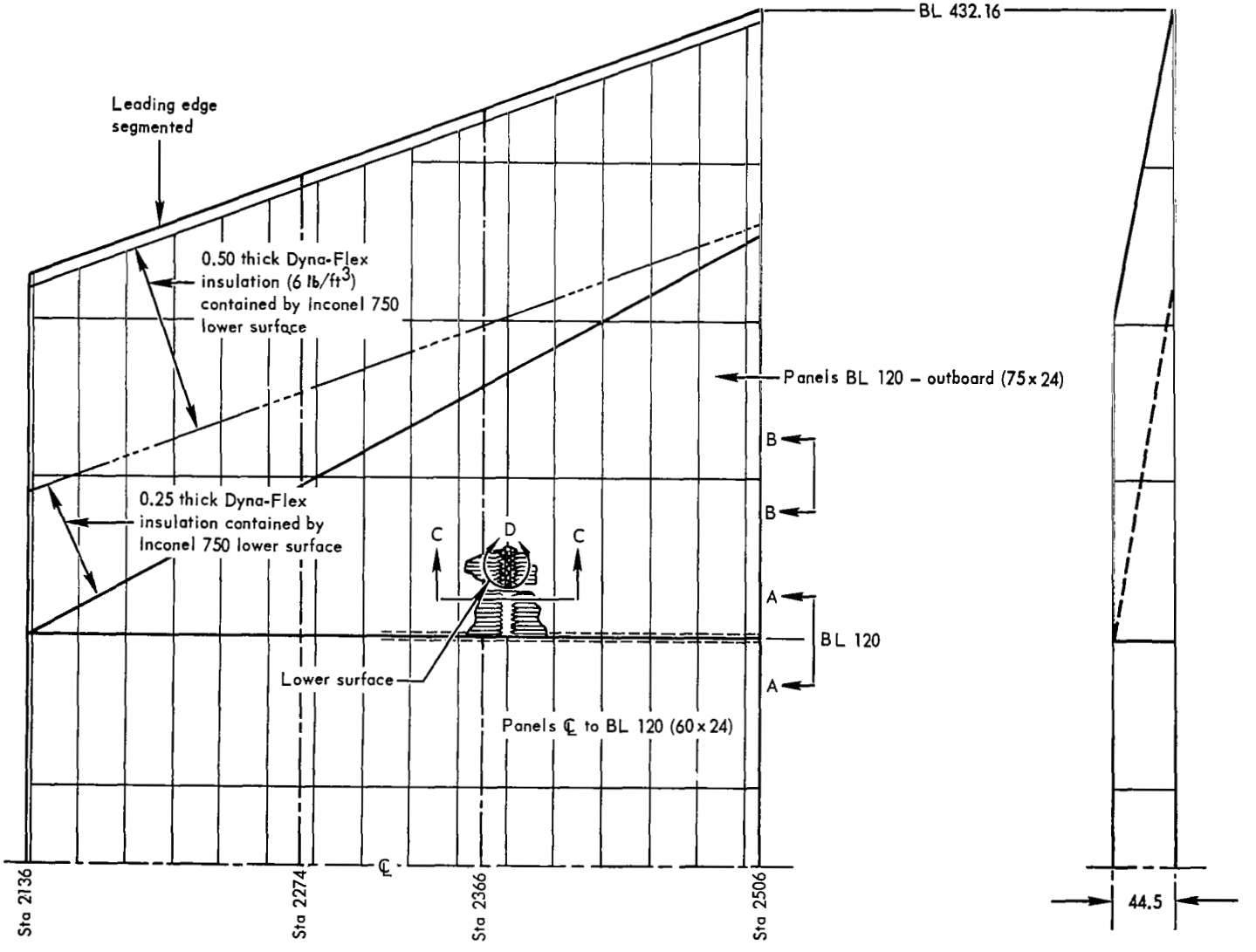

Figure 47A. Semimonocoque chordwise-stiffened primary-structure concept

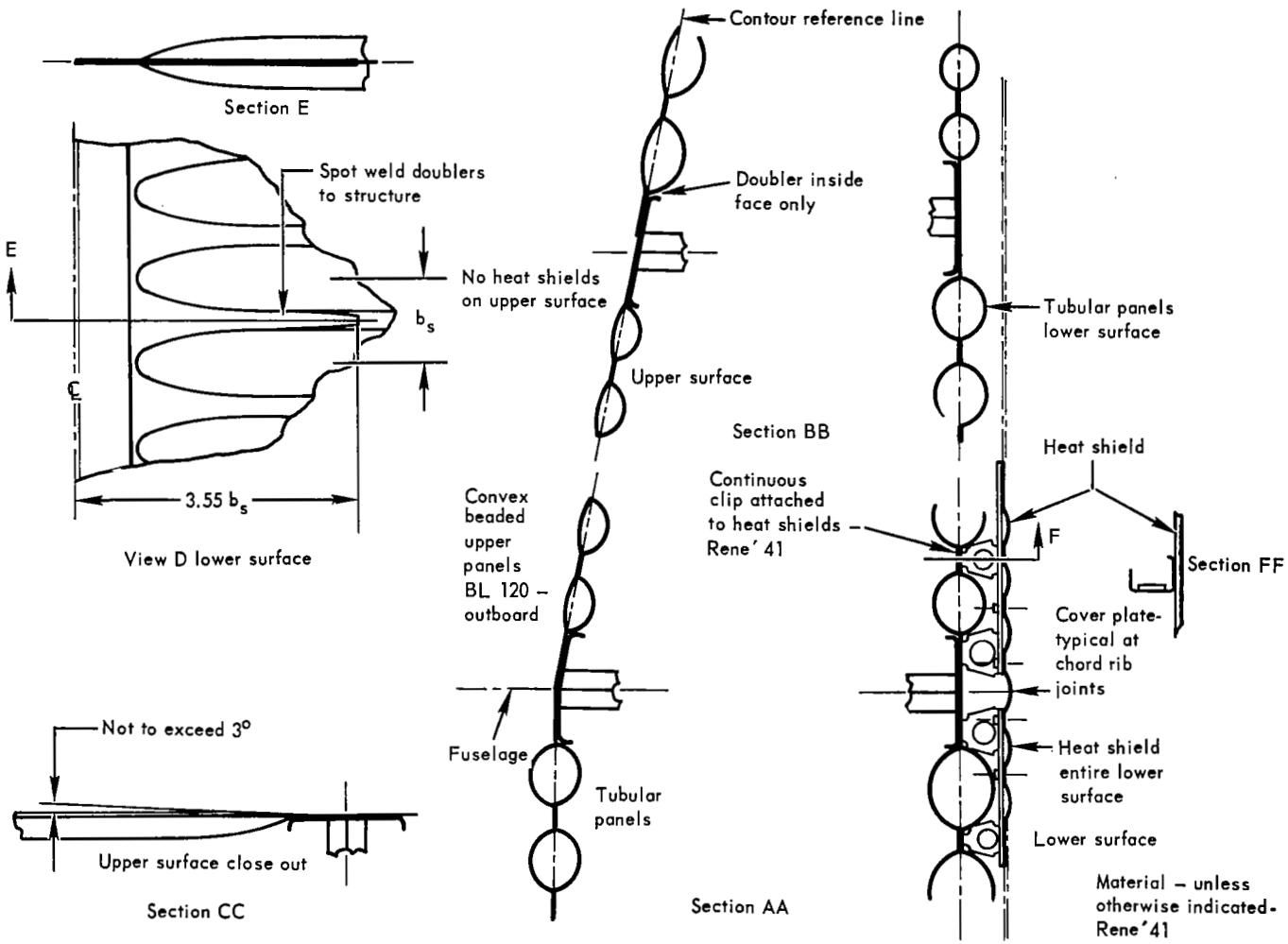

Figure 47B. Details of semimonocoque chordwise-stiffened primary-structure concept

Detailed transient thermal analyses were conducted for the thermal-protection arrangements to determine local stresses and deflections from temperature gradients through the panel structure.

Isotherms were derived for the various thermal-protection arrangements. Figures 48 and 49 show structure and heat-shield temperatures for the thermal-protection arrangement which has no insulation on the lower surface (+2.0-g condition).

To obtain final internal loads, the statically determinate redundant-model was economically developed by decoupling the chordwise bending and axial stiffnesses across the spars of the spanwise redundant model. From the semimonocoque spanwise intermediate-screening panel-sizing results, which were based on the intermediate-screening redundant-model loads analysis, the equivalent extensional and shear stiffenesses were input into the final redundant-model analysis. Thermal data based on no insulation and external loads were input for each flight condition, resulting in the internal loads shown in table 29. Good agreement between the input and the actual final stiffnesses calculated were noted. Because the ribs are discontinuous for this concept, the chordwise airloads and thermal loads are zero, as indicated in table 29. Also, the spanwise thermal loads are small, providing a minimum-thermal-stress wing concept.

In determining optimum rib and spar spacings, surface panels, caps, webs, heat shields, closeouts, fasteners, oxidation penetration, vertical posts, and slip-joint assemblies at each rib and spar intersection were considered. Surface panels were analyzed for the most critical condition, the +2.0-g maneuver. A spar spacing of 90 in. was used, since it permitted use of minimum-gage webs of 0.015-in. thickness for the semimonocoque spanwise concepts; however, with the use of two spars at the end of each panel bay in the statically determinate concept, a possibly greater span spacing can be used to reduce weight. With this spar spacing, the rib spacings were varied to determine element sizes and total wing weights. The optimization results for the inboard area B (BL 120 to BL 212) shown in figure 50 indicate an optimum rib spacing of 50 in. for the beaded concept with no insulation. This same type of rib-spacing optimization was made for the various insulated arrangements at the center, inboard, and outboard areas of the wing investigation section. All rib spacings resulted in the use of minimum-gage rib webs (0.015 in.)

Structural sizing was not conducted for the third thermal-protection arrangement, with insulation only on the lower surface outboard area, since the outboard panels for the no-insulation arrangement were minimum gage (t = 0.015 in.) for the lower surface and near minimum gage (0.016 in.) for the upper surface. Therefore, the use of insulation, with its required packaging, would increase the wing weight above the saving of 0.001 in. on the upper surface.

A summary of unit weights for no-insulation and two thicknesses of insulation inboard, presented in table 30, indicates a slight weight advantage for the no-insulation arrangement. Therefore, the fully shielded statically determinate concept with no insulation was selected for detailed cost, performance, and reliability evaluation.

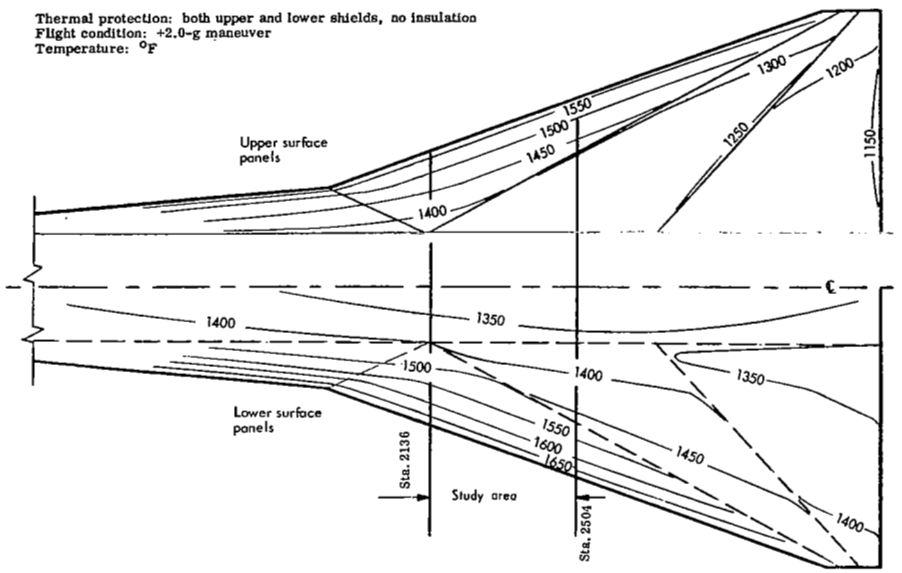

Figure 48. Temperature isotherms for shielded statically determinate structural panels

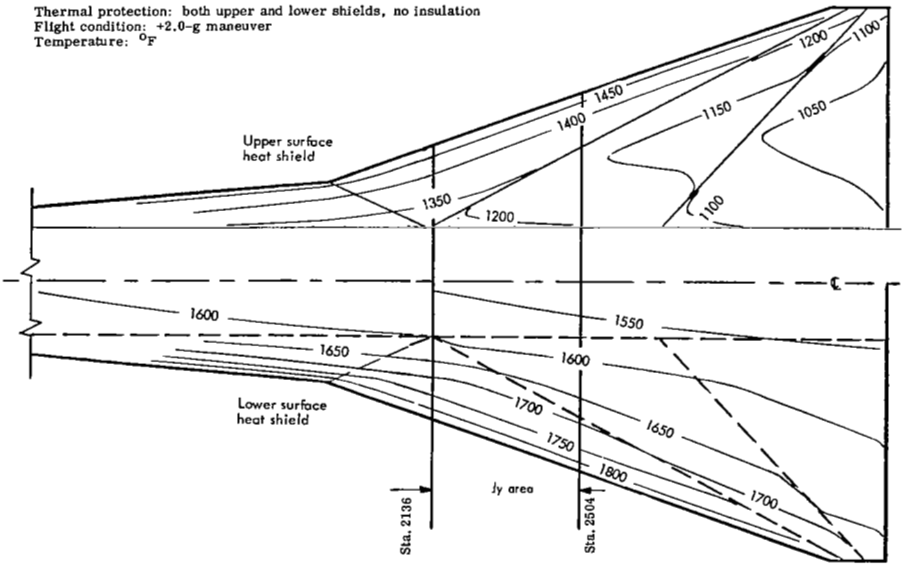

Figure 49. Heat-shield temperatures for shielded statically determinate structural panels

TABLE 29. – FINAL REDUNDANT-MODEL LOADS FOR STATICALLY DETERMINATE SPANWISE-STIFFENED PANELS (AVERAGE LOADS BETWEEN STA. 2274 AND 2366)

Wing panel location	Direction	Ultimate loads, lb/in.[a]					
		-0.5-g condition		+2.0-g condition		Cruise condition	
		Upper	Lower	Upper	Lower	Upper	Lower
$\mathcal{L}$ - BL 120 Area A	N_x	0(0)	0(0)	0(0)	0(0)	0(0)	0(0)
	N_y	181(-35)	-180(35)	-616(-118)	616(118)	-293(-14)	291(15)
	N_{xy}	0(0)	0(0)	0(0)	0(0)	0(0)	0(0)
BL 120 to BL 212 Area B	N_x	0(0)	0(0)	0(0)	0(0)	0(0)	0(0)
	N_y	76(-45)	-77(37)	-535(-65)	535(65)	-245(40)	246(-25)
	N_{xy}	13(-10)	-13(9)	-147(-16)	147(16)	-43(-8)	65(12)
BL 212 - outboard Area C	N_x	0(0)	0(0)	0(0)	0(0)	0(0)	0(0)
	N_y	29(-85)	-28(81)	-201(-35)	201(27)	-92(10)	89(-10)
	N_{xy}	11(-107)	-7(107)	-119(-40)	119(40)	-52(5)	52(-5)

[a]Values within parentheses are thermal loads; values not within parentheses are airloads; negative values indicate compression; positive values indicate tension.

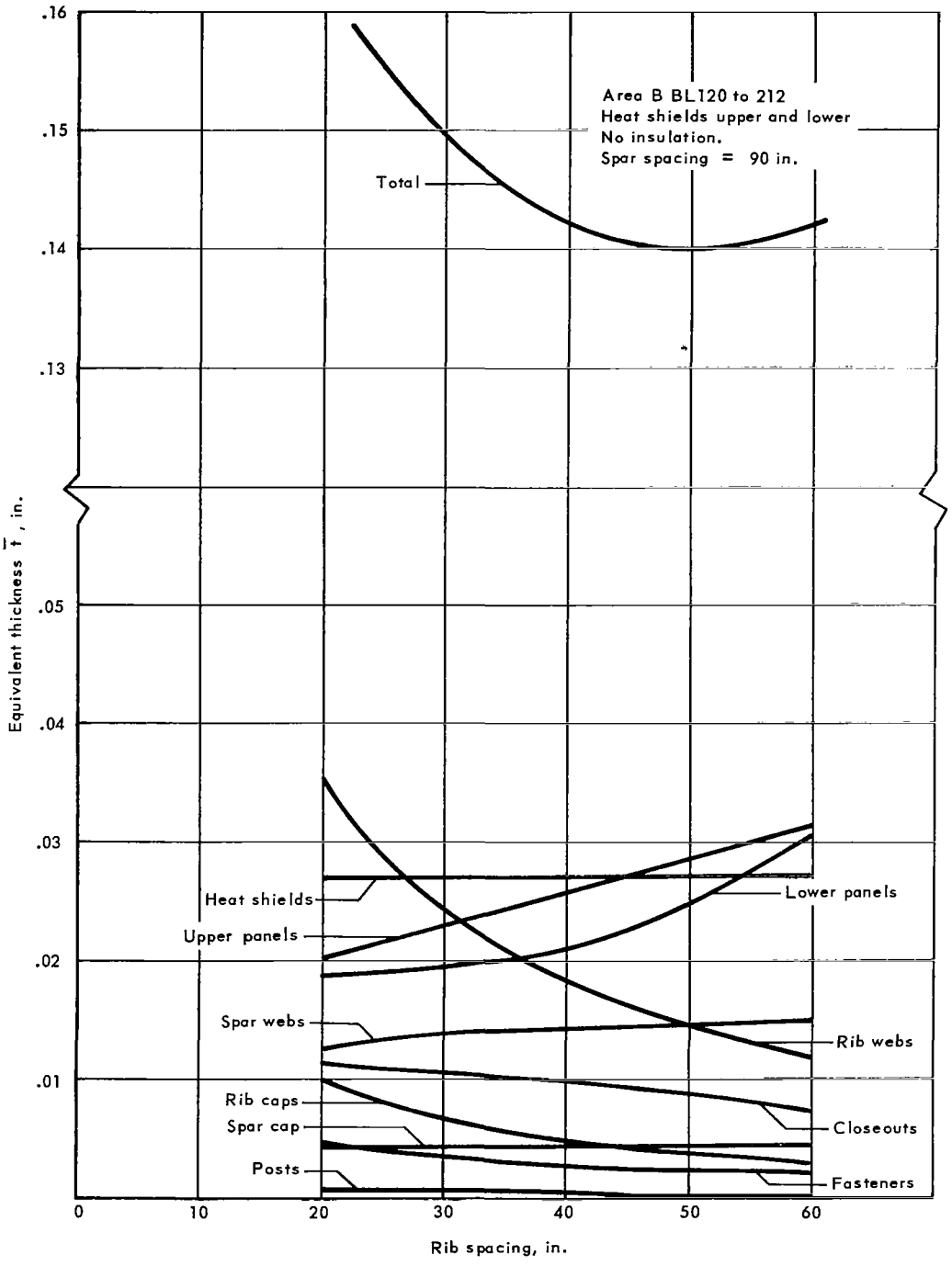

Figure 50. Optimum rib spacing for statically determinate beaded concept

TABLE 30. – WEIGHTS OF STATICALLY DETERMINATE CONCEPTS WITH VARIOUS THERMAL-PROTECTION ARRANGEMENTS

Panel concept[a]	Thermal-protection system[b]	Item, in. $\frac{\bar{t}}{L}$ [c]	Center Area A	Inboard Area B	Outboard Area C	Average	Weight, lb/ft^2 Average
Beaded skin	Heat shields, no insulation	$\frac{\bar{t}}{L}$	$\frac{0.1214}{60}$	$\frac{0.1399}{50}$	$\frac{0.1292}{40}$	0.1293	5.550
Beaded skin	Heat shields, 1/8 in. insulation lower surface from $\mathcal{C}_L$ to BL 212 (Areas A and B)	$\frac{\bar{t}}{L}$	$\frac{0.1223}{60}$	$\frac{0.1390}{50}$	$\frac{0.1292}{40}$	0.1294	5.554
Beaded skin	Heat shields, 1/4 in. insulation lower surface from $\mathcal{C}_L$ to BL 212 (Areas A and B)	$\frac{\bar{t}}{L}$	$\frac{0.1209}{60}$	$\frac{0.1416}{50}$	$\frac{0.1292}{40}$	0.1296	5.562

[a] Lowest-weight semimonocoque spanwise-stiffened concept.

[b] Heat shields on all exposed wing areas.

[c] L = rib spacing.

A summary of the panel configuration for the selected concept is presented in table 31 for the center, inboard, and outboard areas of the wing-investigation section. As indicated, the beaded panel is near or at minimum gage except for the center A and inboard B upper surface panels which are not minimum gage because of larger compression airloads.

The beaded-panel semiapex angle was held at 77.5 deg, the same as for the spanwise concept. To provide heat-shield support-clip attachment surfaces, the flats between beads were set at 0.50 in. The corrugated heat shield with multiple supports and Dyna-Flex insulation packaged in foil was used in this analysis

The statically determinate detail breakdown of wing equivalent thicknesses and weights are shown in table 32 for primary-structure panels, panel closeouts, rib and spar caps, webs, posts, corrugated heat shield, oxidation losses, and fasteners. A spanwise weight distribution was used to obtain an average unit weight of 5.55 lb/ft^2 for the entire wing cross-section. The primary-structure panels represent approximately 35 percent of the total wing weight. The statically determinate fuselage incurs a 10 percent weight penalty over the semimonocoque and monocoque concepts due to added fuselage skin and frames, fuselage local fittings and reinforcements.

The final structural design for the statically determinate beaded concept is shown in figures 51A and 51B. Panel dimensions are 90 in. by 60 in. for area A, 90 in. by 50 in. for area B, and 90 in. by 40 in. for area C. A ball slip joint, providing wing-surface continuity, is located at each spar-rib intersection, with adequate tolerance to permit unrestrained thermal expansion in the chordwise direction.

Rib and spar webs are of 60-deg circular-arc corrugated (sine-wave) construction, fabricated from Rene' 41. The flanged sheetmetal rib and spar caps, which are also fabricated from Rene' 41, are melt-through welded to the vertical webs.

TABLE 31. – FINAL GEOMETRY FOR LOWEST-WEIGHT STATICALLY DETERMINATE PANELS

Wing area	Surface	$\bar{t}$, in.	t, in.	R, in.	L, in.	Pitch, in.
A $\mathcal{Q}_L$ - 120	Upper	0.0314	0.024	1.000	60	4.905
	Lower	0.0211	0.016	1.200	60	5.686
B BL 120-212	Upper	0.0291	0.022	1.300	50	6.077
	Lower	0.0253	0.019	1.600	50	7.248
C BL 212-350	Upper	0.0206	0.016	0.750	40	3.929
	Lower	0.0199	0.015	1.350	40	6.272

$\bar{t}$ = panel equivalent thickness.
L = panel length (rib spacing).
b = 0.5 in. flat.
Critical flight condition on all wing areas = +2.0-g

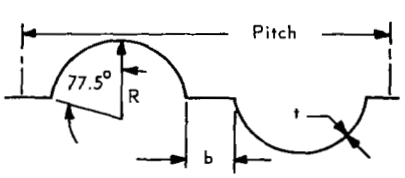

TABLE 32. – BREAKDOWN OF WING WEIGHTS FOR STATICALLY DETERMINATE PANELS WITH FULL HEAT SHIELDS AND NO INSULATION

Item		Equivalent thickness, $\bar{t}$, in.		
		Center, A	Inboard, B	Outboard, C
Panels	Upper	0.0314	0.0291	0.0206
	Lower	0.0211	0.0253	0.0199
Caps	Spar, upper	0.0022	0.0022	0.0022
	Spar, lower	0.0022	0.0022	0.0022
	Rib, upper	0.00165	0.0020	0.0025
	Rib, lower	0.00165	0.0020	0.0025
Closeouts	Upper	0.00338	0.00408	0.0026
	Lower	0.00387	0.00482	0.0041
Webs	Rib webs	0.0126	0.0144	0.0120
	Spar webs	0.0157	0.0147	0.0084
Web intersections	Total	0.00039	0.00044	0.00032
Insulation	Total		–	–
Heat shields		0.0131	0.0263	0.0359
Oxidation	Total	0.00231	0.00162	0.00714
Fasteners	Total	0.00226	0.00254	0.00294
Vertical shear fittings		0.0076	0.00819	0.00594
Total, in.		0.1214	0.1399	0.1292
Unit wt, lb/ft^2		5.21	6.00	5.54
Average unit wt, lb/ft^2			5.55	

[a]Area A: a = 90 in., b = 60 in.
Area B: a = 90 in., b = 50 in.
Area C: a = 90 in., b = 40 in.

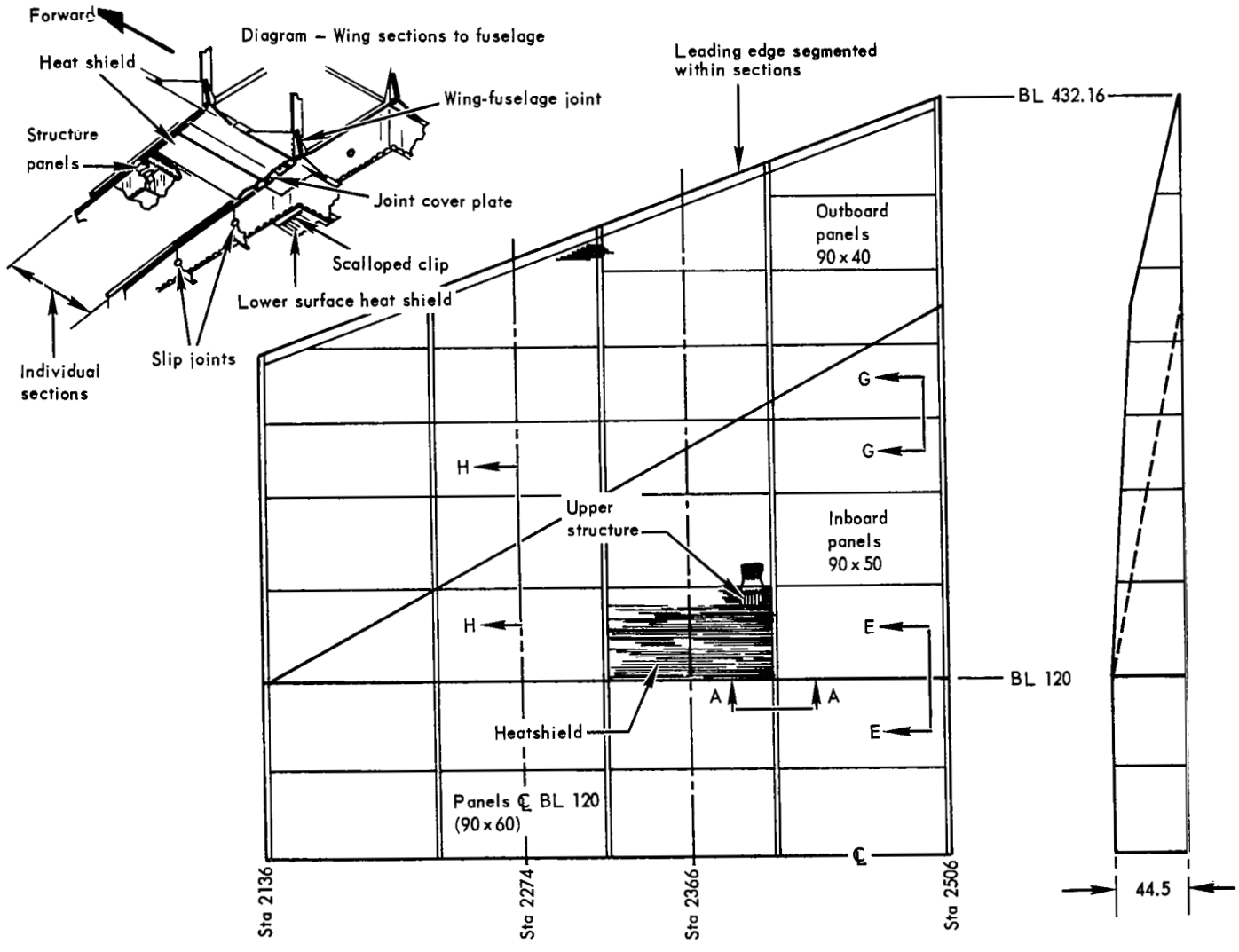

Figure 51A. Statically determinate beaded primary-structure concept

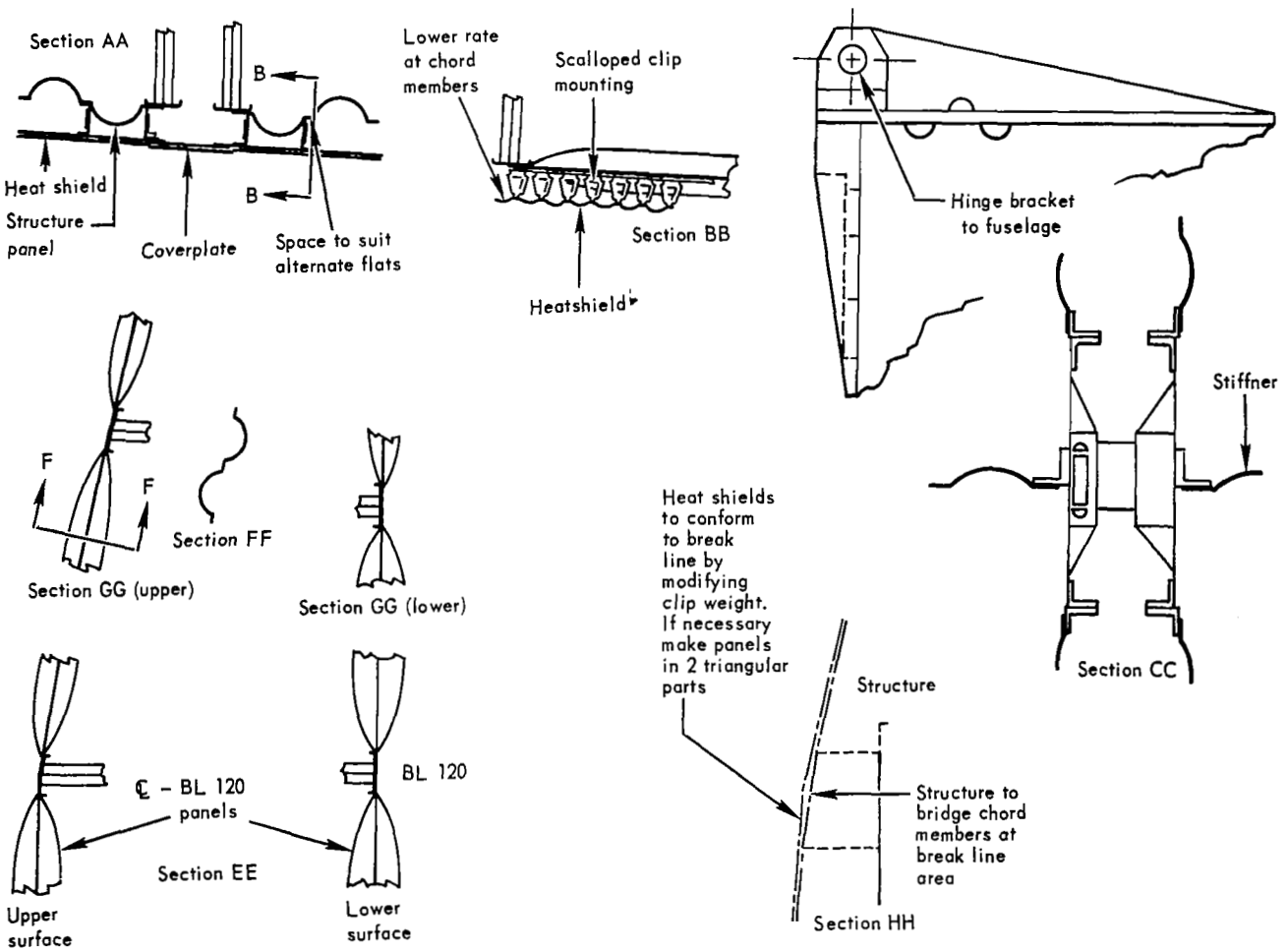

Figure 51B. Details of statically determinate beaded primary-structure concept

Primary-Structure Weight Summary

Table 33 presents a summary of the concept weights and table 34 the associated margins of safety established for each of the six structural concepts. As indicated in table 34, the margins of safety were determined for the critical ultimate flight-load condition, panel flutter, wing flutter, sonic fatigue, load fatigue, and creep.

Ultimate-load analysis. – The margins of safety for the ultimate flight load are zero or near zero for minimum-weight design. However, as presented in table 34, the load margin of safety for the beaded concept is as high as 0.43 because of the use of minimum-gage materials.

Panel-flutter analysis. – A detailed panel-flutter analysis of the concepts indicates that the panels are stable and substantially exceed the flutter factor-of-safety requirement of 1.3. The panel-flutter margins of safety are shown in table 34.

Wing-flutter analysis. – Wing flutter was investigated by applying the results of the redundant analyses to the maximum-weight climb and acceleration region of the trajectory. The investigation showed that an adequate margin on airspeed and dynamic pressure (beyond the required 1.3 factor) is available over the design flight path and that the concepts are not critical in flutter. The margins of safety for wing flutter are large, as shown in table 34.

Sonic-fatigue analysis. – Analyses conducted to determine the effects of random sound pressures on the six concepts indicate that the allowable sound-pressure level (dB/Hz) is greater than the maximum predicted sound-pressure level of the 0.007-q criterion for upper and lower surfaces for both concepts. The application of the 0.022-q criterion on the lower surface during cruise also results in root-mean-square stresses less than fatigue-limit allowable stress. The resulting margins for sonic fatigue are shown in table 34. This analysis provides an interim basis for determining the fatigue resistance of the structure on an empirically derived nominal vibratory stress of typical flight hardware. However, for the primary structures of this study, further sonic-fatigue testing is necessary to determine the actual boundary conditions and the detailed design refinements for the primary structure and its attachments.

Fatigue analysis. – Fatigue analysis was conducted to establish allowable design stress levels for primary structures to meet the life requirements specified. The load-fatigue margins of safety presented in table 34 are based on the best available data and specified assumptions. Experimental evaluation of designs with reasonable simulation of loading spectra is essential to demonstrate acceptable fatigue quality in addition to care given to detail during design and fabrication of the structural eliments.

Creep analysis. – Creep margins of safety were established for the most critical area for each concept. The effects of compressive thermal strains on creep buckling and tensile thermal strains on total plastic deformation can be neglected, due to stress relaxation. Thus, only airloads were used to determine applied stresses for creep at elevated temperatures. The allowable compressive stresses under creep conditions were determined by using isochronous stress-strain curves. The resulting margins of safety are shown in table 34.

TABLE 33. – CONCEPT WEIGHTS

Concept	Unit weight, lb/ft^2				
	Wing section A	Wing section B	Wing section C	Section average	Total wing[a] average
Monocoque					
Waffle	10.717	12.033	9.437	10.494	10.380
Honeycomb-core	6.250	6.346	6.752	6.472	6.585
Semimonocoque spanwise					
Beaded	4.457	5.377	5.374	5.060	6.197
Tubular	4.824	5.610	5.699	5.376	6.532
Semimonocoque chordwise					
Tubular	6.948	6.797	6.333	6.666	7.412
Statically determinate					
Spanwise beaded	5.210	6.005	5.542	5.550	6.769[(b)]

[a]Baseline vehicle total wing unit weight includes basic wing, elevons, and leading edge; wing area = 10 095 ft^2.

[b]Statically determinate fuselage penalty of 0.365 lb/ft^2 not included. Total wing average with penalty = 7.134 lb/ft^2.

TABLE 34. – STRUCTURAL MARGINS OF SAFETY

Concept		Ultimate load		Panel flutter[a]		Wing flutter	Sonic fatigue[b]		Load fatigue[b]		Creep[c]	
	Surface / Section	Upper	Lower	Upper	Lower		Upper	Lower	Upper	Lower	Upper	Lower
Monocoque	A	0.00	0.00	d	83.0	1.3+	11.2	9.66	5.82	4.52	2.70	4.68
Waffle	B	0.00	0.00	135.0	135.0		13.2	13.1	2.31	6.77		
	C	0.00	0.00	92.0	6.77		10.1	1.16	1.50	2.89		
	A	0.00	0.00	d	42.6	1.3+	5.54	5.90	3.01	1.89	2.28	2.59
Honeycomb-core	B	0.00	0.00	46.2	51.1		5.62	6.04	0.70	1.46		
	C	0.00	0.00	58.4	5.31		7.04	0.96	0.36	1.32		
Semimonocoque spanwise	A	0.03	0.43	d	3.00	1.3+	2.16	1.22	4.75	0.13	5.00	1.82
Beaded	B	0.04	0.30	7.90	8.69		2.76	2.51	11.33	0.54		
	C	0.04	0.30	5.71	8.79		1.80	0.18	3.05	1.06		
	A	0.00	0.10	d	2.69	1.3+	3.09	1.47	11.89	0.15	3.68	1.56
Tubular	B	0.03	0.09	7.11	5.53		2.75	2.38	8.41	0.34		
	C	0.00	0.13	5.79	3.88		1.92	0.00	1.55	0.37		
Semimonocoque chordwise	A	0.02	0.01	d	12.4	1.3+	5.16	4.84	6.78	2.78	1.14	0.68
Tubular	B	0.00	0.16	51.5	12.8		2.53	5.86	0.17	2.92		
	C	0.04	0.00	53.8	18.7		3.98	0.65	0.29	2.05		
Statically determinate	A	0.10	0.01	d	2.61	1.3+	1.88	1.17	2.58	0.003	6.35	1.42
Spanwise beaded	B	0.03	0.08	5.72	7.30		2.68	2.66	4.32	0.54		
	C	0.13	0.01	4.64	11.90		1.33	0.31	1.53	1.52		

[a](λ/λ_{CR}) value for panel flutter.

[b]MS = (F/f)-1. For sonic fatigue, F = rms stress, f = normalized stress; for fatigue, F = fatigue allowable, f = applied limit stress.

[c]Critical area ℄ to BL 120. Critical failure mode for all areas – creep buckling at t = 6680 hr, except for the chordwise concept which is critical for creep buckling at t = 30 hr.

[d]Surface not exposed to airflow.

It is of interest to note that total creep did not exceed 0.2 percent, which is an acceptable allowable creep. Consequently, it appears that it is not necessary to develop new materials with higher creep resistance than Rene' 41 for the specified life. This was not known at the time the 0.5-percent allowable creep was specified for this study; this was done in the event that 0.2-percent creep would be exceeded for all primary-structure concepts and result in excessive weight if creep were the critical design criterion. In addition, an allowance of 0.5-percent creep in present material would in the future be an actual creep of less than this when improved materials become available.

Primary-structure weight comparison. – The wing-section weight analysis resulted in the following ranking of primary-structure concepts: semimonocoque spanwise beaded, semimonocoque spanwise tubular, statically determinate spanwise beaded, monocoque honeycomb-core sandwich, semimonocoque chordwise tubular, and monocoque waffle. The tubular panel is the most efficient concept for inplane compression loadings, and the beaded panel is the most efficient concept for bending loads. However, if bending due to normal pressure is the design mode, as it is for the wing since optimum panels are large, the beaded concept is considerably lower in weight than the tubular concept. Therefore, it is concluded that caution should be applied in using only inplane compression weight-strength data for concept selection.

The spanwise concepts are lower in weight than the chordwise concepts. Spanwise panel orientation provides support of lift forces without increased spar cap area, as required with chordwise panel orientation. Probably more significant, however, is the effect that chordwise bending stiffness has on thermal load in the wing. A greater temperature gradient exists through the depth of the wing than through the fuselage. Consequently, the wing, if not integrally fastened to the fuselage, would bow more than the fuselage in the chordwise direction. However, the wing and fuselage are integrally attached, and the higher the chordwise wing stiffness the greater the forced body bending. The chordwise-stiffened wing bends the fuselage more than the spanwise-stiffened wing, which is relatively flexible in the chordwise direction since it derives its chordwise stiffness only from rib caps. Therefore, the spanwise concepts have lower thermal loads, resulting in lighter weight.

In comparing the statically determinate and chordwise concepts, the statically determinate design permits a different gradient and a different mean temperature between the wing and fuselage without thermal stress. This concept provides no resistance to thermal bowing of the fuselage in the chordwise direction and no resistance to differential expansion between the wing and fuselage. While the statically determinate concept requires additional fuselage and fitting weights, the weight is still less than the chordwise-stiffened concept because of spanwise stiffening and thermal-stress alleviation provided by the statically determinate concept. However, the statically determinate concept is not lowest in weight because the semimonocoque spanwise concepts also have low thermal stress, require no fittings, and require no added fuselage stiffening.

Results show the monocoque waffle to be about 4.0 lb/ft^2 heavier than honeycomb structures. Initial screening (see table 10) indicated honeycomb to be heavier than waffle; moreover, waffle is considered to be of more state-of-the-art construction. However, the initial screening was based only on inplane compressive loads for an arbitrarily selected relatively small panel size. These factors yielded minimum gage for both waffle and honeycomb panels with total honeycomb weight less favorable because more edge-member weight had been estimated for honeycomb in initial screening.

However, the detail analysis shows honeycomb edge-member weight to be less than half that used initially. The detail analysis with optimum-size panels (including effects of pressure), shows that the honeycomb structure has half the substructure weight of the waffle-panel structure. In addition, when air-pressure loads were included in the analysis, the waffle panels were shown to be less efficient than honeycomb. Consequently, the honeycomb-core sandwich structure is considerably lighter than the waffle monocoque structure. This result indicates that initial screening should include effects of both substructure and pressure loads.

Since monocoque panels support biaxial loads, they might be expected to be of minimum weight. However, two factors result in the spanwise semimonocoque structures having less weight than the monocoque structures. The semimonocoque spanwise beaded and tubular concepts are new and were found to be more efficient than the honeycomb-core sandwich concept. Another reason that semimonocoque spanwise structure is lighter than monocoque is that chordwise thermal loads are imposed only on the rib caps and thus the wing deflects at little constraint to accommodate the missmatch between wing and fuselage gradients and the rib caps have higher allowable stress than the panels. Monocoque structure provides chordwise stiffening (like the chordwise-stiffened semimonocoque structure) which offers bending resistance to any missmatch of the temperature gradients between the wing and fuselage, thus resulting in high thermal stress. A better match of temperatures and gradients might be achieved by using thermal protection on the upper surface and additional thermal protection on the lower surface. However, based on semimonocoque chordwise-stiffening results, the reduction in primary-structure weight may be less than the weight of the added thermal-protection system. The two spanwise semimonocoque concepts each require shields to provide a relatively smooth surface, so the beneficial thermal effects of shields are inherent in the concepts.

Nonoptimum factors. – Panel nonoptimum factors, as determined from the final detail designs for area B of each wing concept, are presented in table 35. The panel nonoptimum factor (ratio of panel, closeout, and fastener weight to panel weight) is a function of closeout design, method of attachment, and panel size and geometry.

The monocoque panels have the highest nonoptimum factor of all the concepts on their upper surfaces because of the inherent heavy closeout design (waffle panels require alignment of fastener shear force with panel centroidal axis, honeycomb panels require both face sheets to be load-carrying) and minimum-gage panels. In addition, the waffle concept has the smallest panel dimensions and weight of closeouts and fasteners has a larger effect on the total weight of the panel. The lower surface monocoque panels, which are subjected to higher chordwise inplane and normal loads, are not minimum gage, and the closeout design does not represent an appreciable change from the upper-surface closeout design; hence, the panel weights have a larger effect and the nonoptimum factors decrease.

The spanwise beaded and statically determinate concepts have the same panel configuration (beaded) and are single-skin panels which require internal and external finger doublers for the panel closeout. The lower-surface panels, which are designed by the normal pressure, have near minimum-gage panel thicknesses, whereas the upper-surface panels are subjected to compression loads and minimum-gage panels are not adequate. Since panel weight has the most influence on the nonoptimum factors, the surfaces with the near minimum-gage panels (lower) have the largest nonoptimum factors.

TABLE 35. – SUMMARY OF NONOPTIMUM FACTORS

Concept	Panel dimensions, in.	Nonoptimum factor[a] wing area B	
		Upper	Lower
Monocoque			
Waffle	20 x 40	1.35	1.30
Honeycomb-core sandwich	40 x 80	1.26	1.23
Semimonocoque spanwise			
Beaded	40 x 90	1.20	1.31
Tubular	40 x 90	1.15	1.14
Semimonocoque chordwise			
Tubular lower, convex beaded upper	75 x 24	1.20	1.25
Statically determinate			
Spanwise beaded	50 x 90	1.18	1.24

[a]Ratio of panel, closeout, and fastener weight to panel weight.

The closeout and panel thicknesses for the spanwise tubular panels are near minimum gage for both surfaces; hence, the nonoptimum factors are approximately the same.

The chordwise panel nonoptimum factors for the tubular lower surface panels are higher than for the convex-beaded upper surface panels. The upper surface loads are low and require closeout and panel thicknesses that are near minimum gage; whereas, the lower surface is subjected to higher loads and requires greater panel and closeout thicknesses.

The lower surface tubular panel is more efficient for compression and bending loads than the convex-beaded upper surface configuration. Because of this higher structural efficiency, the lower surface panels are only 15 percent heavier than the upper surface panels, but due to high compression loads require closeouts that are 45 percent heavier. The lower surface panels have the largest nonoptimum factor due to the greater influence of closeout weight on the nonoptimum factor.

Total wing weight. – Total wing weights are determined for each concept, using the wing-section weights and the scaling relationships established from the redundant-model analyses of the total wing. The average wing weights (lb/ft^2) for the baseline (550 000-lb) vehicle, including elevon and leading-edge weights, are shown in table 33. The statically determinate concept incurs a fuselage weight penalty, over the other concepts, of 3685 lb. This is 0.365 lb/ft^2 of wing unit weight, based on the planform area, and must be added to the statically determinate weights given in table 33 to obtain a true weight comparison.

The results of the total wing-weight investigation provided the following ranking of structural concepts: semimonocoque spanwise beaded, semimonocoque spanwise tubular, monocoque honeycomb-core sandwich, statically determinate spanwise beaded, semimonocoque chordwise tubular, and monocoque unflanged waffle. As indicated in table 33, the total wing weight of the honeycomb sandwich concept is lower than that for the statically determinate concept, which is a change from the wing-investigation section analysis ranking discussed earlier. Honeycomb is lighter for the total wing because of better efficiency in the high-load area of the aft wing.

HEAT-SHIELD WEIGHT ANALYSIS

The heat-shield weight evaluation consisted of a weight investigation (including cost, performance, and reliability) of the candidate concepts and a final design in which the most promising heat shield was evaluated on each of the primary-structure concepts.

The heat-shield weight analysis for both refurbishable and permanently attached shields was made in terms of temperature requirements, materials, aspect ratio, and width, and was based on a multiple of the overall panel dimensions of a typical semimonocoque spanwise tubular panel. The refurbishable heat-shield concepts considered are shown in figure 11, and the permanently attached heat shields are shown in figure 12.

Materials Selection

Figure 52 shows heat-shield temperature versus distance from the leading edge along Sta. 2360 (the wing investigation section). The plot is for a typical semimonocoque spanwise concept with insulation on the lower surface outboard of the one-third chordline. The upper surface temperatures of figure 52 are for the -0.5-g maneuver condition and the lower surface temperatures are for the +2.0-g condition. As indicated in the figure, the lower surface temperature varies from 1945°F to 1555°F with a reduction to 1900°F after 5 in. The upper surface heat-shield temperatures range from 1785°F to 1280°F. In view of the temperature range, Haynes 25, René 41, and TD NiCr were evaluated as candidate materials.

The corrugated heat-shield design was used in determining the weights of the three candidate materials as a function of temperature. For this evaluation, a maximum moment of 17 in.-lb/in. was used for the design. On the basis of lowest weight, the results, which are presented in figure 53, indicated that Rene' 41 is the most suitable material for heat-shield application below 1800°F and TD NiCr is the best material above 1800°F. Therefore, TD NiCr was selected for the row of shields adjacent to the leading edge on the lower surface.

Refurbishable Heat Shields

Since most heat shields are made of Rene' 41, the weight investigation of refurbishable heat shields (fig. 11) was conducted using heat shields of this material. The heat-shields were arranged on a typical spanwise tubular panel (46 in. by 92 in.). The design temperature and pressure were 1600°F and ±1.0 psi (ultimate), respectively. The closed-form equations of optimization used for this evaluation are presented in section 19 of reference 5.

The basic data obtained for each candidate heat shield included a plot of equivalent thickness $\bar{t}$ versus panel size and maximum deflection versus panel size. A typical example of these data is presented in figures 54 and 55 for the corrugated multiple-supported heat shield. A summary of the maximum deflection and weight for each of the refurbishable heat shields is presented in table 36.

These results indicate the following ranking, based on weight, for the refurbishable heat shields: corrugated skin multiple supports, corrugated skin simple supports, corrugated skin hat-section stiffened clip-supported, and flat-skin dimple-stiffened. The

corrugated skin multiple-supported heat shield of lowest weight has a support spacing of 13.1 in., maximum deflection of 0.242 in., and an equivalent thickness $\bar{t}$ of 0.0131 in. As a typical example, a summary of design data is presented in figure 56 for this design.

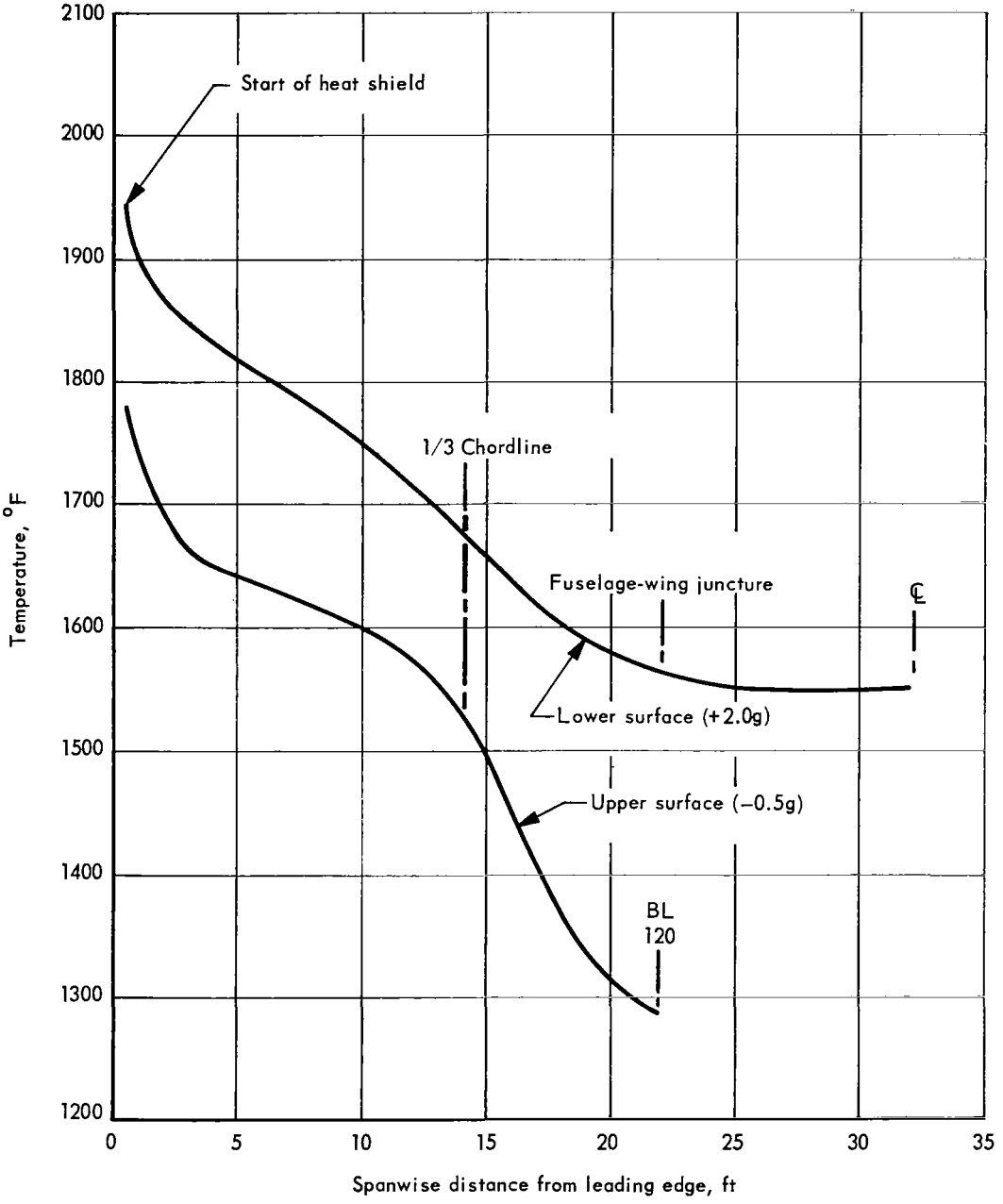

Figure 52. Heat-shield temperature vs spanwise distance from leading edge along station 2360

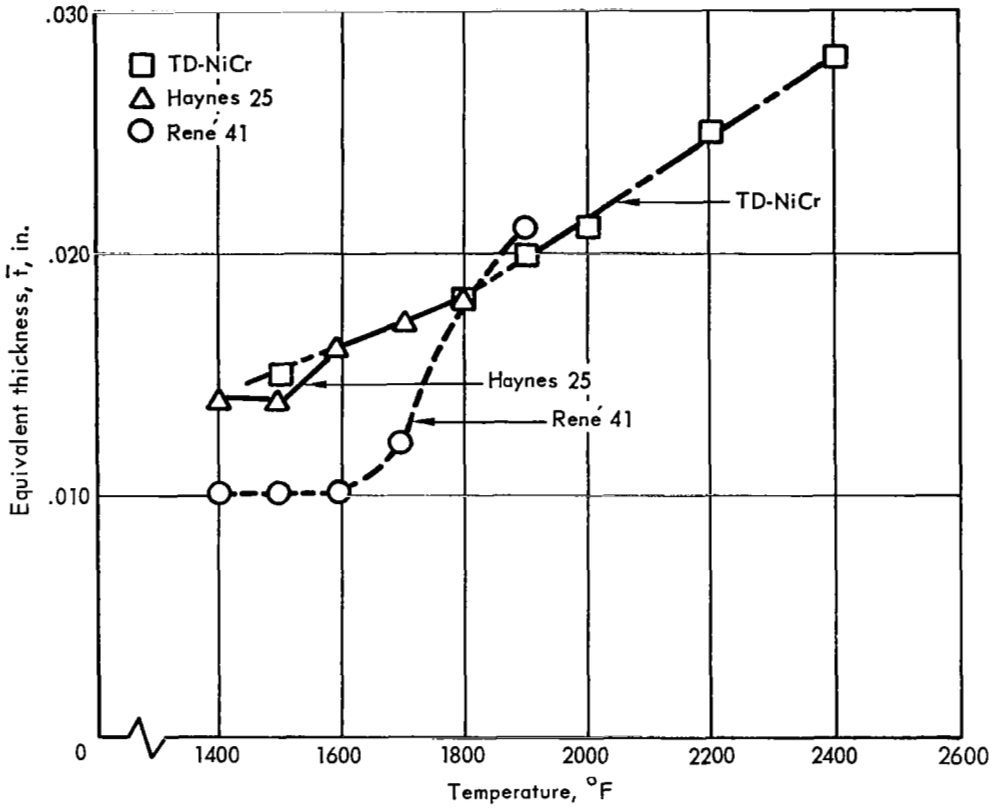

Figure 53. Comparison of heat-shield materials

The corrugated simply-supported heat shield has minimum-gage corrugation thickness of 0.010 in. and a length of 15.3 in. The equivalent thickness $\bar{t}$ and maximum deflection for this design are 0.0147 in. and 0.360 in., respectively.

The corrugated hat-section stiffened clip-supported shield has a minimum-gage corrugation thickness of 0.010 in., aspect ratio of 1.0, and width of 15.3 in. The equivalent thickness $\bar{t}$ and maximum deflection for this design are 0.0165 in. and 0.380 in., respectively.

The flat-skin dimple-stiffened heat-shield has a minimum-gage flat-skin thickness of 0.015 in. and a minimum-gage dimpled-skin thickness of 0.010 in., aspect ratio of 1.0, and width of 15.3 in. The equivalent thickness $\bar{t}$ and maximum deflection for this design are 0.0298 in. and 0.173 in., respectively.

Panel-flutter analyses of the heat shields were conducted. For the refurbishable heat shields, the spring constants included the flexibility of the heat-shielded edge closeout, the support clip, and the primary-structure panel. The primary-structure panel is regarded as shielded from the aerodynamic environment when the refurbishable heat shield is employed. The refurbishable shields are stable; they have panel-flutter factors of safety exceeding the required 1.3.

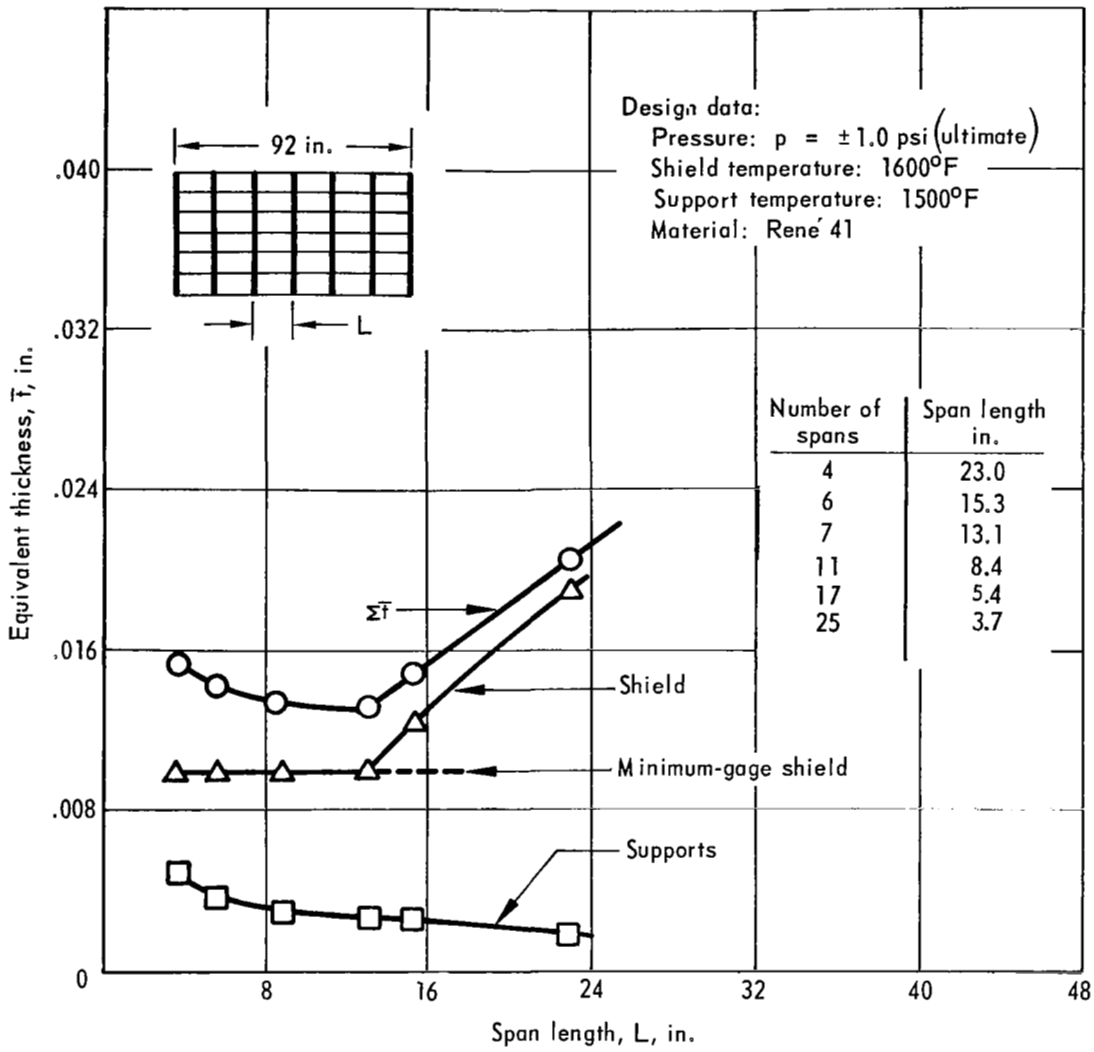

Figure 54. Span length vs equivalent thickness for multisupported corrugated heat shield

The structural design sketches for the four refurbishable heat-shield concepts are shown in figures 57, 58, 59, and 60.

Permanently Attached Heat Shields

The weight investigation conducted on the permanently attached heat shields (fig. 12) utilized the same material, shield arrangement, design temperature, and pressure as just discussed for the refurbishable heat-shield concepts.

A summary of the support spacing, maximum deflection, and weight for the two permanently attached heat-shield concepts is presented in table 36.

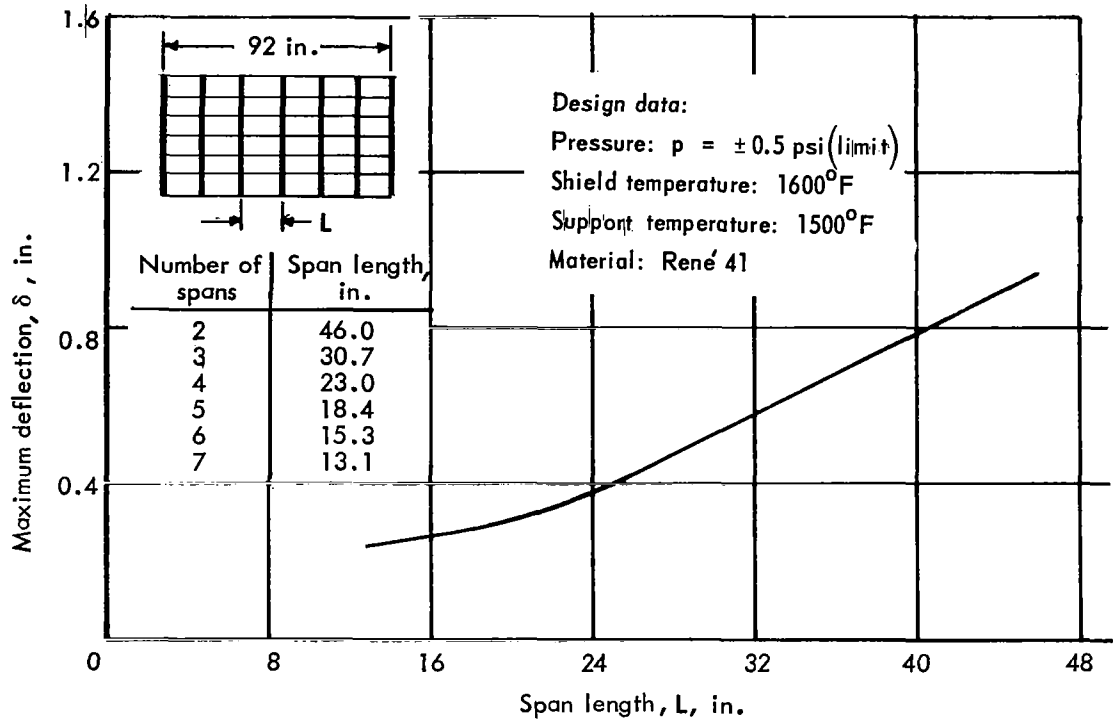

Figure 55. Span length vs deflection for multisupported corrugated heat shield

The lowest weight concept, modular simply supported, has a minimum-gage corrugation thickness of 0.010 in. and a support spacing of 10.4 in. The equivalent thickness $\bar{t}$ and maximum deflection are 0.0118 in. and 0.195 in., respectively.

The modular cantilevered concept has a minimum-gage corrugation thickness of 0.010 in. and a maximum allowable length of one pitch of the primary-structure panel, 2.61 in. The equivalent thickness $\bar{t}$ and maximum deflection are 0.0123 in. and 0.0073 in., respectively. For the panel-flutter analysis on the permanently attached heat shield, both the heat shield and primary-structure panel were required to be flutter free. The permanently attached shields are flutter critical, because the primary-structure panel has an allowable flutter parameter that is less than the applied dynamic pressure. This is because the chordwise stiffness of the spanwise-oriented tubular concept is low. The structural design sketches for the two permanently attached shields are shown in figures 61 and 62.

Heat-Shield Concept Selection

On the basis of weight and deflection, the summary of heat-shield data presented previously in table 36 indicate that the corrugated heat shield with multiple supports is the leading candidate for the refurbishable shield, and for the permanently attached shield, the simply supported modular shield is lowest in weight.

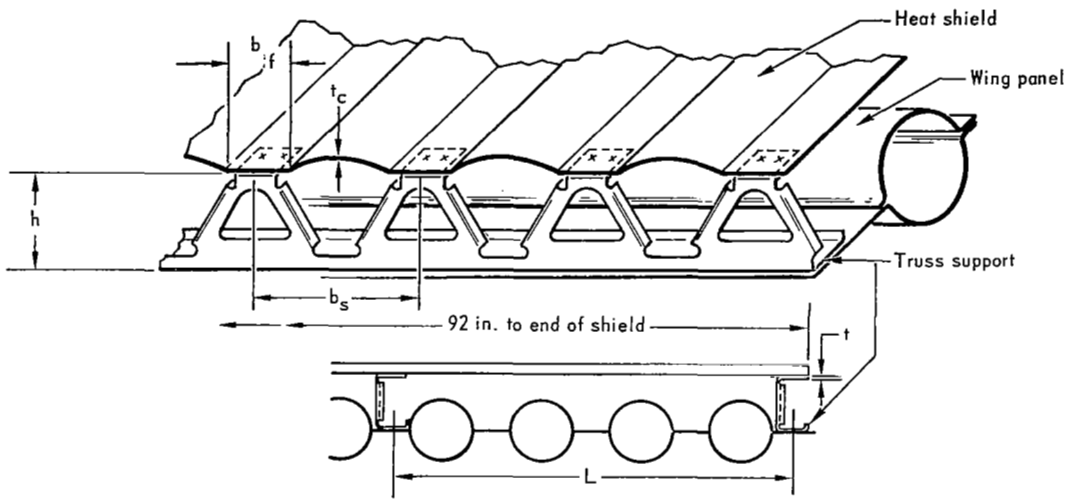

Geometry

Panel length	Support span, in.	Supports required	t_c in.	b_f in.	b_s in.	t in.	h in.	$\bar{t}_{truss}$ in.	$\bar{t}_{shield}$ in.	$\Sigma\bar{t}$ in.	δ in.
92	13.1 [a]	8	.010	.31	1.20	.023	1.172	.0028	.0103	.0131	.242
92	15.3	7	.0122	.37	1.48	.023	1.190	.00245	.0124	.01485	.260
92	23.0	5	.0185	.57	2.20	.023	1.277	.00175	.0190	.02075	.347

[a] Minimum-weight design

Figure 56. Corrugated multisupported heat-shield concept

TABLE 36. – HEAT-SHIELD DATA [a, b]

Heat shield concept		Panel aspect ratio	Support spacing, in.	Maximum deflection, in. [b]	$\Sigma\bar{t}$ in.	Weight, lb/ft^2
Refurbishable	*Corrugated skin hat-section* stiff. with clip supports	1.0	15.3	0.380	0.0165	0.707
	Corrugated skin with simple supports	–	15.3	0.360	0.0147	0.630
	Corrugated skin with multiple supports	–	13.1	0.242	0.0131	0.562
	Flat-skin dimple-stiffened with clip supports	1.0	15.3	0.173	0.0298	1.28
Permanently attached	Modular, simply supported	–	10.4 [c]	0.195 [d]	0.0118	0.507
	Modular, cantilevered	–	2.61 [c]	0.0073 [d]	0.0123	0.528

[a] Design temperature = 1600°F; oxidation effects not included.

[b] Thermal deflections not included.

[c] Maximum length allowed due to high bending in wing-panel tube wall from heat-shield loads.

[d] Local deflections of supports not included.

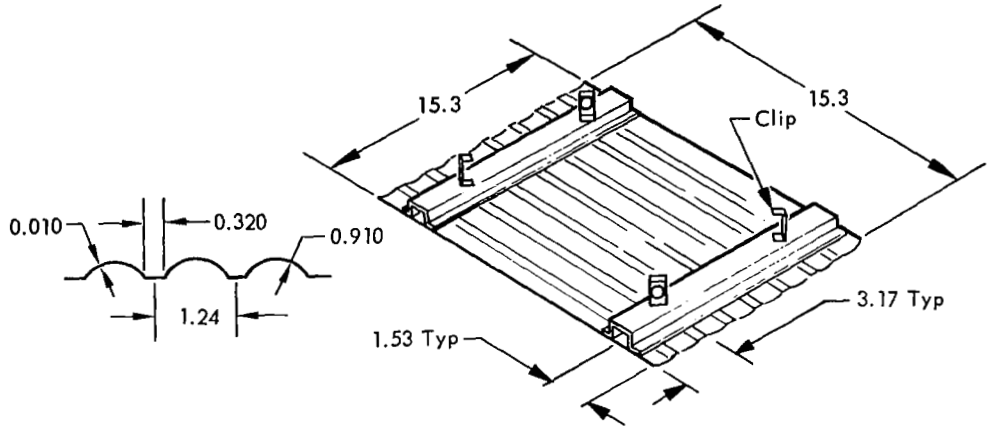

Figure 57. Refurbishable corrugated heat-shield concept, hat-section stiffened and clip supported

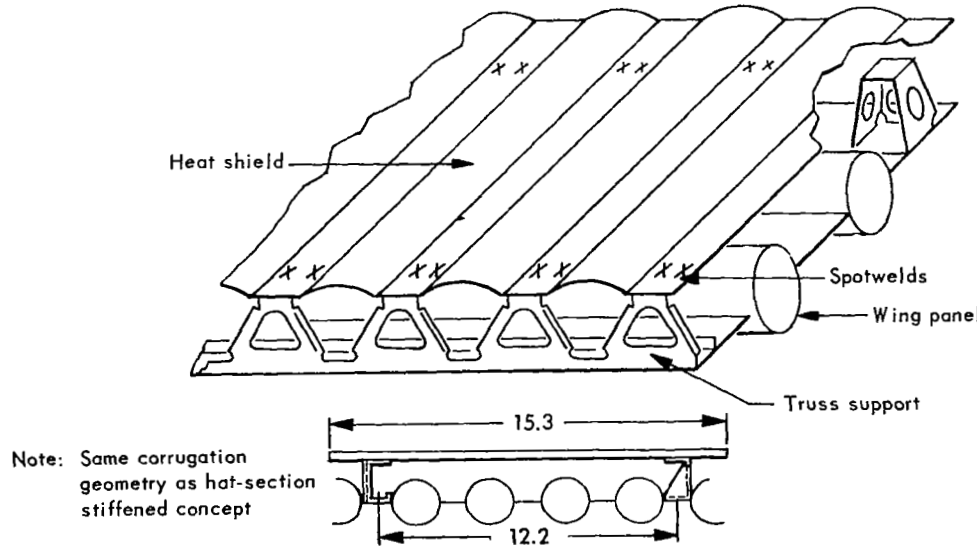

Figure 58. Refurbishable corrugated heat-shield concept with simple supports

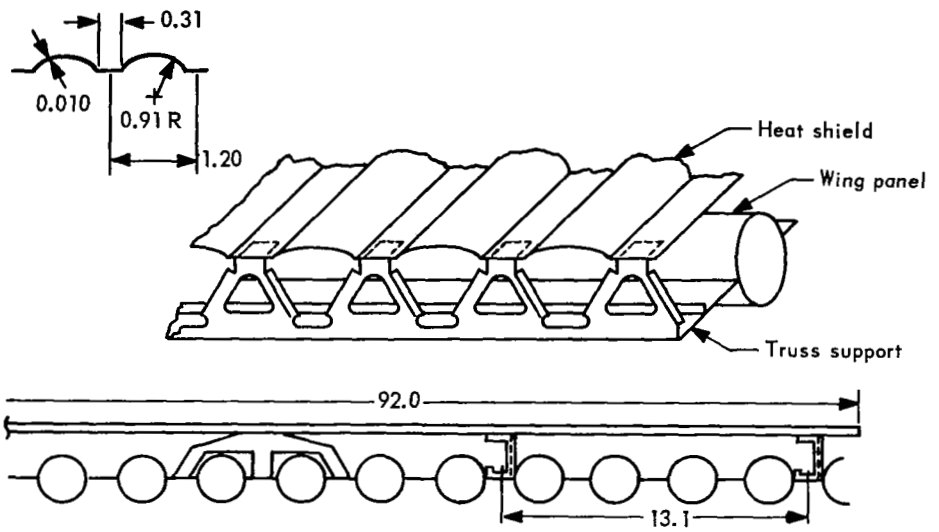

Figure 59. Refurbishable corrugated heat-shield concept with multiple supports

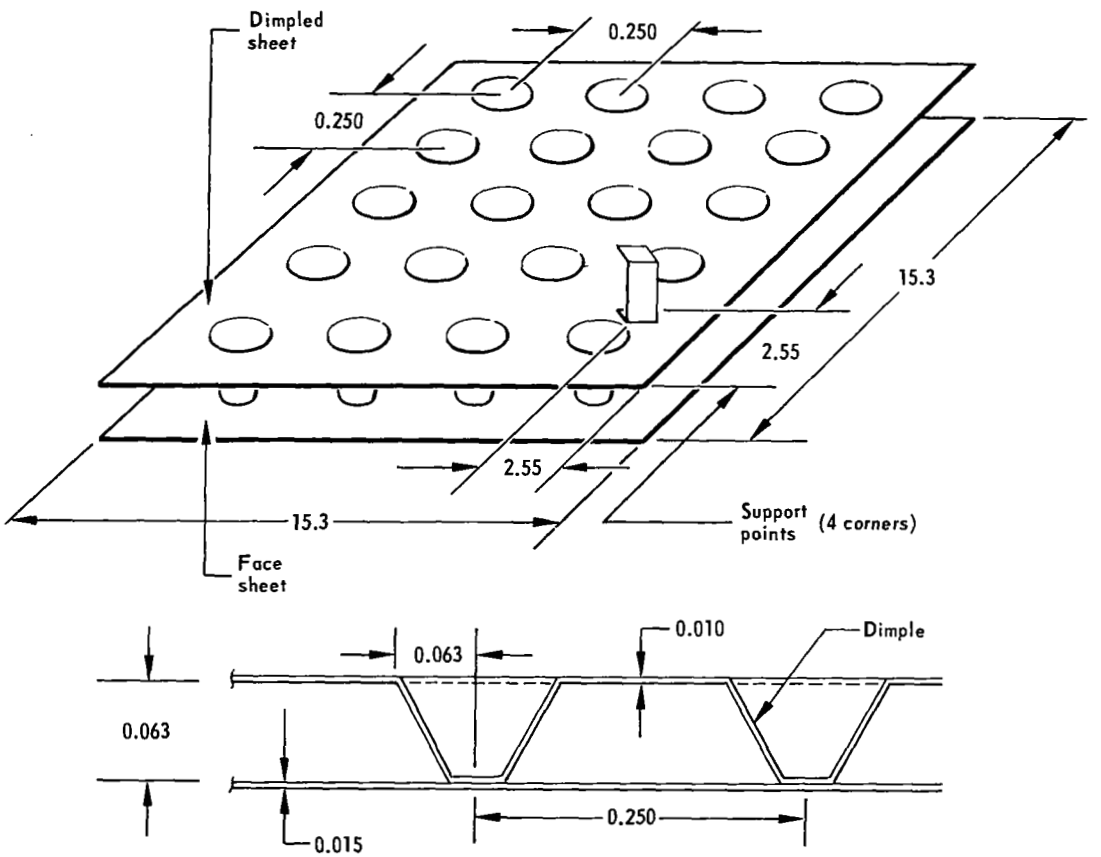

Figure 60. Refurbishable flat-skin dimple-stiffened heat-shield concept with clip supports

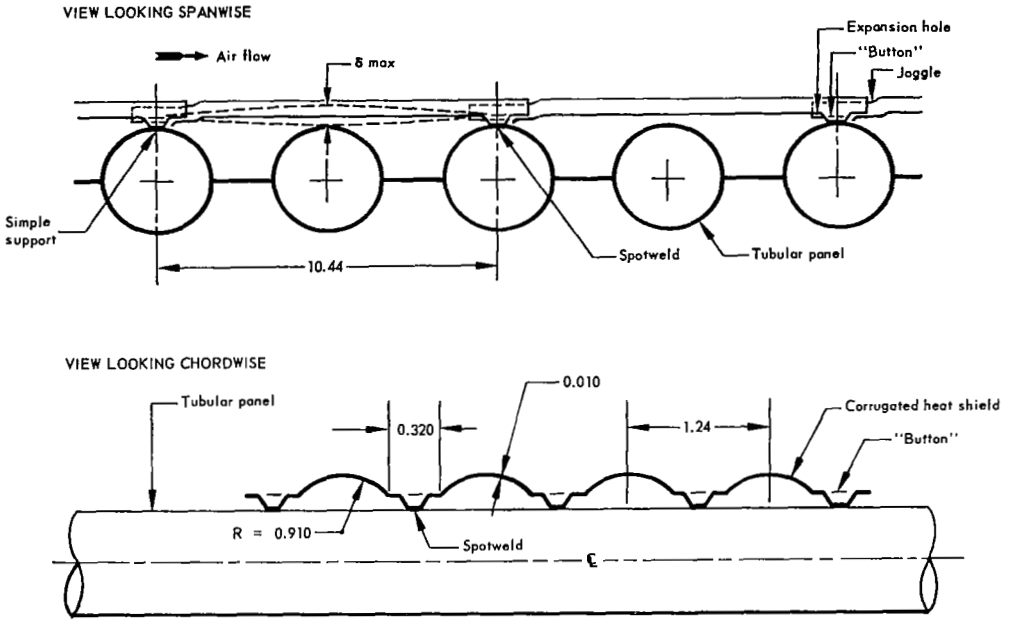

Figure 61. Simply supported modular heat-shield concept with permanently attached interlocking joint

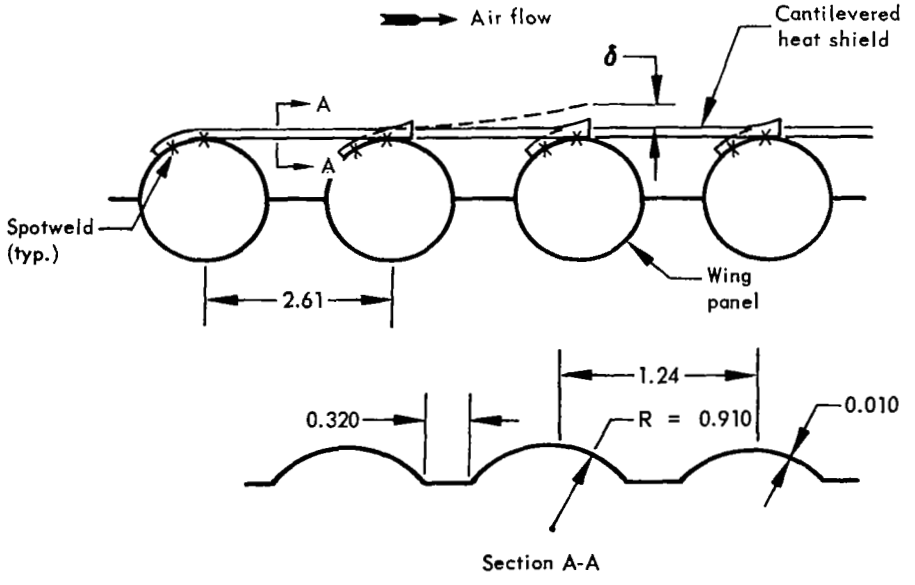

Figure 62. Cantilevered modular permanently attached heat-shield concept

The results of the panel-flutter analysis indicated that the refurbishable shields are stable but the permanently attached shields are flutter critical. In decreasing the rib and spar spacing to overcome the flutter instability of the permanently attached shield, the total wing substructure weight is increased significantly beyond that of the refurbishable shield (additional $\bar{t} = 0.204$ in. or 8.7 lb/ft^2).

The multisupported refurbishable heat shield is of large single-piece construction and affords an appreciable cost advantage over the other refurbishable shield concepts as well as the permanently attached shield concepts.

The flat-skin dimple-stiffened refurbishable shield reduces the flow disturbances and local heating due to cross flow as compared to the corrugated concepts, but it entails a weight penalty.

Based on the results presented above and the cost, performance, and reliability data presented in later sections, the corrugated heat shields with multiple supports was selected for application to the primary-structure concepts. A drawing of the heat-shield design is presented in figure 63.

The weights which were presented in an earlier section for the final six primary-structure concepts included the corrugated shield with multiple supports. Temperature and weight data for this heat-shield design on the spanwise semimonocogue structure are shown in table 37.

TABLE 37. – WEIGHT OF THE CORRUGATED HEAT SHIELD WITH MULTIPLE SUPPORTS ON SEMIMONOCOQUE SPANWISE-STIFFENED STRUCTURE

Surface	BL	Heat-shield design temperature, °F	$\bar{t}_{hs}$, in.	$\bar{t}_{oxid}$, in.	$\bar{t}_{clip}$, in.	$\Sigma \bar{t}$, in.	Unit weight, lb/ft^2
Upper	120 to 212	1600	0.0103	0.00005	0.00294	0.0133	0.570
Upper	212 to 350	1700	0.0125	0.00066	0.00300	0.0162	0.693
Lower	℄ to 120	1600	0.0103	0.00055	0.00280	0.0136	0.586
Lower	120 to 212	1600	0.0103	0.00093	0.00280	0.0140	0.602
Lower	212 to 350	1750[a] 1900[b]	0.0142 0.0196	0.00505 0.00207	0.00346 0.00855[c]	0.0252[d]	1.082

[a] BL 212 to BL 304.

[b] BL 304 to BL 350, TD NiCr heat shield and clips.

[c] Includes fasteners.

[d] Weighted average.

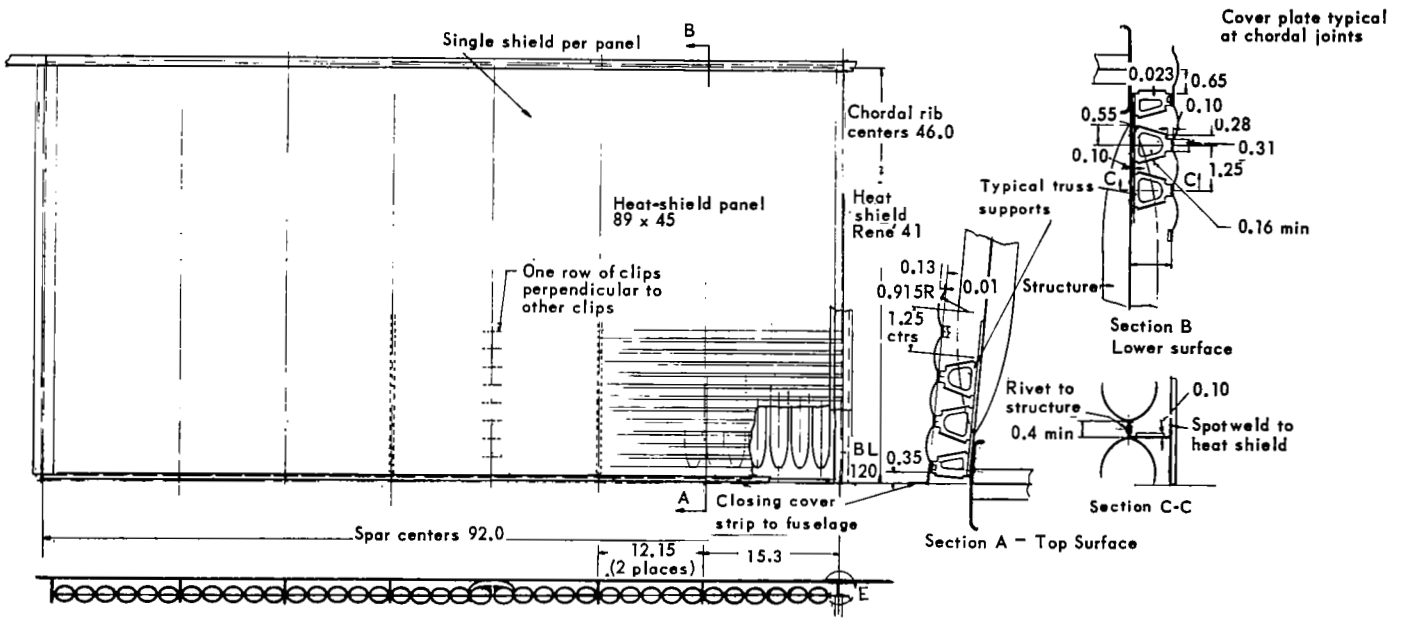

Figure 63. Corrugated heat-shield concept with multiple supports

LEADING-EDGE WEIGHT ANALYSIS

The leading-edge analysis consisted of a parametric thermal analysis, selection of the best material, structural sizing of the arrangements for the segmented and continuous concepts, and final selection of the best leading-edge concept for evaluation on each of the primary-structure concepts.

Materials Selection

The materials considered for the parametric thermal analysis were Ta-10W (tantalum alloy), Cb-752 (columbium alloy), and the dispersion-strengthened alloy TD NiCr. A discussion of these materials was presented earlier in the materials analysis section. On the basis of radiation-equilibrium temperatures, the tantalum alloy Ta-10W was originally considered the leading candidate.

Plasma-jet test results (presented in the materials section) indicated that although the porous tantalum metal concept results in improvements by a factor of 2 over the previously tested sheet specimens with the same Sn-Al coating, a sheet specimen with disilicide coating showed an even more marked improvement. Therefore, the disilicide-coated sheet was considered for detailed evaluation. However, results of a two-dimensional thermal analysis, the lower-curve in figure 64, indicated temperatures lower that the radiation-equilibrium temperatures which would allow use of the super-alloy TD NiCr. Figure 64 is a plot of temperature versus material thickness for Ta-10W, Cb-752, and TD NiCr. Initially, internal-radiation effects only were evaluated for a hot-load-carrying arrangement (no insulation at the René 41 leading-edge spar).

The transient-temperature analysis of figure 64 indicates that a maximum of 2200°F is achieved by increasing the leading-edge thickness to about 0.125 in., thus permitting use of TD NiCr. TD NiCr does not require an oxidation-resistant coating. Therefore, lateral conduction and heat-sink cooling are beneficial for cruise vehicle application, since the leading edge radius is small and the period of peak heating is of short duration.

Continuous Leading Edge

Using the parametric thermal analysis of figure 64, the continuous leading-edge designs were investigated in terms of thermal strains, reusability requirements (depth of oxidation penetration, coating life, low-cycle fatigue), and local buckling.

The leading-edge pressures used for the investigation are shown in table 38. These pressures are based on the differences between internal and aerodynamic pressures.

Initial continuous-leading-edge analysis indicated that the net stress for the refractory-metal concepts is tension, thereby eliminating the local buckling problems The $\alpha\Delta T$ product for the leading edge is less than that for the primary wing structure. In addition, life of previous silicide coatings is much less than the required 4460 hr and no tests of the R512E coating have been performed to date on full size leading edge segments in a realistic environment. Furthermore, to repair the coating of a refractory-metal leading edge, the component must be removed and recoated. Moreover, to prevent eutectic reaction, ceramic spacers are

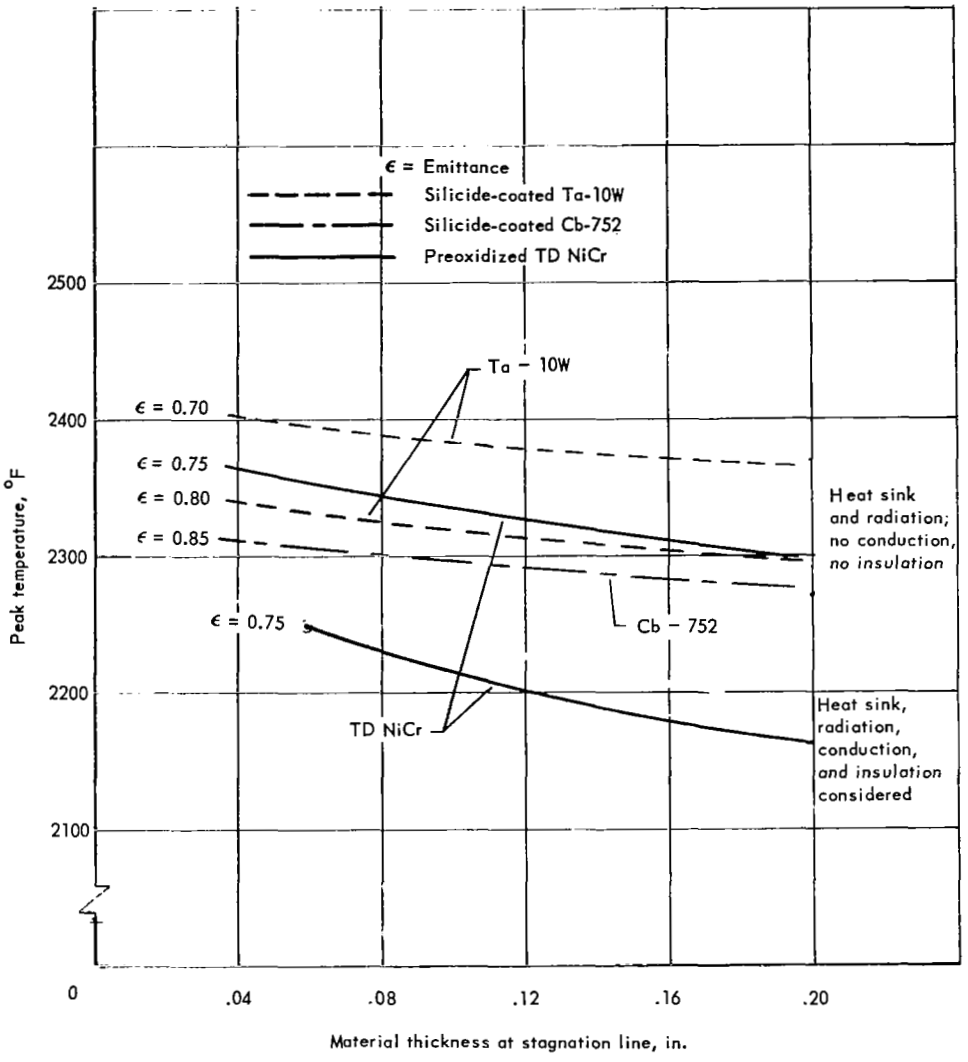

Figure 64. Peak temperature at leading-edge stagnation line vs material thickness and emittance

TABLE 38. – LEADING-EDGE DESIGN PRESSURES

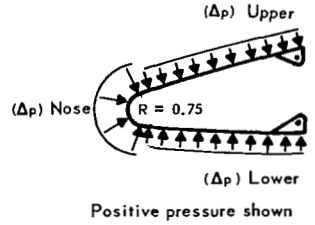

Condition / Surface	Limit Δp, psi		
	-0.5-g	+2.0-g	Cruise
Δp Nose	1.95	2.9	0.83
Δp Upper	-0.1	-0.27	-0.08
Δp Lower	-0.3	0.53	0.44

required at the interface between the coated refractory metals and the adjacent René 41 structure. Because of the unsatisfactory reusability evaluation, the coated refractory-metal leading edge concepts were excluded from further consideration.

For the compression-critical TD NiCr leading-edge, the initial hot-load-carrying concepts proved unsatisfactory because of local buckling. However, increases in thickness, with corresponding reductions in temperatures and thermal gradients, led to an insulated concept that possesses adequate buckling strength (maximum temperature of 2200°F). Local buckling is precluded in the curved section because of its thickness; and, in the regions adjacent to the curved section, corrugations provided to nest with the heat shield (see fig. 65) can relieve the compressive stresses. Maximum oxide penetration for the TD NiCr concepts, based on stagnation-point temperatures and a vehicle life of 10 000 hr, is less than 0.002 inch. Thus, the insulated design using TD NiCr was selected as the best continuous-leading-edge concept and was further evaluated for low-cycle fatigue. Due to the high thermal strains, the low-cycle fatigue life was 12 flights, well below the acceptable level of 8110 flights.

The best continuous-leading-edge concept (the insulated design using TD NiCr, fig. 65) has a unit weight of 8.31 lb/ft^2 and a high margin of safety based on local buckling.

A summary of design and weight data for both continuous and segmented leading edges is presented in table 39.

The design drawing for the continuous leading-edge is presented in figure 65. The curved section is machined from bar stock and the flats are formed from sheet and attached to the main wing structure with brackets located between the heat-shield beads. The attachment brackets are spotwelded to the leading-edge spar cap on one side and fastened to the removable leading edge with screws on the other. Sealed non-slip overlapping joints are provided between the leading edge and heat shield and also between the relatively long segments. Washouts of the heat-shield corrugations, carried into the flats of the leading edge to relieve compressive thermal strains, are symmetrical about a median contour to minimize aerodynamic drag and local heating.

Segmented Leading Edge

The insulated TD NiCr concept was evaluated for the segmented leading edge based on the reasons stated in preceding sections. Designs involving different leading edge and flat thicknesses were evaluated, using the identical procedure used for the continuous leading edge (thermal strain, reusability requirements, and local buckling).

Figure 66 shows the results of the detailed thermal analysis of the insulated TD NiCr design with a material thickness of 0.125 in. at the radius. Temperatures and gradients at the stagnation area are shown for the three flight conditions and temperatures for the flats behind the radius are given for design thicknesses of 0.060 in. and 0.030 in. (minimum gage). A flat thickness of 0.030 in. with a T_{max} of 2025°F was selected on the basis of lower weight, since thermal stresses were approximately the same for both thicknesses.

The leading-edge pressures used for the segmented leading-edge analysis are identical to those used for the continuous leading-edge and were presented in table 38.

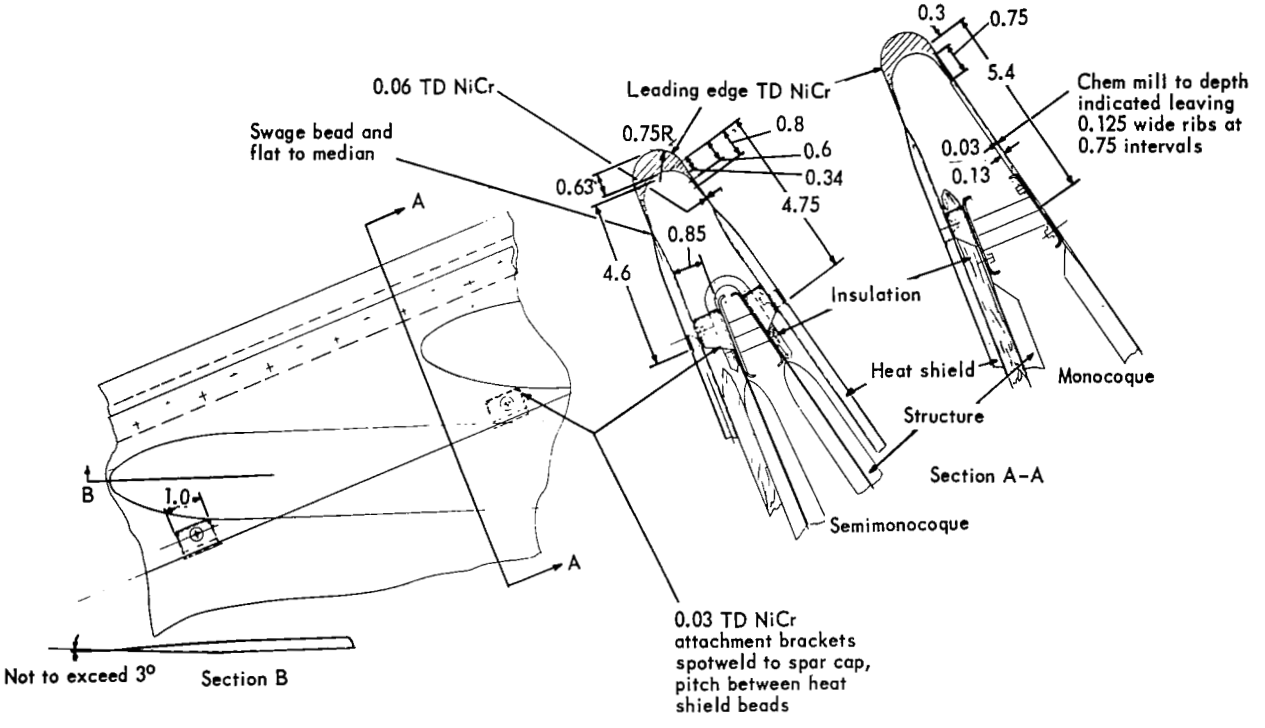

Figure 65. Continuous leading edge

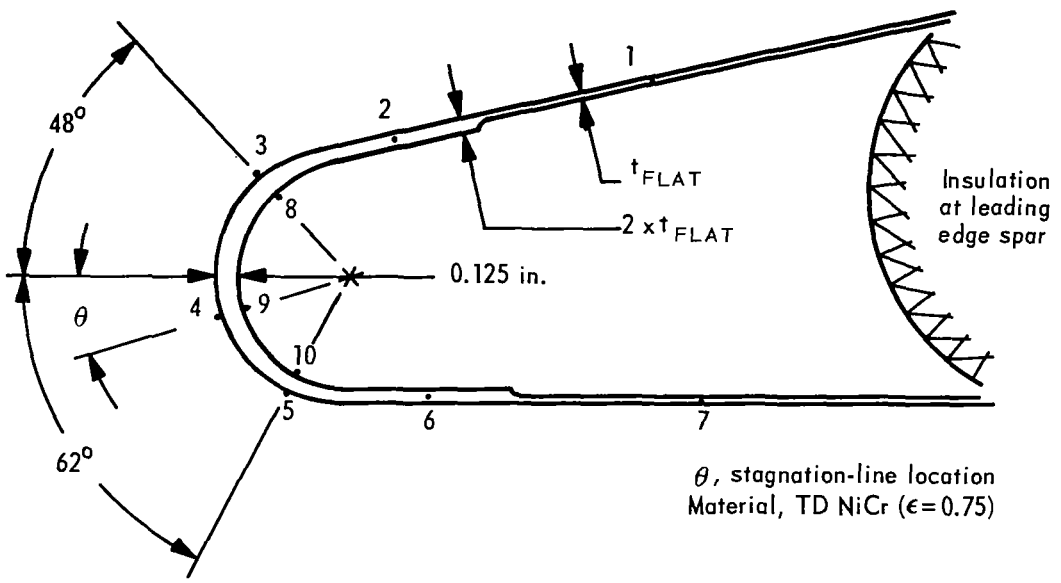

Thermal model of cross-section normal to leading-edge sweep

Temp location \ Condition	Temperature, °F					
	-0.5-g		+2.0-g		Cruise	
t_{FLAT}, in.	0.03	0.06	0.03	0.06	0.03	0.06
T(1)	1925	1860	1795	1785	1340	1340
T(2)	1940	1890	1875	1865	1480	1495
T(3)	1975	1960	2005	1985	1625	1615
T(4)	2055	2045	2200	2190	1795	1790
T(5)	1920	1910	2135	2115	1770	1760
T(6)	1845	1860	2065	2015	1630	1645
T(7)	1765	1770	2025	1985	1515	1515
T(3) − T(8)	5	5	0	0	0	0
T(4) − T(9)	10	10	10	10	5	5
T(5) − T(10)	0	0	5	5	5	5

Figure 66. Detail temperatures for heat-shielded and insulated leading-edge concept with stagnation-area thickness of 0.125 in.

TABLE 39. - LEADING-EDGE DESIGN AND WEIGHT DATA FOR SELECTED CONCEPTS

Item	Selected leading-edge concept	
	Continuous leading-edge concept	Segmented leading-edge concept
Leading-edge material	TD NiCr	TD NiCr
Leading-edge, in.	0.625	0.125
Flat thickness, in.	0.060	0.030
Segment length, in.	–	20.0
Maximum temperature, ^{o}F (stagnation point, +2-g condition)	2050	2200
Maximum limit elastic thermal strain, ϵ_T, in./in.	-0.00647	-0.000850
Maximum depth of oxidation, δ, in./side (stagnation point, 10,000-hr vehicle life)	0.00151	0.00165
Local buckling margin of safety	High	0.43
Low-cycle fatigue life, flights	12	11.9×10^5
Unit weight, lb/ft^2	8.31	4.89

The thermal strains for the selected design were based on a plane-strain analysis and then adjusted to account for end effects (secondary thermal stress near the stress-free end of the segment).

The maximum thermal stresses at the stagnation line of the segmented leading edge are quite low, and low-cycle fatigue lift substantially exceeds the requirement of 8110 flights. Hence, it was not necessary to optimize length on the basis of low-cycle fatigue and end effects. The length of the segmented leading edge was optimized by considering weight, strength, performance, and aerodynamic heating. Since proportions of the segmented leading-edge cross-section (nose thickness of 0.125 in. and flat thickness of 0.030 in.) were selected to minimize weight and thermal stresses, the optimum segmented length was determined by holding cross-section dimensions constant and varying only the length.

The optimum length of the leading-edge segment for the monocoque concept (based on minimum structural weight and drag penalty), was 20.0 in. Figure 67 shows the optimum length for the monocoque concept. The same procedure was used to determine the optimum length for the semimonocoque concept. However, ultimate strength limits the semimonocoque segment length to 20.0 in., so this length was selected. The drag penalty (fuel increment due to deflections, joints, and fasteners) shown is based on an equivalence between fuel and structure weight of 1.5 to 1.0, respectively. This ratio was determined from results of the vehicle-performance interaction evaluation. Since fewer attachment fittings are required, the weight of the leading-edge segment decreases with increasing segment length.

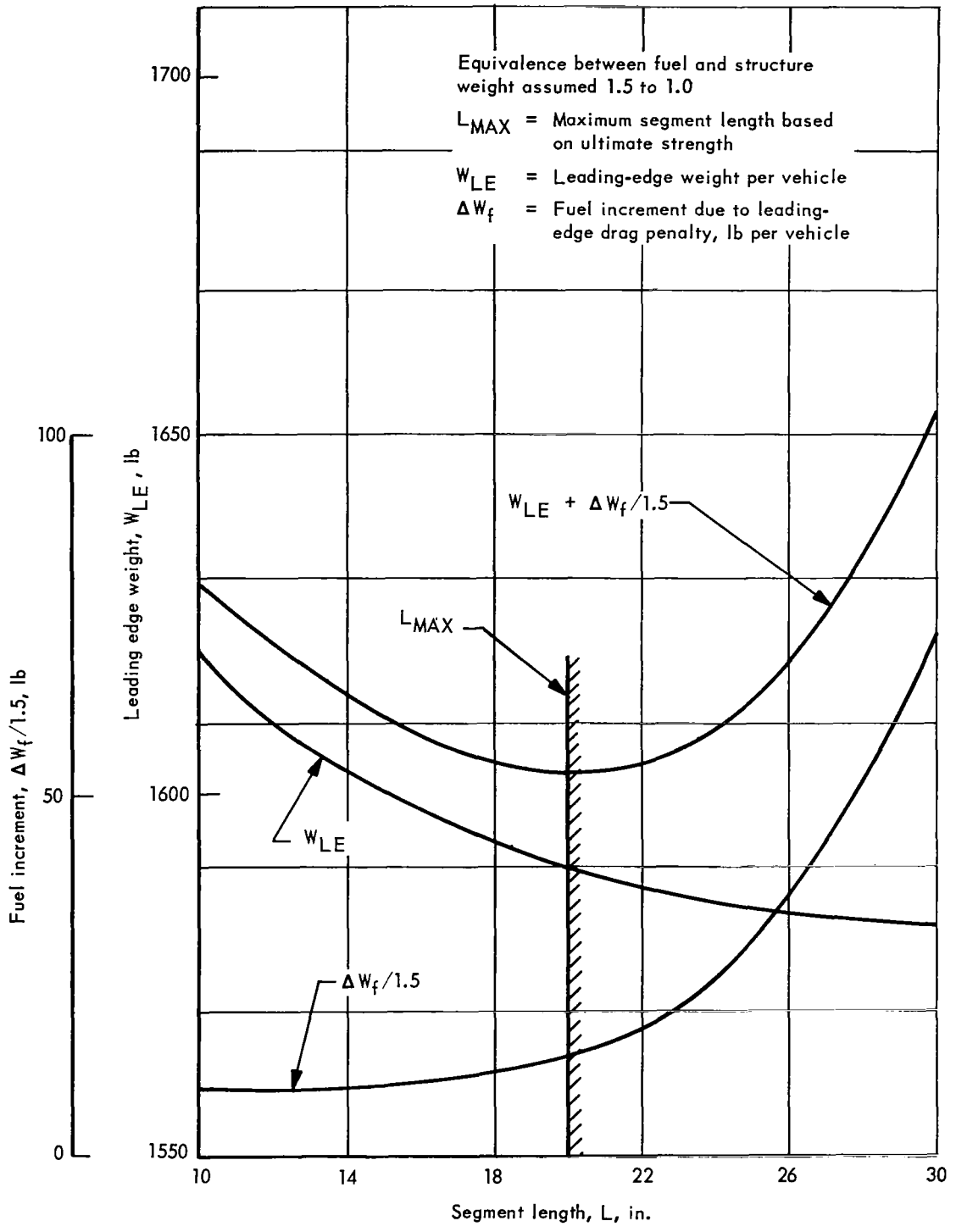

Figure 67. Optimum length of segmented leading edge for monocoque concept

Additional aerodynamic heating occurs because of local changes in flow angle resulting from the segmented leading-edge distortions. For example, based on a leading-edge segment length of 20.0 in., forward deflection of the segmented leading-edge stagnation line increases stagnation temperature by $15^{\circ}F$. Net inward deflection of the center of the lower surface at the trailing edge of the leading edge due to pressure and thermal effects for the +2.0-g condition decreases the temperature $80^{\circ}F$. Corresponding net deflection of the extreme ends of the aft lower surface of the leading edge is outward relative to the wing reference surface, and the local temperature is increased $70^{\circ}F$.

The segmented leading-edge has a unit weight of 4.89 lb/ft^2 and a local buckling margin of safety of 0.43. A summary of design and weight data is presented in table 39.

The design drawing for the segmented leading-edge is presented in figure 68.

The nose section of the segmented leading-edge is chem-milled from 0.125 in. sheet prior to forming. The removable leading edge is screw-attached to the main wing structure hinges. Overlapping joints are provided between the leading edge and heat shield and also between adjoining segments. Heat-shield corrugations are washed out adjacent to the leading edge joint. This approach results in maximum uniformity and also reduces the cost of the leading-edge, but requires a thermal-expansion joint for the heat shield along the leading-edge in each bead of the heat shields.

Leading-Edge Concept Selection

A summary of design and weight data for the selected continuous and segmented leading-edge concepts was presented in table 39. Because of the high thermal strains, the low-cycle fatigue life of the continuous leading edge is very deficient (only 12 flights). The selected segment length of 20 in. leads to low strains and long life for the segmented leading edge. As shown, unit weights for the continuous and segmented leading edge are 8.31 lb/ft^2 and 4.89 lb/ft^2, respectively. The unit weights include insulation and the effects of oxidation.

Based on these results and the cost, performance, and reliability data presented in later sections, the segmented leading-edge was selected for application to the primary-structure concepts. The total weight of the leading edge for the entire wing is:

Primary structure	Leading-edge weight, lb
Monocoque	1700
Semimonocoque	1956
Statically determinate	1956

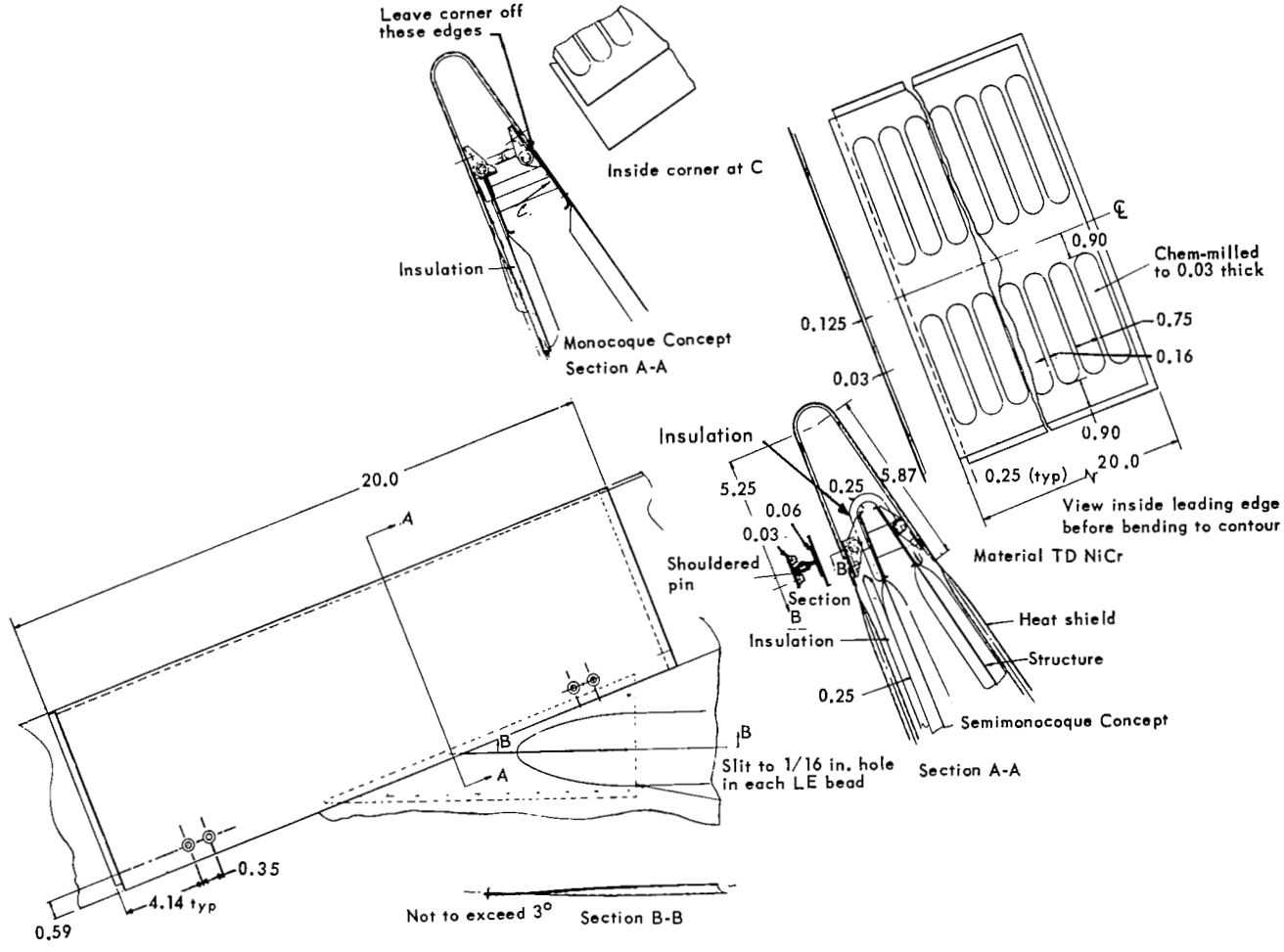

Figure 68. Segmented leading edge

COST ANALYSIS

Cost comparisons of candidate wing structures were made for the three general categories of primary structures, heat shields, and leading edges.

Primary Structures

The cost analyses of the six primary structures consisted of obtaining costs for the wing investigation area and then determining total wing costs for the baseline vehicle.

The typical arrangement and geometry of the wing-investigation area manufacturing segment assumed for detailed costing of the primary structure is shown in figure 69, and the costs are given in table 40.

This segment (one-half shown) consists of 1874 ft^2 of planform area located between stations 2136 and 2506. The wing segment is further divided into three zones (A, B, and C), which represent typical types of structures as determined by detailed analyses. The basic elements consist of the structural panels and substructure. The heat-shield cost information (including insulation) presented on page 128 was used in establishing total concept costs. The substructure costs consist of chordwise ribs, spars, leading-edge spar, and breakline spar. The assembly costs for the substructure are based on the number of spar/rib intersections in the wing manufacturing segment and a costing factor used to account for the type and complexity of the joint involved.

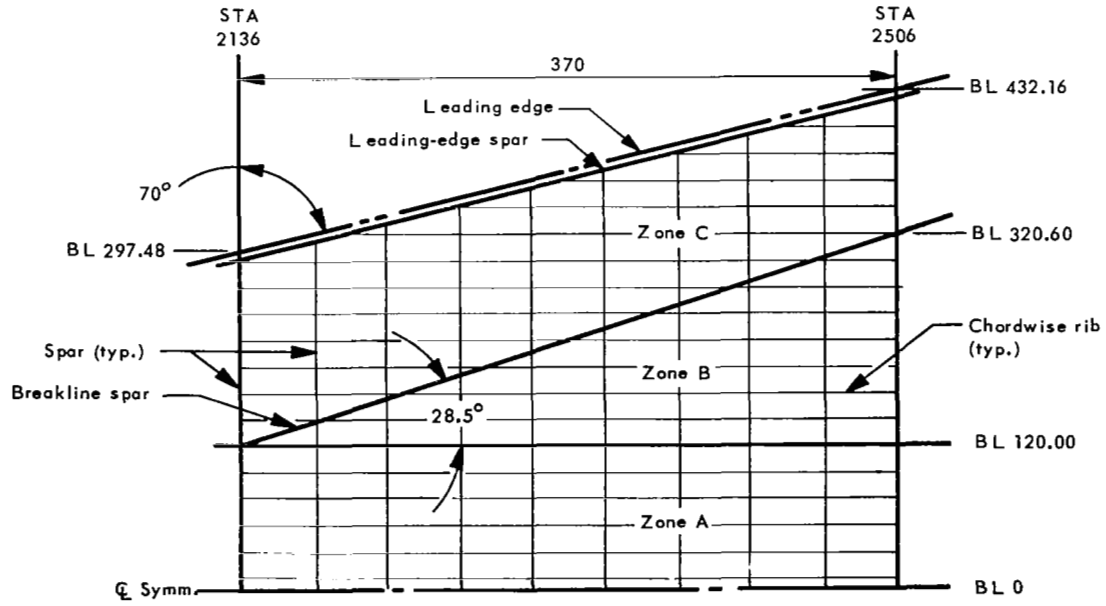

Figure 69. Wing investigation area costing segment

TABLE 40. – PRIMARY-STRUCTURE MANUFACTURING COSTS FOR WING INVESTIGATION AREA FOR 100-VEHICLE PRODUCTION RUN

Structure Concept	Monocoque		Semimonocoque			Statically determinate
			Spanwise		Chordwise	Spanwise
	Waffle	Honeycomb-core	Tubular	Beaded	Convex beaded/tubular	Beaded
Labor, $	$222 030	$198 740	$112 442	$106 889	$148 038	$136 453
Material, $	461 400	213 964	126 900	120 953	150 741	137 624
Tooling, $	35 125	28 507	33 708	40 922	31 083	42 442
Total cost per unit, $	718 555	441 211	273 050	268 764	329 862	316 519
Weight, lb	9 760	5 970	4 958	4 670	6 150	4 843
Dollars per lb	73	74	55	58	53	65
Dollars per ft^2	779	480	296	291	358	343

[a]Costed area = 922 ft^2.

Monocoque waffle concept. – Cost evaluation of this concept included an aspect ratio-cost sensitivity study in addition to determination of cost data for the minimum-weight arrangement. The chordwise ribs were considered as being continuous from the leading edge to the trailing edge of the manufacturing segment. The chordwise-rib fabrication entails joining the segmented webs and continuous caps by melt-through welding of the cap to the webs, using a tracer-controlled gantry-mounted welding head. Welding is accomplished on-station in the wing subassembly fixture. After the melt-through operation, the overlapping edges of the webs are spotwelded for the depth of the beam.

Fabrication of the spar structural elements follows a similar procedure, except that the web has a different configuration, and the length of the spar segment as assembled is a function of the spacing of the chordwise ribs.

The substructure assembly is fabricated by loading the rib and spar segments into a horizontal fixture, maintaining contour and beam spacing. The various substructure elements are secured at the intersections by resistance welding and mechanical fasteners. Splice plates are added to the upper and lower caps at each intersection. The substructure is aged and oxidized as a unit prior to fitup and assembly of the structural panels.

The substructure costs developed in detail for the monocoque waffle concept (1.8 aspect ratio) were factored to develop a cost for each of the other monocoque aspect ratios. Substructure fabrication labor and material costs were factored as a ratio of the linear feet of structural elements to the linear feet in the 1.8 aspect ratio. Substructure assembly labor and material costs were factored as a ratio of the number of structure intersections.

Tooling costs for the spars, breakline (wing one-third high point), and leading-edge beams were assumed to be constant. Tooling for chordwise ribs was factored

by the ratio of linear feet of structure, with compensation for the impact that the similarity of the ribs within the fuselage area would have on this tooling cost. Substructure assembly tooling costs were assumed to be constant, since a major part of this cost results from the massive assembly fixture required to mate the various structural elements. The monocoque waffle panels were assumed to be machined from plate stock by electrical/chemical milling. After machining of the panel pockets, a secondary machining operation removes the risers in the flanged attaching areas.

After aging, panels are fitted to substructure, trimmed to size, drilled, and assembled with Rene' 41 plate nuts and screws. Figure 70 shows total manufacturing costs for the selected wing area (922 ft^2) of monocoque waffle panels for various aspect ratios at 10-, 100-, and 500-vehicle production quantities. As indicated, for greater quantities of vehicles, the effect of panel aspect ratio on cost is negligible.

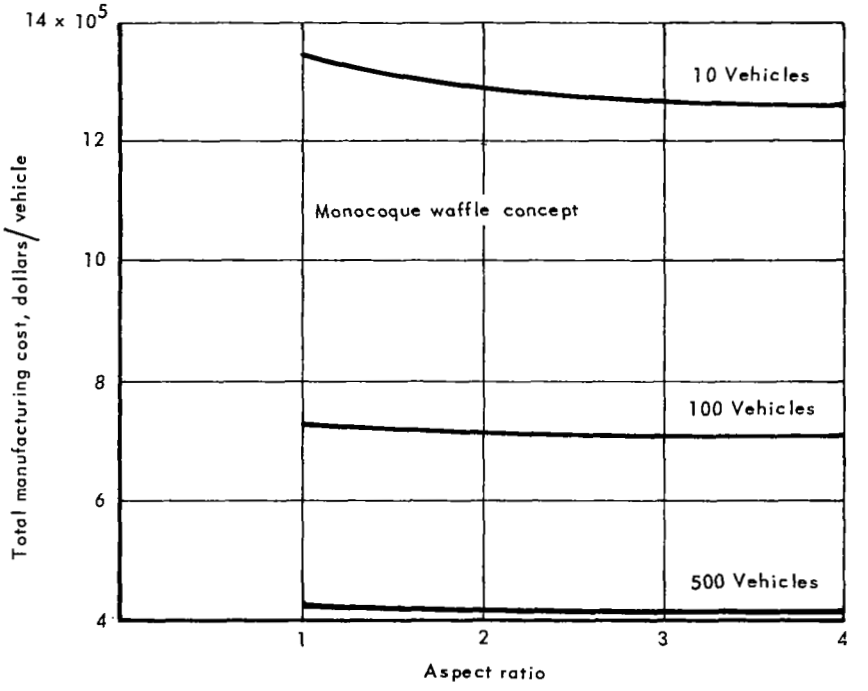

Figure 70. Total unit manufacturing cost vs aspect ratio for monocoque waffle concept

Monocoque honeycomb concept. – The costs determined for the substructure of the waffle concept, as just described, were factored on the basis of the ratio of linear feet of spar and ribs, and the number of spar and rib joints considering the type and complexity of the joint.

The honeycomb-sandwich panels are fabricated by resistance welding of the cellular-shaped foil-ribbon core to the face sheets. The honeycomb sandwich is considered to be sealed and pressurized with helium at 2 psia to prevent oxidation and corrosion of the interior of the panel.

Semimonocoque spanwise tubular concept. – The costs developed for the substructure of the waffle concept, as described above, were factored to develop substructure costs for this concept. However, the fabricated sheetmetal panels were costed in detail, with variations appropriate to each wing structural-panel concept. For the spanwise tubular concept, the halves of the panels are formed in a three-stage forming operation with two interstage anneals. The annealing operation is performed in a controlled-atmosphere furnace, with subsequent bath cooling. Typical panels were costed for each zone of the wing surface, with consideration given to changes in material and shape of panel. Panel halves are assembled with blanked doublers and spot-welded to form a complete structural panel. Heat-shield components are added as appropriate. The complete panel is then aged and oxidized and finally fitted to the substructure and trimmed, drilled, and assembled.

Semimonocoque spanwise beaded-skin concept. – The method used for determining the cost data for the concept above was similarly applied to define detailed panel and substructure costs for the beaded-skin concept. The cost of the wing-investigation area for this concept is shown in table 40.

Semimonocoque chordwise convex-beaded tubular concept. – The substructure costs developed earlier were factored to develop costs for this concept. The fabricated sheetmetal structural panels were costed in a manner similar to that previously described for the spanwise tubular concept, with variations appropriate to this panel concept, such as the number of individual forming tools for panels along the leading edge and the elimination of upper surface heat shields.

Statically determinate concept. – The substructure costing methods described earlier were also applied to determine the detailed cost data for the statically determinate, spanwise beaded-skin concept. Additional requirements for spanwise beams, machined ball/slip joint between wing boxes, and fuselage hinge/support attachment were also considered. The added cost of the slip joints and fuselage fittings, including forging costs, machining, and locating, are reflected in the substructure costs.

Wing cost comparison. – Table 40 lists the primary-structure costs for the wing investigation area and indicates that the semimonocoque spanwise beaded-skin concept provides the lowest cost in terms of dollars per square foot ($\$291/ft^2$).

Total wing costs. – The wing-section costs of table 40 were used to develop total wing costs for the baseline vehicle. As shown in table 41, the semimonocoque spanwise beaded-skin concept has the lowest cost in dollars per square foot ($\$767/ft^2$) and the monocoque waffle concept is the most expensive ($\$1719/ft^2$).

Table 41 shows waffle fabrication costs to be the greatest of the concepts studied. This high cost is attributable to machining by electromechanical milling of superalloy plates of about 1.0 in. in thickness. Consequently, labor, material, and tooling costs are each the greatest of all concepts. The statically determinate structure is second highest in fabrication costs because of added labor, material, and tooling for the multiplicity of attachments between the wing bays and the fuselage. Honeycomb-core sandwich is next highest in cost because of its complex sandwich construction. The semimonocoque chordwise concept is more costly than the semimonocoque spanwise concepts primarily because the chordwise concept has lower structural efficiency and is heavier. The tubular semimonocoque spanwise concept is more costly than the spanwise beaded

concept, because the tubular panel is made of two skins welded together, whereas the beaded panel is formed simply by beading a single skin. In addition, the beaded panel is the most efficient panel structurally, resulting in lowest weight; thus although it is more costly than tubular per pound, its low weight results in lowest total wing cost.

TABLE 41. - TOTAL WING-STRUCTURE MANUFACTURING COSTS FOR 100-VEHICLE PRODUCTION RUN (GROSS TAKEOFF WEIGHT = 500 000 LB)

Primary structure concept	Monocoque		Semimonocoque			Statically determinate
			Spanwise		Chordwise	Spanwise
	Waffle	Honeycomb-core	Tubular	Beaded	Convex-beaded/tubular	Beaded
Labor, $ x 10^3	4 247	3 218	2 457	2 357	3 386	3 846
Material, $ x 10^3	11 138	5 337	4 086	3 964	4 834	5 276
Tooling, $ x 10^3	1 414	1 024	1 133	1 176	1 186	1 299
Total cost, cost, $ x 10^3	16 799	9 579	7 676	7 497	9 406	10 421
Weight, lb	99 876	61 568	60 771	57 391	69 657	63 170
Dollars/lb	168	156	126	131	135	165
Dollars/ft^2	1 719	980	785	767	962	1 066

[a]Total costed wing area = 9774 ft^2.

Heat Shields

Cost analyses were conducted for two refurbishable and two permanently attached heat shields. All were evaluated through their use with the tubular primary structure for a panel size of 92 in. by 46 in.

For the refurbishable heat shields, the corrugated multiple-supported and flat-skin, dimple-stiffened concepts were studied. The corrugated shields with hat-section and with simple supports were not costed, since they are heavier than the corrugated shield with multiple supports (see table 36). For costing permanently attached modular heat shields, the simply supported and cantilevered versions were used.

The cost study was conducted in sufficient detail to produce an estimate of the tooling required for fabrication and assembly. Figure 71 shows relative costs of the four concepts evaluated as a function of number of vehicles and indicates small changes in heat-shield costs after 200 vehicles. Table 42 presents costs in dollars per square foot for 100 vehicles. The results of this cost evaluation indicate that the corrugated-skin multiple support heat shield is the least costly (24.5 dollars/ft^2 for 100 vehicles). Considering cost, as well as the weight, performance, and reliability evaluation factors,

the corrugated-skin multiple support heat shield was selected for application to the various primary structures.

Leading Edges

Cost evaluation of leading-edge concepts was made for both the continuous and segmented designs. The leading-edge cost data, including the data for labor and materials for 100 vehicles, are presented in table 43 in terms of dollars per pound and dollars per linear foot. These data indicate that the segmented leading-edge concept has the lowest cost. The higher cost per pound for the segmented leading edge on the monocoque structure is due to attachment considerations. However, the segmented leading edge is heavier for the semimonocoque and statically determinate structures, so all segmented costs are about the same in dollars per linear foot of leading edge. For the segmented concept, which was selected for application to all primary-structure concepts, the total wing leading-edge cost per linear foot for the baseline vehicle is 427 dollars for all primary-structure concepts.

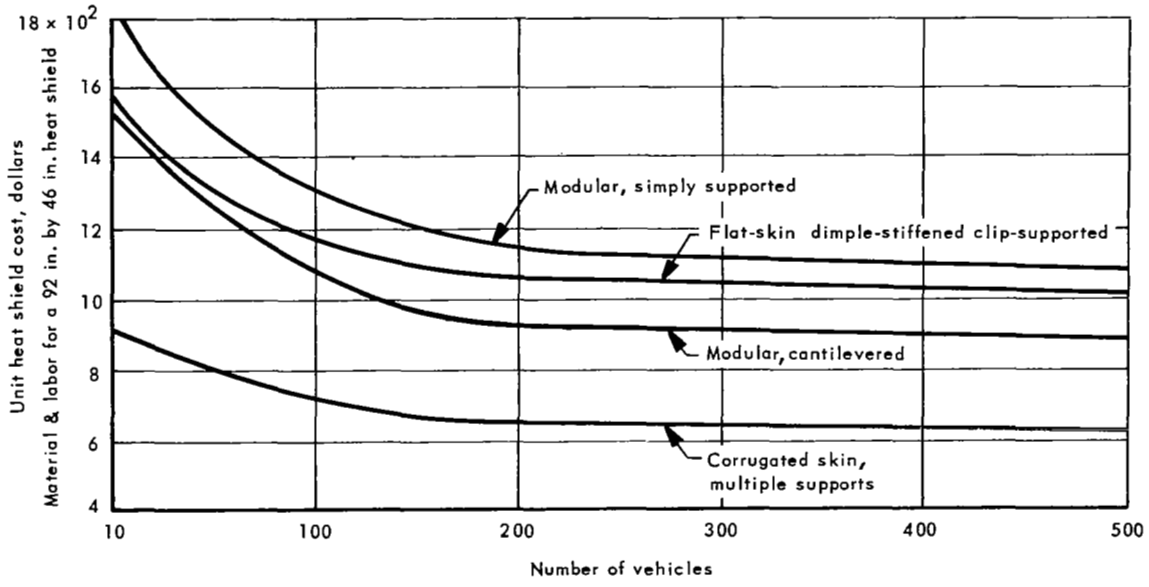

Figure 71. Unit heat shield cost vs number of vehicles

TABLE 42. – SUMMARY OF HEAT-SHIELD COST EVALUATION FACTOR DATA FOR 100-VEHICLE PRODUCTION RUN

Cost evaluation factor	Heat-shield concept			
	Refurbishable		Permanently attached	
	Corrugated skin multiple supports	Flat-skin dimple-stiffened clip-supported	Simply supported	Cantilevered
Material and labor, $ per ft^2	24.5	40.1	44.2	36.4

TABLE 43. – LEADING-EDGE COST EVALUATION FOR WING EVALUATION AREA WITH 100-VEHICLE PRODUCTION RUN

Leading-Edge Concept	Primary structure	Dollars/lb			Dollars/linear ft		
		Labor	Material[b]	Total	Labor	Material[b]	Total
Segmented[a]	Monocoque	22.90	77.55	100.45	97.40	329.60	427.00
	Semimonocoque and Statically determinate	19.90	67.40	87.30	97.40	329.60	427.00
Continuous	Monocoque	51.33	199.13	250.46	387.01	501.34	888.35
	Semimonocoque and Statically determinate	47.50	180.22	227.72	394.79	497.68	892.47

[a]20-in. segments.

[b]TD NiCr.

PERFORMANCE ANALYSIS

Performance degradation caused by aerodynamic drag losses is presented in terms of fuel increment resulting from surface roughness and wing distortion for constant mission range. The fuel increments due to the various types of surface roughness, which were discussed earlier in the concept evaluation procedure section, were based on the parametric design curves presented in figures 72 through 75. Results of performance evaluation of the candidate heat-shield concepts include the required fuel increment due to the deformation of the primary structure.

Primary Structures

The performance penalties resulting from the combined roughness and distortion of the wing are summarized in table 44 for the candidate structural concepts.

Monocoque waffle. – The surface finish of the wing skin of the concepts evaluated is smooth enough to result in no performance losses due to uniformly distributed (sand-grain) roughness. The waffle panels undergo three-dimensional surface distortion, which results in a fuel increment of 31 lb. The waffle panels are connected with a butt joint every 43 in., measured in the chordwise direction. The corrugated heat shield has a lap joint every 43 in. These sheetmetal joints, plus those of the segmented leading edge, produce a fuel penalty of 19 lb. The corrugated heat shield and the end closeouts for the heat-shield corrugations result in a fuel loss of 118 lb. The wing deflections for the cruise loads were used to determine the fuel penalty due to wing deformation, which is 611 lb. The total fuel increment due to the combined roughness and distortion of the monocoque wing concept is 779 lb.

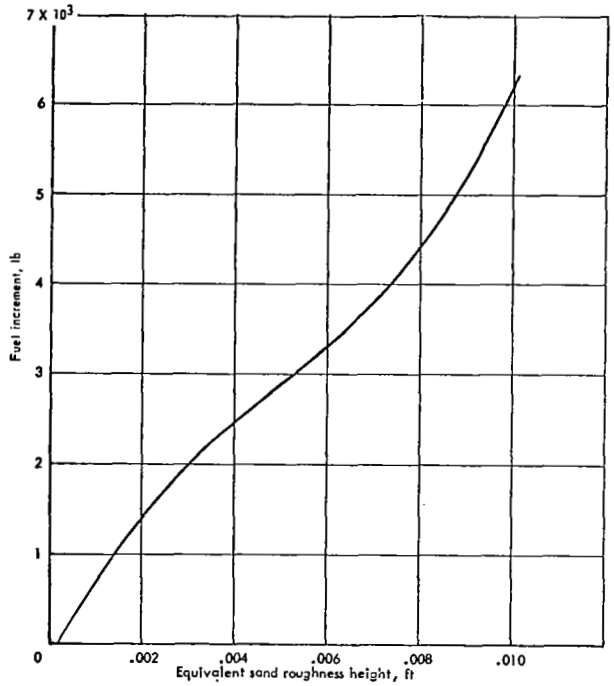

Figure 72. Fuel increment required to compensate for uniformly distributed roughness on wing surface for constant mission range

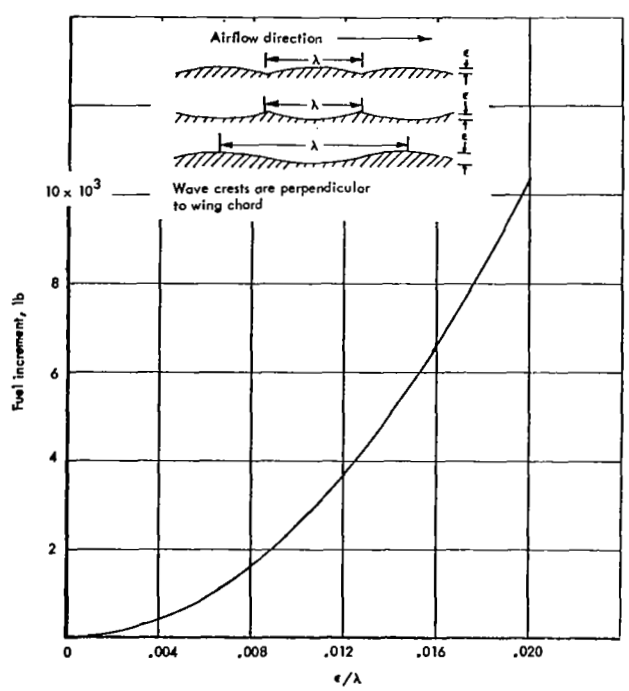

Figure 73. Fuel increment required to compensate for uniform waviness over wing surface for constant mission range

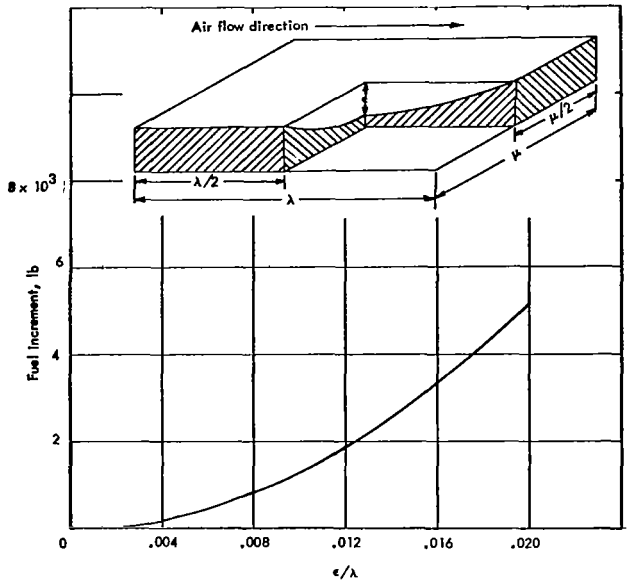

Figure 74. Fuel increment required to compensate for uniform three-dimensional waviness over wing surface for constant mission range

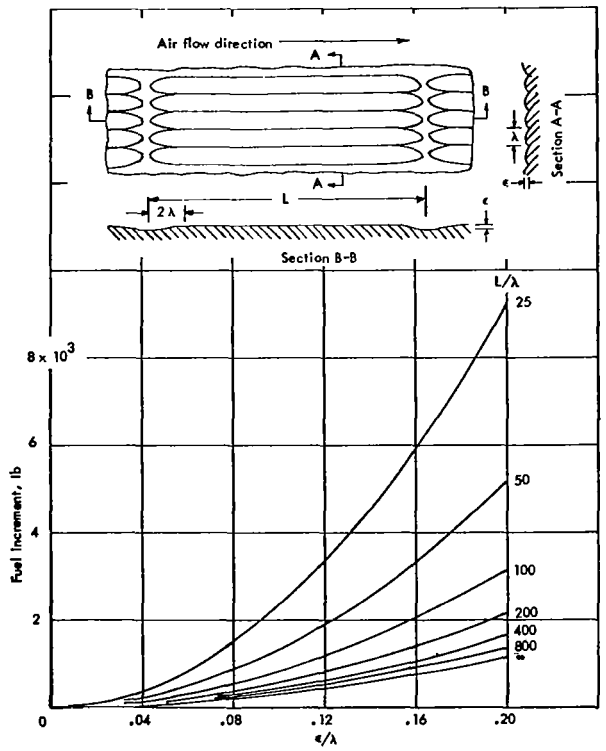

Figure 75. Fuel increment required to compensate for uniform corrugation in wing surface for constant mission range

TABLE 44. – PRIMARY-STRUCTURE CONCEPT PERFORMANCE EVALUATION (FUEL INCREMENT REQUIRED TO PERFORM CONSTANT-RANGE MISSION)

Primary structure concept	Monocoque waffle	Monocoque honeycomb-core sandwich	Semimonocoque spanwise tubular	Semimonocoque spanwise beaded skin	Semimonocoque chordwise tubular/ convex beaded	Statically determinate beaded skin
Fuel increment due to uniformly distributed roughness, lb	0	0	0	0	0	0
Fuel increment due to sheetmetal joints and fasteners, lb	19	155	23	23	32	30
Fuel increment due to surface waviness, lb	31	282	73	81	159	195
Fuel increment due to corrugation, lb	118	118	427	427	1841	427
Fuel increment due to deformation of primary structure, lb	611	458	314	314	521	388
Total fuel increment for wing-structure concept, lb	779	1013	837	845	2553	1040
Total fuel increment due to nominal wing roughness and distortion, lb	1110	1110	1110	1110	1110	1110
Net fuel increment due to wing roughness and distortion, lb	-331	-97	-273	-265	+1443	-70
Fuel mass fraction	0.3994	0.3998	0.3995	0.3995	0.4026	0.3999

Monocoque honeycomb sandwich. – The fuel penalty caused by three-dimensional distortion of the honeycomb panels is 282 lb. This value is larger than that for the monocoque waffle concept because of larger thermal deflections (thermal gradients) imposed on the honeycomb sandwich. The joints, fasteners, and the segmented leading edge cause a fuel penalty of 155 lb. The corrugated heat shield on the lower outboard surface results in a fuel increment of 118 lb. The fuel penalty attributed to the wing distortion is 458 lb. The total fuel increment required to compensate for the roughness and deformation of this wing concept is 1013 lb.

Semimonocoque spanwise tubular. – This concept has corrugated heat shields on all exposed surfaces and a segmented leading-edge. The fuel penalty caused by three-dimensional panel distortion is 73 lb. The lap joints of the heat shield, spaced every 90.0 in., and the sheetmetal joints of the leading-edge have a fuel penalty of 23 lb. The fuel penalty due to the corrugations on the upper and lower heat shield is 427 lb. The fuel penalty attributed to the wing distortion is 314 lb. The total fuel penalty for the combined roughness and wing distortion is 837 lb.

Semimonocoque spanwise beaded skin. – This primary-structure concept incorporates the corrugated heat shield and a segmented leading edge. The fuel penalties resulting from the sheetmetal joints, corrugations, and primary-structure deformations are identical to those of the previous primary-structure concept. The surface

panels of these wing concepts are subject to three-dimensional distortion, which introduces an 81-lb fuel penalty. The total fuel penalty for the concept due to the roughness and distortion of the wing is 845 lb.

Semimonocoque chordwise convex-beaded/tubular. – This candidate wing concept has a convex-beaded panel configuration on the upper surface of the wing and a corrugated heat shield covering the lower wing surface. The fuel penalty produced by three-dimensional distortion is 159 lb. The lap joints of the heat shield, spaced every 24 in., and the sheetmetal joints of the segmented leading,edge installation introduce a fuel loss of 32 lb. The convex beads of the upper wing skin have an end closeout every 24 in. The fuel penalty due to the corrugations of the upper wing skin and the corrugations of the lower surface heat shield is 1841 lb. The fuel increment attributed to the wing distortion is 521 lb. The total fuel increment required to compensate for the roughness and deformation of this wing concept is 2553 lb.

Statically determinate. – This concept has the leading edge and corrugated heat shield employed by the spanwise-stiffened semimonocoque concepts. The fuel penalty due to the heat-shield corrugations is 427 lb. The lap joints of the heat shield result in a fuel penalty of 30 lb for the sheetmetal joints and fasteners. The surface panels distort three-dimensionally, producing a fuel penalty of 195 lb. The fuel penalty for the wing deformation is 388 lb, and the total fuel increment required to compensate for the roughness and distortion of the wing is 1040 lb.

Fuel increment summary. – The performance penalties resulting from the various types of roughness and distortion of the wing are summarized for the six candidate wing concepts in table 44. The total fuel increment for the combined roughness and distortion of each of the candidate wing concepts is compared to the fuel increment of 1110 lb, allowed to compensate for the assumed roughness of the nominal wing, which was 1.10 times smooth wing drag. The net difference between the fuel increment determined for a wing concept and the nominal 1110 lb fuel increment is also listed in table 44 for each of the candidate wing concepts. As shown in table 44, the concept fuel increments are less than the nominal fuel increment except for the chordwise concept, which is more than twice the nominal fuel increment and which results in a figure 1.23 times smooth surface wing friction drag.

The fully heat-shielded surfaces have no appreciable drag increase over a relatively smooth (partially shielded) concept, such as the waffle. However, unshielded upper surface panels with beads protruding into the airstream (chordwise concept) provide the most drag, even though the beads are oriented in the direction of flow.

Using the net fuel increments for each concept, the fuel mass fractions for the baseline vehicle shown in table 44 were determined for input into the interaction evaluation factor investigation, and as shown, the fuel mass fractions are essentially the same for all concepts with the exception of the chordwise concept which has the highest performance penalty.

Heat Shields

The performance degradation resulting from surface roughness, sheetmetal joints and fasteners, surface waviness, corrugations, and deformation of the primary wing

structure has been evaluated for the four heat-shield arrangements applicable to the spanwise tubular structure. These evaluations are summarized in table 45. Wing deflection drag (deformation of primary structure) is included to indicate relative drag of heat shields. The surface finish on all heat-shield concepts was considered to be sufficiently smooth to cause no performance penalties.

TABLE 45. – HEAT-SHIELD CONCEPT PERFORMANCE EVALUATION (SEMIMONOCOQUE SPANWISE TUBULAR PRIMARY-STRUCTURE FUEL INCREMENT REQUIRED TO PERFORM CONSTANT-RANGE MISSION)

Upper surface heat-shield concept Lower surface heat-shield concept	Corrugated Corrugated	Flat-skin dimple-stiffened Flat-skin dimple-stiffened	Simply supported modular Corrugated	Cantilevered modular Corrugated
Fuel increment due to uniformly distributed roughness, lb	0	0	0	0
Fuel increment due to sheet-metal joints and fasteners, lb	23	31	58	149
Fuel increment due to surface waviness, lb	73	43	5	5
Fuel increment due to corrugations, lb	427	0	231	231
Fuel increment due to deformation of primary structure, lb	314	314	314	314
Total fuel increment due to wing roughness and distortion, lb	837	388	608	699
Total fuel increment due to nominal wing roughness and distortion, lb	1110	1110	1110	1110
Net fuel increment due to wing roughness and distortion, lb	-273	-722	-502	-411

Refurbishable heat shields. – The corrugated sheetmetal heat shield on the upper and lower wing surfaces was considered first. The surface of the corrugated heat shields suffers three-dimensional wave distortion, resulting in a fuel penalty of 73 lb. In addition, the skin of this heat shield has a rear-facing lap joint every 90 in., which with the joints and fasteners necessary to the segmented leading edge cause a fuel penalty of 23 lb. The corrugations of the heat shield and the end closeouts of the corrugations near the leading edge result in a fuel penalty of 427 lb. Since all heat-shield concepts were applied to the same primary structure, the fuel increment of 314 lb due to the deformation of the primary structure is common to all concepts. The total fuel increment due to the roughness and distortion of the wing for the corrugated heat shield concept is 837 lb.

The second concept considered has a flat dimple-stiffened skin on the upper and lower surfaces. These panels are subject to three-dimensional wave distortion, and the fuel increment due to this surface waviness is 43 lb. The panels also have a chordwise butt joint every 15.3 in. The fuel penalty due to these sheetmetal joints and those

of the segmented leading edge is 31 lb. The total fuel increment for the combined roughness and distortion of the wing with the flat-skin dimple-stiffened heat shield is 388 lb.

Refurbishable/permanently attached heat shield combinations. – The simply supported modular heat shield on the upper wing surface and the corrugated heat shield on the lower surface of the wing was the first combination of heat-shield concepts considered. The fuel penalty resulting from the panel three-dimensional surface waviness is 5 lb. The skin of the modular concept has a rear-facing chordwise lap joint every 10.4 in., and the lower surface has a lap joint every 90 in. These sheetmetal joints, combined with the joints and fasteners of the segmented leading edge, result in a fuel penalty of 58 lb. The corrugations on the lower-surface heat shield cause a fuel penalty of 231 lb. The total wing fuel penalty for this arrangement of heat shields is 608 lb.

The second arrangement has the cantilevered modular heat shield on the upper surface and the corrugated heat shield on the lower surface. The surface waviness is identical to that of the third concept. The cantilevered modular heat shield has a rear-facing chordwise lap joint every 2.61 in. The fuel penalty for the lap joints and the sheetmetal joints of the leading edge is 149 lb. The total fuel increment resulting from the roughness and distortion of this wing concept is 699 lb.

Fuel increment summary. – The fuel increments of the four heat shield concepts are less than that of the nominal wing, resulting in a payload decrement for each of the candidate heat-shield systems. The fuel increment due to drag is about 450 lb less for the flat-skin dimple-stiffened heat shield than for the corrugated shield; however, the weight of the flat-skin dimple-stiffened heat shield adds 1500 lb for the partially shielded monocoque wing concepts and about 9000 lb for the fully shielded wing concepts. Consequently, the corrugated shield with multiple supports was selected for all structures. In addition, as indicated previously in the cost analysis section, the corrugated shield with multiple supports is also the lowest cost shield.

Leading Edges

The performance degradation resulting from sheetmetal joints and fasteners and the corrugations and closeouts has been evaluated for the segmented and the continuous leading-edge concepts. The end closeouts for the corrugated heat shields are located in the leading edge for the continuous leading-edge concepts. The segmented leading edge is U-shaped and the end closeouts of the corrugations are located in the heat shield just behind the leading edge. The geometric characteristics of the end closeouts are the same for both of the leading-edge concepts and result in identical performance degradation. Because of a joggle joint at the attachment of the leading edge with the wing panel, there is a fuel penalty of 10 lb for either concept. In addition to the joggle joint, the segmented leading edge has an expansion gap between each 20-in. segment. Each segment is fastened to the wing structure with flush-mounted screws. Because of the drag contributed by the expansion gaps and the flush-mounted screws as well as load deflection, the fuel penalty associated with the segmented leading edge adds another 10.2 lb. Therefore, the fuel/payload increments for the continuous and segmented leading edges are 10 lb and 20.2 lb, respectively.

RELIABILITY ANALYSIS

The parametric variations of the factors of safety that affect reliability as measured by weight were determined for low, nominal, and high structural reliability and for -0.5-g, +2.0-g, and cruise load conditions. These parameters encompassed heat shields, leading edges, and primary-structure concepts. Creep and fatigue were analyzed in detail; but it was found that the +2.0-g maneuver condition with short-time material properties was the most critical design condition.

Primary Structures

Relative structural reliability (sensitivity) was based on average unit weights for the entire wing cross-section. To determine average unit wing weights, a spanwise distribution based on total wing cross-section weights in the center A, inboard B, and outboard C wing areas was used for the wing-investigation area. Then total weights were obtained. The wing weights include upper and lower surface panels, spar caps and webs, rib caps and webs, heat shields, insulation, panel closeouts, oxidation penetration, corner posts, and fasteners.

The reliability evaluation results for the six primary structures are shown in table 46 for the wing-investigation area and the total wing. The monocoque waffle results show constant variation in average wing weight of about 1.0 lb/ft^2 between levels of reliability. For the monocoque honeycomb-core sandwich concept, the constant variation in average wing weight is about 0.20 lb/ft^2 between levels of reliability.

TABLE 46. - RELIABILITY EVALUATION WING WEIGHTS FOR BASELINE VEHICLE

Structural concept	Reliability level	Investigation Area Avg. unit weight, lb/ft^2	Total wing weight, lb [a]	Total wing average unit weight, lb/ft^2 [b]
Monocoque waffle	Low	9.446	94 388	9.350
	Nominal	10.494	103 086	10.212
	High	11.402	110 373	10.933
Monocoque honeycomb-core sandwich	Low	6.285	63 254	6.266
	Nominal	6.472	64 778	6.417
	High	6.739	66 756	6.613
Semimonocoque spanwise tubular	Low	5.058	61 114	6.054
	Nominal	5.376	63 981	6.338
	High	5.755	67 418	6.678
Semimonocoque spanwise beaded-skin	Low	4.640	56 753	5.622
	Nominal	5.060	60 601	6.003
	High	5.519	64 766	6.416
Semimonocoque chordwise tubular	Low	5.959	67 000	6.637
	Nominal	6.666	72 867	7.218
	High	7.134	76 742	7.602
Statically determinate spanwise beaded	Low	5.139	62 607	6.202
	Nominal	5.550	66 380	6.575
	High	5.912	69 763	6.911

[a] Includes elevon and basic wing weights less leading-edge weight.

[b] Wing area = 10,095 ft^2.

For the spanwise tubular concept, the results indicate variations in wing weight of about 0.30 lb/ft^2. For the beaded-skin concept, a constant variation of about 0.4 lb/ft^2 was indicated.

The chordwise concept results indicate variations in wing weight of about 0.65 lb/ft^2 between the low and nominal reliability levels and about 0.45 lb/ft^2 between the nominal and high reliability levels. The statically determinate concept results indicate variations in wing weight of about 0.40 lb/ft^2.

For the fatigue reliability evaluation, discrete loading spectra were used to arrive at a loading distribution (actual number of cycles applied at discrete load levels) for cumulative damage analysis. A fatigue-life versus allowable-stress plot, based on Palmgren-Miner cumulative damage theory, provided a direct-reading method of determining the potential penalty (reduced allowable stress) for increase in lifetime. Results of the fatigue-reliability evaluation are shown in figure 76. Fatigue-life requirements for low, nominal, and high levels of reliability were based on scatter factors of 1.0, 1.5, and 2.0, respectively, applied to the specified vehicle life of 10 000 hr at 1400°F. Between low and nominal levels of reliability, the allowable mean stress at cruise decreased 6 ksi.

The effect of creep on primary-structure panel design was determined for the cruise-condition loads and temperatures, and scatter factors corresponding to low and high levels of reliability were applied to the total cruise time. The resulting structures, optimized for creep only, accounted for only 70 percent of the weight of structures designed for the maneuver conditions and checked for creep life. Therefore, creep conditions had to be evaluated, although they are not critical to the design.

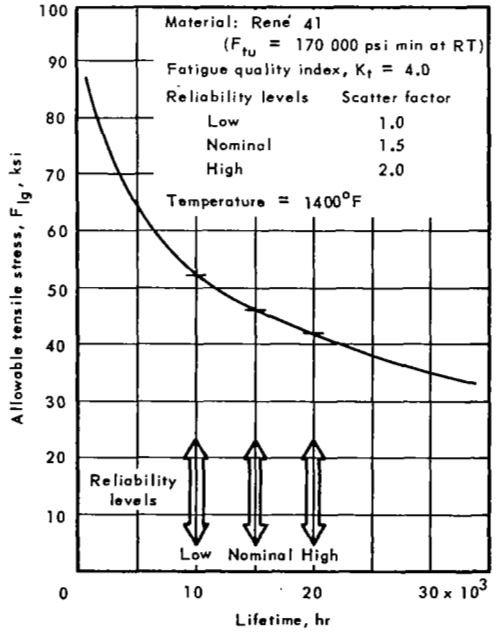

Figure 76. Allowable tensile stress for fatigue of René 41

Heat Shields

Results of the heat-shield reliability evaluations are shown in table 47, with heat shields applicable to a typical spanwise tubular panel (46 in. by 92 in.). For each load factor, the optimum heat shield consists of minimum-gage skin with the support spacing decreased to allow for increased pressure loading. Thus, variation in the panel equivalent thickness $\bar{t}$ is due only to changes in support spacing. The multi-supported corrugated heat shield, for example, has support spacing of 15.3 in., 13.1 in., and 11.5 in. for the three levels of reliability.

Panel sizes for the flat-skin dimple-stiffened concept are 23 in., 15.3 in., and 15.3 in. Because only heat-shield sizes that are multiples of the primary-structure panel size are considered in the heat-shield evaluation, the support spacing and $\bar{t}$ for nominal and high factors of safety are identical. The next larger size (23 in.) would have larger bending moments than allowed by minimum-gage design.

The weights of the two modular concepts are not affected by variations in factor of safety, since they are not influenced by the support spacing of the primary-structure panel.

The results indicate that reliability (weight sensitivity) had little influence upon final selection of the heat-shield concept.

Leading Edges

The leading-edge reliability-evaluation results are shown in table 48. As indicated, the segmented leading edge provides considerably more flights than the continuous concept; and the nominal design for the segmented leading edge more than satisfied the vehicle design-life of 8110 flights. The continuous leading-edge concept does not meet the life requirements for any level of reliability studied.

TABLE 47 – HEAT-SHIELD RELIABILITY EVALUATION[a]

Heat-shield concept		Equivalent panel thickness, $\bar{t}$, in.		
		Low ultimate load factor = 1.5 p_{ult} = 0.75 psi	Nominal ultimate load factor = 2.0 p_{ult} = 1.0 psi	High ultimate load factor = 2.5 p_{ult} = 1.25 psi
Refurbishable	Corrugated, multisupported	0.0127	0.0131	0.0135
	Flat-skin dimple-stiffened, clip-supported	0.0291	0.0298	0.0298
Permanently	Modular simply supported	0.0118	0.0118	0.0118
	Modular cantilevered	0.0123	0.0123	0.0123

[a] p_{limit} = 0.5 psi

TABLE 48. – LEADING-EDGE RELIABILITY EVALUATION

Structural arrangement	Leading-edge life (number of flights)		
	Level of reliability [a] [b] [c]		
	Low scatter factor = 1.0	Nominal scatter factor = 1.5	High scatter factor = 2.0
Segmented leading edge t_{NOSE} = 0.125 in. t_{FLAT} = 0.030 in. Length = 20.0 in. [d]	10.0×10^6	11.9×10^5	2.5×10^5
Continuous leading edge t_{NOSE} = 0.625 in. t_{FLAT} = 0.060 in.	74	12	2

[a] Scatter factor applied to low-cycle fatigue strain allowable.

[b] Fatigue quality index, K_Q = 2, applied to limit elastic thermal strain.

[c] Analysis of end effect based on reference 41.

[d] For cumulative fatigue damage analysis, -0.5-g and +2.0-g conditions are assumed to occur for one of ten flights.

Summary of Concept Reliability Evaluation

Reliability-evaluation results for the selected monocoque, semimonocoque, and statically determinate primary-structure concepts are summarized in figure 77 for the wing investigation area and in figure 78 for the total wing. As shown, for low, nominal, and high levels of reliability they represent ultimate factors of safety of 1.5, 2.0, and 2.5 respectively. Average unit wing weights were based on loads for the +2.0-g maneuver condition.

As shown in figure 77, the chordwise concept is lower in weight than the honeycomb-core sandwich for the low but not high reliability. This is due to the minimum-gage restraint of the honeycomb sandwich.

The total wing weight evaluation of figure 78 indicates that the minimum-gage honeycomb-core sandwich is heavier than the statically determinate concept for the low reliability. However, the honeycomb sandwich is lower in weight than both the statically determinate and tubular concepts at high factors of safety (2.5) – an indication of higher honeycomb efficiency in the higher load ranges.

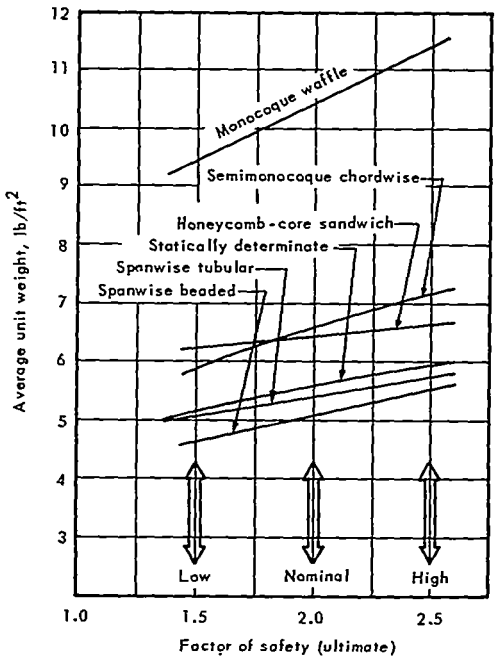

Figure 77. Wing investigation area weights vs factor of safety

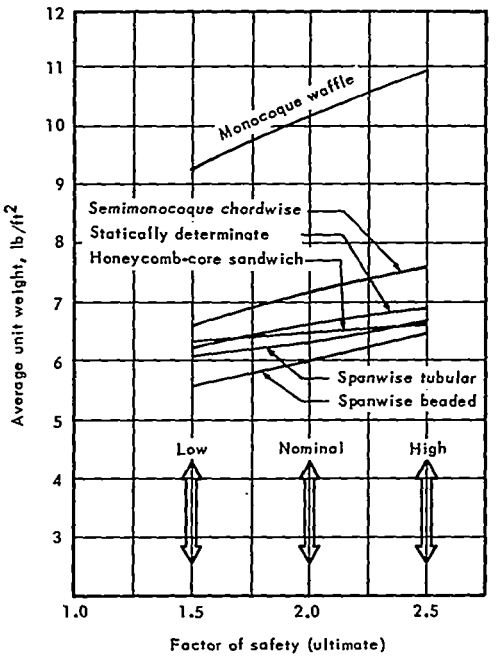

Figure 78. Total wing weights vs factor of safety

INTERACTION OF EVALUATION FACTORS

Total-system costs were determined for each primary-structure concept at each level of reliability. The segmented leading edge and the multiple-support corrugated heat shield concepts were used for each structure.

Results of these determinations are given in tables 49A and 49B in dollars and in cents per ton-mile, respectively. These tables indicate that the semimonocoque spanwise beaded-skin concept has the lowest total-system cost. The spanwise tubular concept is the next lowest-cost concept. The tables also show that the minimum total-system-cost is about 74.7 billion dollars (36.4 cents per ton-mile) for the fleet requirement specified and that fleet procurement costs are 5.7 billion dollars or 9.35 billion dollars with spares. The tables also show that there is a significant cost difference of 6 billion dollars (3 cents per ton-mile) between the minimum-cost and next-lowest-cost primary structure. In addition, improved reliability from low to nominal or nominal to high for any of the concepts adds approximately 5 billion dollars to the total-system-cost, except for the honeycomb sandwich low-to-nominal reliability, which is about 3 billion dollars. The minimum-weight beaded concept reliability can be substantially increased over that of the next best structure for the same total-system cost. The differences in roughness drag and initial cost between concepts have insufficient effect on total-system-cost to change the effect of weight differences. One exception is that at high levels of reliability, honeycomb, even though it is more costly to fabricate than the next heavier concept, offers lower total-system cost; consequently their ratings change with reliability level.

Table 50 shows wing-weights and their relative ratings for the baseline-size vehicle, and their relation to minimum total-system-cost with optimum-size vehicles. The tubular concept is 5.3 percent heavier than the beaded-skin concept, but the total system cost is 8.3 percent greater. The third-ranking primary structure is the honeycomb-core sandwich. This concept is 6.1 percent heavier and 11 percent more costly than the minimum-weight concept. Statically determinate, chordwise-stiffened, and waffle are more costly, respectively, than the first three concepts. It should be noted that small weight increases cause large cost increases. The weight order of concepts, which varies by as little as 5 percent, controls the total-system-cost in the same order, but to a greater degree than this amount.

A plot of total-system-cost (in terms of cents per ton-mile) as it varies with vehicle size (expressed as gross takeoff weight) is given in figure 79 for the different structural concepts. The minimum-cost beaded panel concept permits a vehicle-length variation of 350 to 488 ft or, expressed as gross takeoff weight, a variation of from 620 000 to 1 200 000 lb at less cost than the next-lowest-cost tubular wing structure vehicle. Moreover, the order of structure selection remains unchanged regardless of vehicle size for the range given in figure 79. In particular, for the 550 000-lb baseline vehicle on which basic analyses were performed, this holds true.

A plot of minimum-total-system cost (in terms of cents per ton-mile) as it varies with wing unit weight for both the optimum-size vehicle and the corresponding baseline-size vehicle for the various structural concepts (at nominal factor of safety) is given in figure 80. The waffle concept costs are large because at the waffle-concept weight, the vehicle has little payload. Consequently 1023 vehicles (see table 49A) instead of 129

TABLE 49A. – COST BREAKDOWN IN DOLLARS FOR EACH PRIMARY STRUCTURE AT EACH LEVEL OF RELIABILITY

Structure concept	Level of reliability	Vehicle weight, lb	Vehicle length, ft	Wing unit weight, lb/ft^2	Payload, lb	Fleet size, no. veh.	Cost per vehicle, millions
Semimonocoque spanwise beaded	Low	923 970	427	7.126	95 942	115	45.390
	Nominal	882 621	418	7.454	85 068	129	43.818
	High	836 824	407	7.784	74 056	149	42.036
Semimonocoque spanwise tubular	Low	874 287	416	7.497	83 324	132	43.330
	Nominal	840 670	408	7.716	75 618	145	42.025
	High	791 110	395	7.924	66 349	166	40.097
Monocoque honeycomb-core	Low	842 818	408	7.598	77 478	142	44.108
	Nominal	835 241	406	7.748	74 179	148	43.812
	High	799 753	398	7.841	68 388	161	42.368
Statically determinate spanwise beaded	Low	836 318	407	7.897[b]	71 933	153	43.603
	Nominal	797 493	397	8.186	62 906	175	41.997
	High	762 021	388	8.462	55 322	199	40.493
Semimonocoque chordwise tubular	Low	799 766	398	7.898	65 283	168	40.615
	Nominal	726 862	379	8.251	51 669	213	37.665
	High	709 737	375	8.596	45 085	244	36.827
Monocoque waffle	Low	599 236	344	9.809	20 903	526	34.475
	Nominal	562 904	334	10.432	10 748	1023	31.440
	High	529 254	323	10.888	3 323	3310	27.183

Structure concept	Cost oper vehicles, billions	Initial investment[a], billions	DOC, billions	IOC, billions	Total operational cost, billions	Total system-cost, billions	Relative total-system-cost
Semimonocoque spanwise beaded	5.204	8.689	43.327	16.625	59.952	68.641	
	5.666	9.354	46.821	18.567	65.388	74.742	1.00
	6.244	10.186	51.175	21.094	72.270	82.455	
Semimonocoque spanwise tubular	5.720	9.430	47.351	18.917	66.268	75.698	
	6.113	9.994	50.301	20.678	70.979	80.973	1.083
	6.648	10.757	54.028	23.435	77.463	88.219	
Monocoque honeycomb-core	6.262	10.214	49.606	20.194	69.800	80.015	
	6.497	10.558	51.381	21.053	72.434	82.993	1.110
	6.815	11.008	53.528	22.641	76.169	87.178	
Statically determinate spanwise beaded	6.668	10.816	53.004	21.717	74.721	85.538	
	7.344	11.796	57.984	24.600	82.584	94.380	1.263
	8.051	12.822	63.194	27.731	90.925	103.747	
Semimonocoque chordwise tubular	6.843	11.052	56.012	23.734	79.746	90.798	
	8.019	12.747	64.748	29.454	94.202	106.949	1.431
	8.985	14.167	72.536	33.612	106.148	120.315	
Monocoque waffle	18.142	27.599	134.453	70.450	204.903	232.501	
	32.177	48.247	245.120	135.739	380.859	429.106	5.741
	89.973	133.278	737.475	435.156	1,172.630	1,305.908	

[a] Includes spares.
[b] Includes weight of fuselage body penalty.

TABLE 49B. – COST BREAKDOWN IN CENTS PER TON-MILE FOR EACH PRIMARY STRUCTURE AT EACH LEVEL OF RELIABILITY

Structure concept	Level of reliability	Vehicle weight, lb	Vehicle length, ft.	Wing unit weight, lb/ft^2	Payload, lb	Fleet size, no. veh.	Cost oper vehicles, cents/ton-mi
Semimonocoque spanwise beaded	Low	923 970	427	7.126	95 942	115	2.533
	Nominal	882 621	418	7.454	85 068	129	2.758
	High	836 824	407	7.784	74 056	149	3.039
Semimonocoque spanwise tubular	Low	874 287	416	7.497	83 324	132	2.784
	Nominal	840 670	408	7.716	75 618	145	2.975
	High	791 110	395	7.924	66 349	166	3.236
Monocoque honeycomb-core	Low	842 818	408	7.598	77 478	142	3.048
	Nominal	835 241	406	7.748	74 179	148	3.162
	High	799 753	398	7.841	68 388	161	3.317
Statically determinate spanwise beaded	Low	836 318	407	7.897[b]	71 933	153	3.245
	Nominal	797 493	397	8.186	62 906	175	3.574
	High	762 021	388	8.462	55 322	199	3.918
Semimonocoque chordwise tubular	Low	799 766	398	7.898	65 283	168	3.331
	Nominal	726 862	379	8.251	51 669	213	3.903
	High	709 737	375	8.596	45 085	244	4.373
Monocoque waffle	Low	599 236	344	9.809	20 903	526	8.830
	Nominal	562 904	334	10.432	10 748	1023	15.661
	High	529 254	323	10.888	3 323	3310	43.791

Structure concept	Initial investment[a] cents/ton-mi	DOC, cents/ ton-mi	IOC, cents/ ton-mi	Total operational cost, cents/ton-mi	Total-system-cost cents/ton-mi	Relative total-system-cost
Semimonocoque spanwise beaded	4.229	21.09	8.09	29.18	33.41	
	4.555	22.79	9.03	31.82	36.38	1.00
	4.957	24.91	10.26	35.17	40.13	
Semimonocoque spanwise tubular	4.589	23.04	9.21	32.25	36.84	
	4.864	24.48	10.07	34.55	39.41	1.083
	5.235	26.29	11.41	37.70	42.94	
Monocoque honeycomb-core	4.971	24.14	9.83	33.97	38.94	
	5.138	25.00	10.25	35.25	40.39	1.110
	5.356	26.05	11.02	37.07	42.43	
Statically determinate spanwise beaded	5.264	25.80	10.57	36.37	41.63	
	5.741	28.22	11.97	40.19	45.93	1.263
	6.240	30.75	13.50	44.25	50.49	
Semimonocoque chordwise tubular	5.379	27.26	11.55	38.81	44.19	
	6.204	31.51	14.34	45.85	52.05	1.431
	6.895	35.30	16.36	51.66	58.56	
Monocoque waffle	13.432	65.44	34.28	99.72	113.16	
	23.482	119.30	66.06	185.36	208.84	5.741
	62.866	358.92	211.79	570.71	635.58	

[a] Includes spares.
[b] Includes weight of fuselage body penalty.

TABLE 50. – WING WEIGHTS AND RELATION OF WING WEIGHT TO TOTAL-SYSTEM-COST

Wing primary-structure concept	Weight comparison for baseline-size vehicle[a]		Minimum TSC[b] comparison for optimum-size vehicles[c]
	Wing weight,[d] lb/ft^2	Relative weight	Relative cost
(1) Semimonocoque spanwise beaded	6.20	1.000	1.000
(2) Semimonocoque spanwise tubular	6.53	1.053	1.083
(3) Monocoque honeycomb-core	6.58	1.061	1.110
(4) Statically determinate spanwise beaded	6.77	1.092	1.263
(5) Semimonocoque chordwise tubular	7.41	1.195	1.431
(6) Monocoque unflanged waffle	10.38	1.674	5.741

[a]Gross takeoff weight = 550 000 lb.
[b]TSC = procurement cost and operating costs for a 205 x 10^9 ton-mile fleet mission.
[c]Gross takeoff weight and fleet size = variable.
[d]Wing weights are given in lb per ft^2 of planform wing area.

for the minimum-weight beaded-skin concept are required to perform the fleet mission requirements. Figure 80 shows the effect of increasing unit wing weight, which if extrapolated to about 12.0 lb/ft^2, would show the total-system-cost approaching infinity, since at this weight the payload is zero.

Baseline-vehicle-size wing weights are shown in addition to the optimum-size vehicle data because the unit wing weights for the baseline vehicle are comparable to one another, whereas the optimum-size vehicle unit weights vary as a function of vehicle size. This consistency for baseline-size vehicle wing unit weights enables estimates to be made of how other concepts calculated for the baseline-size vehicle, such as those dropped out by intermediate screening, compare with the listed concepts. For instance, the semimonocoque spanwise trapezoidal corrugation concept wing average weight is 7.45 lb/ft^2 (see ref. 5), which from figure 80 indicates a weight and a total-system-cost that are greater than all but the waffle concept.

Figure 80 indicates that the semimonocoque chordwise, statically determinate (with body penalty), and honeycomb structures have total-system-costs that fall on the curve drawn through the semimonocoque spanwise concepts and the waffle concept. The chordwise concept has twice the roughness-drag fuel increment of the other concepts. The statically determinate wing structure requires additional fuselage weight

over the other concepts, and the honeycomb concept has the highest fabrication cost of all concepts except waffle which has a high total-system-cost primarily because of its excessive weight. Consequently, a weight change of structure due to efficiency change is most responsible for the change in total system cost.

The total-system-cost results enable an estimate to be made of what the penalty is for a one pound increase in total wing weight with a resulting reduction of one pound in payload. This penalty for the most efficient structure is about \$7000/lb., i.e., the total-system-cost or loss in revenue attributed to costs is \$7000 for each airplane for a one pound increase in structure weight for each airplane. This amounts to about \$900 000 total-system-cost for the fleet of vehicles for the semimonocoque spanwise-beaded wing structure where total wing weight of each airplane is increased by 1 lb or by 0.00006 lb/ft^2. Therefore, it appears that considerable effort is warranted to remove unnecessary weight from the structure of a hypersonic cruise vehicle.

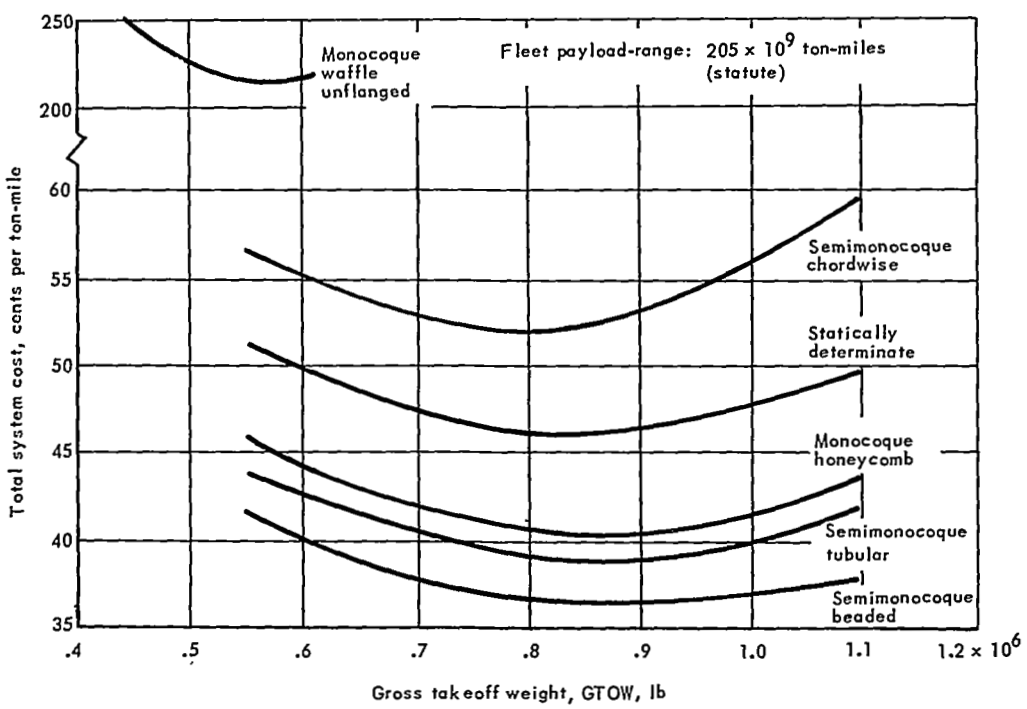

Figure 79. Total-system-cost for optimized vehicles of various wing constructions

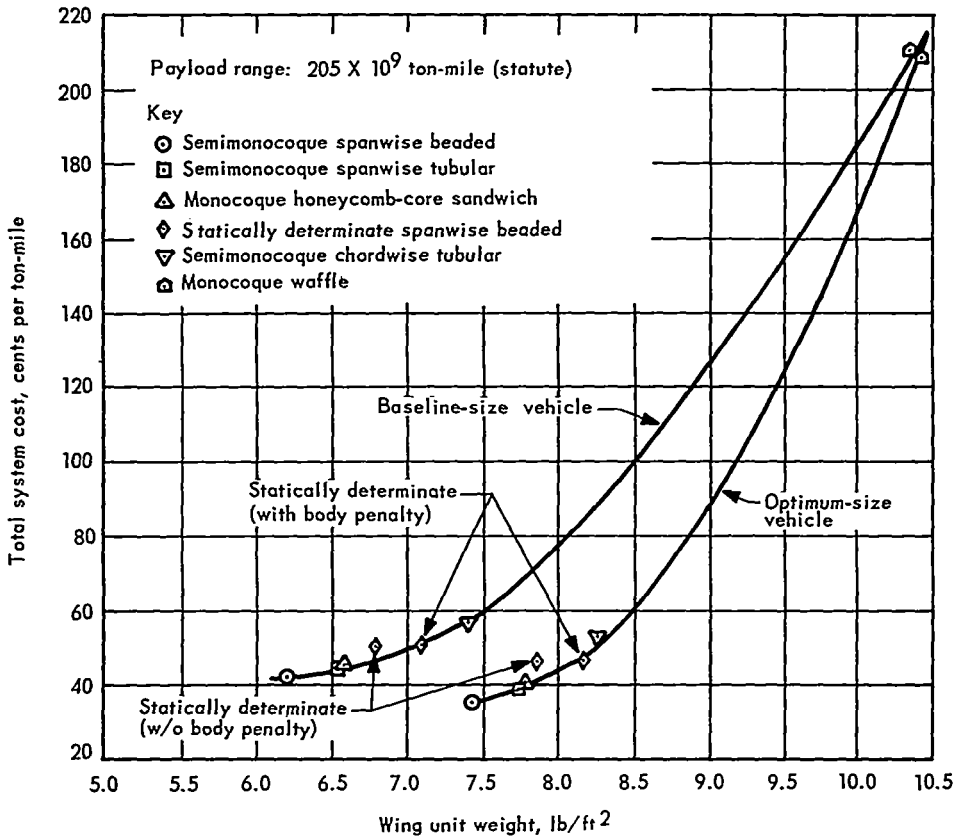

Figure 80. Total-system-cost for baseline and optimum-size vehicles of various wing constructions

CONCLUSIONS

Conclusions resulting from the investigation to provide the experimental and theoretical data to support selection of a lightweight, hot-wing structure for a hypersonic cruise vehicle are as follows:

Based on minimum-total-system cost, the interaction evaluation of the four factors of weight, cost, performance, and reliability established the following ranking of wing primary structures:

(1) Semimonocoque spanwise-stiffened beaded skin
(2) Semimonocoque spanwise-stiffened tubular
(3) Monocoque honeycomb-core sandwich
(4) Statically determinate spanwise beaded skin
(5) Semimonocoque chordwise-stiffened tubular lower surface and convex-beaded upper surface
(6) Monocoque unflanged waffle

All of the primary structures analyzed are satisfactory from the standpoint of utlimate load, wing flutter, panel flutter, sonic fatigue, fatigue, and creep, and they require no refurbishment throughout the life of the vehicle. Minimum-weight construction requires insulation at the outboard lower surface, which minimizes the thermal stresses and limits the primary-structure temperatures to approximately 1600°F.

The most favorable heat shield for use with the primary structures is a large corrugated skin, of the same size as the primary-structure panel, with multiple supports. The total drag of the spanwise semimonocoque structures, which utilize these shields on all exposed surfaces, proved to be less than the partially shielded honeycomb structure. This fact was mainly attributed to the smaller number of sheetmetal joints exposed to the airstream and a small panel deflection penalty.

For the leading edge, a segmented slip-jointed type, which is insulated from the primary load-carrying structure, was selected, since its life is greater than the vehicle-life requirement whereas the continuous-type does not meet the service-life requirements.

To satisfy the requirement of 10 000 hr of life, Rene 41 superalloy is the most satisfactory material for the primary structures and most heat shields. The additional weight to accommodate depth of attack due to oxidation is small. The choice of material for the heat shields adjacent to the leading edge and for the leading edge is the dispersion-strengthened alloy TD NiCr. The use of radiation-equilibrium temperatures for selecting the leading-edge material is not satisfactory; instead, a two-dimensional thermal analysis considering material thickness, lateral conduction, and internal radiation is required. No refurbishment of leading edges or heat shields is required throughout the life of the vehicle.

Refractory metals are not required for a Mach 8 wing application. The metal selected for the primary structures and most of the heat shields, René 41, can be successfully stretch-formed for stiffened-panel configurations requiring at least 39-percent elongation. In addition, it can be successfully formed and welded (by

resistant spot or TIG welding) in the annealed condition followed by aging.

Panel-element tests performed in this study agreed reasonably well with the theory; however, exceptions were noted, indicating a need for further tests.

It is essential to consider local and general instability in wing-panel optimization to satisfy the inplane compression and shear, and normal pressure loads. Thermal loads are important to design, and a proper thermal-protection system can reduce weight. It was found that the wing inplane airloads are low for a Mach 8 wing application, even during the +2.0-g maneuver. Light loads tend to yield large panels; therefore, air-pressure loads become significant in panel design. With reference to the wing study section, aeroelastic loads agree well with rigid loads. Because of the low loads at outboard locations, selection of material minimum-gage thickness is important to design for such areas, and for other areas for the more efficient structures.

One of the most important results of the investigation is the rating system developed. The interrelation of the evaluation factors of weight, cost, and performance for various levels of reliability on the basis of total-system cost is applicable to any combination of structural concepts. Of the four basic evaluation factors, weight has the most influence on total-system cost. For instance, although fabrication costs were higher than the next heavier concept at high factors of safety, honeycomb has a lower total-system cost. For the performance (roughness-drag) factor, the fuel-penalty increments for all structural concepts are somewhat less than the value used for the nominal wing condition, which was a skin-roughness drag of 10 percent greater than the smooth-surface skin drag, except that the chordwise-stiffened semimonocoque concept had twice this drag-induced fuel-penalty increment. Therefore, performance has little influence on the interaction evaluation. Furthermore, the minimum total-system-cost concept at nominal reliability remains minimum-cost at both low and high reliability levels. There is a system-cost change relative to the other concepts at the same level of reliability for the honeycomb concept. At a high level of reliability, honeycomb has the second lowest total-system cost.

The primary-structure concept with the least weight, fabrication cost, and total-system cost, the semimonocoque spanwise-stiffened beaded skin, has a significantly lower total-system cost than the next best concept. The minimum-weight beaded-skin structure permits a factor of 2 variation in vehicle weight for less total system cost than the next-lowest-weight structure. In addition, the order of structure concepts remains unchanged regardless of vehicle size for the range evaluated; in particular, this is the case for the baseline vehicle (550 000 lb) on which all in-depth analyses were performed.

APPENDIX A

PANEL-ELEMENT TESTING

Panel-element tests to substantiate, and if necessary refine, the methods of analysis and the concept designs were conducted in parallel with the theoretical analysis and the latter portion of the material-screening testing. These tests were conducted on semimonocoque panels, since the initial weight-screening results indicated that these panels are generally lower in weight than the monocoque panels and less information exists for tests of the semimonocoque panels. Twenty-one structural element panels were designed, fabricated of René 41, and tested in accordance with the structural-element test schedule outlined in table 51. As indicated, the concepts included the tubular, beaded, corrugation-stiffened, trapezoidal-corrugation, circular-arc corrugation web, and channel spar cap. Since some of these concepts are new, validation of local buckling and end-closure design was required.

End closeouts (8 in. by 17 in.), crippling (8 in. by 17 in.), column (30 in. by 17 in.), and inplane shear (17 in. by 17 in.) tests were conducted at room temperature and at 1400°F for evaluation of the structural concepts. The information obtained from these tests included evaluation of end-closure designs; evaluation of joining methods; combined effects of temperature and load; and substantiation of element and panel shear, crippling, and compression panel buckling stresses.

Fabrication

Resistance spotwelding was used for the stiffened-panel configurations, and melt-through welding for the cap-web specimens. Crippling and end-closeout panels were saw cut from full-length panels and ends of crippling panels; one end of each end-closeout panel was cast in Densite or Pyroform for testing. Tubular and corrugation-stiffened skin panels were formed on a multistage high-pressure Version-Wheelon press. Multistage hydraulic forming in a Clearing 1500-ton press was used for the beaded-skin concept. Power-brake forming was used for the trapezoidal-corrugation concept.

The manufacturing processes used for the fabrication of the test panels included interstage annealing for several of the panel configurations. Therefore, mechanical property tests were conducted to establish the material characteristics resulting from these processes.

Test Procedure

The test setups for the room- and elevated-temperature compression tests of the panel, crippling, end closeout, and spar-cap crippling specimens were essentially the same. Typical setups for the crippling and compression panel tests are shown in figure 81, positioned in the compression bay of a testing machine of suitable capacity. These specimens are located between a baseplate and a compression-head test fixture. The initial alignment of the compression surfaces was held to within ±0.005 in. across the total bearing surfaces of the loading fixture.

TABLE 51. – STRUCTURAL-ELEMENT TEST SCHEDULE

Test-panel configuration	Type of test	Number tested					
		End closeout	Crippling		Panel		Inplane shear
	Temp, °F	RT	RT	1400	RT	1400	RT
Tubular 		1	1	1	1	1	–
Beaded 		1	1	1	1	–	–
Corrugation-stiffened 		1	1	1	1	1	–
Trapezoidal-corrugation 		–	1	1	1	1	–
Shear web 		–	–	–	–	–	2
Channel spar cap 		–	1	–	–	–	–
Total number of panels		3	5	4	4	3	2
Grand total							21

The general arrangement for the inplane shear test is shown in figure 82. The test panel is mounted in a cantilever-type loading test fixture. Flexure pivots are incorporated in the test fixture design at each of the four corners to eliminate the friction associated with pin connections. A hydraulic jack was used to apply vertical loading to the cantilevered test fixture.

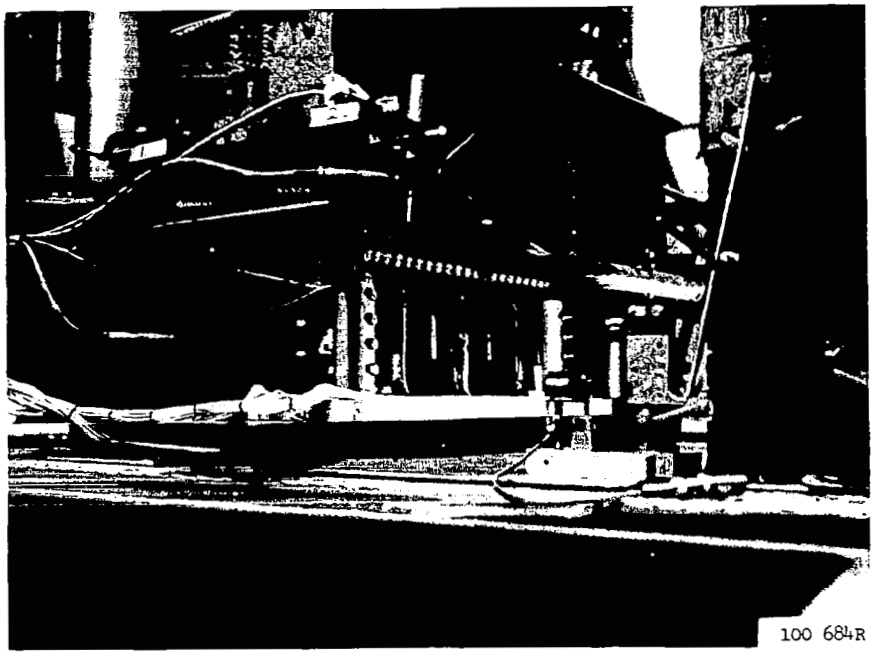

Typical crippling panel test

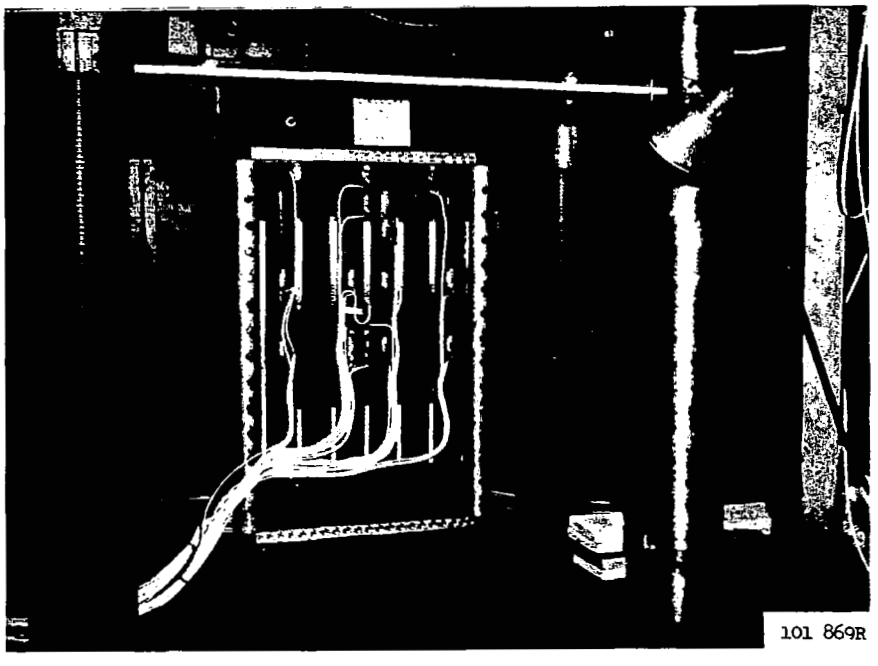

Typical compression panel test

Figure 81. Typical room-temperature compression-test setups

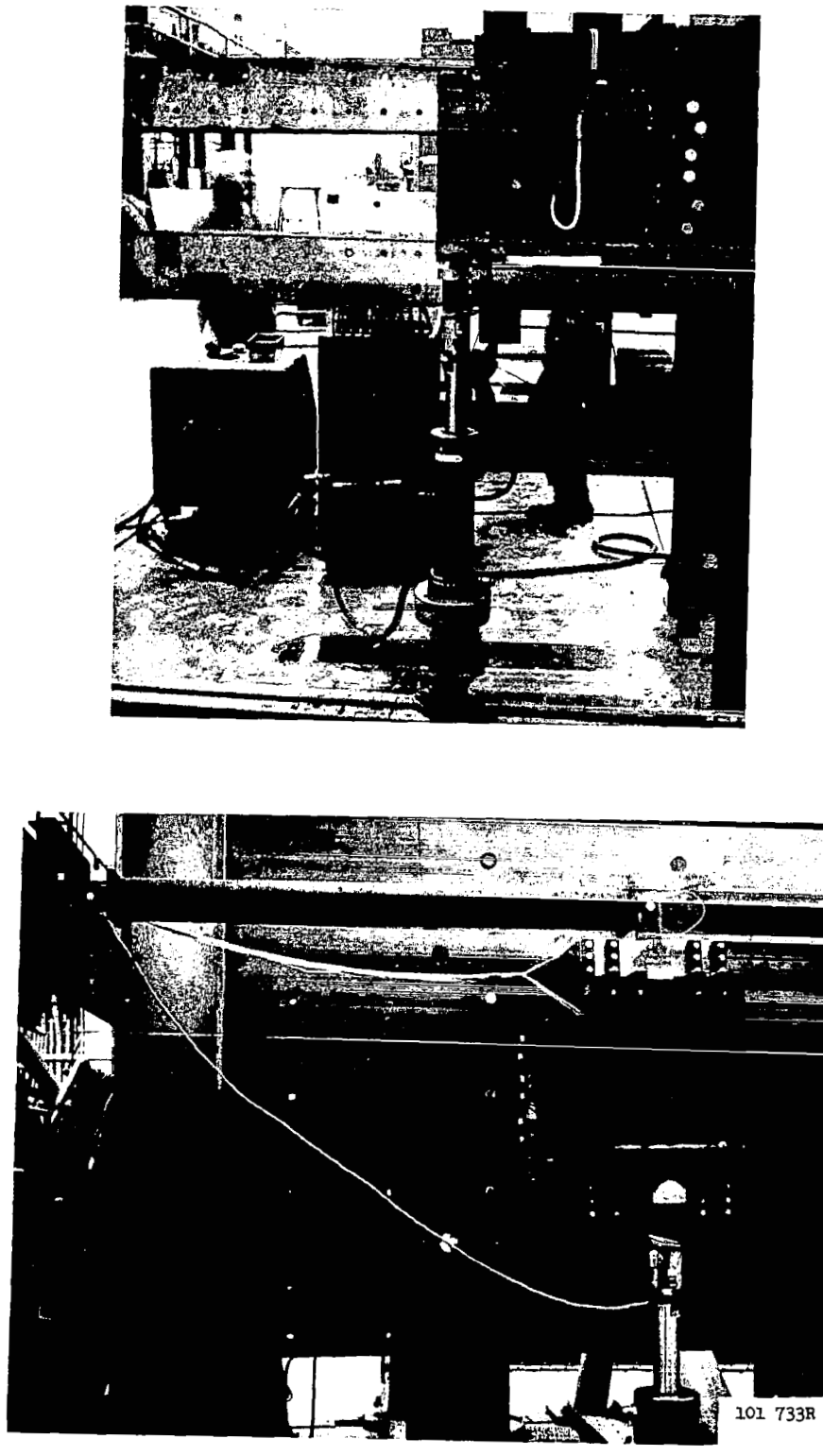

Figure 82. Test setup for inplane shear-panel tests

Comparison of Analysis and Test Results

A summary of the correlation between the analysis and test results of the structural element test specimens is presented in table 52. The following observations are pertinent:

(1) The initial compression buckling stress test results correlated reasonably well with initial buckling stress predictions whenever it was possible to positively identify initial buckling in either the room- or elevated-temperature tests. This correlation was noted for about half the tests. The correlation with theory for the remaining tests indicated variations of approximately 50 percent. Table 52 gives reasons for the disagreements when possible. Tests in which the variation is not explainable indicate a need for further tests.

(2) The tubular and beaded-skin configurations exhibit the same sensitivity to initial imperfections and other disturbances as found in axially compressed large thin cylindrical shells. Consequently, a conservative method of predicting compression buckling was employed. Even with this conservative method, large variations between test and theory were noted, as described above.

(3) All of the configurations exhibit about a ±10 percent variation in thicknesses across their widths, resulting from the forming process. This is within the normal tolerance of the sheet material. The analytical methods show significant fluctuations with these thickness variations; however, fair agreement exists between test and theory when the thickness used in calculations is based on the lower limit of the tolerance.

(4) The corrugation-stiffened concept demonstrated substantial post-buckling strength. Therefore, this configuration has a higher potential than the initial buckling analysis allows, providing permanent set due to inelastic deformation after initial buckling is acceptable. The test results indicated a variation of more than 20 percent over the predicted values for four of the tests performed. Of these tests, three were comparisons of the failure stresses.

(5) Panel instability was observed in several of the tests of 30-in. specimens, and the test loads agreed favorably with the analysis based on orthotropic theory for plates simply supported on all four sides. It is shown that the wide-column analysis used in the optimization of these configurations is a simplified form of the orthotropic plate theory (n=0). This theory is valid for panel width-to-length ratios of 2 or more when the unloaded edges are supported but it is conservative for ratios less than 2. However, the wide-column analysis is valid for any width-to-length ratio when tested with unsupported edges. It is concluded that the test panels demonstrated in part the validity of the theory. However, no tests were performed for unsupported edges, for buckling due to inplane shear, or for bending due to lateral pressure. Since the optimum ratio for the hypersonic-vehicle wing structure is greater than 2, the use of wide-column analysis in the optimization program is also valid.

(6) The configuration composed of a single beaded skin is susceptible to a local instability mode with a very short transverse half-wavelength, which can be predicted with reasonable accuracy. This mode of failure was accounted for in the analysis.

(7) The shear-panel test specimens correlated within 7 percent of the calculated initial buckling stresses.

(8) The measured initial buckling stress on the spar cap was within 5 percent of the calculated initial buckling stress.

TABLE 52. – SUMMARY CORRELATION OF STRUCTURAL-ELEMENT TESTS

Panel concept	Test type	Test temp., °F	Calculated Stresses		Avg. test stresses		Remarks
			Initial buckling,[a] psi	Failure, psi	Initial buckling, psi	Failure, psi	
Tubular	Closeout	RT	105 300 L	105 300 C	83 000	85 000	End doublers were too short
	Crippling	RT	105 300 L	105 300 C	88 000	90 400	Uneven load distribution
	Crippling	1400	78 500 L	78 500 C	66 700	66 700	Some detached spotwelds
	Panel[c]	RT	105 300 L	105 300 C	73 800	73 800	Some detached spotwelds; and unknown amount of bending load was applied in test
	Panel[c]	1400	78 500 L	78 500 C	80 200	80 200	None
Beaded	Closeout	RT	130 000 L	130 000 C	74 500	84 600	End doublers were too short
	Crippling	RT	130 000 L	130 000 C	96 700	105 000	Proportional limit being approached and actual values for the tested sheet unknown
	Crippling	1400	92 500 L	92 500 C	65 400	72 200	
	Panel	RT	27 900 L	27 900 L	32 600	42 600	Some postbuckling behavior
Corrugation-stiffened	Closeout	RT	22 200 L	55 000 C	26 300	47 300	Failure in edge support due to eccentric loading
	Crippling	RT	22 200 L	55 000 C	26 000	69 200	Substantial postbuckling strength indicated in test
	Crippling	1400	16 200 L	41 500 C	30 000	43 700	Unknown
	Panel[c]	RT	22 200 L	32 900 P	24 700	39 600	Eccentric end loading and a panel bowing imperfection of 0.10 measured at midpanel
	Panel[c]	1400	16 200 L	24 000 P	17 300	32 000	Some postbuckling behavior
Trapezoidal corrugation	Crippling	RT	69 600 L	86 600 C	69 600	92 400	None
	Crippling	1400	50 800 L	64 300 C	54 500	66 800	None
	Panel[b,c]	RT	69 600 L	75 200 P	69 300	75 600	None
	Panel[b,c]	1400	50 800 L	55 100 P	49 800	49 800	Panel instability with possible interaction with initial buckling
Circular arc Corrugation	Shear	RT	41 200 L	44 200 P	38 500	40 500	None
Shear panel		RT	38 700 L	43 300 P	38 400	38 400	
Spar cap	Crippling	RT	110 000 L	133 500 C	104 000	127 200	Slight eccentric cap loading

[a]Code for type of buckling: L local, P panel, C crippling.
[b]Tested with clamped loaded edges; all other types of panels tested with simple support-loaded edges.
[c]All panels tested for panel buckling were 30 in. long.

REFERENCES

1. Heldenfels, R. R.: Structural Prospects for Hypersonic Air Vehicle. ICAS paper, 1966.

2. Plank, P. P.; and MacMiller, C. I.: Analytical Investigation of Candidate Thermal-Structural Concepts Applicable to Wing, Fuselage, and Inlet Structure of a Manned Hypersonic Vehicle. AFFDL-TR-66-15, 1966.

3. Plank, P. P.: Hypersonic Thermal-Structural Concept Trends. SAE paper 660678, 1966.

4. NASA-SP-148. Conference on Hypersonic Technology, Ames Research Center, 1967.

5. Plank, P. P.; Sakata, I. F.; Davis, G. W.; and Richie, C. C.: Substantiation Data for Hypersonic Cruise Vehicle Wing Structure Evaluation. NASA CR-66897-1, -2, -3, 1970.

6. Rising, J. J.: Aerodynamic Performance Coefficients for a Proposed Delta-Wing Body, Manned Hypersonic Vehicle. Lockheed-California Company Aerodynamic Memorandum Report No. 40, 1966.

7. Fully Automatic Computer Technique of Sizing for Manned Hypersonic Vehicles. Lockheed California Company Computer Control No. 2802, 1966.

8. Ames Research Staff.: Equations, Tables and Charts for Compressible Flow. NACA Report 1135, 1953.

9. Liepman, H. W.; and Rosko, A.: Elements of Gasdynamics. John Wiley & Sons, 1957.

10. Dyer, I.; Franken, P. A.; and Ungar, E. E.: Noise Environments of Flight Vehicles. Noise Control, Jan-Feb 1960.

11. Eldred, K.; Roberts, W.; and White, R.: Structural Vibrations in Space Vehicles, WADD TR 61-62.

12. Lockheed-California Company. Volume 11-C, Airframe Design, LR 19839.

13. Hansen, C. F.: Approximations for the Thermodynamic and Transport Properties of High Temperature Air. NASA TR R-50, 1959.

14. Beckwith, I. E.: Similar Solutions for the Compressible Boundary Layer on a Yawed Cylinder with Transpiration Cooling. NASA TR R-42, 1959.

15. Beckwith, I. E.; and Gallagher, J. J.: Local Heat Transfer and Recovery Temperatures on a Yawed Cylinder at a Mach Number of 4.15 and High Reynolds Numbers. NASA TR R-104, 1961.

16. Bushnell, D. M.: Interference Heating on a Swept Cylinder in Regions of Intersection with a Wedge at Mach Number 8. NASA TN D-3094, Dec 1965.

17. Thomas, A. C.; Perlbachs, A.; and Nagel, A. L.: Advanced Reentry System Heat Transfer Handbook for Hypersonic Flight. AFFDL-TR-65-195, Jun 1966.

18. Schultz, H. D.: Thermal Analyzer Computer Program for the Solution of General Heat Transfer Problems, Lockheed-California Company. LR 18902 Jul 1965.

19. Eckert, E. R. G.: Survey of Heat Transfer at High Speeds. WADC TR-54-70, Apr 1954.

20. Spalding, D. B.; and Chi, S. W.: The Drag of a Compressible Turbulent Boundary Layer on a Smooth Flat Plate With and Without Heat Transfer. Journal of Fluid Mechanics, Vol. 18, Jan 1964.

21. Schlichting, H.: Boundary Layer Theory. McGraw-Hill, New York, 1960.

22. Pagel, L.: et al: ASSET, Correlative Analysis of Heat Transfer Data. AFFDL-TR-65-31, Vol. IV, Apr 1966.

23. Schultz, H. D.: Hypersonic Boundary Layer Transition. Lockheed-California Company, LR 21245, Dec 1967.

24. Jillie, D. W.; and Hopkins, E. J.: Effects of Mach Number, Leading-Edge Bluntness, and Sweep on Boundary-Layer Transition on a Flat Plate. NASA TN D-1071, 1961.

25. Personal Communication, F. L. Guard, Lockheed-California Company and R. D. Banner, NASA Flight Research Center, Edwards Air Force Base, California, Nov 1967.

26. Benson, J. L.: Computer Program for the Design and Analysis of Hypersonic Inlets. Lockheed-California Company, LR 18079, Aug 1964.

27. Jakob, M.: Heat Transfer, Volume II. John Wiley & Sons, New York, 1949.

28. McAdams, W. H.: Heat Transmission. McGraw-Hill, New York, 1933.

29. Haggenmacher, G. W.: Preparation of Data for the Redundant Structures Analysis Programs. Lockheed-California Company, LR 13091, Feb 1964.

30. Hubka, R. E.: Structural Optimization of Six Different Types of Rectangular Plates Subjected to Combined and Biaxial-Compressive Loading. Lockheed-California Company, LR 21662, 1968.

31. Bohon, Herman; and Anderson Melvin S.: Role of Boundary Conditions on Flutter of Orthotropic Panels. AIAA Journal Vol. 4 No. 7, R 41-1248, Jul 1966.

32. Lockheed Flutter and Matrix Algebra System (FAMAS).

33. Lockheed-California Company. Structural Life-Assurance Manual (SLM No. 5), Sonic Fatigue Prevention.

34. McGowan, P. R.; et al: Structural Design for Acoustic Fatigue. ASD TDR 63-820, Oct 1963.

35. Lockheed-Georgia Company. C5A Final Sonic Fatigue Analysis. LG 1VS58-1-3 Feb 1968.

36. Miles, J. W.: On Structural Damage Under Random Loading. Journal of the Aeronautical Sciences, Volume 30, No. 11, Nov 1954.

37. Freberg, C. R.; and Kemter, E. N.: Elements of Mechanical Vibration. John Wiley & Sons, Inc., New York, 1949.

38. Philips, E. P.: Fatigue of René 41 Under Constant and Random Amplitude Loading at Room and Elevated Temperatures. NASA TN D3075, Langley Research Center, Nov 1968.

39. Lockheed-California Company. Structural Life Assurance Manual. 1968.

40. Manson, S. S.: Thermal Stress and Low-Cycle Fatigue. McGraw Hill Book Company, New York, 1966.

41. Heldenfels, R. R.: The Effect of Nonuniform Temperature Distributions on the Stresses and Distortions of Stiffened-Shell Structures. NACA TN 2240, Nov 1950.

42. Aker, L. J.: A Digital Computer Program for Calculating Airplane Turbulent Skin Friction Drag. LR 19620, Apr 1966.

43. Peterson, J. B.: A Comparison of Experimental and Theoretical Results for the Compressible Turbulent-Boundary-Layer Skin Friction with Zero Pressure Gradient. NASA TN D-1795, Mar 1968.

44. Goddard, F. E.: Effect of Uniformly Distributed Roughness on Turbulent Skin-Friction Drag at Supersonic Speeds. Journal of the Aero/Space Sciences, Jan 1959.

45. Hoerner, S. F.: Fluid Dynamic Drag, 1965.

46. Smith, K. G.: The Increase in Wave Drag at Supersonic Speeds Due to Surface Waviness. Royal Aircraft Establishment Technical Report No. 65173, Aug 1965.

47. Czarnecki, K. R.; and Monta, W. J.: Pressure Drags Due to Two-Dimensional Fabrication-Type Surface Roughness on an Ogive Cylinder at Transonic Speeds. NASA TN D-3519, Aug 1966.

48. Elliot, R. D.: A Digital Computer Program for Calculating Pressure Distributions and Aerodynamic Coefficients of Warped Wings of Arbitrary Planform in Supersonic Flow. LR 18764, Feb 1966.

49. Jones, R.: Weight Synthesis and Sensitivity Programs, Lockheed-California Company, LR 21205, 1967.

50. Morris, R. E.: A Study of Advanced Airbreathing Launch Vehicles with Cruise Capability, Vol. V; Economics Model LR 21042, Lockheed-California Company, Feb 1968, NASA CR 73198.

51. Brewer, G. M.: The Learning Curve in the Airframe Industry. Masters Thesis, Air Force Institute of Technology, SLSR-18-65, Aug 1965.

52. Lemcoe, M. M.; and Trevino, Jr., A.: Determination of the Effect of Elevated Temperature Material Properties of Several High Temperature Alloys. ASD-TDR-61-529, Jun 1962.

53. Wichorek, Gregory R.; and Stein, Bland A.: Experimental Investigation of Aluminide-Coated Ta-10W for Heat-Shield Applications. NASA TN D-5524, 1969.

NASA-Langley, 1970 — 2 CR-1568